

INTERNATIONAL RESEARCH AND REVIEWS IN
ENGINEERING

VOLUME - 1

EDITOR

ASSOC. PROF. DR. SELAHATTİN BARDAK

**DECEMBER
2023**

 **SERÜVEN**
YAYINEVİ



Genel Yayın Yönetmeni / Editor in Chief • C. Cansın Selin Temana

Kapak & İç Tasarım / Cover & Interior Design • Serüven Yayınevi

Birinci Basım / First Edition • © Aralık 2023

ISBN • 978-625-6760-80-6

© copyright

Bu kitabın yayın hakkı Serüven Yayınevi'ne aittir.

Kaynak gösterilmeden alıntı yapılamaz, izin almadan hiçbir yolla çoğaltılamaz.

The right to publish this book belongs to Serüven Publishing. Citation can not be shown without the source, reproduced in any way without permission.

Serüven Yayınevi / Serüven Publishing

Türkiye Adres / Turkey Address: Kızılay Mah. Fevzi Çakmak 1. Sokak

Ümit Apt No: 22/A Çankaya/ANKARA

Telefon / Phone: 05437675765

web: www.serüvenyayınevi.com

e-mail: serüvenyayınevi@gmail.com

Baskı & Cilt / Printing & Volume

Sertifika / Certificate No: 47083

INTERNATIONAL RESEARCH AND REVIEWS IN ENGINEERING

VOLUME 1

December 2023

Editor

Assoc. Prof. Dr. SELAHATTİN BARDAK

CONTENTS

Chapter 1

A SERIOUS GAME FOR OCCUPATIONAL HEALTH AND SAFETY TRAINING IN A CONSTRUCTION SITE

Seda ÇELLEK¹, Mehmet ÖZDEMİR², Kaan ERARSLAN³.....1

Chapter 2

TORSIONAL ANALYSIS OF DRIVESHAFT WITH FINITE ELEMENT METHOD

Sümeyye Erdem..... 17

Yusuf Dilay 17

Chapter 3

THE NECESSITY AND ADMISSIBILITY OF GAINING ANDROID SMARTPHONES' ROOT PRIVILEGES

Tayfun Yıldırım..... 31

Nursel Yalçın 31

Chapter 4

INTEGRATED PLANNING OF PUBLIC TRANSPORTATION SYSTEMS IN SMART CITIES – ISTANBUL CASE STUDY

Mesut SAMASTI 47

Chapter 5

COMPARISON OF MONOSTATIC AND MULTISTATIC RADAR-BASED MICROWAVE IMAGING SYSTEMS

Ali Recai Celik 77

Chapter 6

ELECTROSTATIC AND ELECTROTHERMAL THRUSTERS

Hakan BUCAK..... 89

Chapter 7

VALIDATION OF A NUMERICAL METHOD FOR AERODYNAMIC PERFORMANCE ESTIMATION OF WING-IN-GROUND-EFFECT

Yüksel ERASLAN 109

Chapter 8

FUTURE SUSTAINABLE ENERGY IN AUTOMOTIVE: FUEL CELLS

Yasin Furkan GORGULU 123

Chapter 9

ANALYSIS AND SIMULATION OF TWO ZVT BOOST CONVERTERS
WITH ACTIVE SNUBBER CELL

| | |
|----------------------------------|-----|
| <i>Hilal Sebnem Gecmez</i> | 135 |
| <i>Naim Suleyman Ting</i> | 135 |

Chapter 10

TREATMENT OF AMOXYCILLIN WASTES USING ADVANCED
OXIDATION PROCESSES

| | |
|-----------------------------|-----|
| <i>M. Fatih ERGİN</i> | 153 |
|-----------------------------|-----|

Chapter 11

MODELING AND MANUFACTURING OF MINI PRUNING ROBOT
PROTOTYPE

| | |
|--------------------------|-----|
| <i>Faruk GÜNER</i> | 175 |
| <i>Hilmi ZENK</i> | 175 |

Chapter 12

FOOD WASTE MANAGEMENT IN THE FOOD SUPPLY CHAIN AND
SUSTAINABILITY

| | |
|---------------------------------------|-----|
| <i>Fatma Zehra YAKUT</i> | 195 |
| <i>Mukaddes KILIÇ BAYRAKTAR</i> | 195 |
| <i>Cengiz ÇETİN</i> | 195 |

Chapter 13

PREDICTIVE MODELING OF R&D EXPENDITURES FOR TURKEY:
SVR KERNEL VARIATIONS

| | |
|-----------------------------|-----|
| <i>Didem GULERYUZ</i> | 215 |
| <i>Pelin AKIN</i> | 215 |

Chapter 14

APPLICATION OF ANFIS AND ANNS MODEL IN THE PREDICTION
OF DRYING KINETICS OF FIRE HOSE IN A MICROWAVE DRYER

| | |
|---------------------------------|-----|
| <i>Halil Nusret BULUŞ</i> | 237 |
| <i>Aytaç MORALAR</i> | 237 |
| <i>Soner ÇELEN</i> | 237 |

Chapter 15

INVESTIGATION OF THE PERFORMANCE OF A PCM-BASED
PASSIVE BATTERY THERMAL MANAGEMENT SYSTEM UNDER
DIFFERENT GEOMETRICAL, AMBIENT AND MATERIAL
CONDITIONS

Bariş KAVASOĞULLARI 255

Mücahit Emin KARAGÖZ..... 255

Mehmet Nurullah ÖNEL 255

Chapter 16

MOTH-FLAME OPTIMIZATION ALGORITHM FOR DISASSEMBLY
LINE BALANCING PROBLEM UNDER THE TRUNCATED LEARNING
EFFECT

Halime SOMTÜRK 277

Mehmet Duran TOKSARI 277

Chapter 17

INVESTIGATION OF CFD ANALYSIS OF RECTANGULAR SHAPE
OF TALL BUILDINGS AT DIFFERENT ASPECT RATIOS FOR SAME
CROSS-SECTIONAL AREA

Ahmet ŞUMNU 301

Chapter 18

REVIEW OF BRAKING AND BATTERY SYSTEMS IN ELECTRIC
VEHICLES

Mehmet ŞEN 323

Muciz ÖZCAN 323

Chapter 19

THE ART OF TIMELESS LEATHER: SUSTAINABILITY AND LIFE
CYCLE ASSESSMENT OF THE LEATHER INDUSTRY

Fazlı AKYÜZ 345

Nuray Olcay IŞIK EMEKSİZ 345

Khashim BEGALIEV 345



Chapter 1

A SERIOUS GAME FOR OCCUPATIONAL HEALTH AND SAFETY TRAINING IN A CONSTRUCTION SITE

*Seda ÇELLEK*¹, Mehmet ÖZDEMİR², Kaan ERARSLAN³*

* Corresponding author

¹ Assist.Prof.Dr., Ahi Evran University, Engineering Faculty, Geological Engineering, 40100, Kırşehir, TURKEY, e-mail: sedacellek@ahievran.edu.tr, ORCID: 0000-0001-9675-5691

² Res.Assist.PhD., Kütahya Dumlupınar University, Engineering Faculty, Mining Engineering, 43100, Kütahya, TURKEY, e-mail: mehmet.ozdemir@dpu.edu.tr, ORCID: 0000-0002-8164-8874

³ Prof.Dr., Kütahya Dumlupınar University, Engineering Faculty, Mining Engineering, 43100, Kütahya, TURKEY, e-mail: kaan.erarslan@dpu.edu.tr, ORCID: 0000-0002-1875-4009

1. Introduction

The basic conceptual approach of occupational health and safety (OHS) is to prevent accidents and hazardous events before they occur (Bastos et al., 2013). Cognitive and qualified training of the workers in a workplace is a crucial trivet serving this purpose (Palka, 2017). In many countries, work law and legislation oblige OHS training before and during the life of workplaces regarding İLO standards (Alli, 2008; Legislation, 2022). A well-trained staff means workers equipped with the necessary knowledge, behavioral culture, and reflexes. Otherwise, training may not be stated as satisfactory. Recent visual technologies are evolving rapidly and are utilized in different disciplines such as healthcare, industrial branches, advertising, education, etc. (Blumberg et al., 2013). OHS training is one of the fields in which new technologies, approaches, materials, and digital transformation can find comprehensive and various applications.

The computer game sector is an active industrial field due to increasing employment capacity and huge economic volume. On the other hand, games and gamification are also helpful, motivating, and powerful educational tools when pedagogically well designed and properly used (Caponetto et al., 2014). Gamification can be described as developing a digital game environment and scenario for a severe case/non-entertainment case to increase the motivation and interest of the user on that issue (Educause, 2011). Morschheuser et al. (2018) state that since the 2010s, gamification has become one of the leading technologies and software. Hybridization and cooperation of classical education methods and new technological approaches may give better results after scientific research and pedagogical design (Bai et al., 2020). Connolly et al. (2012) state that playing computer games is related to perceptual, cognitive, behavioral, affective, and motivational impacts and outcomes. The knowledge acquisition/content understanding and affective and motivational outcomes seem the most frequent results and impacts.

Various researches have revealed the effect and power of games for a better understanding, enhanced level of consciousness, and joyful training process (Gee, 2005; Erarslan, 2005). Another issue is its positive effect on students' engagement are studied by Seixas et al. (2016) The positive impact of gamification on academic performance and social behaviors has also been determined (Díaz-Ramírez, J., 2020). Krath et al. (2021) explained how gamification supports positive affect and motivation, behavior change, and learning, and the need to study the current theoretical understanding of the psychological mechanisms of gamification. The authors also clarify the issue of gamification, game-based education, and serious game terms.

The construction industry also has an application field of game-based training for OHS training. A serious game is considered a promising tool to

engage learners and enhance their retention of important concepts (Greuter et al., 2012). It has been shown that a serious game can be a suitable manner for training in the construction industry (Din and Gibson, 2019; Mohd et al., 2019). Besides scientific studies, commercial applications can also be found in the market (Alhadef, 2014; Construction Simulator, 2022).

In this work, a first-person role-playing game (FP-RPG) type serious game is developed to be applied in occupational health and safety training and testing. The case study was developed for a construction site as the construction industry is one of the most dangerous industrial branches (EUStat, 2020) and the level of involvement in the accidents arising from workers or the work team is fairly remarkable (Haslam et al., 2005). The three-dimensional model of a skyscraper under construction is used as the training and testing environment. After the scene organization in the Unity 3D game engine, the code scripts required to realize the scenario was written in the C# programming language. This descriptive paper presents the theoretical perspective, methodology, program codes, functions, and application stages.

2. Material and Method

This work intends to develop a tool supporting the classical and current digital training methods. Previous studies and research in the literature have already shown that classical approaches and new technologies may give better results together.

The application scenario is based on a PC-based/Web-based first-person role-playing (FP-RPG) type game. It aims to assist the awareness of personal protective equipment and test/teach the basic knowledge of occupational health and safety training. The flowchart of the game-building process is shown in Fig. 1.

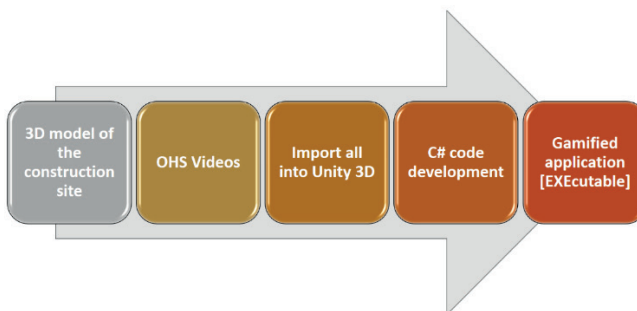


Fig.1. *The process of game building.*

The stages during the game's development can be described as conceptual/theoretical outline, designing the physical components in the game scene, and code development.

2.1. *Conceptual/theoretical outline*

The philosophical backbone and the functional design of the game make the training and testing work together in case of repeatedly playing. The conceptual/theoretical aspect of the game preparation includes the items given below:

i. The knowledge content of the game should cover the subjects related to the accidents occurring most frequently. High occurrence frequency indicates a problem related to weakness in training and application. Hence, primary and critical knowledge should be gathered and added to the game scenario regarding the accident statistics.

ii. The model should reflect a realistic scene where the construction work will occur. Undoubtedly, the construction sites do not have a static appearance and dynamically change day by day. So, a rational instantiation representing the training content should be prepared.

iii. The game should serve awareness of the use of personal protective equipment (PPE). Many accidents still occur due to disregarding the importance of PPE. Picking up the necessary PPEs on the game site should increase the score. This action aims to give consciousness and behavioral improvement.

iv. The knowledge that the trainee is expected to have should be imposed by watching the video clips in the game. Here, the classical teaching methods and thereafter the game application may take place to yield a better result.

v. The game should stimulate learning and have a reward mechanism. This is realized by collecting points to reach a specific score mostly. This is to engage in the activity and boost the trainee's concentration during the training.

vi. The game should be able to support teaching and testing simultaneously. Correct answers to the questions directed at the construction site will increase the score. However, the trainee should be given more than one chance while selecting the correct answer. This approach is a kind of teaching method. In other words, teaching is embedded within the tests using multiple answering trials and repeatedly playing the game.

vii. The game should provide interactive learning and testing while moving on the construction site and taking the messages addressing the subconscious. The first-person role-playing game style serves this purpose better.

viii. There should be a mechanism to prevent continuing the game when personal protective equipment is not taken.

2.2. *Designing the game scene*

In this work, the theory shaping the game is realized in Unity 3D, one of the leading game engine platforms. It is a superior system in which many games and applications have been developed. It has been preferred due to its applicability to various devices, from low to high-performance hardware. Besides, it is the development platform of over 70% of the top 1000 games and over 50% of mobile applications (Unity 3D, 2022). Unity 3D is a cross-platform software in which the application can be switched to various application fields. A Unity 3D game or application can be PC-based web-based, for smartphones, virtual reality headsets, augmented reality smart glasses, IOS and Android mobile devices, consoles like Play Station and Xbox (Fig. 2).

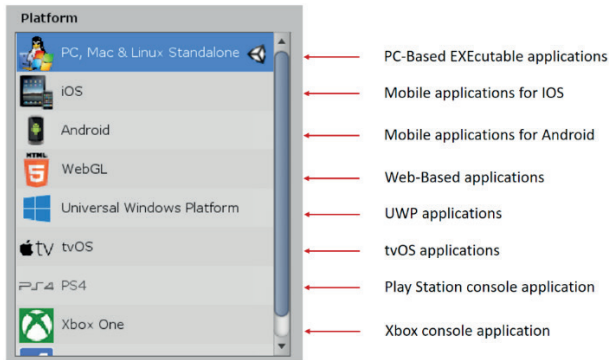


Fig. 2. *Standard platforms, supported by Unity 3D.*

The scene is added previously prepared necessary visual materials like the 3D model of a skyscraper under construction, 3D models of personal protective equipment, occupational health and safety video clips, and the question boards. Personal protective equipment models like safety helmets (Muradyan, 2021), safety glass (Vinigor, 2018), safety boots (Unwave, 2019), life vests (Ramifara, 2021), safety gloves (Rubiez, 2018), fire extinguishers (Red2000, 2020), construction harness (Purdue Envision Center, 2019), fire axe (Denis_cliofas, 2020) and 10 OHS video clips (SafetyAnimation, 2022) are other materials and components of the scene on which the application is developed (Fig. 3).

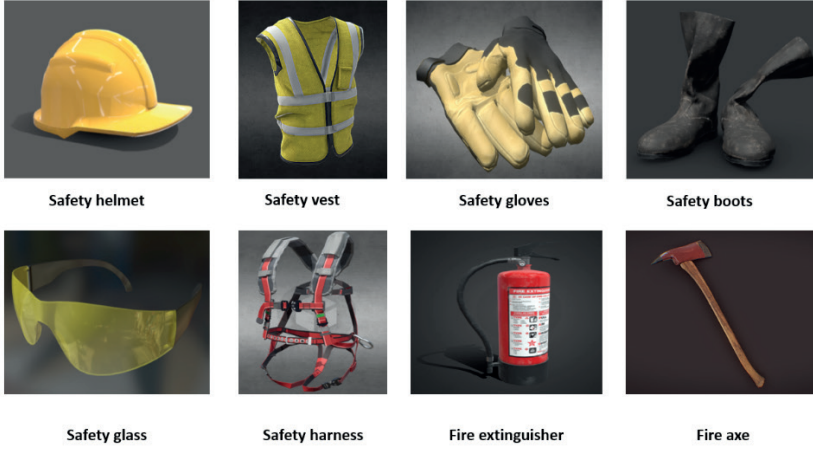


Fig. 3. *Personal protective equipment used in the scene.*

The next step is to develop the first-person role-playing game (FP-RPG) player control, camera control, and game score codes in C#. Here, the FP-RPG character is controlled by the player in the application. The scripts are written and compiled in MS Visual Studio 2019 Community. After compilation, building and running the PC-based executable application is obtained.

In the training and testing scenario, the player moves through the construction site, picks up the animated personal protective equipment, and answers the questions related to the OHS video clips to increase the score.

2.3. *The skyscraper under construction*

The most critical asset in the scene is the 3D model of the skyscraper under construction (MattQ012, 2019), taken from the Sketchfab model database (Sketchfab, 2022). The sophisticated building has more than 15 levels (Fig. 4, 5, and 6). It has a mine-craft game-type structure. All other assets are placed on the different levels and parts of the skyscraper.

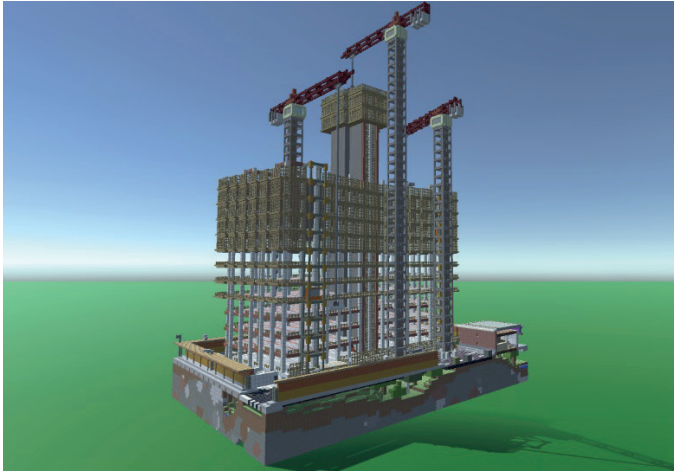


Fig. 4. *The skyscraper used for the scene.*



Fig. 5. *Side view of the skyscraper.*



Fig. 6. *The model view at entrance.*

2.4. *Training OHS videos and question themes*

Besides the PPE, another major trivet of the game is the OHS video files and the question boards placed near them. Ten video files were selected regarding the most frequently occurring accidents (Williams et al., 2018; SafetyAnimation, 2022). The OHS themes of the video files and the related questions are as follow:

- i. Electrical devices, cables, and precautions
- ii. Gaps and falling-down
- iii. Safety goggles and eye protection
- iv. Safety harness and working at high places
- v. Safety helmet against falling pieces
- vi. Walking and working carefully always
- vii. Accidents due to machines
- viii. Careless behaviors due to phone use
- ix. Accidents sourced by head-banging
- x. Foot protection and protective boots

2.5. *C# program scripts*

The theoretical background and scene preparation is completed with the C# codes. Three script files were written in the game project to realize the scenario. The C# files were implemented for player control, camera control, and game control.

PlayerControl.cs file provides the player's movement controls. The classical keys on the keyboard that are used to move forward, backward, right, left, up (ascending), and down (descending) are W, S, D, A, Q, and E keys. Besides, arrow keys are also available for directional movement.

CameraControl.cs script directs the camera according to mouse movement to look at the right, left, up, and down.

GameControl.cs is the code file for destroying the game objects selected or touched and increasing the game score appearing on the screen.

The developed codes are dragged to the necessary assets and related parameters on the Inspector window. When the application is started, it has the characteristics of a first-person shooter game (Fig. 7).



Fig. 7. The scene appearance and some of the codes of the project in Unity 3D 2019.1.14.

3. Implementation of the Game

The game has a design similar to commercial games. The purpose of this is the thought that the game setup that people afford to buy will be more attractive and serve the purpose of the study more. The design is aimed to embody the ideas and intentions stated in the conceptual and theoretical plan.

The game starts by reading the notice at the entrance of the skyscraper construction site (Fig. 8).



Fig. 8. Entry of the construction site with site safety notice.

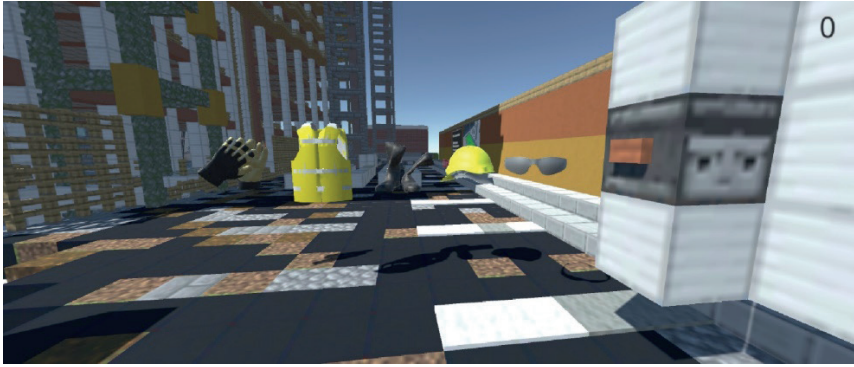


Fig. 9. Personal protective equipment must be picked up to go into the site.

The player has zero points at this point. In order to advance into the building, he/she must first take the personal protective equipment that he will encounter at the entrance. This equipment attracts attention by rotating in the air, similar to commercial games (Fig. 9). When animated PPE is taken, 10 points are earned for each. The player can collect eight PPE up to the top of the skyscraper.

The OHS training videos were used to provide both the training and testing function of the game (SafetyAnimation, 2022). It is possible to watch these looping videos on the panels located at different points of the skyscraper construction repeatedly. The videos have been selected in accordance with the development purpose of the game. Next to each video panel is a related and contextual question. This type of fiction aims to test whether the player perceives the message in the video (Fig. 10). The correct answer is worth 10 points.

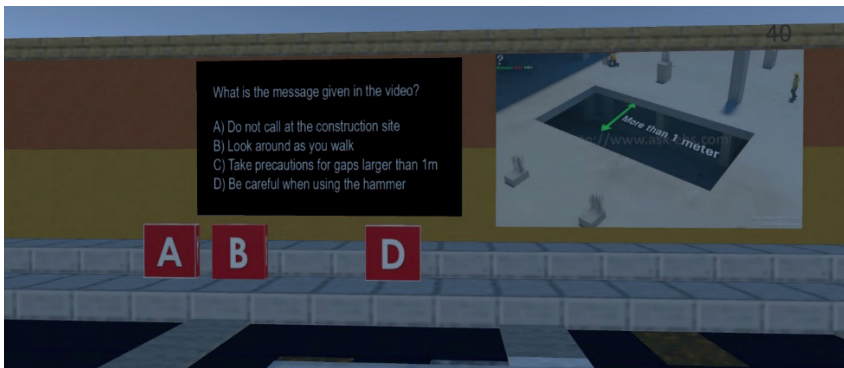


Fig. 10. The video clip and the related question board.

The educational dimension planned to be in the game setup is provided by giving the player a chance to choose until he/she finds the correct answer to the question. This way, the player can go through the options until he finds the right answer, and the points are gained. The player will purposely mark the correct answer when he plays again. In other words, he has now learned the message of the video. With this character, the game can simultaneously be used as a training and testing tool.

While going to the top of the skyscraper, the player must find a PPE or video prepared on each floor and collect points. The location of the game items results in the player going to almost all parts of the tower under construction (Fig. 11 and Fig. 12).

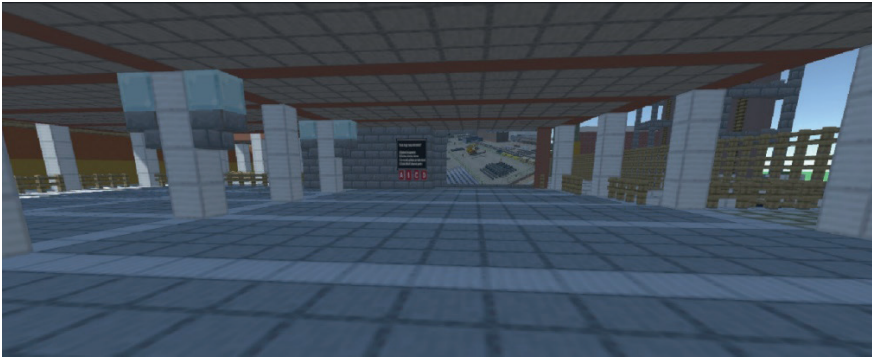


Fig. 11. *The video clips and the question boards were located in various building parts.*

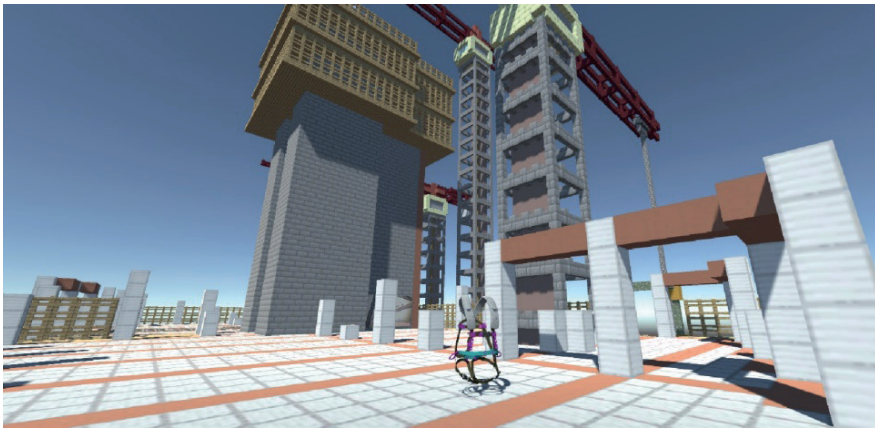


Fig. 12. *Personal protective equipment at different places on the construction site.*

The maximum score to be earned in the game is 180. There is no time limitation. Eight PPE and ten OHS videos were placed in different parts of the skyscraper construction. The repetition of the game aims to consolidate the given knowledge, express the correct information, and increase

consciousness. The game's most essential and fundamental success criterion is that the acquired knowledge can turn into behavior when the trainee goes to an accurate construction site.

As a final inference, it can be said that the player (trainee) has the opportunity to learn and test his knowledge on the game scene simultaneously. In the game, the concepts and issues such as training and testing in a game atmosphere, no time anxiety, visual encounter with the basic information, imposing of OHS messages to the subconscious by watching, interactive learning, and taking tests while walking around the construction site, rewarding knowledge, and increasing interest in training are aimed to be gathered. After repeatedly executing and testing the game it has shown that it can accomplish the functions.

4. Conclusion and Recommendations

In this study, a serious game was developed for occupational health and safety training and testing and was applied to a model of a skyscraper under construction. The study's primary purpose is to develop a technological tool that will support the training program for OHS in the construction sector, which is one of the sectors with the most significant dangers and risks. The serious game's scene components are a 3D model of a skyscraper under construction, personal protective equipment, OHS video files, and related question boards. The game has a design in the style of a first-person role-player game and is similar to the concept and fiction of popular commercial games. It has a structure that makes learning enjoyable, understanding and testing easier, and rewarding knowledge. The player (trainee) earns points during the game by collecting his/her personal protective equipment and answering the relevant questions next to the OHS videos. In the conceptual background of the game, cognitive learning, awareness, concentration on the subject, and transformation of knowledge into behavior are aimed. Messages for the subconscious are intended to be given through gamification. The game scenario was developed in the Unity 3D engine, and the events taking place on the scene were coded with C#. With the approach developed in the study, a sustainable and expandable system that can be applied in the construction sector has been created. It also sets an example for the concept of digital transformation in terms of content and application.

The scope of the study is primarily to develop a new tool to support education. The developed system has been successfully tested. In the next stage, it will be beneficial to continue under the headings of training of students, training of workers, training of trainers. Also, as an approach, it will have the opportunity to be used and updated in many construction activities.

References

- Alhadeff. (2014). Serious Games for Construction Workers with Limited On-Site Experience, Serious Game Market, <https://www.seriousgamemarket.com/2014/03/serious-games-for-construction-workers.html>.
- Alli, B.O. (2008). *Fundamental Principles of Health and Safety*, International Labor Organization, Geneva, ISBN 978-92-2-120454-1, p. 221.
- Bai, S., Hew, K.F., Huang, B. (2020). Does gamification improve student learning outcomes? Evidence from a meta-analysis and synthesis of qualitative data in educational contexts. *Educational Research Review*, 30, 100322, <https://doi.org/10.1016/j.edurev.2020.100322>.
- Bastos, A., Sá, J.C., Silva, O. (2013). The Importance of Training for Preventing Occupational Risks. *Proceedings Cicot 2013, Working Conditions International Congress, Portugal*, ISBN: 978-989-97762-6-5 print, pp. 308-312.
- Blumberg, F.C., Almonte, D.E., Anthony, J. S., Hashimoto, N. (2013). Serious games: What are they? What do they do? Why should we play them? In K. E. Dill (Ed.), *The Oxford Handbook of media psychology*, Oxford, United Kingdom: Oxford University Press, 334–351.
- Caponetto, I., Earp, J., Ott, M. (2014). Gamification and education: A literature review. In C. Busch (Ed.), *Proceedings of the 8th European conference on games based learning*, Nr Reading: Acad Conferences Ltd, pp. 50–57.
- Connolly, T.M., Boyle, E.A., MacArthur, E., Hainey, T., Boyle, J.M. (2012). A systematic literature review of empirical evidence on computer games and serious games. *Computers & Education*, 59(2), 661–686, <https://doi.org/10.1016/j.compedu.2012.03.004>.
- Construction Simulator. (2022). *Construction Simulator 3*. Astragon Entertainment GmbH, <https://www.construction-simulator.com/en>.
- Denis_cliofas. (2020). Fire axe, Sketchfab models, <https://sketchfab.com/3d-models/fire-axe-b9d83055bb3b467c88496299c27ceae0>.
- Díaz-Ramírez, J. (2020). Gamification in engineering education–An empirical assessment on learning and game performance. *Heliyon*, 2020, 6(9), <https://doi.org/10.1016/j.heliyon.2020.e04972>.
- Din, Z.U. and Gibson, Jr G.E. (2019). Serious games for learning prevention through design concepts: An experimental study. *Safety science*, 115, 176-187.
- Educause. (2011). 7 things you should know about gamification. <http://www.educause.edu/library/resources/7-things-you-should-know-aboutgamification>.
- Erarslan, K. (2005). *A System for Virtual Reality Applications on 3D Geological Models and Mine Design*. 19th Intl. Mining Congress and Exhibition of Turkey, June 9-12, Izmir, pp. 299-303.
- EUStat. (2020). *EUStat Statistics Explained*, <https://ec.europa.eu/eurostat/statisti>

cs-explained/index.php?title=Accidents_at_work_statistics#Accidents_2010_to_2018.

Gee, J.P. (2005). Learning by Design: good video games as learning machines. *E-Learning*, Volume 2, Number 1, 5-16.

Greuter, S., Tepe, S., Peterson, J.F., Boukamp, F., d'Amazing, K., Quigley, K., Wakefield, R. (2012). Designing a game for occupational health and safety in the construction industry. In *Proceedings of The 8th Australasian Conference on Interactive Entertainment: Playing the System*, pp. 1-8.

Haslam, R.A., Hide, S.A., Gibb, A.G., Gyi, T.Pavitt, D.E., Atkinson, S., Duff, A.R. (2005). Contributing factors in construction accidents. *Applied ergonomics*, 36(4), 401-415.

Krath, J., Schürmann, L., Korflesch, H. (2021). Revealing the theoretical basis of gamification: A systematic review and analysis of theory in research on gamification, serious games and game-based learning, *Computers in Human Behavior*, 125, 106963, 33, <https://doi.org/10.1016/j.chb.2021.106963>.

Legislation. (2022). Legislation for the Training of Occupational Health and Safety Training of Workers. *Turkish Work Law*, <https://www.mevzuat.gov.tr/File/GeneratePdf?mevzuatNo=18371&mevzuatTur=KurumVeKurulusYonetmeligi&mevzuatTertip=5>.

MattQ012. (2019). Under Construction Skyscraper, Mineopolis, <https://sketchfab.com/3d-models/under-construction-skyscraper-mineopolis-0bdaa-04334b2470690f61da73431bdd2>.

Mohd, N.I., Ali, K.N., Bandi, S., Ismail, F. (2019). Exploring gamification approach in hazard identification training for Malaysian construction industry. *International Journal of Built Environment and Sustainability*, 6(1), 51-57, DOI:10.11113/ijbes.v6.n1.333.

Morschheuser, B., Hassan, L., Werdere, K., Hamarid, H. (2018). How to design gamification? A method for engineering gamified software. *Information and Software Technology*, 95, 219-237.

Muradyan, H. (2021). Safety helmet, Sketchfab models, <https://sketchfab.com/3d-models/safety-helmet-f9c17905f17a45d885442ebace25a66f>.

Palka, D. (2017). The role and importance of training for improving the safety and awareness of the technical staff in the mining plant. In *CBU International Conference Proceedings*, Vol. 5, pp. 1195-1198.

Purdue Envision Center. (2019). Construction harness, Sketchfab models, <https://sketchfab.com/3d-models/construction-harness-41638e5ec5264ed481d7cda-15806ca0e>.

Ramifara. (2021). Life vest model, Sketchfab models, <https://sketchfab.com/3d-models/life-vest-model-f4160b557ee34182a33af737d2f9d397>.

Red2000. (2020). Realistic fire extinguisher, Sketchfab models, <https://sketchfab.com/3d-models/realistic-fire-extinguisher-8b52b1f4c4c44bb9866146f60dbe534c>.

- Rubiez. (2018). Mechanical Gloves, Sketchfab models, <https://sketchfab.com/3d-models/mechanical-gloves-f3fed278f56e49528c78e6c4c311777d>.
- SafetyAnimation. (2022). ASK-EHS Occupational Health & Safety Animation, <https://www.youtube.com/channel/UCaEmkOaYKdcw8EXfmMut7zg>.
- Seixas, L.R., Gomes, A.S., Filho, I.J.M. (2016). Effectiveness of gamification in the engagement of students. *Computers in Human Behavior*, 58, 48-63.
- Sketchfab. (2022). Sketchfab Inc, <https://sketchfab.com>.
- Unity 3D. (2022). Unity Technologies, <https://unity.com>.
- Unwave. (2019). Kizra boots, Sketchfab models, <https://sketchfab.com/3d-models/kizra-boots-fac9f2745c0f47f5b4e63e2aaf8228f8>.
- Vinigor. (2018). Glasses Yellow, Sketchfab models, <https://sketchfab.com/3d-models/glasses-yellow-2c38a0d71fc64064b162b33154334265>.
- Williams, O.S., Hamid, R.A., Misnan, M.S. (2018). Accident Causal Factors on the Building Construction Sites: A Review. *International Journal of Built Environment and Sustainability*, 5(1), 78-98. <https://doi.org/10.11113/IJBES.V5.N1.248>.



Chapter 2

TORSIONAL ANALYSIS OF DRIVESHAFT WITH FINITE ELEMENT METHOD

Sümeyye Erdem¹

Yusuf Dilay²

1 Öğr. Gör., Karamanoğlu Mehmetbey Üniversitesi, Teknik Bilimler Meslek Yüksekokulu, <http://orcid.org/0000-0002-5518-2716>

2 Dr. Öğr. Üyesi, Karamanoğlu Mehmetbey Üniversitesi, Teknik Bilimler Meslek Yüksekokulu, <http://orcid.org/0000-0002-5365-5137>

1. INTRODUCTION

Driveshaft can be defined as machine elements that transfer rotational moment. They are widely used in motion transmission in mechanical systems. Especially if there are vertical or horizontal differences between two shaft axes, the use of driveshaft is inevitable. Since these shafts transmit rotational torque, they are subjected to overloads, stresses and torsion. Driveshafts are used to transmit torque and power, subjecting them to high dynamic torsional and shear stresses (Nadeem et al., 2018). These machine elements can transmit rotational movements without disturbing the existing stiffness. The main damage mechanism that occurs in machine parts operating under dynamic stresses is fatigue damage (Santecchia et al., 2016; Tarakçı et al., 2021). Fatigue is one of the main damage mechanisms for Driveshaft (Göksenli and Eryürek, 2009; Çivi and Tahralı, 2021). Driveshafts are generally manufactured from hollow shafts. The strength of hollow shafts increases and they become lighter. The shafts are made of high quality steels and the joint forks are welded to the end. In machine tool construction, Driveshaft are used to drive the spindle of multi-spindle drill presses and to drive the tables of small milling machines. It can also compensate for misalignments caused by spindle position. This is achieved by mutual centering of the spindle flanges by means of a centering piece or a centering collar (Güllü and Özdemir, 2000).

Long-term operation of driveshaft and the overloads to which they are exposed cause costly problems as well as shortening the life of the shaft. In order to prevent these damages and costs and to improve the shaft, Von Mises (equivalent) stress and displacement values were analyzed. Within the scope of the research, safety factor values were calculated based on safety coefficient values and fatigue tests in the driveshaft designed in accordance with DIN 5480 standard. In cases where the equivalent stress is higher than normal, improvement suggestions are made.

2. Materyal ve Yöntem

The research material of the study is the driveshaft used in cars. The technical dimensions of the solid modeling of the analyzed propeller shaft prepared using SolidWorks program are given in Figure 1. It is possible to improve the design or directly intervene in the design from the elements of the propeller shaft consisting of many parts. The driveshaft considered in the research is composed of a stab flange and auxiliary flange elements. The moment value applied to the driveshaft is taken from the company catalogs. During the analysis, a moment of 120000 [Nmm] was applied to the driveshaft. 30MNB5 material was used in the propeller shaft, C45 material was used in the shaft, AISI 5120 (20MnCr5) material was used in the spindle, and C45 material was used in the auxiliary flange. Some technical properties of the materials are given in Table 1-4.

Table 1. Material properties of the flange element

| Flange (30MNB5) | Properties |
|-----------------------|------------------------|
| Modulus of Elasticity | 210 GPa |
| Yield Strength | 510 MPa |
| Poisson Ratio | 0,3 |
| Density | 7860 kg/m ³ |

Table 2. Material properties of the driveshaft element

| Driveshaft (C45) | Properties |
|------------------|------------------------|
| Yield Strength | 500 MPa |
| Tensile Strength | 700 MPa |
| Density | 7,85 g/cm ³ |

Table 3. Material properties of the spindle element

| Spindle [AISI 5120 (20MnCr5)] | Properties |
|-------------------------------|------------|
| Yield Strength | 540 MPa |
| Tensile Strength | 1000 MPa |
| α_2 (Joint angle) | 20° |

Table 4. Material properties of the auxiliary flange element

| Auxiliary Flange (C45) | Properties |
|------------------------|------------------------|
| Yield Strength | 500 MPa |
| Tensile Strength | 700 MPa |
| Density | 7,85 g/cm ³ |

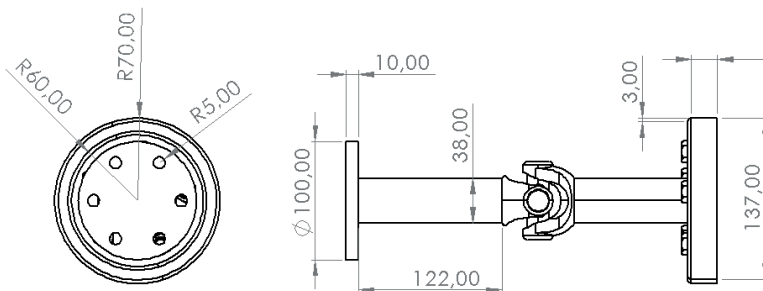


Figure 1. Technical drawing of the driveshaft

The driveshaft was solid modeled with Solidworks software (Figure 2). Then, the stress distributions occurring on the driveshaft were simulated with the finite element package software Ansys Workbench under different loads, moments and operating environments. The analyzes were carried out as three-dimensional linear static. The obtained torsion analysis results are given as outputs of Ansys Workbench package software. Driveshaft operation was evaluated and simulated for the application conditions. The moment on the driveshaft is calculated by equation (1).

$$T = F \times a \quad (1)$$

In equality;

$T =$ Moment (Nm, lbf ft)

$F =$ Applied force (N, lbf)

$a =$ Moment arm (m, ft)

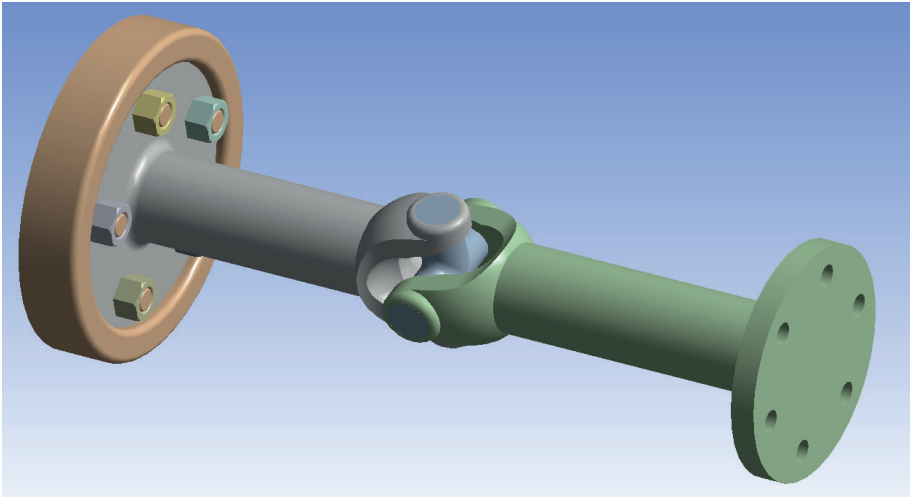


Figure 2. Solid model drawings of driveshaft

In the first step of the analysis process carried out in the simulation environment with the finite element method, the meshing of the driveshaft model, in other words, the separation of the model into the most appropriate small parts, was performed (Figure 3). The “meshing” functions of Ansys Workbench software were utilized to create the finite element structure of the propeller shaft. A total number of 24912 elements and 68346 total nodes were obtained for the driveshaft.

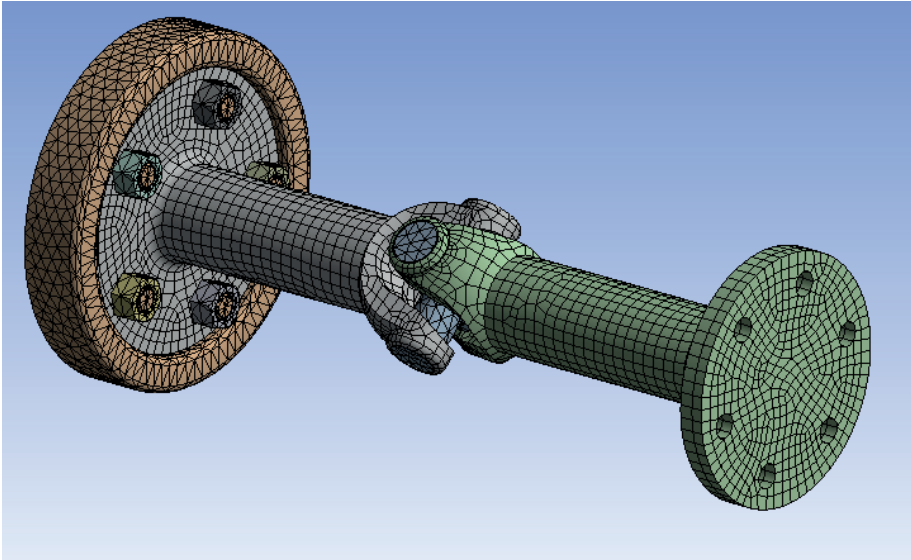


Figure 3. Finite element structure of the driveshaft model

A torque of 1200000 Nmm was applied clockwise on the circular surface of the driveshaft auxiliary flange (Figure 4).

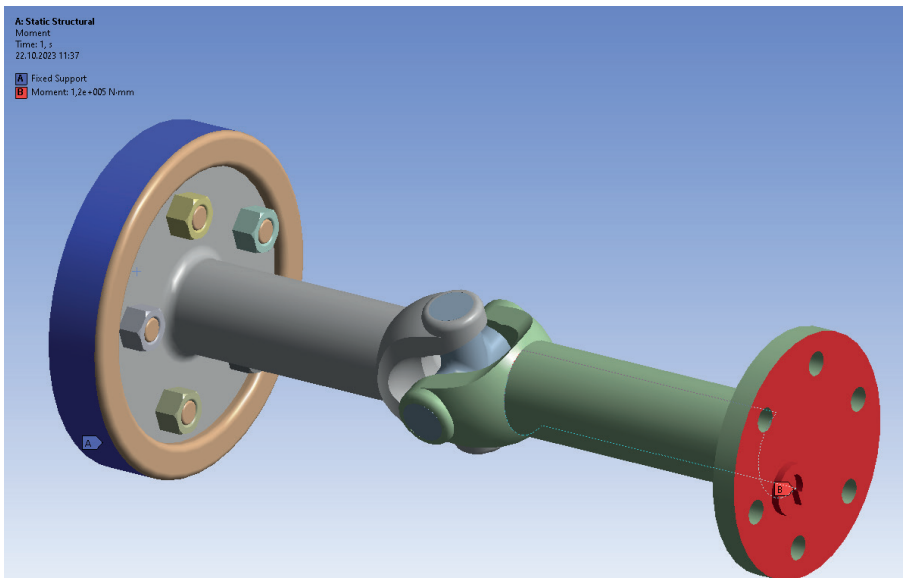


Figure 4. Boundary conditions and definition of moment

3. RESEARCH FINDINGS AND DISCUSSION

After the moment analysis solution process, the stress distributions occurring on the propeller shaft are given in Figure 5. When the structure of the driveshaft is examined, it is seen that the maximum equivalent stress is in the spindle. The maximum stress value is 108.26 MPa. When this value is evaluated in terms of material, it is below the yield strength. When the stresses on the other structural elements were examined (Figure 6-9), it was determined that the stress distribution under the applied loads remained within the yield strength limits of the material. The maximum equivalent stress and the safety coefficients obtained according to the yield strength of the material for Figures 6-9 are given in Table 5. When the equivalent stress values of all structural elements are analyzed, it is seen that the driveshaft operates safely without damage under the application conditions.

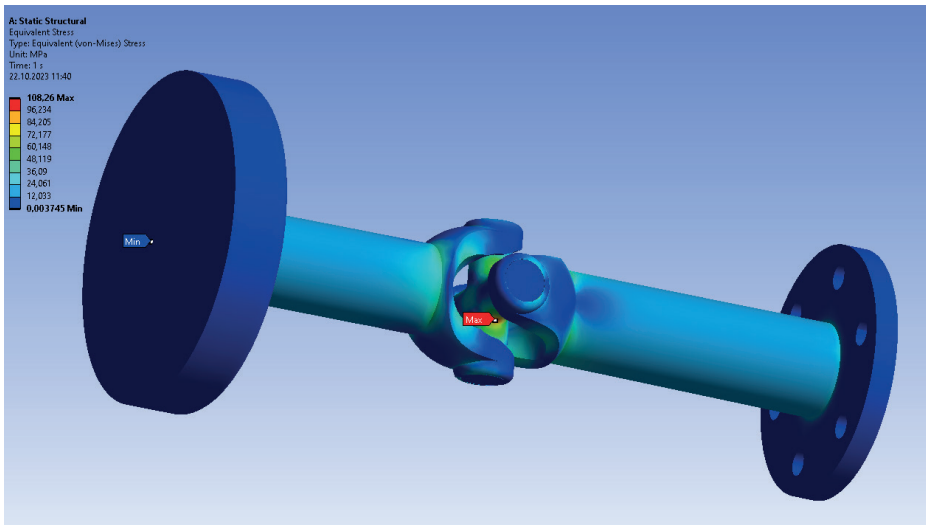


Figure 5. Distribution of equivalent stresses for the whole structure

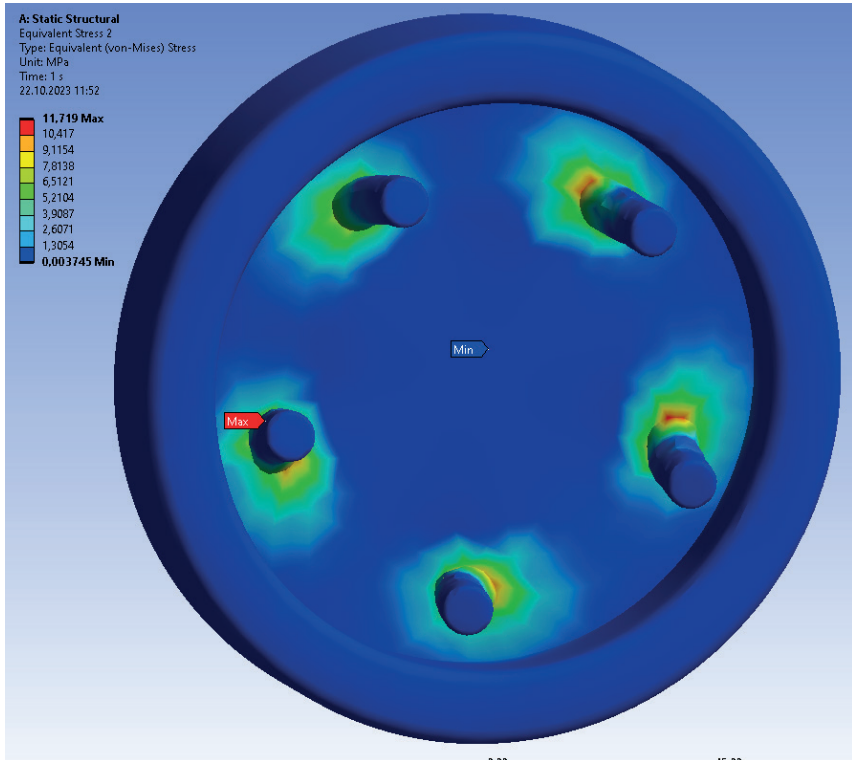


Figure 6. Equivalent stress distributions for flange

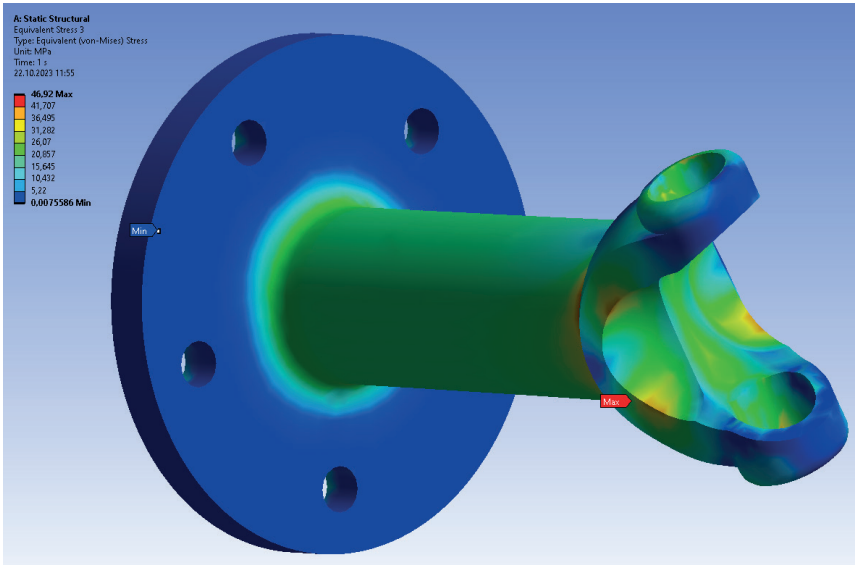


Figure 7. Equivalent stress distributions for driveshaft

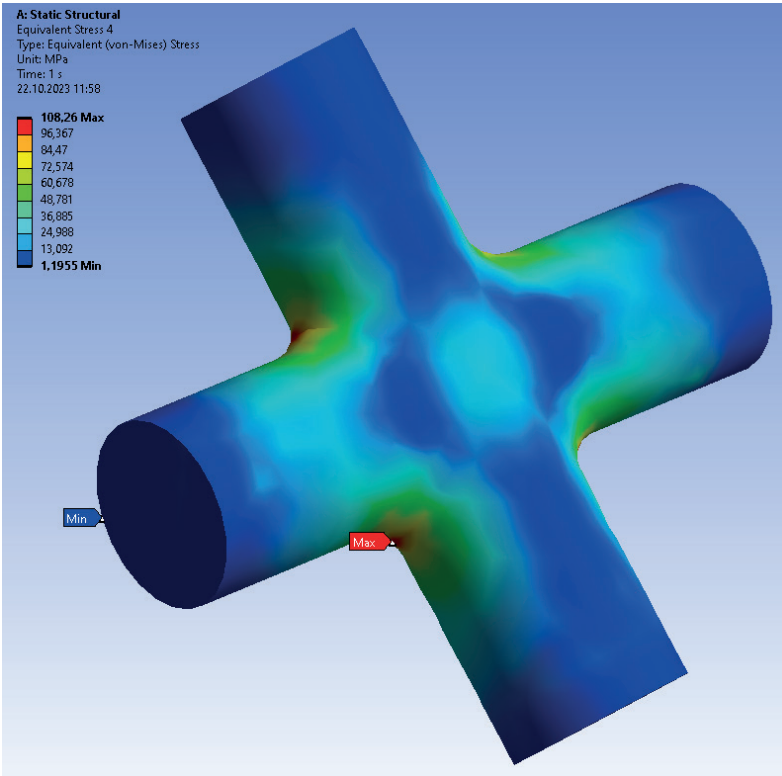


Figure 8. Equivalent stress distributions for the spindle

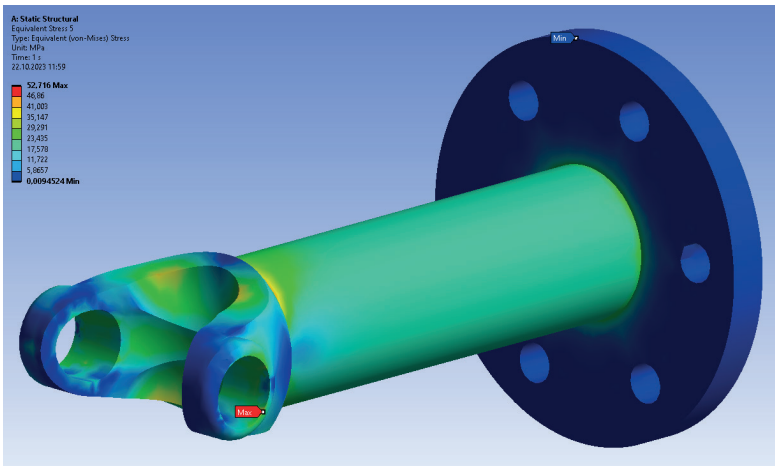


Figure 9. Equivalent stress distributions for auxiliary flange

Table 5. Working safety coefficients calculated for driveshaft

| Driveshaft elements | Material yield strength [σ_{yield}] [MPa] | Max. equivalent stress [σ_{eq}] [MPa] | Safety coefficient [k_s] = [$\sigma_{yield} / \sigma_{eq}$] |
|---------------------|---|---|--|
| Flange | 510 | 11,719 | 43,519 |
| Driveshaft | 500 | 46,92 | 10,656 |
| Spindle | 540 | 108,26 | 4,987 |
| Auxiliary flange | 500 | 52,716 | 9,484 |

In the research, displacement analysis was performed under the effect of moment applied to the propeller shaft. After the analysis, the total displacement value occurring on the driveshaft is given in Figure 10. When the structure of the driveshaft was examined, it was seen that the total displacement value was at the auxiliary flange. The total displacement value was found to be 0.16472 mm. Displacement values were also calculated on other structural elements (Figures 11-14) The values obtained according to the displacement analysis for Figures 11-14 are given in Table 6.

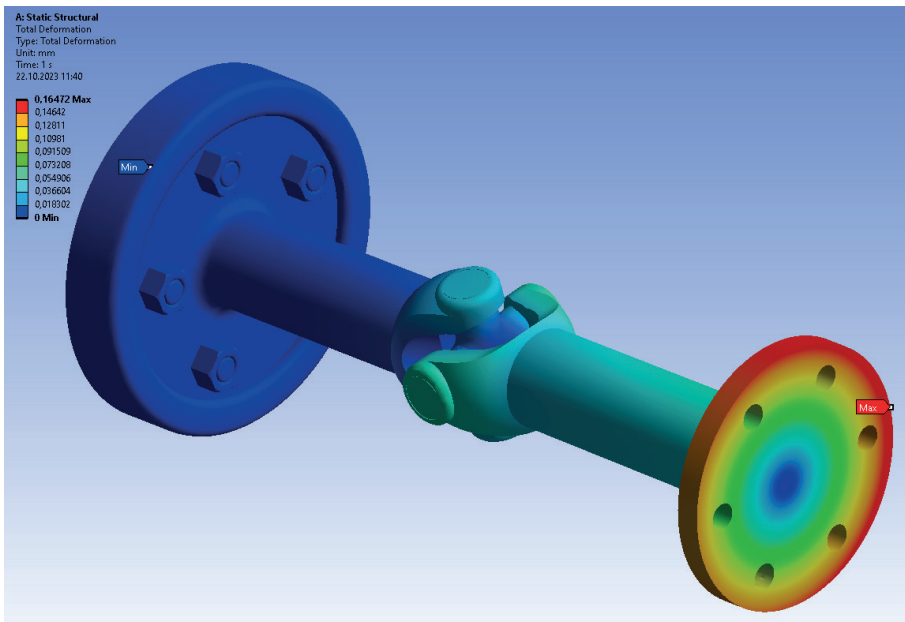


Figure 10. Driveshaft maximum total displacement distribution

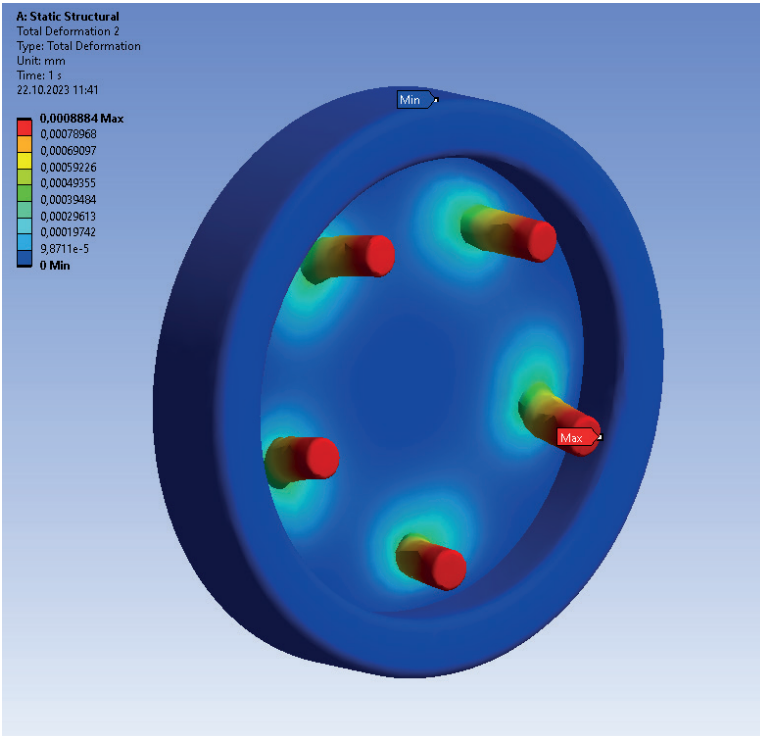


Figure 11. Displacement distributions for flange

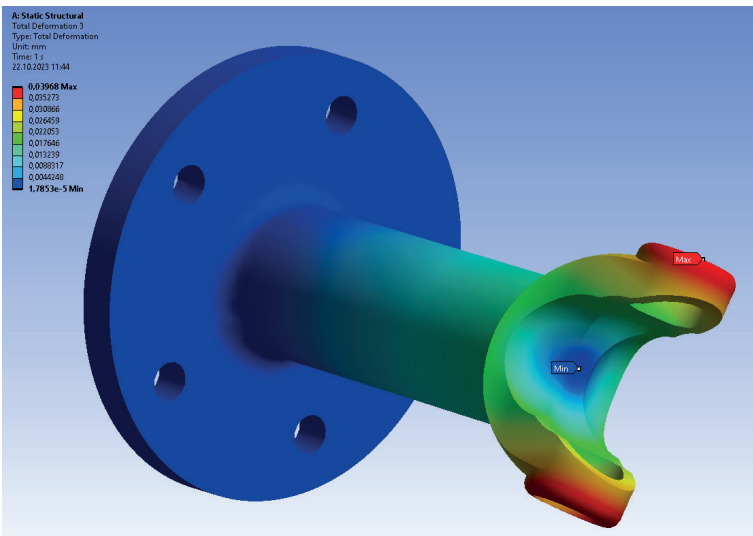


Figure 12. Displacement distributions for driveshaft

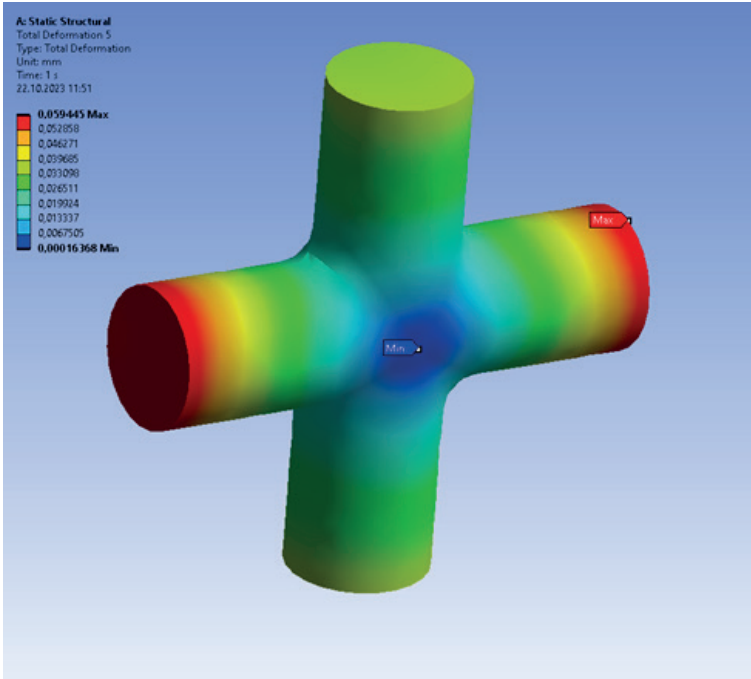


Figure 13. Displacement distributions for the spindle

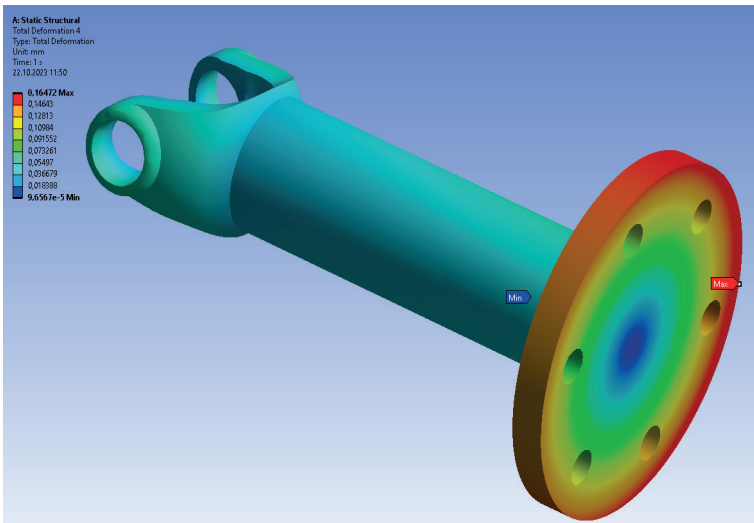


Figure 14. Displacement distributions for auxiliary flange

Table 6. Calculated displacement values for driveshaft

| Driveshaft elements | Displacement Values (mm) |
|---------------------|--------------------------|
| Flange | 0,0008884 |
| Driveshaft | 0,03968 |
| Spindle | 0,059445 |
| Auxiliary flange | 0,16472 |

After the analysis, the safety factor value on the driveshaft was calculated and given in Figure

15. The blue color indicates the maximum safety factor on the driveshaft and the red color indicates the minimum safety factor. The safety factor value of the driveshaft was found to be maximum 15 and minimum 0.

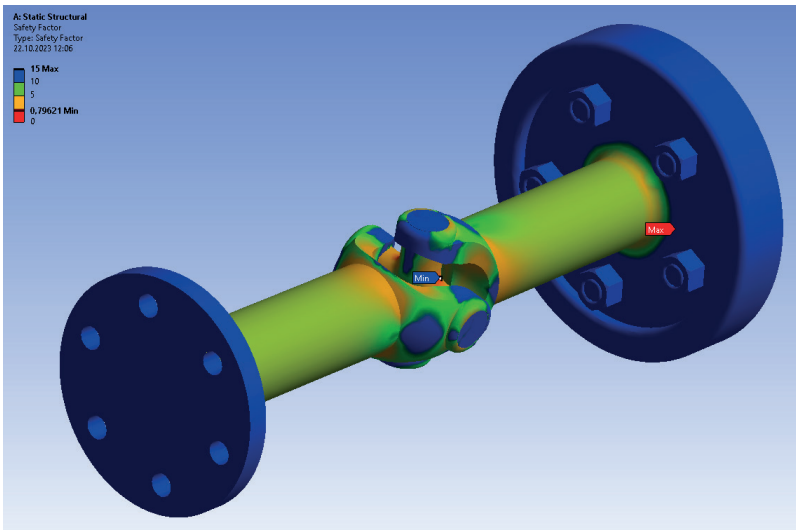


Figure 15. Safety factor of the driveshaft

4. CONCLUSION

In this study, three-dimensional solid modeling of the driveshaft was made, stress and displacement analysis of the modeled driveshaft under normal conditions were simulated and the safety factor of the driveshaft was calculated. The results obtained as a result of the analyzes are given below.

a. For the whole propeller shaft construction, the maximum equivalent stress value was found to be at the spindle of the propeller shaft. It is 108.26 MPa.

b. The maximum equivalent stress value was determined as 11.719 MPa on the flange element, 46.92 MPa on the driveshaft element, 108.26 MPa on the on the spindle element and 52.716 MPa on the auxiliary flange element.

c. The maximum total displacement for the driveshaft was found to be 0.16472 mm at the auxiliary flange element.

d. The displacement value was determined as 0.0008884 mm on the flange element, 0.03968 mm on the driveshaft element, 0.059445 mm on the spindle element and 0.16472 mm on the auxiliary flange element.

e. Safety factor values of the driveshaft were calculated. The maximum safety factor value was found to be 15 on the driveshaft. The minimum safety factor value was found to be 0 on the spindle.

f. In the simulation, no damage was found on the driveshaft construction. It was determined that the driveshaft element and structural elements bear the forces at different points applied within the elastic deformation limits of the materials used.

Material tests of Driveshaft designed and manufactured from different materials and shapes are necessary. Since real driving tests are time-consuming and costly, the strength analysis of the products to be designed with 3D solid modeling techniques and finite element method will minimize unnecessary time loss. In this context, the data obtained in the virtual environment should be interpreted very well before manufacturing and experimental studies should be directed where necessary.

REFERENCES

- Çivi, C., Tahralı, N. (2021). Driveshaft Strength and Fatigue Life Analysis Case Study: 4x2 Commercial Vehicle Driveshaft. *International Journal of Engineering Research and Development*, 13(2), 329-338.
- Goksenli, A., & Eryurek, I. B. (2009). Failure analysis of an elevator drive shaft. *Engineering Failure Analysis*, 16(4), 1011-1019. doi:10.1016/j.engfailanal.2008.05.014.
- Güllü, A., Özdemir, A., (2000). "Metal Vocational Knowledge" Milli Eğitim Basımevi, İstanbul.
- Nadeem, S. K. S., Giridhara, G., & Rangavittal, H. K. (2018). A Review on the design and analysis of composite drive shaft. *Materials Today: Proceedings*, 5(1), 2738-2741. doi:10.1016/j.matpr.2018.01.058.
- Santecchia, E., Hamouda, A. M. S., Musharavati, F., Zalnezhad, E., Cabibbo, M., El Mehtedi, M., & Spigarelli, S. (2016). A Review on Fatigue Life Prediction Methods for Metals. *Advances in Materials Science and Engineering*, 2016, 1-26. doi:10.1155/2016/9573524.
- Tarakçı, S., Aldemir, O., Efe, I. Ş. I. K., & Özdemir, S. (2021). Design and production of torque measurement system over driveshaft. *Balıkesir University Journal of Institute of Science and Technology*, 23(1), 234-242.



Chapter 3

THE NECESSITY AND ADMISSIBILITY OF GAINING ANDROID SMARTPHONES' ROOT PRIVILEGES

Tayfun Yıldırım¹

Nursel Yalçın²

¹ Tayfun Yıldırım, Gazi University, Institute of Informatics, Department of Computer Forensics, 0000-0001-8942-6953

² Assoc. Prof. Nursel Yalçın, Gazi University, Faculty of Education, Department of Computer and Educational Technologies Education, 0000-0002-0393-6408

*This work was composed from MSc Thesis named "Analysis of android smartphones in the context of digital forensics: Processes, methods and the legal dimension". Author: Tayfun Yıldırım. Supervisor: Assoc. Prof. Nursel Yalçın. 2023. Gazi University, Institute of Informatics, Department of Computer Forensics.

I. INTRODUCTION

Digital forensics is a branch of science that provides evidence to be presented to the court as a documentation by collecting digital devices and analyzing them. By reaching the material truth through this branch of science, it is possible to catch the perpetrators, punish them or acquit the innocent or prevent the crimes planned to be committed (Kılıç, 2012).

Digital forensics: It is the whole of the stages of examining digital evidence on digital media of various qualities by applying scientific methods to reach the material truth, preserving the integrity of the digital evidence related to the crime, making it ready to be presented to the judicial authorities in an understandable way without being corrupted, and applying certain scientific techniques (Ekizer, 2014).

According to the theory known as “Locard’s Principle of Change” by Criminologist Prof. Edmond Locard, before a perpetrator leaves the crime scene, he will either leave a trace of himself there or carry a trace of there on himself. Since this evidence are concrete evidence, they are very important as they cannot be refuted by abstract witness statements. The principle of change is valid in the field of digital forensics as well as in the physical environment of a crime scene. In this respect, it is very difficult to act on information technology systems without leaving any indications, just as every behavior in the physical environment leaves indications (Başlar, 2019).

The Android operating system is the most widely used operating system in all devices with a 38.33% market share among all operating systems in November 2023 (StatCounter, 2023).

Since smartphones are relatively more affordable than personal computers, it can be much easier to reach these devices. And it is possible for people in the low-income group without using any digital device other than smartphone, and basically continue their lives with the operations they do on their smart phones. If these people commit a crime, there is the potential to have large amounts of digital evidence on their smartphones relates to the crime (Petraityte, Dehghantanha, and Epiphaniou, 2017).

Smartphones are constantly carried with their owners, often physically held closer to them than other potential digital devices, such as computers. The size of these devices to be carried in the pocket makes it easier for people to carry these devices with them, causing them to be in constant interaction throughout the day. For these reasons, the evidence potential of these devices is greatly increased following factors like: the possibility of the devices were taken to the area where the crime was committed; the possibility of the formation of location information as a result of communicating with people by using a smart phone at the scene; the possibility of audio, video recording

or photographing at the scene with a smartphone; the possibility of criminal messaging recordings on the smartphone. Moreover, it is likely to commit crimes by using these devices directly as a tool. Because smart phones have very powerful hardware and functions today, and they can contain rich data types that equivalent to personal computers (Walnycky et al., 2015). Smartphones have become the most critical and important piece of evidence in many investigations (Kim and Lee, 2020).

Although the methods used in digital forensics have developed, the previously developed forensic methods may become dysfunctional with the continuous technological developments and the updating of the versions of operating systems and applications. For this reason, digital forensics is a science that still needs development and needs to be studied continuously.

For example, it is very important to gain root privileges during the examination of Android smartphones, and it is getting harder and harder to gain root privileges on newly released Android smartphones and operating system versions.

Because it is often necessary to gain root privileges to effectively perform forensic investigations of Android smartphones and reach the material truth. However, gaining root privileges can be seen as unlawful method. In this study, acceptability of gaining root privileges also discussed.

II. IMPORTANCE, ADMISSIBILITY AND CHALLENGES OF GAINING ROOT PRIVILEGES

A. Root Privileges

Rooting Android smartphones is like having administrator privileges using the “sudo” command in the Linux operating system. As a matter of fact, since Android is based on Linux, just as it is necessary to have administrative authority with the use of the “sudo” command line to perform many development or modification operations in the Linux operating system, root privileges are required to have broad authorities on Android smartphones (Hoog, 2011).

With root privileges, it is possible to make changes to system files, access system files and important files where application’s data are stored. Although it is possible to access user data without root privileges, this data will often be too limited.

ADB (Android Debug Bridge) commands will need to be used when it is desired to take a logical or physical image from an Android smartphone with a computer on the workstation. It is possible to take both logical and physical images with ADB commands. However, additional components and applications must be installed like BusyBox application on the device to

obtain a physical image.

Android Debug Bridge (ADB) system consists of three elements: client, daemon, and server. The client runs on the computer in the workstation and sends commands to the device. The daemon runs in the background of the Android smartphone, executing the commands that the client sends to it. The server handles the communication between the daemon and the client. It is possible to backup non-rooted device data via an application on Android smartphone or ADB commands, or to obtain data from the device through the information provided by the content providers (Lin, 2018).

For ADB commands to be executed, USB debugging mode must be turned on from the target device (Figure 1) and this permission must be given to the computer on the workstation (Figure 2).

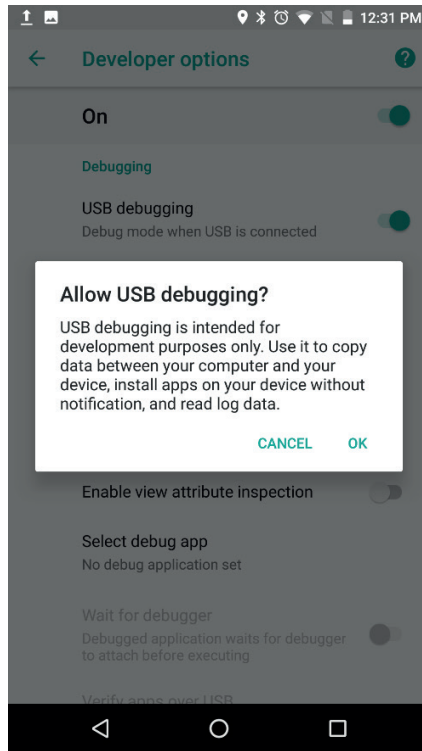


Figure 1. Enabling USB debug mode on target device.

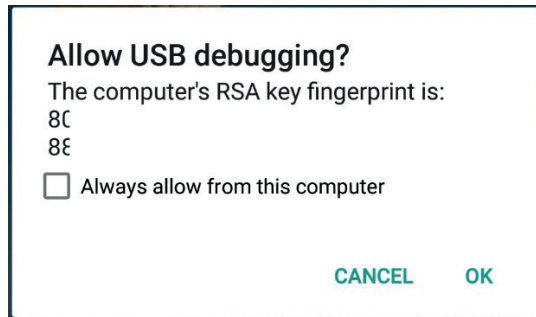


Figure 2. Screenshot of the smartphone that shows giving permission to use ADB commands on target device from workstation specific computer.

After connecting an Android smartphone to the workstation, then binding to the terminal of the target device with root privileges with the command “adb shell su”, the screen that appears in the superuser application is shown whether to allow root privileges on the device (Figure 3).

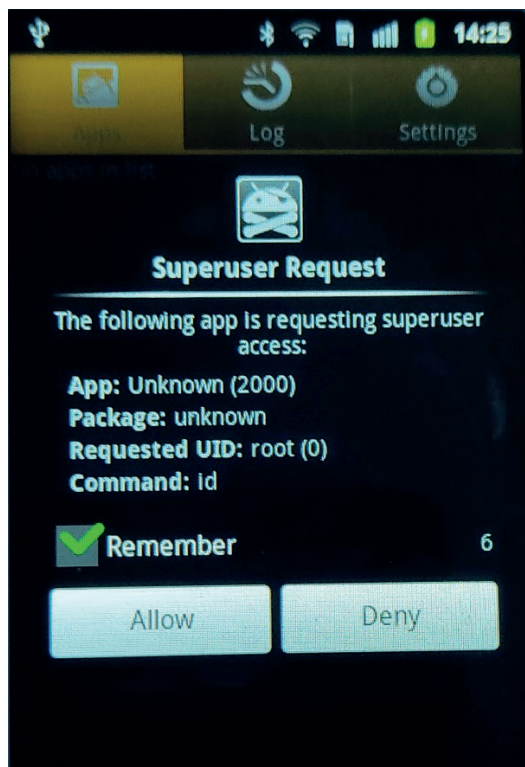


Figure 3. Permitting to using root privileges of the Android Smartphone.

The command prompt screen showing that the device can be accessed to the /data directory without encountering any problems on the rooted device by typing the “ls /data” command on the computer at the workstation (Figure 4).

```
tyfn@tyfn-VirtualBox:~$ adb -d shell
$ su
# ls /data
log
dontpanic
cache
misc
local
data
app-private
app
property
radio
anr
dalvik-cache
lost+found
gps
soundbooster.txt
system
secure
backup
tombstones
#
```

Figure 4. Checking if root privileges has been acquired by digital forensic examiner or has not from workstation computer command prompt.

The command prompt screen showing that many permissions, and the permission to view the subfolders and subfiles information in the /data directory are denied, even when the workstation is requested to examine the base directories of the target device (Figure 5).

```

C:\Users\avtay\AppData\Local\Android\Sdk\platform-tools>adb shell
gm5plus_s_sprout:/ $ ls
ls: ./vndservice_contexts: Permission denied
ls: ./verity_key: Permission denied
ls: ./ueventd.rc: Permission denied
ls: ./plat_hwservice_contexts: Permission denied
ls: ./nonplat_hwservice_contexts: Permission denied
ls: ./init.zygote32.rc: Permission denied
ls: ./init.usb.rc: Permission denied
ls: ./init.usb.configfs.rc: Permission denied
ls: ./init.recovery.qcom.rc: Permission denied
ls: ./init.rc: Permission denied
ls: ./init.environ.rc: Permission denied
ls: ./init.carrier.rc: Permission denied
ls: ./init: Permission denied
acct          d          firmware          oem          proc          storage
bt_firmware  data      mnt              persist      res           sys
bugreports   default.prop  nonplat_file_contexts  plat_file_contexts  root         system
cache        dev        nonplat_property_contexts  plat_property_contexts  sbin        tombstones
charger      dsp        nonplat_seapp_contexts  plat_seapp_contexts  sdcard      vendor
config       etc        nonplat_service_contexts  plat_service_contexts  sepolicy
1|gm5plus_s_sprout:/ $ ls /data
ls: /data: Permission denied

```

Figure 5. ADB commands that shows without root privileges it is not possible to access /data directory that contains user data, and even to view some directories on the smartphone flash memory.

As seen above, it is not possible to access the /data directory where user data is stored without having root privileges. Therefore, even when a logical image of the device is desired, the data in this directory will not be available.

B. Importance of Root Privileges

There are basically two different ways to obtain data on Android smartphones. One of them is taking the logical image, while the other is taking the physical image. The importance of rooting Android smartphones in terms of digital forensics is gathered at the point of obtaining data with these two different ways.

If it is preferred to logically obtain data from Android smartphones, it will not be possible to access the /data directory where the user data is stored or the /system directory where the system files are stored (Skulkin, Tindall, and Tamma, 2018c). If these directories cannot be reached, although it is possible to obtain various data via Android backup files or content providers, the data obtained will be very poor compared to the data that can be acquired with gaining root privileges. In fact, Android applications can prevent the data that can be obtained with the Android backup feature with a Boolean type code called as a flag that they add to the manifest.xml file (Breitinger and Baggili, 2019). Again, content providers are the data that an Android application shares with other applications and it is obvious that these applications will keep this data within a certain limit.

To take the physical image of the target device with software tools, it is a requirement to have root privileges. It is not possible to take the physical image of the device in any way with software tools without having root privileges.

With the physical image, it is possible to create a byte-to-byte copy of the flash memory of the target device. In this way, not only the file system, but also the unallocated space of the device's flash memory can be obtained. Therefore, data deleted by the user can also be recovered by obtained physical image.

With hardware level methods like JTAG or Chip-off, the physical image of the target device can be taken without gaining root privileges. However, the implementation of both methods has great difficulties. The implementation of the JTAG method may not always result in success or it may not be possible because the smartphone manufacturer has closed the JTAG inputs on the circuit board (Skulkin, Tindall, and Tamma, 2018b). Besides that, Chip-off method is much more time consuming and costly than JTAG, and it may harm hardware of device (Skulkin, Tindall, and Tamma, 2018a).

At the same time, software tools such as LiMe or AMExtractor must be used to obtain the volatile memory of the Android smartphone. However, to use these software tools on the target device, it is mandatory to have root privileges of the target device. The Linux kernel source code of the target device is needed for LiMe (504ENSICS Labs, 2014). It can be found on the manufacturer's website or other resources. Along with the Linux kernel source code, the file named "config.gz" must be obtained from the /proc directory of the device's file system and this file which is related to target device kernel must be cross compiled with the Linux kernel source code. Later, by transferring the module created by LiMe to the target device, volatile memory can be obtained. However, this Linux kernel source code may not be available for every target device because the manufacturer does not share the kernel source code, or the kernel source code has not been published by a third source. This reduces the effectiveness of the tool called LiMe.

Although the Linux kernel source code is not required to use the AMExtractor tool, it is necessary to learn the various features of the RAM (Random Access Memory), to create the kernel module based on these features, and to obtain the data of the volatile memory by transferring the created kernel module file to the device (Haiyu Yang, 2022).

However, root privileges are needed both to obtain the "config.gz" file of the target device for the LiMe tool, and to obtain various features of the RAM for the AMExtractor tool. Again, it is obligatory to have root privileges during the transfer of the created module to the device for acquiring volatile memory.

Therefore, obtaining useful data for forensic analysis on the target device without having root privileges will be very limited.

C. Legal Acceptability of Gaining Root Privileges

When it comes to ensuring data security, the confidentiality, integrity, and availability of evidence, known as the CIA trio, will be evaluated. These

basic principles, which have their roots in providing data privacy on a military basis, are also used in ensuring data security for organizations (Samonas and Coss, 2014). Confidentiality of evidence means taking precautions and measures so that only authorized persons can access the data. Integrity, on the other hand, is that the wholeness of the data is maintained continuously, and its accuracy is not lost. Availability means that it is possible to access the data by authorized persons when necessary.

These features can also be applied to the admissibility of digital evidence by courts. Ensuring the confidentiality of the evidence is important in terms of the privacy of personal data through the investigation, and the fundamental rights and freedoms of the suspect. Preserving the integrity of the evidence is a necessity to be able to prove that the alleged crime was committed by the defendant. Availability, on the other hand, is an essential for the competent authorities like judge, lawyer, or prosecutor to examine the digital evidence during the trial and form the judgment.

Having the integrity feature of digital evidence will also mean that evidence has the accuracy and reliability. It demonstrates that the data on the device preserved without any changes since the first acquisition of the digital evidence (University Of East London and Ay, 2020). By ensuring this feature, the existing digital evidence does not undergo any changes during all processes from obtaining it to its presentation to the court and afterwards during its storage. Thus, that the originality of the data created by the user can be preserved at all stages (Alfred and Scott, 1997).

Since appellate proceedings can take a long time, an environment that will constantly protect the integrity and especially the authenticity of the digital evidence should be provided even after the convict (Granja and Rafael, 2017).

Rooting Android smartphones will inevitably cause a change in the target device. Therefore, since the integrity of digital evidence cannot be protected by rooting, it can be claimed that it is unlawful evidence.

However, as explained above, it is very important to gain root privileges for Android smartphones to obtain many user data. Otherwise, the material truth may not be reached, and the perpetrators may not be punished.

Gaining root privileges of Android smartphones does not corrupt or change user data. It causes a change only at the system level (Almehmadi and Batarfi, 2019) (Hassan and Pantaleon, 2017). In addition, after the physical or logical image of the target device is taken, it is possible to undo the rooting process and restore the device's system to its original state.

Processes made in digital forensics operations should be reasonable and reliable (McKemmish, 2008). Therefore, the analyzes made within the scope

of digital forensics should also have the quality of justifiability, it should be explained why the root privileges were gained and the user data was not changed in any way (Montasari, 2016).

In this context, another situation that should be considered is that if it is possible to reach the material truth with evidence other than digital evidence, it is necessary to be just content with this evidence. Otherwise, the balance between fundamental rights and freedoms against public interest may be disrupted. Considering the best evidence rule, the use of digital evidence obtained because of gaining root privileges can be used as a last resort (Mason and Seng, 2017). The Turkish Law of Criminal Procedure states that if other non-digital evidence is sufficient to reach the truth, should be contented with these non-digital evidence (CMK, 2004).

However, in an investigation, the Android smartphone's evidential value is important, and if it is necessary to refer to this evidence in reaching the material truth, this situation can be overcome with documentation, which is the cornerstone of digital forensics. With documentation, it is necessary to present the digital evidence as a whole by considering all aspects of how it was obtained and what it relates to (Tenhunen, 1997). Using the "Five Ws" (and one H) questions, by explanations of where, when, why, who, what, and how questions, the processes of gaining root privileges can be presented in the documentation (Cosic and Baca, 2010).

The judge, lawyer or prosecutor may not have sufficient technical knowledge about the authenticity of digital evidence (Montasari, 2016). Although gaining root privileges does not affect user data, the running principles of the Android operating system should be effectively disclosed to the court subjects with the documentation. Thus, it will be efficient to discuss digital evidence. It is great importance for defense lawyers to have knowledge of the authenticity of digital evidence. Otherwise, the digital evidence presented to the courts can be accepted as accurate digital evidence (Roscini, 2016). In this respect, it is very important for the trial subjects to have basic knowledge of the Android operating system architecture in terms of reaching the material truth. During the acquisition of root privileges, discussing whether the limit is exceeded, and the user data has been modified will help to give an accurate convict.

It has great importance that the user data remains unmodified to ensure authenticity. In this way, it will be possible to prove that the user data on the target device was created by the suspect (Antwi-Boasiako and Venter, 2017). In terms of reaching the material truth, the protection of the authenticity of the digital evidence is more important than the integrity feature. As a matter of fact, the integrity is not an absolute condition, but is important in relation with the authenticity. Therefore, with the authenticity preservation of the digital evidence, mandatory changes to be made on the digital evidence can

be accepted (Mason and Seng, 2017). Otherwise, if data is obtained from the target devices by logical acquisition, the rejection of these digital evidence may occur due to the lack of complete physical image and so integrity feature. Today, in many digital devices, it may not be possible to take the physical image of the target device for various reasons such as password protection and lack of access authorization. Rejecting the obtained logical image, on the ground that it does not have integrity feature, will cause most of the digital evidence to be unavailable in trials and so reaching to truth for punishing perpetrators or acquitting innocents.

In this context, digital forensics experts can reveal that they did not change any user data by documenting the processes they made while gaining root privileges, with the timestamps, video recording of the smartphone and workstation screen, and reporting the processes to the finest detail. Performing this process with technically competent digital forensics experts, it should be ensured that the user data part of the target device is not changed, and that the system part is changed only to gain root privileges so that no damage is caused to the operability of the device. In the created documentation, it should also be explained why gaining root privileges is necessary to access user data. Thus, the admissibility of digital evidence by the courts will be protected.

The integrity of the evidence must also be protected after gaining the root privileges, during the chain of custody (Antwi-Boasiako and Venter, 2017). Since the device will be rooted, different forensic experts should take this situation into account when analyzing the device. Since experts who do not know about this situation or do not take it into account may think that their actions will not be allowed by the target device anyway, and they may cause loss or change of user data.

One of the principles used for the acceptance of digital evidence in the United States is the Dauber test method. In this method, the admissibility of digital evidence is not tied to strict principles, but it is evaluated whether the accepted scientific methods are applied according to the type of digital evidence (Montasari 2016). Rooting of Android smartphones has also been widely used in many academic studies like analysis of TikTok application (Khoa et al., 2020), analysis of instant messenger applications (Mahajan, Dahiya, and Sanghvi, 2013), analysis of Wickr application (Mehrotra and Mehtre, 2013), acquisition of Android smartphone volatile memory (Yang et al., 2016). Therefore, it is obvious that rooting is a scientific method in digital forensics investigation of Android smartphones. So, gaining root privilege is forensically sound if user data is not modified or lost (Kong, 2015).

Otherwise, if the data obtained by not making any changes in the target device with traditional approaches, it may cause that many perpetrators cannot be punished, and justice cannot be established. As explained in

the “Introduction” section, Android smartphones are the most widely used smartphones in the World, and because these devices are in constant interaction with the perpetrators, their potential evidence value in a crime committed is quite high.

D. Challenges

Rooting Android smartphones is not a simple process and requires competence. It is obligation to apply different methods according to each Android operating system version or phone brand and model.

In operating system versions prior to Android 5.0.0, it is possible to gain root privileges by installing a file that will change the system data over the bootloader, which will be accessed by using various key combinations during startup of the device, without the need to unlock the bootloader. However, unlocking the bootloader is a must for Android 5.0.0 and higher versions. Once the bootloader is unlocked, it is possible to gain root privileges with a special recovery system file (like TWRP) to be installed (Skulkin, Tindall, and Tamma, 2018d).

Many Android smartphones only permit unlocking the bootloader on the condition of deleting the data on the device. In these cases, instead of gaining root privileges by unlocking the bootloader, it is necessary to gain root privileges by finding a different vulnerability. If a different vulnerability cannot be found, a forensic investigation will have to be made on the data that can be accessed in a limited way. Unlocking the bootloader may cause the Android smartphone to crash and not start (soft brick/hard brick), loss of the manufacturer’s warranty, and security vulnerability (Skulkin et al., 2018c).

III. RESULT AND DISCUSSION

The process of gaining root privileges causes changes only at the system files level on the target device. It does not change any user data of the device. However, this process is not a simple process and requires competence. In case of an unsuccessful attempt, irrecoverable data loss may occur. By demonstrating the necessity of gaining root privileges and no user data has been changed, the admissibility of the digital evidence obtained by gaining root privileges can be ensured. Thus, this digital evidence will be accepted as lawful evidence by the courts.

If there is no previous experience in successfully rooting the relevant device or operating system version, practices should not be carried out directly on the target device, and root privileges should be successfully acquired on an exact sample device. The process steps applied in successful acquisition should be detailed, and the same steps should be applied to the target device to prevent the user data of the target device from being modified or lost.

For all these reasons, the digital forensics expert to gain root privileges must be quite competent. Whether it is necessary to gain root privileges should be evaluated by considering the balance between the benefit that is thought to be gained in terms of each concrete case and fundamental rights and freedoms. It should be evaluated whether it is possible to reach the material truth with any other evidence other than the data to be obtained from the Android smartphone, and the process of gaining root privileges should be used as a last resort. Because after gaining root privileges on the device, system data will change. If it is necessary to gain root privileges, it should be tried to gain authority with minimal changes in system files and user data should not be damaged by any means. While gaining root privileges, it is necessary to act in such a way that it is possible to undo rooting. (Akarawita, Perera, and Atukorale, 2015).

If it is possible to reach the material truth with the limited data that can be obtained on the Android smartphone without gaining root privileges, should be contented with this limited data. The aim of the Criminal Law is to reach the material truth, and fundamental rights and freedoms of individuals should not be harmed by going beyond this purpose.

IV. CONCLUSION

Smartphones are pocket-sized and the users is constantly interacting with their smartphones. Android smartphones are dominantly used in the smartphone market. For this reason, the potential of the Android smartphones containing evidence in relation to a committed crime is quite high. It is not possible to access the directories where Android smartphones store user data without root privileges. For this reason, even if a logical image is taken without root privilege, many user data will not be obtained. Besides that, the physical image of the device will not be obtained with software tools. Obtaining the physical image is very important in terms of digital forensics, since the physical image also contains data that has been deleted by the user. In traditional digital forensics approaches, it is foreseen that no changes should be made to the device. For this reason, gaining root privilege should be used as a last resort. If it is possible to reach the material truth with other evidence, should be contented with just other evidence without making any changes in the Android smartphone. Although gaining root privileges causes changes in the data on the target device, this change only occurs in system files level. Therefore, gaining root privileges by competent forensic experts will be effective in reaching the material truth. At the same time, it can be proven that no modification has been made in the user data, by documenting every step of the process of gaining root privileges, supported with video recordings. Thus, the claim that the digital evidence has been altered can be refuted and its legality can be preserved.

REFERENCES

- 504ENSICS Labs. 2014. “LiME (Linux Memory Extractor).”
- Akarawita, Indeewari, Amila Perera, and Ajantha Atukorale. 2015. “ANDROPHSY - Forensic Framework for Android.”
- Alfred, Menezes, and Vanstone Scott. 1997. *Handbook of Applied Cryptography*. CRC press.
- Almehmadi, Tahani, and Omar Batarfi. 2019. “Impact of Android Phone Rooting on User Data Integrity in Mobile Forensics.” Pp. 1–6 in *2019 2nd International Conference on Computer Applications & Information Security (ICCAIS)*. IEEE.
- CMK. 2004. *Ceza Muhakamesi Kanunu*.N. 5271.
- Antwi-Boasiako, Albert, and Hein Venter. 2017. “A Model for Digital Evidence Admissibility Assessment.” Pp. 23–38 in *IFIP International Conference on Digital Forensics*. Springer.
- Başlar, Yusuf. 2019. “Adli Bilişim Sürecinde Karşılaşılan Sorunlar ve Çözüm Önerileri.” *TBB Dergisi* (2020 (148)).
- Breitinger, Frank, and Ibrahim Baggili, eds. 2019. “If I Had a Million Cryptos: Cryptowallet Application Analysis and a Trojan Proof-of-Concept.” in *Digital Forensics and Cyber Crime*. Vol. 259, *Lecture Notes of the Institute for Computer Sciences, Social Informatics and Telecommunications Engineering*. Cham: Springer International Publishing.
- Cosic, Jasmin, and Miroslav Baca. 2010. “Do We Have Full Control over Integrity in Digital Evidence Life Cycle?” Pp. 429–34 in *Proceedings of the ITI 2010, 32nd International Conference on Information Technology Interfaces*. IEEE.
- Eki zer, A. Hakan. 2014. “Adli Bilişim (Computer Forensics).” Retrieved December 22, 2022 (URL: <https://www.ekizer.net/adli-bilisim-computer-forensics/>, Last Access Date: 22.12.2022.).
- Granja, Fernando Molina, and Glen D. Rodríguez Rafael. 2017. “The Preservation of Digital Evidence and Its Admissibility in the Court.” *International Journal of Electronic Security and Digital Forensics* 9(1):1–18.
- Haiyu Yang. 2022. “AMExtractor.”
- Hassan, Mohamed, and Lutta Pantaleon. 2017. “An Investigation into the Impact of Rooting Android Device on User Data Integrity.” Pp. 32–37 in *2017 Seventh International Conference on Emerging Security Technologies (EST)*. Canterbury: IEEE.
- Hoog, Andrew. 2011. “Android and Mobile Forensics.” in *Android forensics*. Waltham, MA: Syngress.
- Khoa, Nghi Hoang, Phan The Duy, Hien Do Hoang, and Van-Hau Pham. 2020. “Forensic Analysis of TikTok Application to Seek Digital Artifacts on Android Smartphone.” Pp. 1–5 in *2020 RIVF International Conference on Computing and Communication Technologies (RIVF)*. IEEE.

- Kim, Dohyun, and Sangjin Lee. 2020. "Study of Identifying and Managing the Potential Evidence for Effective Android Forensics." *Forensic Science International: Digital Investigation* 33:200897.
- Kılıç, Mehmet Serkan. 2012. "İşletim Sistemlerinin Adli Bilişim Açısından İncelenmesi." Yüksek Lisans Tezi, Polis Akademisi Güvenlik Bilimleri Enstitüsü, Ankara.
- Kong, Joe. 2015. "Data Extraction on Mtk-Based Android Mobile Phone Forensics." *Journal of Digital Forensics, Security and Law* 10(4):3.
- Lin, Xiaodong. 2018. "Android Forensics." Pp. 335–71 in *Introductory Computer Forensics*. Springer.
- Mahajan, Aditya, M. S. Dahiya, and Hitesh P. Sanghvi. 2013. "Forensic Analysis of Instant Messenger Applications on Android Devices." *ArXiv Preprint ArXiv:1304.4915*.
- Mason, Stephen, and Daniel Seng. 2017. *Electronic Evidence*. University of London Press.
- McKemmish, Rodney. 2008. *When Is Digital Evidence Forensically Sound?* Springer.
- Mehrotra, Tarun, and B. M. Mehtre. 2013. "Forensic Analysis of Wickr Application on Android Devices." Pp. 1–6 in *2013 IEEE International Conference on Computational Intelligence and Computing Research*. IEEE.
- Montasari, Reza. 2016. "Digital Evidence: Disclosure and Admissibility in the United Kingdom Jurisdiction." Pp. 42–52 in *Global Security, Safety and Sustainability-The Security Challenges of the Connected World: 11th International Conference, ICGS3 2017, London, UK, January 18-20, 2017, Proceedings 11*. Springer.
- Petraityte, Milda, Ali Dehghantanha, and Gregory Epiphaniou. 2017. "Mobile Phone Forensics: An Investigative Framework Based on User Impulsivity and Secure Collaboration Errors." Pp. 79–89 in *Contemporary Digital Forensic Investigations of Cloud and Mobile Applications*. Elsevier.
- Roscini, Marco. 2016. "Digital Evidence as a Means of Proof before the International Court of Justice." *Journal of Conflict and Security Law* 21(3):541–54.
- Samonas, Spyridon, and David Coss. 2014. "The CIA Strikes Back: Redefining Confidentiality, Integrity and Availability in Security." *Journal of Information System Security* 10(3).
- Skulkin, Oleg, Donnie Tindall, and Rohit Tamma. 2018a. "Chip-Off." in *Learning android forensics: analyze android devices with the latest forensic tools and techniques*. Packt Publishing Ltd.
- Skulkin, Oleg, Donnie Tindall, and Rohit Tamma. 2018b. "JTAG." in *Learning android forensics: analyze android devices with the latest forensic tools and techniques*. Packt Publishing Ltd.
- Skulkin, Oleg, Donnie Tindall, and Rohit Tamma. 2018c. *Learning Android Forensics: Analyze Android Devices with the Latest Forensic Tools and Techniques*. Packt Publishing Ltd.

- Skulkin, Oleg, Donnie Tindall, and Rohit Tamma. 2018d. "Recovery and Fastboot." in *Learning android forensics: analyze android devices with the latest forensic tools and techniques*. Packt Publishing Ltd.
- StatCounter. 2023. "Operating System Market Share Worldwide." *StatCounter Global Stats*. Retrieved December 9, 2022 (URL: <https://gs.statcounter.com/os-market-share>, Last Access Date: 15.12.2023.).
- Tenhunen, Matti. 1997. "The Integrity of Electronic Evidence." *Integrity and Internal Control in Information Systems: Volume 1: Increasing the Confidence in Information Systems* 153–86.
- University Of East London, and Ofori Ay. 2020. "Digital Forensics Investigation Jurisprudence: Issues Of Admissibility Of Digital Evidence." *Journal of Forensic, Legal & Investigative Sciences* 6(1):1–8. doi: 10.24966/FLIS-733X/100045.
- Walnycky, Daniel, Ibrahim Baggili, Andrew Marrington, Jason Moore, and Frank Breiting. 2015. "Network and Device Forensic Analysis of Android Social-Messaging Applications." *Digital Investigation* 14:S77–84.
- Yang, Haiyu, Jianwei Zhuge, Huiming Liu, and Wei Liu. 2016. "A Tool for Volatile Memory Acquisition from Android Devices." Pp. 365–78 in *IFIP International Conference on Digital Forensics*. Springer.



Chapter 4

INTEGRATED PLANNING OF PUBLIC TRANSPORTATION SYSTEMS IN SMART CITIES – ISTANBUL CASE STUDY

Mesut SAMASTI¹

¹ TUBITAK TUSSIDE, Kocaeli Turkey
E-mails: mesut.samasti@tubitak.gov.tr, mesutsamasti@gmail.com

1. Introduction

With the increasing risks of global warming, countries have started to develop new policies to reduce carbon emission rates. The Kyoto Protocol is one of these policies, which aims to reduce greenhouse gases by 5.2% between 2008 and 2012 (Cirman, 2009). Among the preventive actions taken in this context, practices such as installing filters in factory chimneys, expanding the use of alternative green energy, carbon footprint monitoring, and expanding the use of electric vehicles have been implemented.

Since industrial establishments are predominantly located in the outskirts of the city, their negative environmental impacts are not directly noticed by individuals. However, air pollution, noise pollution, and negative psychological effects due to time loss due to traffic density are noticed more quickly and closely by individuals. For this reason, the traffic problem is generally considered among the problems that need to be solved with priority in city management. Instead of solving the problem, applications such as improving infrastructure facilities, directing vehicle users to different routes, etc. with local solution proposals to reduce the traffic problem, instead of solving the problem, the significant effect of the problem is spread over a wide area environmentally and the existing effect is less pronounced or felt regionally. However, the total negative environmental impact per unit time period does not change. In this case, solutions to be developed for traffic should be sought with holistic approaches.

Traffic is formed depending on the vehicle density of the movements of individuals between departure and arrival points in transportation processes. Excessive idle capacities of individual vehicle users or inefficiently planned public transportation vehicles increase the vehicle density in traffic. Idle capacities in public transportation cause inefficiency in resource planning since the planning process of different transportation modes or different enterprises serving in the same transportation mode is done independently of each other. In an integrated public transportation system, public transportation vehicles will provide more efficient and comfortable service as resources will be distributed evenly within the system. Even if individual vehicle users do not switch to public transportation systems in the first stage, with the increase in comfort in public transportation systems, individual vehicle users will gradually start to use public transportation systems, which will contribute to a decrease in the number of unit vehicles in traffic, which will contribute to a decrease in traffic density, negative environmental impact, air pollution and negative psychological effects.

The smart city concept, which addresses the services offered in the city holistically with technological awareness, also offers solutions for public transportation and traffic issues. However, since the existing solutions belong

to narrow problems, there is limited efficiency increase. This study aims to establish a conceptual process on how integrated public transportation planning should be done in smart cities, how to collect and analyze which data, and how integrated planning should be done depending on the type of transportation. In this way, it is aimed to use resources more efficiently.

2. Scope

This study covers all passengers served by public transportation systems, the modes of transportation used by these passengers, public transportation vehicles and traffic mobility on the route where the journeys take place. With the integrated public transportation plan, it is foreseen that transportation plans will be made more efficiently with the integrated public transportation plan, the comfort in public transportation systems will increase, more individuals will use public transportation systems, and individual vehicle users will gradually use public transportation systems. In this way, it is thought that traffic density will decrease over time.

3. Problem Definition

Public transportation systems are managed and planned within different enterprises. Each system (bus operators, minibus cooperatives, rail systems, subways, sea lines with ferries, etc.) acts independently of each other. The planning of these transportation systems is not based on the passengers in the general mobility, but only on the passengers using their own systems. In this case, inefficient planning of vehicles providing transportation services and the resources of transportation systems may not be distributed fairly. With this study, "General travel movement will be analyzed and its effect on efficiency will be examined when integrated public transportation planning is made.

4. Literature

In smart cities, when public transportation systems are planned in an integrated manner and the reliability of vehicle scheduling plans is consistent, the waiting time of passengers in public transportation systems decreases and the resource utilization efficiency of the system increases. This increases the attractiveness of public transportation systems, which in turn increases the potential for individual car users to gradually prefer public transportation systems. For this reason, public transport systems in smart cities should be handled with a holistic approach, including the extraction of general passenger mobility (start and end matrices), route optimization, transfer optimization, feeding systems and frequency of trips. The studies so far have been conducted locally within a specific transportation mode or system. In the literature review, the integration of intermediate public transport systems with urban bus systems was examined, and regional solutions were developed by analyzing the profit-loss situations for vehicles (Kalpakçı, 2013). Similarly,

conceptual studies have been conducted on how quality public transportation systems should be (Arslan, 2011), and the integration steps that should be taken have been examined (Deveci, 2015). In the integration phase, studies such as rail public transportation systems (Önder, 2019) and modeling of service vehicles have also been conducted (Altan, 2018). As a result of the research, it was observed that an integrated planning has not yet been made due to the different ownership and operating systems of the systems

4.1. Personalized Transportation Data in Smart Cities

In order to plan integrated public transportation for smart cities, system components should be examined in detail. At this stage, it is first necessary to examine the data of the passengers that ensure the continuity of the system. Passenger data and related vehicle occupancy rates can be determined in different methods. Counting the passengers in the vehicle at certain points, surveys and smart card application are among the known methods. In terms of the consistency of the data, the most accurate result of these methods is the records of smart cards. However, in modes of transportation such as minibuses and minibuses that operate with ticket or cash payment where smart cards are not used, general estimations are made based on surveys and driver observations. In the case of collecting trip data with smart cards, it is possible to determine the trip demand with methods such as artificial neural networks (Topuz, 2008) and to make highly reliable trip optimizations (Deri, 2012).

Increasing integration in public transport service (PTS), multimodal routing and sharing pricing information with passengers in advance have a positive impact on the increased use of public transport systems (Pucher, 1995) (André, 2007). In this context, methods that can perform multi-layered routing activities for personalized transportation information have been developed (Lathia, 2012). In another application, studies have been conducted to provide real-time services using data (Zhang, 2011).

It is also possible to present different scenarios in land use and mobility models in intelligent transportation systems (Tan, 2018). Today, there are applications developed by public institutions serving in this field (Mobiect) as well as applications developed by the private sector (Google Maps, Moovit, Citymapper). In the projects carried out in the European Union, multimodal urban public transportation studies are carried out. Projects such as NODES, CLOSER and Superhub offer door-to-door routing services (TÜSSIDE, Feasibility Report on Personalized Transportation Information in Smart Cities, 2020). However, these applications are unable to analyze individual journey data in an integrated manner, and therefore cannot develop improvement suggestions for the system.

4.2. Smart Stop/Station Systems

Smart Stop applications, which are one of the important components of PTSs, are an important factor in increasing passengers' satisfaction with the use of PTSs. Although there are different regional applications for smart stop applications, in general, different services can be provided within this scope. At smart stops, services such as Air Conditioning, Free Wi-Fi, Smart Card Sales-Filling, Ticket Sales, Payment Vending Machines, Food and other Shopping Vending Machines, Mobile Phone Charging Service, Passenger Guidance Kiosk, Information Screens, Bicycle Parking, UV Air Purification Service, IOT Based Security Monitoring, Light Music Recital can be provided (TÜSSİDE, Smart Station Systems Feasibility Report, 2021). Apart from these services, with the smart interaction between the vehicle and the stop, information such as how long the vehicle stops at which stop, how many passengers get on and off, and when it leaves the stop can be analyzed. With web-based applications, information on when the vehicles will arrive at which stop can be communicated to passengers in advance (Eken, 2014).

4.3. Smart Multimodal Public Transportation

When daily trip data is analyzed, it is measured that the per capita trip rate in Istanbul is 1.74 person/day (İUAP, İstanbul Transportation Master Plan, 2011). There are different applications for smart multimodal public transportation services (TÜSSİDE, Feasibility Report on Multimodal Public Transportation in Smart Cities, 2021):

- Bicycle and electric vehicle rental services with annual subscription in Paris, France,
- Distance-based pricing in Vienna, Austria,
- Congestion-related variable taxation in Singapore,
- Re-planning of transport routes with a focus on efficiency in Barcelona, Spain.

As the subject of this report, these services are not integrated in other systems, but are implemented locally. In the research conducted, it was observed that model proposals for the development of smart public transportation systems were developed (Göl, 2019), transit times between stops were calculated according to the floor press data in public transportation systems (Elmedir, 2014), and smart routing studies were carried out in public transportation systems (Nurkovic, 2015).

4.4. Smart Integrated Traffic Management

While some of the modes of transportation in public transport systems serve in a closed system without being affected by traffic (Bus Rapis System-BRT, Metro, Tram, Finucular, etc.), some modes of transportation serve in an

open system and are directly affected by the traffic situation. For this reason, traffic management is important in PTS planning. In traffic management, traffic flow is controlled with systems such as signaling, electronic control system, 5G, etc., and interventions are made to the traffic flow at certain points when needed. Because reducing the time spent in traffic has significant economic, environmental and psychological effects. For example, when the time spent by drivers stuck in traffic is reduced by 10% using 5G technology in London, it is estimated that it can save £ 880 million annually and reduce CO₂ emissions by 370,000 metric tons per year (TÜSSİDE, Model Development Application in Smart Integrated Traffic Management, 2021).. When traffic is congested in different directions in the morning and evening, the zipper lane system, which can expand and contract, makes it possible for infrastructure resources to be shared fairly by vehicles using the road. For example, it has been simulated that transferring one lane from the less congested direction to the other direction in the morning and evening on the E5 road in Istanbul will significantly relieve traffic congestion, and the addition of a smart controlled intersection can reduce traffic congestion by up to 40%. It is estimated that spending 10 minutes less time in traffic per day will generate an annual economic saving of 6 billion TL (TÜSSİDE, Public Transportation Oriented Istanbul Traffic Planning, 2017).

5. METHOD

This study will develop a conceptual process for integrated public transportation planning in smart cities. Considering the studies in the literature and applications in the field, it has been observed that integrated public transportation planning has not been carried out so far. When the root causes of this are examined, non-standard transportation modes, decentralization of transportation operators, lack of sufficient equipment in vehicles (GPS, smart card payment) and non-standard payment systems are the constraints that make integrated public transportation planning difficult. Even if these data are complete, planning for transportation vehicles that serve as open systems in traffic makes the solution impossible with current optimization approaches. However, when the above constraints are solved or when they can meet in a common denominator, the model to be developed for integrated public transportation planning will enable better planning with heuristic approaches.

A process consisting of 4 stages has been developed for Integrated Public Transportation Planning in Smart Cities.

1. Collecting and analyzing travel data (Process No. 1)
2. Making vehicle inventory and route analysis of the PTS (Process No. 2)

3. Preparation of customized Origin - Destination (OD) matrices (Process No. 3)

4. Preparation of an integrated transportation plan (Process No. 4)

This section will examine the general flow of these 4 processes.

5.1.Collection and Analysis of Trip Data

Some of the methods used in collecting trip data have been mentioned in previous sections. In this section, we aim to identify actual trips and develop solutions by using GPS, residence and workplace/school address location comparisons. **Figure 1** shows the process of how to collect trip data. This process is explained in 4 stages.

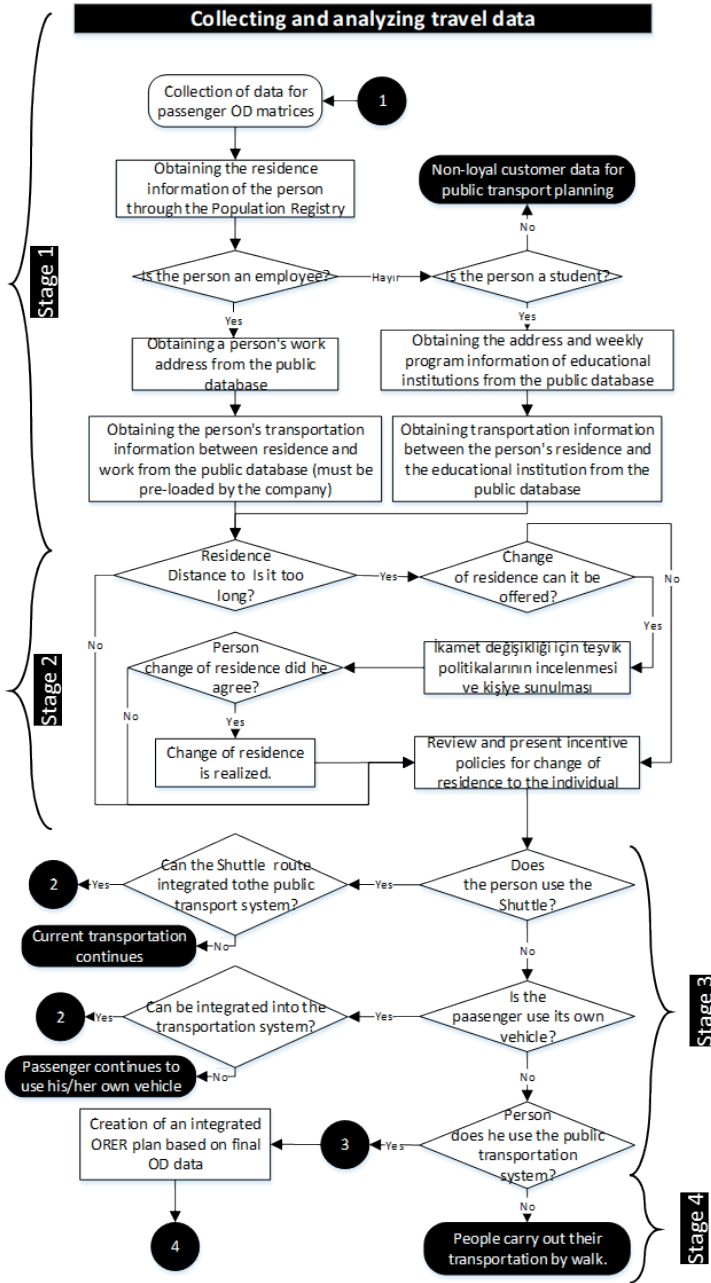


Figure 1. Process of collecting and analyzing trip data

State 1

Journey data is obtained externally through smart card prints, surveys and expert opinions. In order to collect the relevant data more accurately, the person's residence, the location of the institution where the person works or receives

education, and the frequency of visits will be obtained from the relevant public and private institutions, and the journey of the person will be determined more accurately. In the following sections, while analyzing the personalized journey data, validation of this data will be done with smart card prints.

Stage 2

After determining the actual travel movements of the person, when the regular round-trip movement distances of the person during the day are examined, if the person travels over a certain distance, incentive policies are developed for these people and an offer is made to move to a location closer to the work or education institution. Enterprises have long-distance shuttle services such as Kocaeli Gebze - Istanbul Beylikdüzü (108 km), Kocaeli Gebze - Sakarya villages (101 km). There are also individuals who do not use shuttle services but use their private cars to travel between Istanbul and Bursa every day. Such long-distance movements have negative economic, environmental and psychological impacts. Except for family situations that cannot be changed, if the person has the opportunity to move, some of the additional costs spent in traffic can be offered to the person as an incentive by offering special tax advantages for the person. In this case, there will be a reduction in the number of vehicles in traffic, a reduction in environmental impacts and an increase in the quality of life of the person.

Stage 3

After examining people's transportation movements and change of residence, it should be determined whether the person uses an individual vehicle, shuttle service or public transportation. In this case, it is determined how the person currently transfers between which stops on which route in the transportation system. This data will be used as input during the creation of OD matrices. In addition, the route used and which public transportation system the person will be integrated into are also examined in this section. This part of the process should also interact with stages 1 and 2. If the transportation provided by the person with vehicles such as shuttle services and individual vehicles cannot be provided by public transportation, the person will not be included in the integrated public transportation plan, and the person will continue to use the existing transportation facilities.

Stage 4

If there is a potential to include personal transportation information in the integrated public transportation plan, planning is made by taking into account personal transportation information and public transportation vehicle inventory. While planning, the quality of public transportation service is improved by ensuring fair distribution of resources within the system. After the personal transportation data is collected and analyzed, the next process is

the PTS inventory and route analysis.

5.2. Vehicle Inventory and Route Analysis of the PTS

After collecting trip data, PTS inventory and route analysis should be carried out. Determining the existing capacity with these analyses will form the basis for the studies to be carried out for the possibilities of combining different modes of transportation on the same route. The process of conducting vehicle inventory and route analysis of the PTS was examined in 3 general stages. These stages are indicated in **Figure 2** below.

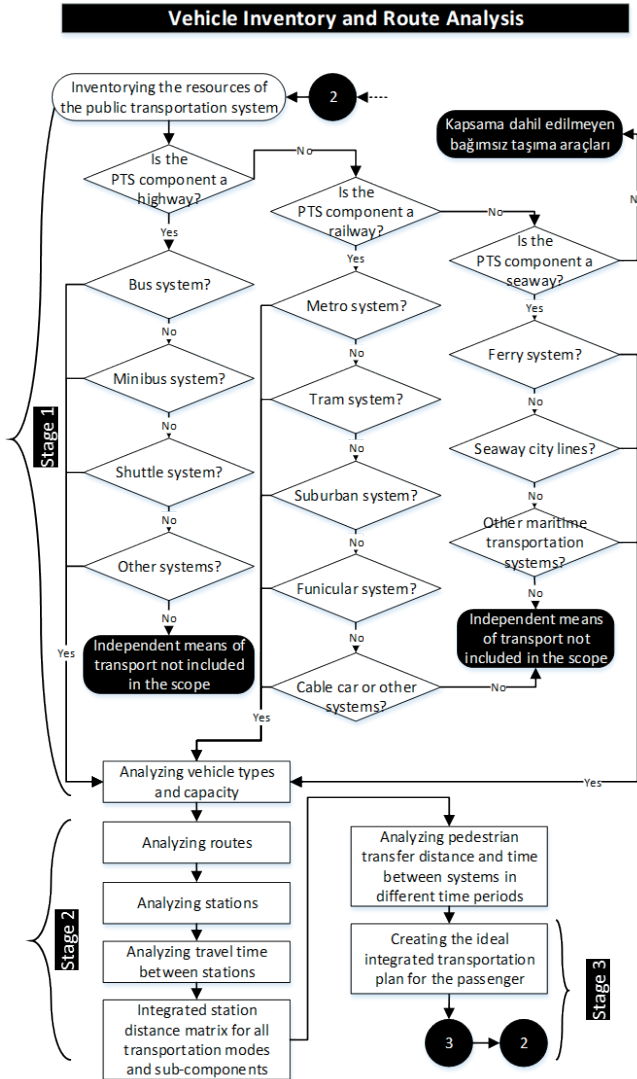


Figure 2. PTS vehicle inventory and route analysis process

Stage 1

The relevant section shown in the process is the section where groupings are made by taking into account the different types of transportation in the public transportation system. In this section, vehicles serving on certain routes in road, rail and maritime transportation types are taken into consideration. Independent vehicles such as taxis, electric scooters, etc. are not included in integrated public transportation planning processes.

Stage 2

After determining the types of operations of the vehicles, it is necessary to determine the capacity of each vehicle, how often trips are made on which routes, the analysis of the stations visited by the route and the trip, the distances between the stations and the travel times in these distances should be extracted on a time basis. Travel time between stations varies according to the traffic density. For this reason, planning should be done by taking hourly traffic densities into account. In addition, transfer times between different vehicles or systems should also be calculated as pedestrian movement. Afterwards, a distance matrix should be created according to the travel legs formed by the stations.

Stage 3

After the distance matrix is analyzed according to time zones, the ideal transportation plan for the passenger can be prepared. At this stage, the next process is to plan which vehicles the traveler will use between the OD points of the journey.

5.3. Preparation of Customized OD (Origin - Destination) Matrices

After the inventory and route analyses of the modes of transportation in the public transportation system are completed, the location and GPS-based travel movements mentioned in Process 1 need to be validated with the existing smart card prints. After validation, the required OD matrices will be created. With the created OD matrices, iterative vehicle assignments will be made according to the densities of the transportation legs between the stations depending on the transportation mode, route and vehicle type of the next process. The process shared in Figure 3 is analyzed in 3 stages

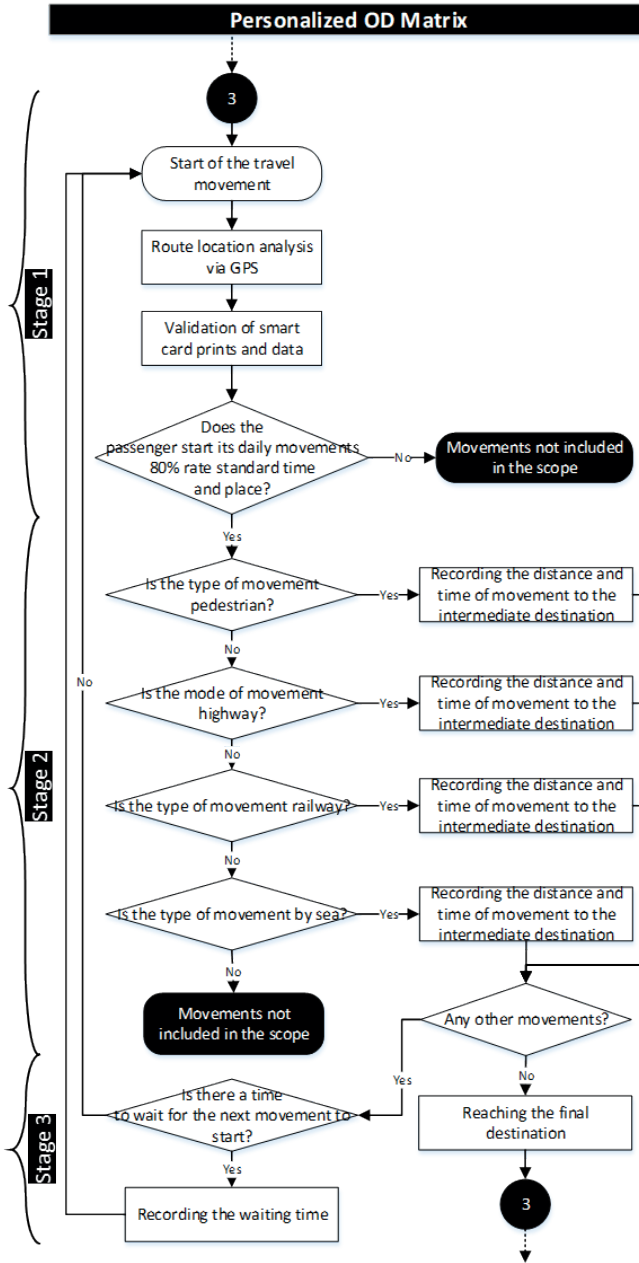


Figure 3. Preparation of customized O-D (Origin - Destination) matrices

Stage 1

The first step in the process is to validate the movement data obtained with GPS and the data obtained from smart cards. Then, individual travel

movements are analyzed again. For example, if a working individual starts his/her first movement at 7:00 in the morning, travels for 60 minutes, ends his/her movement at a different point, starts moving again from his/her current location after a certain period of time (between 5-8 hours) at the end of the working day and goes to the same location in 60 minutes and does this regularly during working days, this passenger is a loyal passenger. Depending on the traffic, the departure and arrival times may be different, but consistent trips between 2 points constitute the base data to be used for integrated public transportation planning. For this reason, planning will be made based on loyal passengers while creating OD matrices and leg densities. Non-loyal passenger profiles (retirees, day-trippers, etc.) will be positioned in the idle capacities allocated in the capacity in the planning.

Stage 2

Loyal passengers are planned according to the minimum time between the start and end points according to the OD matrices, and information such as when the relevant individual will be on the integrated transportation legs in the journey, how long the transfers will take, how long the journey will take and when it will arrive are cumulatively assigned to the transportation legs considering the new OD matrix. Transfers other than these movements are excluded from the scope.

Stage 3

When the relevant movements are completed cumulatively for all passengers, the station leg densities on the planned model will be prepared according to the improved situation, and the next and final process of integrated transportation planning can begin.

5.4. Preparation of Integrated Public Transportation Plan

Integrated public transportation planning can be carried out after collecting travel data, performing PTS inventory and route analysis, and creating ideal OD matrices for resources. At this stage, since the passenger leg densities between stations are known in the OD matrices, in the method to be developed, the vehicle with the highest capacity will be assigned to the most dense travel leg. In case there are different transportation modes or different operators using the same route, priority will be given in assignments to transportation vehicles such as subway, BRT, suburban, ferries, etc., which are not very flexible because they serve in a closed system. The process in Figure 4 prepared for these activities is analyzed in 3 stages.

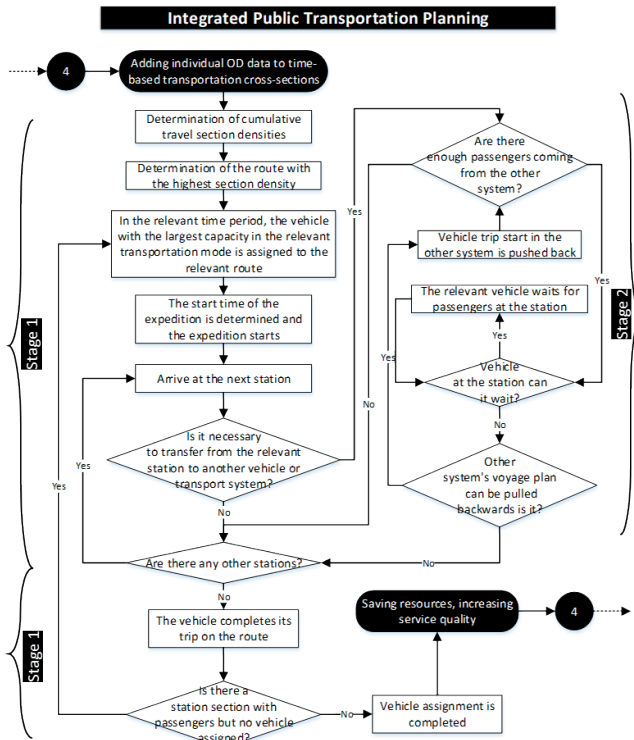


Figure 4. Process of making an integrated transportation plan

Stage 1

Since the densities are calculated cumulatively, the total number of passengers that will pass through the section after the boarding and alighting process is completed at each station constitutes the density of the relevant section. After determining which route has the highest density according to the OD matrix, the highest capacity vehicle is assigned to this route. While this process is being carried out, the assignment is made according to the time period in which the density in the relevant section is in. The assigned vehicle, within the scope of the transportation mode, stops at the stations in order until the trip of the relevant route is completed, performs passenger boarding and alighting movements and completes the trip by unloading all passengers when it arrives at the last station.

Stage 2

After the first vehicle is assigned, according to the OD matrix, when customers who have to change to a different vehicle or system according to the OD matrix get off at the stations where they will transfer, the walking distance and time they will have to walk to get on the next transportation vehicle is defined in previous studies in OD, so it is known when the individual will

arrive at the relevant station. Similarly, there will be new passenger boardings to this vehicle from other systems. At this stage, there may be a waiting period for vehicle A in system X, which is assigned at transfer stations, and a delay in the travel time for vehicle B in transportation system Y, which will be transferred. For this reason, vehicle A, which disembarks passengers at transfer stations, knows when vehicle B from other transportation systems will arrive according to OD data. In order not to reduce the quality of travel service, if there will be enough passengers, vehicle A in system X can be kept waiting at the station for a few minutes for the passengers coming from vehicle B in system Y. Otherwise, vehicle A continues and new arrivals are kept waiting at the station of vehicle A. When the passengers getting off from vehicle A and going to vehicle B in system Y arrive at the relevant system, if the waiting time of the passengers will be too long, the backward timetable of vehicle B can be updated. If the waiting time is too long, other passengers may be dissatisfied, so it should be avoided or reduced as much as possible.

Stage 3

When the assigned vehicle completes the relevant trip, the section densities will change as there will be passenger boarding and alighting from busy sections according to the idle capacity in the vehicle. In this case, the section densities in the system will change. In this case, before the next vehicle is assigned, vehicles are assigned to the busiest routes and legs where no vehicle is assigned. Repetitive processes continue until all passengers in the legs are assigned to public transportation vehicles.

6. Case Study on Integrated Public Transportation Planning

Within the scope of the study, a method proposal has been developed for the advantages to be obtained as a result of integrated planning of public transportation systems. In order to test this method, there is a need for technology improvements such as legislative changes, updating company management structures, common ticketing and fare collection systems. Therefore, it is not very easy to test the relevant system one-to-one. However, it is possible to evaluate the current public transportation planning in Istanbul to identify possible gains. At this point, OD data showing the mobility in the city and the data sets produced by TÜSSİDE in the transportation projects carried out between 2013-2016 were taken as basis. The scenario-based evaluation of the developed method is based on these data sets and certain assumptions for the scenarios, and it is tried to roughly reveal what kind of gains can be achieved if the proposed situation is realized within the scope of the process.

In this context, mobility on specific routes and the resources assigned to the transportation service were considered together. These assessments started by first selecting the routes, then determining the OD mobility in these route regions, then determining the types of transportation in the transportation

service in the region and determining the assigned transportation vehicles and revealing the current situation in the first place. Then, the vehicle assignments in transportation services in these regions were analyzed according to their usage rates and possible gains were analyzed.

In the scenarios based on these analyzes the following assumptions were accepted.

- The activity in the related study, which was taken as a source, continued today,
- The routes of transportation systems remain unchanged,
- Vehicle capacities have not changed,

For the conceptual process developed within the scope of the study, route, district-based OD matrix, types of transportation, vehicle quantities and capacities in various transportation legs throughout Istanbul were determined from the open sources of the relevant operators, and comparative analyses were made before and after the conceptual process.

The following features were taken into consideration when determining the transportation legs.

- Being among the busiest areas of the city in terms of traffic density
- More than one transportation system serving in the transportation leg

Due to the ability of Geographic Information Systems (GIS) to express the real world in a layered way, the scenarios discussed were visually expressed on the map so that the transportation infrastructure and mobility data could be more easily understood by the readers. Within the scope of the study, the transportation service areas of the transportation modes of Istanbul for the scenarios discussed on the map were determined on ArcGIS program, one of the most popular package programs of GIS. The routes used within the scope of rail transportation systems, bus and BRT systems, minibus and midibus transportation systems were positioned on the map.

Within the scope of the discussion, transportation legs that have different characteristics and have the ability to produce important information in the evaluations were examined in detail and the transportation modes and lines belonging to these modes were identified. After this process, the current frequencies of the identified routes were checked through up-to-date data and the capacities offered were calculated considering the time period of the OD matrix. Capacity utilization amounts were calculated by calculating the existing mobilities with the inter-district OD matrix. In the maps below, the routes of transportation types are given separately and holistically.

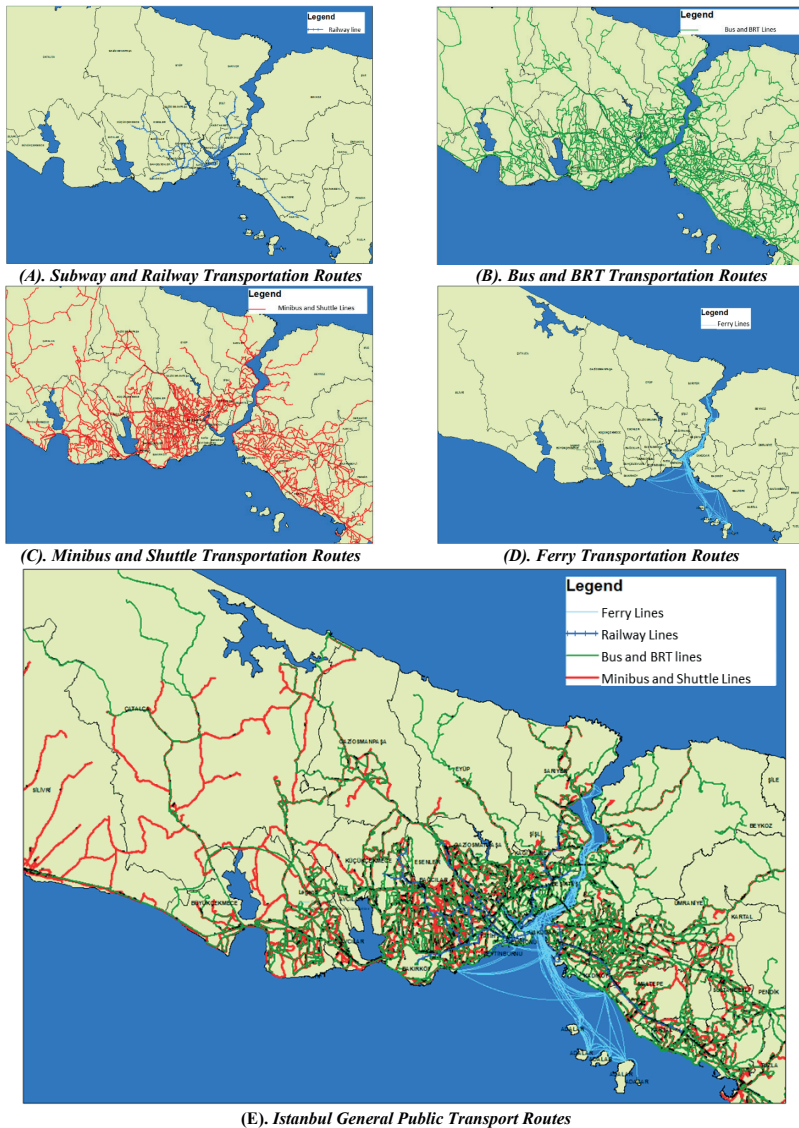


Figure 5. Istanbul Public Transportation and its Components, which are the basis for scenario analysis

While determining 5 different transportation legs throughout Istanbul as a sample case, the legs were determined by considering parameters such as transportation leg density, different transportation systems serving on the same leg, general traffic density, general travel movement. These transportation legs are given in the **Table 1** below.

Table 1. *Types of Transportation in the Transportation Legs Examined in the Case Study*

| Start District | End District | Bus | Minibus | BRT | Subway | Ferry | Reason for selection |
|----------------|--------------|-----|---------|-----|--------|-------|---|
| Zeytinburnu | Bakırköy | + | | + | | | Being a dense section on the E5 highway where there is traffic density, Bus and BRT providing service |
| Esenler | Küçükçekmece | + | + | | | | Bus and minibus service, different scale compared to other legs |
| Bayrampaşa | Yenikapı | + | | | + | | Being a dense area, Bus and subway service |
| Kadıköy | Kartal | + | + | | + | | Being between dense sections, bus, metro and minibus service |
| Kadıköy | Beşiktaş | + | | | | + | Dense cross-section, sea crossing unlike other scenarios, |

As can be seen from the table, although Istanbul is only one city, since the transportation demand of the dense population can be met by many different modes of transportation, different situations can be analyzed and possible benefits related to collective planning can be revealed.

Within the scope of the study, the passenger densities of the vehicles serving in the transportation legs were calculated and scenario analysis of the situations that will occur with the use of idle capacity in a way that will create acceptable density was made. While classifying the densities, the 5-class comfort parameters in public transportation systems (Vuchic, 2015) were taken into account (**Table 2**). The situation where the number of passengers per square meter is 5.5 was assumed to be the theoretical capacity situation and the number of passengers per square meter in the first 4 classes was normalized by the in-vehicle density. In vehicle capacities, it is assumed that the capacity of BRT vehicles is 192, the capacity of buses is 80, (TÜSSİDE, Flexible public transportation model - Bus Report, 2015), metro and trams have an average of 6 sets and each set has a capacity of 200 passengers minibus is 25 passengers. In the scenario analyses, the gains in cases where in-vehicle passenger densities are 50% are analyzed.

Table 2. Classification of passenger densities

| Passenger/ m2 | Travel Condition | In-Vehicle Density |
|------------------|--|-----------------------|
| < 1,5 | Standing independently; Easy getting on and off | 0% - 27% |
| 1,5-3,49 | Partial Contact, Landing and Disembarking with Disturbance | 27,1% - 63% |
| 3,5-4,49 | Intense Contact, Difficulty of Movement | 63,1% - 82% |
| 4,5-5,49 | Pressed Posture, Extremely Difficult Movement | 82,1% - 100% |
| >5,5 | Crushing Loading, Possibility of Injury, Pushing | |

6.1. Zeytinburnu – Bakırköy Transportation Legs

Since the E5 road is an important transportation leg in the traffic flow in Istanbul, the transportation leg between Zeytinburnu and Bakırköy was analyzed in the first stage. The transportation modes and vehicles using the 7 km long transportation leg were identified on the map shown in **Figure 6**. The transportation leg is served by 15 different bus lines with a total of 93 bus trips and 4 different BRT lines with 70 trips. According to the time period of the OD matrix, 20,880 trips are served by these lines. In the data obtained from the OD matrix, 6,847 passengers are served. Capacity utilization of vehicle trips is calculated as 33%.



Figure 6. Zeytinburnu - Bakirkoy Transportation Leg Analysis

As stated in the conceptual process, in transportation types where it is not possible to change the route over the determined transportation section, vehicle trips in the BRT system are assigned first in accordance with the rule

that the vehicle assignment will be made first. Since the average occupancy rate in the currently determined section is calculated as 33%, the density of BRT vehicles was gradually increased and the change in the bus system was observed by acting on 2 different scenarios (Figure 7). In Scenario 1, the capacity utilization of BRT and buses was increased to 40%. Passengers were assigned to all BRT vehicles. In the bus system, after the passenger assignment to the BRT system, a similar assignment was made at 40% occupancy rate. After passenger assignments were completed, the remaining vehicle trips were reserved as idle capacity. In Scenario 2, capacity utilization was increased to 51%. Because 51% of the capacity of the BRT system can serve all passengers in the existing transportation leg, in this case, all bus services in the relevant transportation leg have become idle.

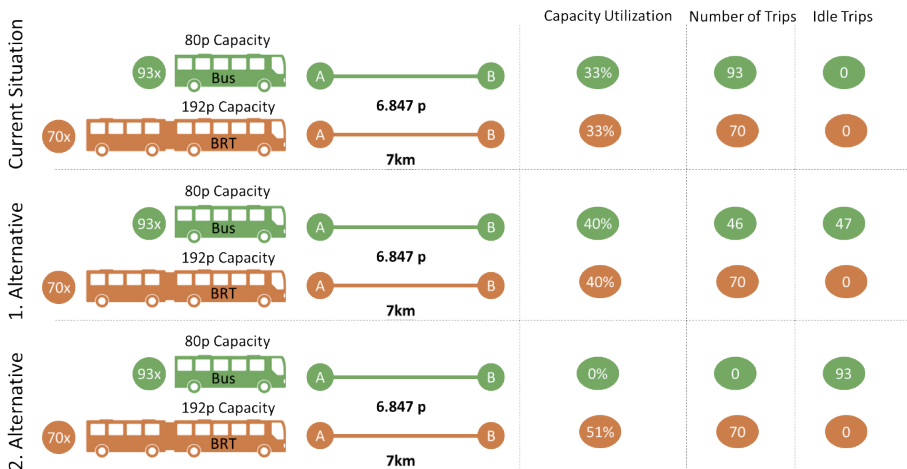


Figure 7. Scenario Analysis for Zeytinburnu - Bakırköy Transportation Leg

6.2. Esenler - Küçükçekmece Transportation Legs

Esenler - Küçükçekmece transportation section has a length of 9 km. When the transportation types serving in this transportation leg are examined, it consists of 10 different bus lines consisting of 30 bus trips and 1 minibus line (Figure 8). According to the time period of the OD matrix, a capacity of 2,600 trips is provided with these vehicles. In the data obtained from the OD matrix, 587 passengers are served. Capacity utilization of vehicle trips is calculated as 23%.

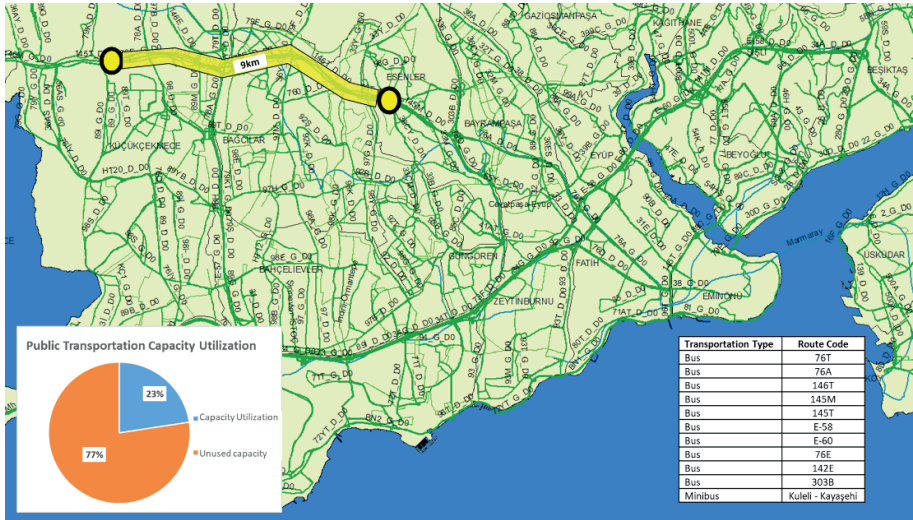


Figure 8. Esenler - Küçükçekmece Transportation Leg Analysis

The transportation modes in this sample segment consist of buses and minibuses. For this reason, there will be no restriction in vehicle assignment priority as in transportation modes with fixed routes. The passenger density in the relevant section was calculated to be 23%. When the passenger density of buses is increased to 25% in Scenario 1, minibus services become idle. When the search is made according to 50%, which is the middle value of the second level of the comfort parameter in public transportation systems, this service can be provided with 15 bus trips in that section. In this case, in addition to 8 minibus trips, 15 bus trips become idle (Figure 9).

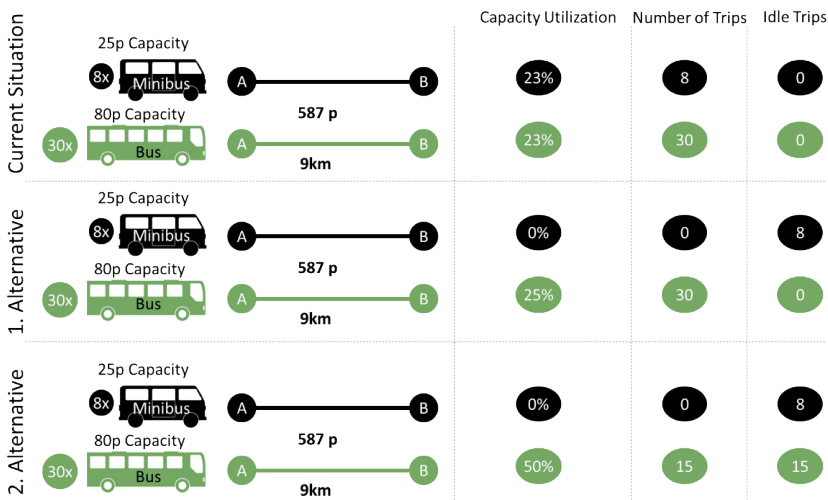


Figure 9. Scenario Analysis for Esenler – Küçükçekmece Transportation Leg

6.3. Bayrampaşa - Yenikapı Transportation Legs

M1 metro line is the first metro route in Istanbul. Within the scope of the analysis, a 5 km transportation leg between Bayrampaşa and Yenikapı was analyzed as an example of the transportation leg in which this transportation system is located (**Figure 10**). There are 134 bus services on 28 different bus lines and Yenibosna - Kirazlı - Yenikapı metro transportation system. A total of 10,720 passenger capacity of bus services and a total of 37,720 passenger capacity of the M1 system, including an hourly capacity of 24,000 passengers, are provided between the specified time periods. When the capacity utilization of the relevant segment is analyzed, it is seen that 9,124 trips were realized. In line with these figures, the capacity utilization rate of the relevant transportation leg is calculated as 26%.



Figure 10. Bayrampaşa - Yenikapı Transportation Leg Analysis

The transportation modes in this section determined as an example consist of bus and metro. For this reason, vehicle assignment should be made primarily on metro vehicles. The passenger density in the relevant section was calculated to be 26%. Considering the current amount of passengers, if the capacity utilization in the metro system increases to 38%, it can serve all passengers. In this case, 133 bus services on the transportation leg become idle. When the capacity utilization rate in the subway is increased to 50%, 4 subway trips become idle in addition to the bus trips (**Figure 11**).

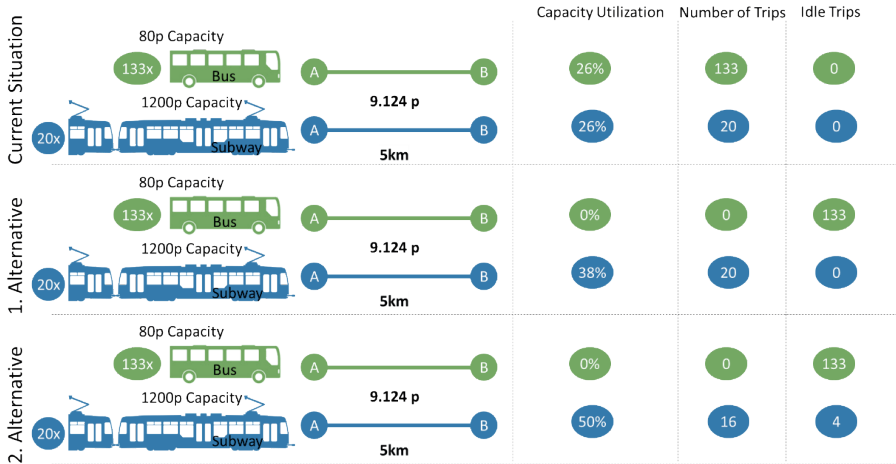


Figure 11. Scenario Analyses for Bayrampasa - Yenikapı Transportation Leg

6.4. Kadıköy – Kartal Transportation Legs

Kartal - Kadıköy transportation leg is one of the busiest transportation legs in Istanbul. The 16 km long transportation leg is served by 3 different transportation systems: bus, minibus and subway (Figure 12). Among the bus systems, 7,440 passenger capacity is served with 15 different routes and 93 trips, minibus system with 8 trips and 200 passenger capacity, M4 Kadıköy – Tavşantepe subway system with 16 trips and 19,200 passenger capacity, totaling 26,840 passenger capacity. When the capacity utilization of the relevant segment is analyzed, it is seen that 10,960 trips were realized. In line with these figures, the capacity utilization rate of the related transportation leg is calculated as 41%. Marmaray (Gebze-Halkalı subway line) is not included in the calculations since Marmaray was not active during the period to which the trip data belongs.



Figure 12. Kadıköy – Kartal Transportation Leg Analysis

The transportation modes in this section are bus, minibus and metro. For this reason, vehicle assignment should be made primarily on metro vehicles. The passenger density in the relevant section was calculated to be 41%. Considering the current amount of passengers, if the capacity utilization in the metro system is increased to 50% and the density of 33 bus services is increased to 50%, all passengers in the section can be served. After the assignment, 59 bus services and 8 minibus services become idle (**Figure 13**).

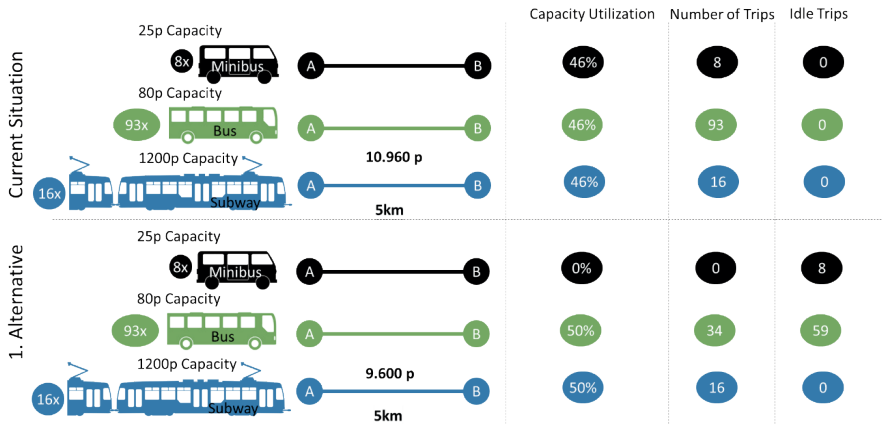


Figure 13. Scenario Analyses for Kadıköy - Tavşantepe Transportation Leg

6.5. Beşiktaş - Kadıköy Transportation Legs

Beşiktaş - Kadıköy transportation section can be realized via 2 different routes. The first is by bus lines (lines 110 and 112) and the second is by sea.

The bus route is 15 km long and the sea route is 6 km long (Figure 14). There were 7,017 trips between Beşiktaş and Kadıköy. The services of bus lines 110 and 112 were discontinued due to the capacity of 11,800 passengers and the shorter distance by sea. Seaway services have a capacity of 11,800 passengers. Since the capacity utilization rate of maritime transportation is 59%, no vehicle assignment has been made for this transportation leg.

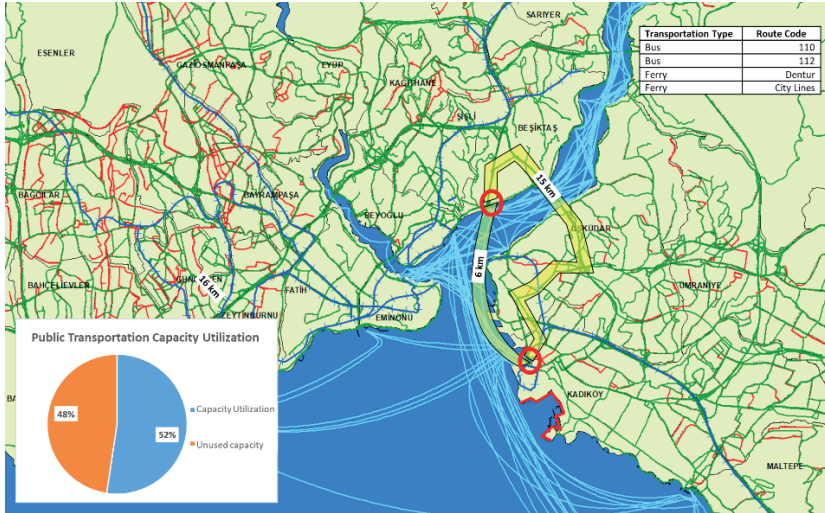


Figure 14. Beşiktaş – Kadıköy Transportation Leg Analysis

6.6. Summary Results of Scenario Analyses

It is estimated that 300 bus trips, 16 minibus trips and 4 metro trips can be saved by applying the developed conceptual process in 5 different transportation legs in Istanbul.

Table 3. Evaluation of Scenario Analysis

| | Description | Zeytinburnu – Bakırköy | Esenler - Küçükçekmece | Bayrampaşa - Yenikapı | Kadıköy - Kartal | Beşiktaş - Kadıköy |
|------------|--------------------------|------------------------|------------------------|-----------------------|------------------|--------------------|
| Route Info | Route Length | 7 | 9 | 5 | 16 | 6 |
| | Capacity Offered | 20880 | 2600 | 37720 | 26840 | 11800 |
| | Current Passenger Number | 6847 | 587 | 9124 | 10960 | 7017 |
| | Capacity Utilization | 0.33 | 0.23 | 0.26 | 0.41 | 0.59 |

| | | | | | | |
|-------------------------|-------------------------|------|-----|-----|-----|---|
| Current Number of Trips | Bus | 93 | 30 | 134 | 93 | - |
| | Minibus | | 8 | | 8 | |
| | BRT | 70 | | | | |
| | Subway | | | 20 | 16 | |
| | Ferry | | | | | 6 |
| Recommended Status | Number of Bus Trips | | 15 | | 34 | |
| | Number of BRT Trips | 70 | | | | |
| | Number of Minibus Trips | | | 16 | 16 | |
| | Capacity Utilization | 0.51 | 0.5 | 0.5 | 0.5 | |
| | Trip savings (Bus) | 93 | 15 | 133 | 59 | |
| | Trip savings (Minibus) | | 8 | | 8 | |
| | Trip savings (Subway) | | | 4 | | |

7. CONCLUSIONS AND RECOMMENDATIONS

Within the scope of this study, a conceptual process for Integrated Public Transportation Planning in Smart Cities has been developed. In order to provide a basis for this process proposal, scenario analyses were carried out for the efficiency of resource utilization in certain parts of Istanbul's public transportation system. In the analyses conducted for sample segments, it has been observed that efficiency can be increased by using idle capacities more effectively in integrated public transportation planning to be realized depending on passenger density.

In addition to the economic return to be obtained with integrated public transportation planning, the comfort of social life will also increase with the decrease in exhaust emission values and the decrease in the number of vehicles in traffic. In this case, preliminary findings have been determined that the capacity can be used better when the general travel movement specified in the problem definition is analyzed and integrated public transportation planning is made.

Prior to the benefits that can be achieved through Integrated Public Transport Planning in Smart Cities, public transport systems need to be managed by a central authority in order to plan with a holistic approach in transport systems. However, there are some processes that need to be completed for planning from a central authority. These are:

Payment with Smart Cards: Necessary arrangements should be made for their use in all modes of transportation

Personal Data Protection Law: The collection and processing of some data that cannot be collected with smart cards (residence address, work

address, school address and GPS location, etc.) may cause uneasiness among people. For this reason, the purpose and scope of the work to be carried out on this data should be clearly stated.

GPS Systems: In-vehicle control systems are indispensable for intelligent public transportation management systems. By using the data generated, recorded and interpreted by these systems, both vehicle utilization efficiency and passenger safety can be increased.

Ownership: The ownership of public transport systems by different institutions or organizations makes it difficult to plan on a common denominator. The planning authority should take initiatives to ensure that vehicles with different ownerships are included in the integrated plan in a complementary and supportive, rather than competitive, role.

Shuttles : Shuttle companies may be distant from environments that may allow their employees to interact with employees of different companies. However, they may change their minds when opportunities such as savings in operating costs through integrated planning and the ability of idle shuttle vehicles to provide services during the day that will sustain their economic activities during the day are pointed out.

Expedition Speed : Travel speeds between systems may vary. This application is cost-oriented in the first stage. In the optimization models to be developed in the future, two-stage models can be used so that one of the objective functions is the shortest time and the other objective is the lowest cost.

Incentivizing Transfers: In integrated public transportation planning, since transportation systems will serve in a way to complement each other, it is necessary to facilitate transfers between systems and to develop incentive policies in terms of fare.

REFERENCES

- Altan, M. k. (2018). Toplu Taşımada Çok lı Karar Verme ve Metropolitan Bir Alanda Servis Araçlarının Modellemesi. *Karaelmas Science and Engineering Journal*, s. 99 - 105.
- André, P. W. (2007). Journey planning based on user needs. *CHI'07 Extended Abstracts on Human Factors in Computing Systems*, 2025-2030.
- Arslan, O. (2011). Kaliteli Bir Toplu Taşıma Sistemi Nasıl Olmalıdır, Münih Örneği. *Ulaştırma kongresi*.
- Cirman, A. D. (2009). The Kyoto protocol in a global perspective. *Economic And Business Review*.
- Deri, A. (2012). Akıllı Kart Verileri Kullanılarak Toplu Ulaşım Yolculuk Talebinin Belirlenmesi ve Sefer Çizelgeleme Optimizasyonu. *Dokuz Eylül Üniversitesi Fen Bilimleri Enstitüsü*.
- Deveci, M. C. (2015). TOPLU ULAŞIMDA ENTEGRASYON BASAMAKLARI: KAVRAMSAL BİR İNCELEME. *TRANSİST 8. Uluslararası Ulaşım Teknolojileri Sempozyumu ve Fuarı*.
- Eken, S. S. (2014). WEB TABANLI AKILLI BİR DURAK SİSTEMİNİN GERÇEKLENMESİ. *Selçuk Üniversitesi Mühendislik, Bilim Ve Teknoloji Dergisi*.
- Elmedir, F. M. (2014). YOLCU KAYIT BİLGİLERİ İLE OTOBÜS SİSTEM HIZININ TESPİTİ. *Transist Ulaşım Kongresi*.
- Göl, B. (2019). Akıllı toplu ulaşım sistemlerinin geliştirilmesine yönelik model önerisi. *Sakarya Üniversitesi, Yüksek Lisans Tezi*.
- İUAP. (2011). *İstanbul Transportation Master Plan*. İstanbul: s.19.
- Kalpakçı, A. (2013). Ara toplu taşıma sistemlerinin şehir içi otobüs sistemleri ile entegrasyonu, İzmir örneği. *Dokuz Eylül Üniversitesi Fen Bilimleri Enstitüsü Yüksek Lisans Tezleri*.
- Lathia, N. C. (2012). Personalizing Mobile Travel Information Services. *Procedia-Social and Behavioral Sciences*, 48, 1195-1204.
- Nurkovic, A. D. (2015). Toplu Taşıma Araçlarıyla Seyahat için Akıllı Yönlendirme. *Akademik Bilişim Konferansı*.
- Organ, İ. G. (2012). Şehir İçi Ulaşım Faaliyetlerinde Kazancın Basit Usulde Vergilendirilmesinin Yaratığı Vergi Adaletsizliği: Denizli Örneği. *Maliye Dergisi*, s. 187-203.
- Önder, H. A. (2019). Türkiye'deki Kentiçi Raylı Toplu Taşıma Sistemlerinin Ulaşım Ana Planları Bağlamında Değerlendirilmesi. *Railway Engineering*, s. 31 - 45.
- Pucher, J. K. (1995). Verkehrsverbund: the success of regional public transport in Germany, Austria and Switzerland. *Transport policy*, 24, 279-291.
- Tan, Y. K. (2018). Smart Cities and Mobility: Does the Smartness of Australian Cities

Lead to Sustainable Commuting Patterns? *Journal of Urban Technology*, 1-25.

Topuz, S. (2008). İstanbul İlindeki Toplu Taşıma Yolculuk Taleplerinin Yapay Sınır Ağlarıyla Modellenmesi. *İstanbul Teknik Üniversitesi, Fen Bilimleri Enstitüsü, Yüksek Lisans Tezi*.

TÜSSİDE. (2015). *Flexible public transportation model - Bus Report*. Kocaeli.

TÜSSİDE. (2017). Public Transportation Oriented Istanbul Traffic Planning.

TÜSSİDE. (2020). Feasibility Report on Personalized Transportation Information in Smart Cities.

TÜSSİDE. (2021). Feasibility Report on Multimodal Public Transportation in Smart Cities.

TÜSSİDE. (2021). Model Development Application in Smart Integrated Traffic Management.

TÜSSİDE. (2021). Smart Station Systems Feasibility Report.

Vuchic, V. (2015). *Urban Transit: Operations, Planning and Economics*. 641p.

Zhang, L. L.-B. (2011). Traveler information tool with integrated real-time transit information and multimodal trip planning: Design and implementation. *Transportation Research Record*.



Chapter 5

COMPARISON OF MONOSTATIC AND MULTISTATIC RADAR-BASED MICROWAVE IMAGING SYSTEMS

Ali Recai Celik¹

¹ Dr. Dicle University Electrical and Electronics Engineering
ORCID: 0000-0002-6917-5170

1. Introduction

Microwaves are waves with frequencies ranging from 300 MHz to 300 GHz (1 m to 1 mm in wavelength) in the electromagnetic spectrum. They are included in the non-ionizing wave class. They are generally used in radar-based far-field applications. Furthermore, thanks to their ability to easily penetrate dielectric materials, their use has become widespread in many near-field applications such as measuring distances, determining the size and properties of objects, detecting cracks in structures, imaging the objects, etc (Xie et al., 2020). Microwave-based measurement systems work on the principle of sending electromagnetic energies to matter in waves. In measurements, the parts of the wave that pass through the material and are reflected are measured.

In this study, firstly, an overview of ‘Microwave Imaging (MI)’, which is one of the important application areas mentioned above, is made. Then, two different measurement setups named as ‘monostatic’ and ‘multi-static’ are examined in detail. The advantages and disadvantages of these methods are mentioned and comparisons are made between them.

2. MI Method

When an electromagnetic wave passes from one medium to another, some of the waves pass to the second medium and some are reflected as seen in Figure 1 (Celik, 2018). The reflection coefficient (Γ) is calculated to find the amount of the reflected wave, and the transmission coefficient (T) is calculated to find the amount of the transmitted wave by using Maxwell’s Equations (Senior and Volakis, 1995). By interpreting these wave quantities, information about the various properties of the examined substance can be obtained.

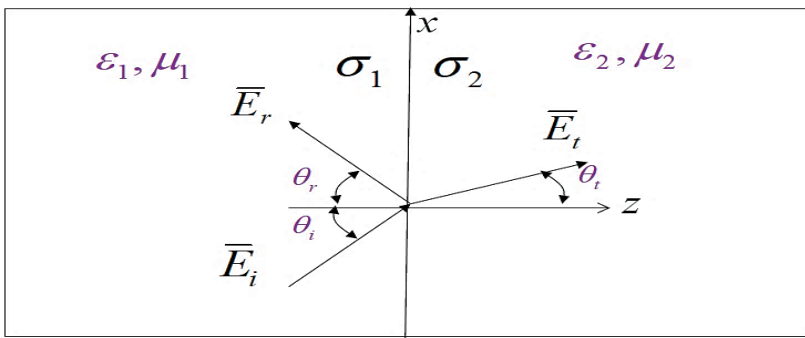


Figure 1. Transition of an electromagnetic wave to a different medium (Celik, 2018)

When calculating the Γ value, Equation (1) is used if the wave is oblique and has perpendicular polarization, and Equation (2) if it has parallel polarization. Since the wave’s arrival and transmission angles will be zero

when the wave is perpendicular, Γ is calculated by using Equation (3). The impedance (η) values in these Equations can be found by Equation (4) where μ is the magnetic permeability of the medium, ϵ is the electrical permeability, σ is the conductivity constant, and the ω is the angular frequency (Ulaby, 2006).

$$\Gamma_{\perp} = \frac{\eta_2 \cos \theta_i - \eta_1 \cos \theta_t}{\eta_2 \cos \theta_i + \eta_1 \cos \theta_t} \quad (1.1)$$

$$\Gamma_{\parallel} = \frac{\eta_2 \cos \theta_t - \eta_1 \cos \theta_i}{\eta_2 \cos \theta_t + \eta_1 \cos \theta_i} \quad (1.2)$$

$$\Gamma = \frac{\eta_2 - \eta_1}{\eta_2 + \eta_1} \quad (1.3)$$

$$\eta = \sqrt{\frac{\mu}{\epsilon - j\frac{\sigma}{\omega}}} \quad (1.4)$$

In Equation 1.4, it will be seen that ϵ or σ increases the reflection, together with the substitution of the η values to be obtained by using different ϵ and σ values in the equations related to Γ . Since both ϵ and σ values of different parts in the internal structure of objects at microwave frequencies are different, the amount of reflected wave varies. Therefore, more different scattering parameters and energy profiles can be obtained. Thus, inferences can be made about the existence, location and size of different parts. Finally, in order to make a clearer determination, the reflected signals are converted into images by subjecting them to various processes such as pre-processing, filtering, calibration, and energy calculation.

In summary, the object detection process is initiated by transmitting a few nanoseconds of short-pulsed electromagnetic energy to the target. The energies passing the target and reflected from the target are detected by the receivers and the obtained data is subjected to image processing.

2.1. Uses of MI

MI can be used in radar-based far-field applications such as target detection and tracking, weather modelling, underground monitoring, etc. Furthermore, due to its ability to penetrate materials, it can also be used in near-field applications such as through-the-wall imaging, biomedical imaging, security scanning, and non-destructive testing. The images of some studies in the literature related to these applications are given in Figure 2-6.

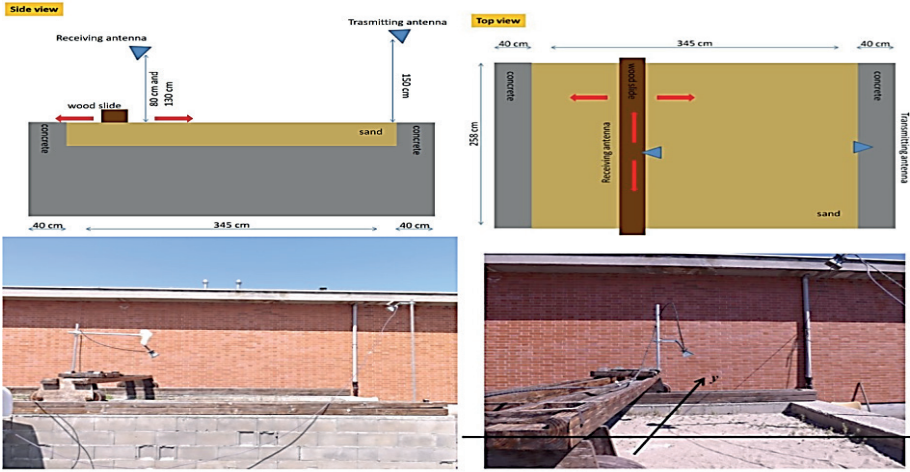


Figure 2. Schematic and real view of a MI measurement configuration for detecting and localizing buried targets (Brancaccio et al., 2021)

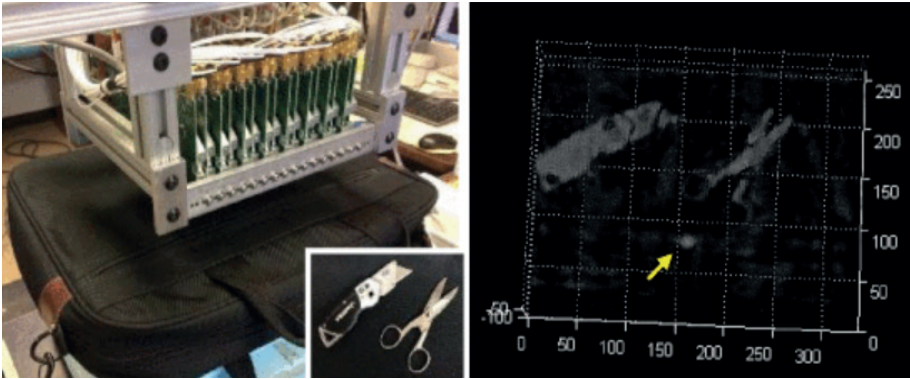


Figure 3. An example of video camera utility for security application with MI (Ghasr et al., 2017)

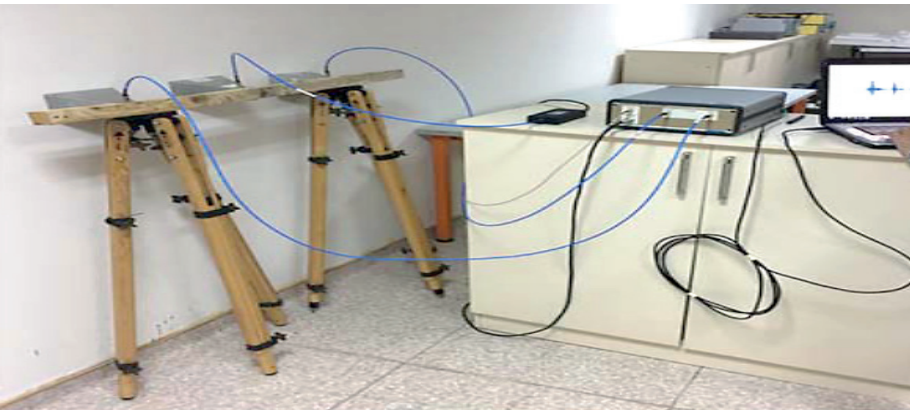


Figure 4. Image of an experimental MI measurement for detection of moving targets behind walls (Yilmaz and Ozdemir, 2017)



Figure 6. An example of the MI system for non-destructive cracks detection (Jiya et al., 2016)

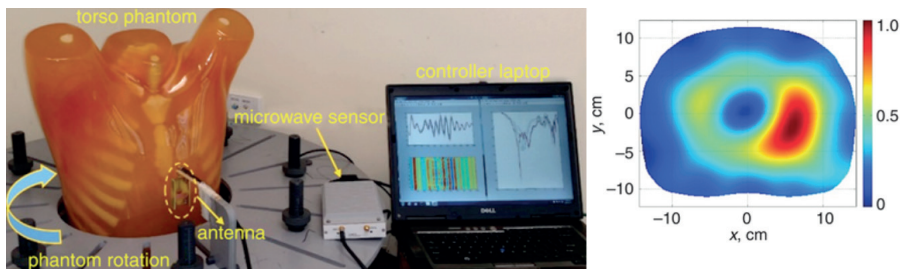


Figure 5. An example of biomedical MI for lung cancer detection (Zamani et al., 2015)

3. Measurement Configuration of MI

There are three MI system structures called monostatic, bi-static, and multi-static according to the measuring setup. In these systems, the scattering parameters, which are defined as the measure of the relations between the waves transmitted and reflected from the circuit gates, are obtained.

In the monostatic system, the same sensor is used for both transmitting and receiving the microwave signals. Therefore, the scattering parameter ' S_{11} ' which allows the determination of the reflection coefficient is measured.

In the bi-static system, one of the two sensors with the same characteristics is used for transmitting microwave signals and the other for receiving them. Thus, the scattering parameter ' S_{21} ' which allows the determination of the transmission coefficient is measured.

In the multi-static system, one of the many sensors with the same characteristics is used for transmitting microwave signals and the others for receiving them. In turn, each antenna acts as a transmitter. Therefore, a large number of scattering parameters such as ' $S_{21}, S_{31}, S_{41}, \dots, S_{12}, S_{32}, S_{42}$

....' are measured. By converting these parameters to the time domain, high-resolution images can be created. In the remainder of this study, the principles, prototypes, designs and differences of the monostatic and multi-static configurations will be investigated, discussed and compared.

3.1. Monostatic System

As mentioned before, a single sensor is used in the monostatic systems. Hence, a rotation system is required in the measurements to recapture and save the S_{11} data at different locations. The monostatic measurement setup is visually given in Figure 7(a), and an example image of a measurement using this setup is given in Figure 7(b) (Bicer and Akdagli, 2017).

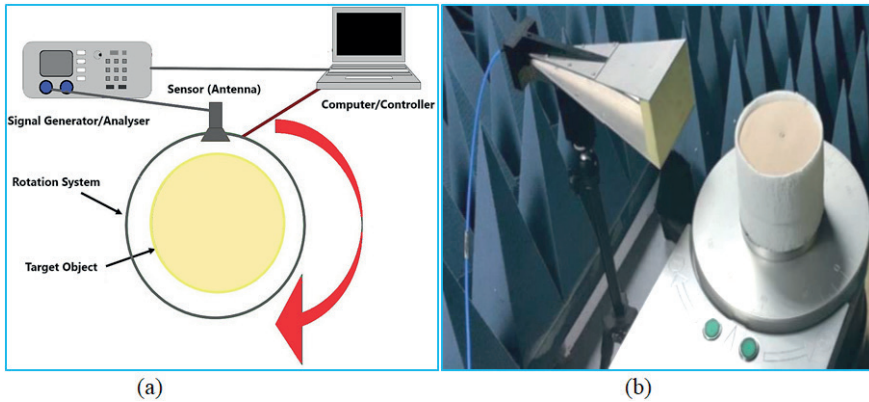


Figure 7. a) *The monostatic measurement setup*

b) *An example image of the experimental monostatic measurement (Bicer and Akdagli, 2017)*

3.2. Multi-static System

The process of acquiring data using multiple sensors in a multi-static system has the same operating logic as the process of obtaining data by rotating a single sensor at certain angles in a monostatic setup. Thus, the sensors do not need to be rotated by a mechanical system in this configuration. The multi-static measurement setup is visually given in Figure 8(a), and an example image of a measurement using this setup is given in Figure 8(b) (Mohammed, 2014).

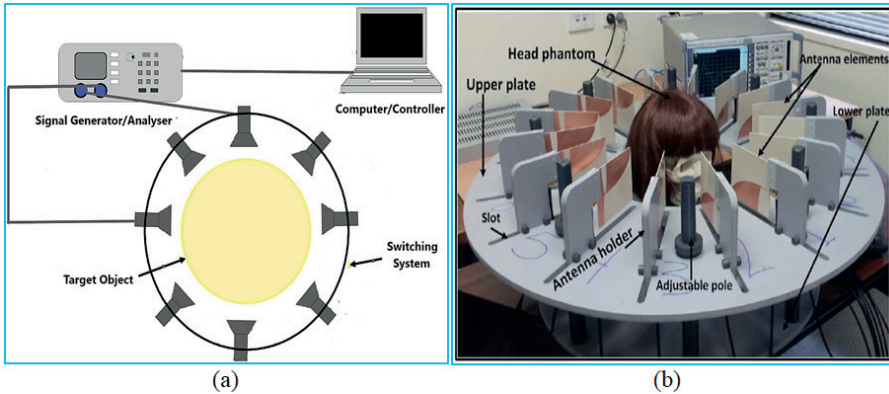


Figure 8. a) *The multi-static measurement setup*

b) *An example image of the experimental multi-static measurement (Mohammed, 2014)*

4. Comparison of Monostatic and Multi-static Systems

As mentioned in the previous sections, radar-based MI systems generate images using backscatter signals from the target object. Thus, information about the properties and internal structure of the object is provided. If a multi-static system is used for measurements, an antenna array and a switch network controller are required. This is a prominent disadvantage of multi-static measurement, as it makes the system complex. However, thanks to more than two sensors in the antenna array, a large number of transmission coefficients can be obtained. Thus, high-resolution images are obtained. This makes multi-static measurement more suitable for clinical applications and is a significant advantage of this system. On the other hand, in the mono-static system, the object is scanned mechanically using a single antenna. The lack of complexity of this system makes measurements easy. However, obtaining low-resolution images is a disadvantage of this system.

Another important issue that needs to be examined regarding systems is the mutual coupling phenomenon. In a multi-static system with a large number of antennas, one antenna can generate an induced current due to current flowing from the antennas located around it. This induced current can deteriorate the characteristics of the antenna by changing some important values such as impedance, radiation pattern, and scattering parameters. However, since decreasing the number of antennas reduces mutual coupling and the complexity of signal processing, this problem will not arise in a monostatic measurement setup where a single antenna is used. This is an important difference that separates the two systems.

Another thing to consider when comparing systems is the size of the antennas to be used. In multi-static systems where measurements are made using antenna arrays, it is desired to have as many sensors as possible.

Therefore, the size of the antennas must be quite small. Due to this necessity, the operating frequency increases, and the penetration of the signal to the target object is insufficient. However, in a monostatic system where a single antenna is used, measurements can be made by adjusting the size of the antenna according to the size of the target object. Therefore, not much effort is spent on size reduction during the antenna design process.

In summary; the negative aspects of the monostatic system are the need for a mechanical system and obtaining low-resolution images. On the other hand, the difficulties of the multi-static system are that it requires a very small size antenna and is affected by mutual coupling. The features, merits, and drawbacks of the two methods are summarized in Table 1. Taking these advantages and disadvantages of the two systems into consideration, researchers are creating radar-based MI configurations. For example, (Fear et al., 2013), (Celik et al. 2019) and (Asok et al. 2022) preferred the monostatic approach for ‘non-invasive breast tumor detection’ with MI, while (Nilavalan et al., 2003), (Xie et al., 2006) and (Godinho et al. 2022) used the multi-static approach for this aim. In the MI for ‘material characterization system’, (Abu-Khousa et al., 2003) chose the monostatic and (Abd Aziz et al., 2021) chose the multi-static method. While (Fallahpour, 2013) used the monostatic system for the ‘embedded passive objects detection’ with MI, (Moulder, 2016) used the multi-static system for the ‘concealed weapons detection’ with MI measurements.

Table1. Comparison of the features of Monostatic and Multistatic MI systems

| Radar-based Monostatic MI Systems | Radar-based Multistatic MI Systems |
|---|---|
| Only one antenna or antenna pair is used | More than two antennas are used |
| Reflection coefficient is obtained | Transmission coefficient is obtained |
| A rotation system is necessary | A switching system is necessary |
| They consist of a simple configuration | They consist of a complex configuration |
| An antenna suitable for the size of the target object is required | A large number of very compact-sized antennas are required. |
| The low-resolution images are obtained | The high-resolution images are obtained |
| There is no mutual coupling | Mutual coupling occurs |

4. Conclusions

In this study, firstly it was primarily mentioned that the use of microwaves, which are included in the non-ionizing wave class, has become widespread in both radar-based far-field and near-field applications. It was emphasized that MI has an important place among these applications, and some systems using MI such as target detection and tracking, through-the-

wall imaging, biomedical imaging, security scanning, and non-destructive testing were demonstrated with various examples. It was explained that the object detection process in MI systems is initiated by transmitting short pulsed electromagnetic energy of a few nanoseconds to the target, then the energies passing through and reflected from the target are detected and the obtained data is subjected to image processing.

Then, monostatic, bi-static and multi-static methods, which are named according to the measurement mechanism in MI systems, were examined in detail and a comparison of monostatic and multi-static methods, which is the main subject of this study, was made. According to this; it was stated that the monostatic system has a simple structure and is not affected by mutual coupling. However, it was explained that this method has disadvantages such as the requirement of a rotation system for scanning, and obtaining low-resolution images.

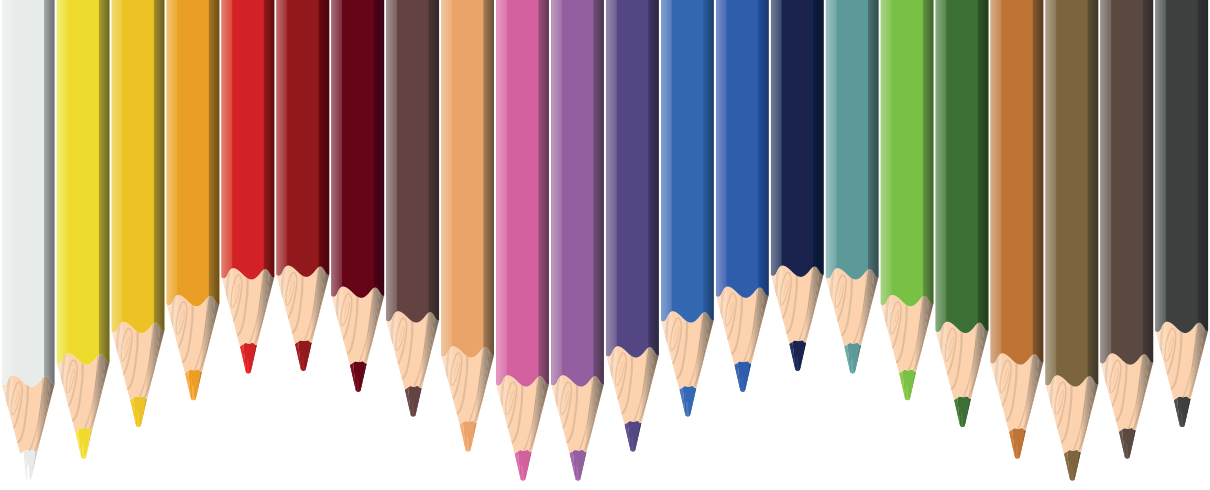
On the other hand, the multi-static system has superior features such as having a fixed mechanism, obtaining a high number of transmission coefficients, forming high-resolution images, and being suitable for clinical applications. However, it was stated that this method also has some drawbacks such as having a complex structure and being affected by mutual matching. At the end of the study, all these features were summarized in a table and the study was concluded.

References

- Xie, Z., Li, Y., Sun, L. et al. (2020). "A simple high-resolution near-field probe for microwave non-destructive test and imaging", *Sensors*, vol. 20, 2670.
- Celik A.R. (2018). "Detection of the breast tumors by ultra-wideband radar based microwave method", Ph.D. Thesis, Dicle University, Diyarbakir, Turkey.
- Senior, T.B.A. and Volakis, J.L. (1995). "Approximate boundary conditions in electromagnetics", *London UK: Institution of Electrical Engineers*, 261.
- Ulaby, F. (2006). "Fundamentals of applied electromagnetics", 5th editon, *Prentice Hall*, Washington
- Brancaccio, A., Leone, G., Pierri, R. and Solimene, R. (2021). "Experimental validation of a microwave imaging method for shallow buried target detection by under-sampled data and a non-cooperative source" *Sensors*, vol. 21(15), 5148.
- Ghasr, M.T., Horst, M.J., Dvorsky, M.R. and Zoughi, R., "Wideband microwave camera for real-time 3-D imaging", *IEEE Transactions on Antennas and Propagation*, vol. 65(1), 258–268.
- Yilmaz, B., Özdemir, C. (2017). "A detection and localization algorithm for moving targets behind walls based on one transmitter-two receiver configuration", *Microw. Opt. Technol. Lett.*, vol. 59, 1252–1259.
- Zamani, A., Rezaeieh, S.A. and Abbosh, A.M. (2015). "Lung cancer detection using frequency-domain microwave imaging", *Electronics Letters*, vol. 51(10), 740–741.
- Jiya, E.A., Anwar, N.S.N. and Abdullah, M.Z. (2016). "Detection of cracks in concrete structure using microwave imaging technique", *International Journal of Microwave Science and Technology*, ID:3195716.
- Bicer, M.B., Akdagli, A. (2017). "An experimental study on microwave imaging of breast cancer with the use of tumor phantom", *Applied Computational Electromagnetics Society Journal (ACES) Journal*, vol. 32(10), 941–948.
- Mohammed, B.J. (2014). "Design and implementation of microwave imaging systems for medical applications", Ph.D. Thesis, The University of Queensland School of Information Technology and Electrical Engineering, Australia.
- Fear, E.C., Bourqui, J., Curtis, C., Mew, D., Docktor, B. and Romano, C. (2013). "Microwave breast imaging with a monostatic radar based system: a study of application to patients", *IEEE Transactions on Microwave Theory and Techniques*, 61(5), 2119–2128.
- Asok, A.O., Gokul Nath, S.J. and Dey, S. (2022). "Non-invasive breast tumor detection with antipodal Vivaldi antenna using monostatic approach". *International Journal of RF and Microwave Computer-Aided Engineering*, vol.32(12).
- Celik, A.R., Kurt, M.B. and Helhel, S. (2019). "An experimental performance investigation of an ultra-wideband directional antenna in the microwave imaging of breast cancer tumor", *Applied Computational Electromagnetics Society Journal*

(ACES) *Journal*, vol.34(10), 1549–1560.

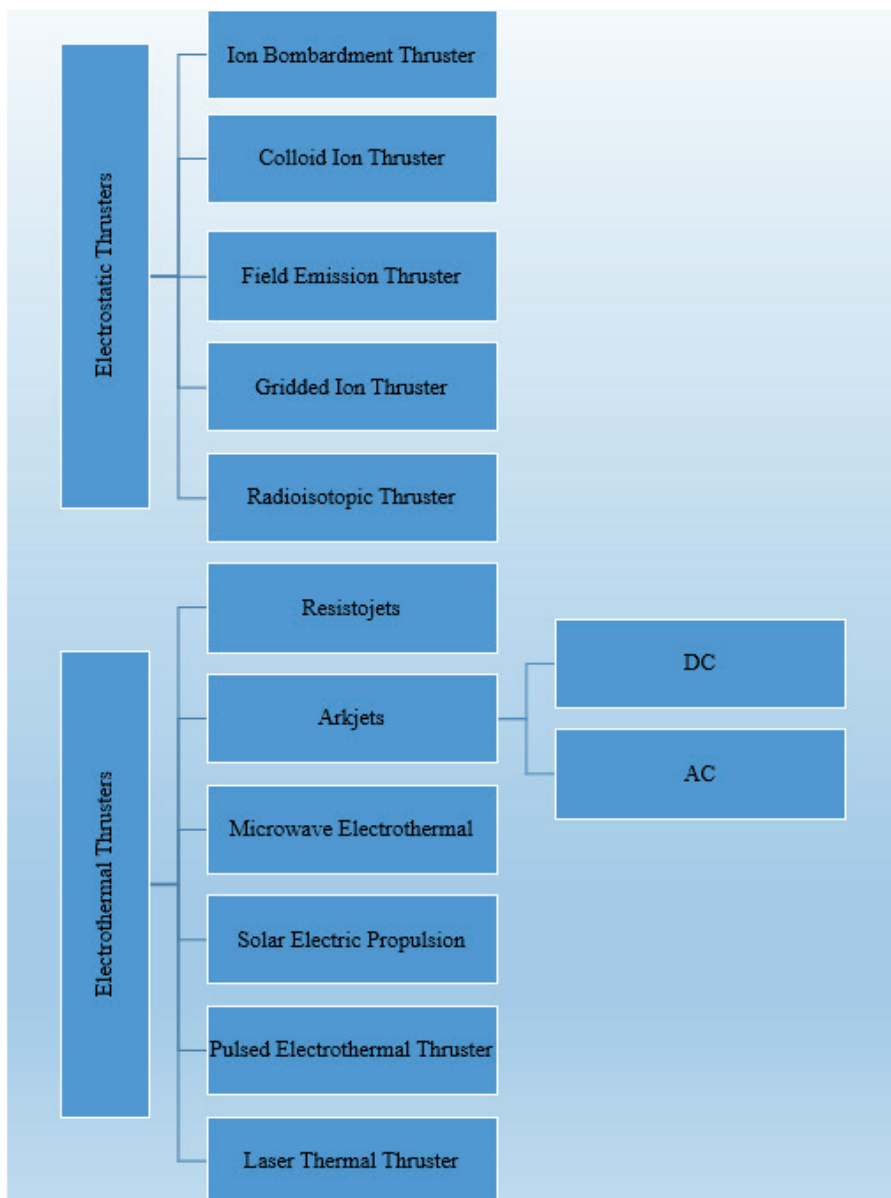
- Xie, Y., Guo, B., Xu, L., Li, J. and Stoica, P. (2006). “Multistatic adaptive microwave imaging for early breast cancer detection”, *IEEE Transactions on Biomedical Engineering*, vol. 53(8), 1647–57.
- Nilavalan, R., Gbedemah, A., Craddock, I., Li, X. and Hagness, S.C. (2003). “Numerical investigation of breast tumour detection using multi-static radar”, *Electronic Letters*, vol. 39, 1787–1789.
- Godinho, D.M., Felício, J.M., Fernandes, C.A. and Conceição, R.C. (2022). “Target selection in multistatic microwave breast imaging setup using dielectric lens”, *16th European Conference on Antennas and Propagation (EuCAP)*, Madrid, Spain, 1–5.
- Abu-Khousa, M., Saleh, W. and Qaddoumi, N. (2003). “Defect imaging and characterization in composite structures using near-field microwave nondestructive testing techniques”, *Composite Structures*, vol. 62(3-4), 255–259.
- Abd Aziz, M.Z.A. Ghani, A.S.A. and Abdullah, N.I. (2021). “Development of 4×4 multistatic microwave imaging system for material characterization”, *IEEE Asia-Pacific Conference on Applied Electromagnetics (APACE)*, Penang, Malaysia, 1-4.
- Fallahpour, M. (2013). “Synthetic aperture radar-based techniques and reconfigurable antenna design for microwave imaging of layered structures”, Ph.D. Thesis, Missouri University of Science and Tech.
- Moulder, W.F. (2016). “Development of a high-throughput microwave imaging system for concealed weapons detection”, *2016 IEEE International Symposium on Phased Array Systems and Technology (PAST)*, Waltham, MA, USA, 1-6.



Chapter 6

ELECTROSTATIC AND ELECTROTHERMAL THRUSTERS

Hakan BUCAK



1. Electrostatic Thrusters

Electrostatic propulsion utilizes a high-voltage electrostatic field for accelerating ions to achieve significant exhaust velocities. The main focus of research and development has been on systems that use positively charged ions as the primary working fluid, with mechanisms in place to neutralize ions after the exhaust. Many electrostatic systems incorporate a gridded arrangement at the exhaust port to confine and generate the required high electric field for ion acceleration. This includes ion bombardment, RIT, and colloid thrusters. In a typical gridded thruster, a DC potential difference of approximately 1 kV exists between an inner grid anode on the plasma chamber and an exit-plane cathode. Multiple grids are employed at the exhaust port to perform various functions such as propellant containment, ion acceleration, and control of beam divergence.

The efficiency of propulsion systems is frequently constrained by radiative heat losses occurring in the propellant heating/ionization chamber, and the power conditioning needs are influenced by the chosen propellant ionization approach. Issues like grid and cathode erosion have hindered the longevity of grid-type electrostatic systems. Continuous advancements in materials, particularly with the use of carbon-carbon composite grids, are anticipated to improve the performance and extend the lifespan of these units.

Electric propulsion has a longstanding and pivotal role in propulsion technology, serving as one of the earliest and most efficient methods for particle acceleration (Cassady et al., 2008). These propulsion systems utilize a fixed electric potential to propel charged ions, giving rise to two primary types of electrostatic accelerators: the gridded ion thruster and the Hall-effect thruster. The distinction between these types lies in the methodologies employed to create the accelerating potential, leading to distinct performance characteristics and technical challenges. Both gridded ion thrusters and Hall-effect thrusters have accumulated extensive flight experience and are widely utilized for tasks such as satellite station-keeping and orbital maneuvering (Curran et al., 1993).

In simpler terms, Electrostatic Thrusters, a widely recognized concept in the realm of electric propulsion, are commonly known as ion propulsion. The underlying principle involves propelling ions through the use of an electrode. These ions are generated by an ion source that releases charged particles into a stream. An accelerating electrode provides a charge opposite to that of the ions, pushing them towards the electrode. After passing through the electrode, a neutralizer releases ions with an equal and opposite charge, ensuring a downstream net charge of zero. The achievable thrust is solely determined by the exhaust velocity, ion mass, and total ion flux (Cassady et al., 2008).

1.1. Ion bombardment thruster

Ion bombardment or electron bombardment thrusters generate positive ions by bombarding neutral propellant atoms in a discharge chamber with thermionically excited electrons. This system typically involves a cylindrical anode as the discharge chamber, featuring a centrally located axial hollow cathode. The heating of the axial cathode results in the thermionic emission of electrons at low amperage (1 to 15 Amps) and low voltage (25 to 30 V DC), which discharge toward the outer anode. To enhance efficiency, a magnetic field is applied in the discharge chamber, increasing the electron path length and residence time, thereby improving collision probability and propellant utilization efficiency (Goebel et al., 2005).

Grids, maintained at different potentials near the exhaust port, enable the acceleration of plasma to exhaust velocities. Subsequently, ions are neutralized in the exhaust by a spray of electrons from a neutralizer cathode, preventing potential differences from pulling ions back into the engine.

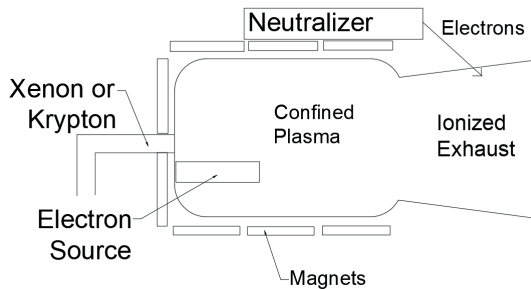
Ion bombardment systems have undergone testing and flights over 30 years in space and 40 on the ground. Various NASA and Air Force low Earth-orbit missions in the 1970s contributed to demonstrating and refining the basic design. For instance, Intelsat VII utilizes 25 mN UK-10 north-south station-keeping units. Higher thrust units have been flight-qualified for east-west station-keeping motors on geosynchronous satellites, requiring about 20 times the Δ -V per year compared to north-south station-keeping at geosynchronous altitudes. A notable mission, Deep Space-1, employs a 30-cm diameter NASA/Hughes xenon-ion engine.

Ground units have been tested with thrusts over 1N and power consumptions ranging from 50 W to 200 kW. Despite occasional temperamental behaviour in gridded acceleration, ion bombardment systems are attractive due to their relatively high performance, extended development heritage, and potential long lifetime. These systems deliver the highest integrated lifetime impulse among currently flying electric propulsion techniques, making them excellent candidates not only for station-keeping but also for primary propulsion. Extensive plans for commercial use include ongoing tests of tiny microthrusters employing a hollow cathode (Jordan, 2000).

Ion thrusters exhibit a distinctive capability to function effectively at high propellant exhaust velocities, with optimal operation achieved at specific impulse rates above 2500s. Challenges in the development of low-power ion thrusters revolve around designing small-sized discharge chambers and neutralizers that can operate effectively at low levels of energy consumption and low propellant flow rates.

A study (Gorshkov, 1998) explores the prolonged operation of thrusters,

exceeding 10 thousand hours, driven by a potent combination of high specific impulse and low thrust levels, arising from limited power. The efficiency of discharge chamber work diminishes due to reduced geometrical size, creating a higher ratio of recombination surface area to discharge chamber volume. As power decreases without altering thruster geometry, maintaining acceptable gas efficiency necessitates reducing mass flow rate, introducing critical power considerations. These findings shed light on the intricate dynamics between discharge chamber geometry, power constraints, and gas efficiency rates, offering insights for the sustained operation of high-specific-impulse, low-thrust propulsion systems.



1.2. Colloid ion thruster

Colloid thrusters propel fine droplets of electrically charged, conducting fluid, generated through a needle, and an electrostatic field accelerates them. This technology, extensively studied in the 1960s and 1970s, encountered challenges associated with high acceleration voltages and degradation. Recent research is concentrating on developing miniaturized, low-power colloid thrusters with reduced acceleration voltages, positioning them as competitive solutions for microspacecraft applications (Tajmar, 2003).

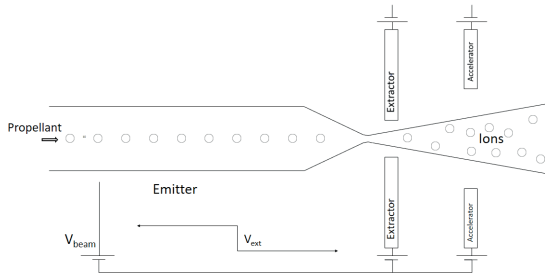
Microthruster systems, offering variable thrust capabilities, play a crucial role in nano and microspacecraft propulsion as well as precise position control. Colloid thrusters, alongside Field Emission Electric Propulsion (FEEP) thrusters, are recognized as efficient solutions for specific impulse and thrust requirements. NASA missions such as LISA, EX-5, and LIRE, which demand precise position control, stand to benefit from microthrusters. Ongoing research is dedicated to compact and efficient colloid thruster systems operating at lower voltages (Hruby et al., 2001).

Colloid thrusters have undergone extensive research as alternatives to chemical propulsion for micro spacecraft. Research initiatives by organizations like Busek Company, MIT, and Yale University aim to develop compact and efficient colloid thruster systems. Advances in electrospray physics, high-voltage electronics, and new propellant fluids contribute to achieving lower

operating voltages and improved performance (Xiong et al., 2002).

Research efforts in colloid thruster minimization involve the integration of micro-pump and micro-thruster systems using Micro-Electro-Mechanical Systems (MEMS) and PCB processing technologies. The micro-thruster operates on the electrical colloid propulsion principle, and researchers are focused on system properties, utilizing direct thrust measurement devices for characterization (Xiong et al., 2002).

The experimental setup for colloid thrusters includes a capillary made of fused silica with specific dimensions. Propellant flow regulation is accomplished through a nitrogen pressure system, and measurements are conducted at room temperature. Different propellant solutions with varying conductivities are utilized, and the mass spectrometer calibration compound is employed for system characterization (Chiu et al., 2005).



1.3. Field emission thrusters

Field Emission Electric Propulsion (FEEP) functions by applying a robust electric field, typically ranging from 8 to 15 kV, to ionize the surface of a working fluid, commonly a liquid metal, generating individual ions instead of droplets. This technique achieves notable efficiency by avoiding heat loss during ionization, utilizing slit or pinhole diameters around one micron in size (Yongjie et al., 2018).

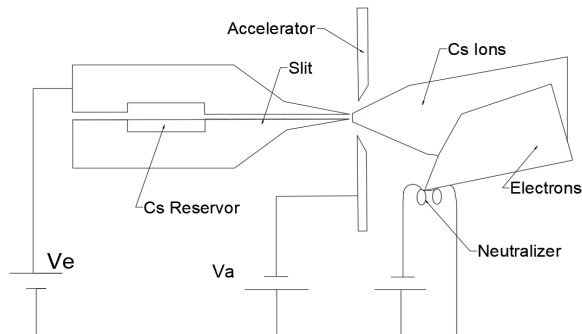
FEEP devices demonstrate reproducibility in short pulse times and small impulse bits, making them well-suited for space missions addressing challenges like atmospheric drag and solar radiation pressure. Flight units developed by Centrosazio and the Austrian Research Center have been employed in various missions and are marketed for science-sensitive station-keeping tasks such as LISA and TPF (Jordan, I. J. E., 2000).

FEEP represents an advanced electrostatic propulsion concept using liquid metal, typically cesium, as a propellant. The FEEP device consists of an emitter and an accelerator electrode, forming a slit with a width of approximately $1 \mu\text{m}$. An applied potential difference of about 10 kV creates a strong electric field at the liquid metal surface, extracting and accelerating

cesium ions. Due to the high emitter-accelerator potential difference, FEEP devices can achieve high specific impulses of approximately 10^4 s. The emitted propellant ions create a localized, high-density ion beam, presenting challenges for neutralization in space environments. The ion beam emitted by FEEP differs significantly from conventional ion thrusters, and few plasma measurements have characterized its neutralization (Tajmar et al., 2004).

Field emission thrusters have emerged as promising propulsion systems for precision-pointing space missions due to their low thrust noise, high controllability, and exceptionally high specific impulse, reaching up to 8000 seconds. Among these, the indium field emission electric propulsion (In-FEEP) thruster, built upon miniaturized indium liquid-metal ion sources (LMIS), has been in development since 1995 and has proven its spaceworthiness. This paper reviews over two decades of research and advancements in In-FEEP thruster technology, focusing on ion emission scalability, optimization, addressing lifetime degradation concerns, and the development of larger propellant reservoirs and thruster module housings. The In-FEEP thruster's excellent robustness, demonstrated through space-proven applications, highlights its potential for precision-oriented missions such as LISA, Terrestrial Planet Finder Darwin, Gravity Field and Steady-State Ocean Circulation Mission (GOCE), and SMART-2. The ongoing efforts in research aim to further enhance the performance and reliability of In-FEEP thrusters, positioning them as a key technology for future space exploration endeavors (Tajmar & Wang, 2000).

FEEP employs an electric field to extract and accelerate atomic ions directly from the surface of a metal exposed to vacuum. For propulsion applications, the most common source is a metallic liquid, with thrust levels ranging from micro- to milli-Newton and specific impulses as high as 12,000 seconds. The power-to-thrust ratio is relatively high at about 60-75W/mN (Tajmar, 2003).



1.4. Gridded ion thruster

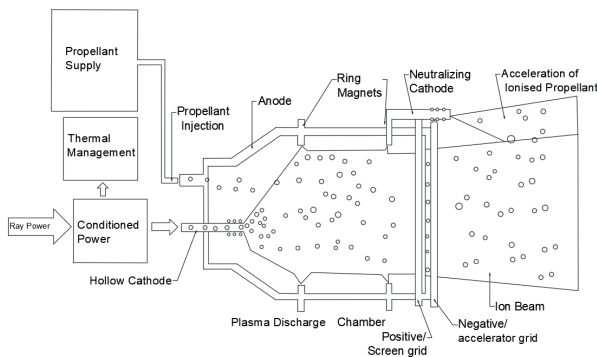
The Gridded Ion Engine (GIE), an electric propulsion (EP) system developed since the 1960s, operates based on the electrostatic energy principle

to accelerate charged particles for thrust generation. GIEs worldwide consist of three major components: the plasma generator, ion accelerator, and electron neutralizer (Yeo et al., 2021) (Mickelsen 1967).

In simpler terms, the plasma generator introduces and ionizes a neutral gas propellant in the discharge chamber using direct current (DC), radio frequency (RF), or microwave discharge methods. These discharge methods categorize the subclasses of GIE. In the ion accelerator, grids with applied voltage accelerate ions from the plasma discharge. The external cathode supplies electrons to neutralize the expelled ions at the electron neutralizer (Yeo et al., 2021).

Gridded ion thrusters (GIT or GIE), with origins dating back to the 1960s and initially proposed by Tsiolkovsky in 1911, generate ions by bombarding a propellant with a high-energy electron beam created through DC, RF, or MW discharge (Kokura et al., 1999). These ions are then expelled through electrically charged grids, including a screening grid and an accelerating grid. The potential difference between these grids determines the propellant's acceleration. Cathode grid acceleration propels the negatively charged anions. Xenon (Xe) is a common propellant, chosen for its ease of ionization, high atomic mass, and low boiling point compared to earlier metallic propellants like mercury or cesium. Ion thrusters, recognized for their high efficiency, are widely used for attitude and trajectory control in geostationary communication satellites and interplanetary missions (O'Reilly et al., 2021).

Ongoing efforts for lightweight spacecraft and system miniaturization aim to address challenges and drawbacks in these systems (Yeo et al., 2021).



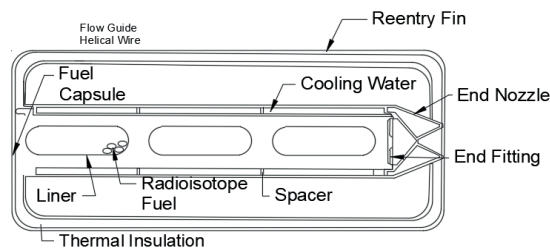
1.5. Radioisotopic Thruster

The Radioisotopic Thruster operates by generating charged colloidal particles within a conceptual framework that involves a thin layer of fuel containing beta-decaying radioisotopes. This fuel layer is distributed across a substantial emitting surface with a net positive charge generated through the decay of radioisotope fuel, often utilizing Cesium-144. The process establishes

a significant potential difference between the surface and space, ranging from approximately 500,000 to 1,500,000 volts. A shield collects electrons emitted from the surface, and the resulting potential difference and current are employed to operate a high-energy colloidal accelerator (Jordan, 2000). Despite the innovative potential of this technique as a power source, practical development has been hindered by safety considerations, including extreme radiation hazards and complexities, with no operational model produced.

Contact-ion thrusters offer an opportunity to achieve enhanced power-to-area ratios, representing notable advancements in space propulsion. These thrusters exhibit a reduction in neutral-atom efflux to below 1%, and the permissible ion current density may surpass that of electron-bombardment thrusters by 5 to 10 times. The durability of the acceleration electrode has been validated, reaching ion current densities as high as 170 amp/m². Under specific conditions, these thrusters reportedly achieve a power-to-area ratio of 170 kW/m² (Tahara & Nishida, 1999).

Furthermore, in efforts to improve thruster efficiency, researchers suggest the application of radioisotope heating to the contact ionizer, potentially reducing power requirements. The Hughes strip-beam contact-ion thruster, considering estimated vaporizer, neutralizer, and accelerator drain powers, is anticipated to be more efficient than electron-bombardment thruster systems. However, practical implementation faces challenges, such as the necessity for a large void fraction to contain helium evolved during decay, potentially increasing thruster weights. Additionally, a significant portion of the projected annual production of Pu-238 in 1970 would be required for a single spacecraft, excluding test and backup systems. This suggests that even with increased production, these thrusters may not find extensive utilization for high-power missions (Mickelsen 1967).



2. Electrothermal

Electrothermal thrusters employ electrical power to heat propellant, inducing expansion through a nozzle to generate thrust. Specific impulse within the range of 200 to 1500 s surpasses that of chemical propulsion, enhancing performance. The adaptability of electrothermal engines allows for the utilization of various propellants, offering flexibility for diverse mission requirements. Among the commonly employed propellants are H₂, He, Li, Be,

B, C, NH_3 , N_2 , N_2H_4 , and B_5H_9 . Hydrogen, in particular, stands out due to its high specific heat and thermal conductivity. Energy sources for electrothermal thrusters encompass solar, laser, and microwave thermal energy, directed towards heat exchangers or propellants to facilitate propulsion.

Within the category, two subtypes are identified as Resistojet and Arcjet. Resistojet elevates propellant temperature through an arc discharge, while Arcjet utilizes a heat exchanger linked to a resistive heater. As per Wollenhaupt et al. (Wollenhaupt et al., 2018), Arcjet demands power ranging from 0.3 to 100 kW, resulting in thrust levels between 200 and 7000 mN, with specific impulse values ranging from 200 to 2000 s. For instance, an Arcjet thruster developed by the University of Stuttgart (Auweter-Kurtz et al., 1996) (Schmidt 2005) utilizes hydrazine and ammonia, delivering thrust within the range of 100-500 mN.

Electrothermal thrusters represent straightforward systems grounded in gas acceleration principles. While their specific impulse falls below that of certain electric systems, it surpasses that of traditional chemical systems. Resistojet and Arcjet stand as classical examples, leveraging electrical heating for thermodynamic expansion and subsequent thrust generation. Resistojets, employing resistive elements, demonstrate compactness and compatibility with various gases, rendering them suitable for applications such as attitude control and stationkeeping (Holste et al., 2020).

These electrothermal systems constitute mature technologies with a record of accomplishment of successful implementation in spacecraft over several decades. However, their specific impulse values remain constrained to levels below 2000 sec, positioning them as suitable choices for near-Earth orbit applications but less so for exploration missions extending beyond low Earth orbit (Cassady et al., 2008).

2.1. Resistojets

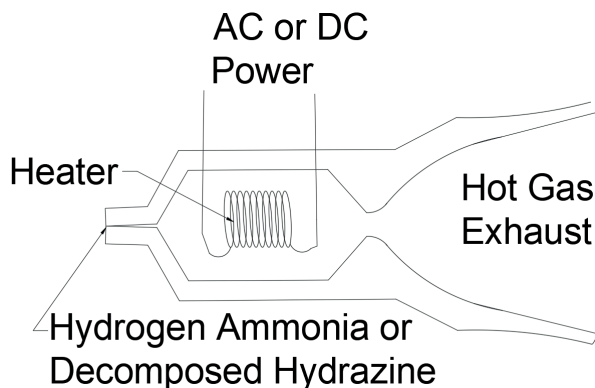
Resistojets operate through the direct ohmic heating of the propellant, involving the passage of the propellant over a tungsten-heating element within a heat exchange chamber before being expelled. While electric heating introduces a more intricate interface compared to chemical propulsion, resistojets demonstrate compatibility with traditional chemical monopropellants or bipropellants in terms of power conditioning and feed systems. These compact and lightweight systems can achieve relatively high thrust levels with voltages of approximately 100V and high current. Notably, hydrazine resistojets have been successfully employed on Iridium satellites for orbit-raising maneuvers, highlighting their suitability for extended multi-hour burns (Jordan 2000).

The utilization of electric heaters to enhance the specific impulse of nitrogen or ammonia propellants in resistojets traces back to the Vela-

1 satellite in 1965. In the 1980s, Aerojet Rocketdyne developed MR-501 Electrothermal Hydrazine Thrusters (EHTs) for North-South Station Keeping (NSSK) applications on geosynchronous communication satellites. The MR-501 EHTs, first deployed in orbit in April 1983 on Satcom 1R, demonstrated successful integration within a short timeframe (Hoskins et al., 2013).

Multipropellant resistojets, crucial for Space Station Freedom's (SSF) final operating configuration, are tailored for drag makeup propulsion, prioritizing longevity and integration over peak performance. These resistojets can operate on various waste gases from the Environmental Control and Life Support System (ECLSS), addressing challenges related to waste disposal and propellant resupply. Under the NASA program, engineering models developed by a collaboration between Rocketdyne and Technion underwent successful testing on a variety of propellants, accompanied by system integration studies and the development of a power controller (Xiong et al., 2002).

Resistojets stand as among the less complex electric propulsion devices, functioning by directing the propellant over an electrically heated solid surface. The specific impulse, influenced by the molecular mass of the propellant and the maximum chamber temperature, typically reaches around 300 seconds. While hydrogen proves to be the most efficient fuel, storage challenges lead to the preference for other propellants such as O_2 , H_2O , CO_2 , NH_3 , CH_4 , and N_2 . The efficiency of resistojet thrusters ranges from 65% to 85%, with losses occurring in areas such as heat transfer and the dissociation of propellant byproducts. A notable drawback is the relatively inefficient heat transfer from the resistance element to the gas stream. Various resistance element designs, including coils of wire and geometric shapes, aim to maximize heat transfer to the gas flow (Curran et al., 1993).



2.2. Arcjets

The fundamental principle underlying thermal arcjet thrusters is the utilization of an electric arc to heat the propellant, causing the expansion of the resulting hot gas in a divergent nozzle. This approach, akin to chemical

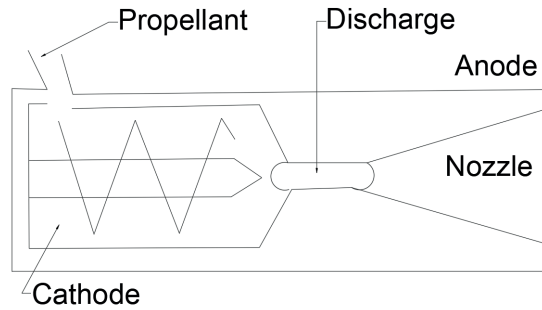
thrusters, attains higher mass-specific energies due to its independence from the energy content of the propellant. Achieving specific impulses of up to 2,000 seconds is possible, surpassing the capabilities of conventional chemical thrusters.

In the general design, a tungsten alloy nozzle is employed, featuring a cathode and anode mounted coaxially and separated by a high-temperature insulator. Arc stabilization and constrictor wall cooling are facilitated through the tangential injection of propellant gas. Thermal arcjets are categorized based on power levels, ranging from 100 W to 100 kW (Wollenhaupt et al., 2018).

Arcjets, similar to resistojets, are categorized as electrothermal devices. They overcome the wall temperature limitation of resistojets by internally depositing power through an electric arc. The arc, typically formed between a cathode and an anode that serves as the supersonic nozzle, results in a non-uniform, high-temperature core. While this characteristic reduces propulsive efficiency, it leads to high specific impulse. Arcjets can be classified based on power, and their performance advances are influenced by materials and thermal design. Arcjets occupy an intermediate position on the specific impulse scale and compete with plasma thrusters in geostationary applications (Martinez-Sanchez & Pollard 1998).

Various types of arcjets exist, employing diverse methods of propellant heating, including DC current heating, AC current heating, RF heating, and laser-thermal heating. DC arcjets, utilized on satellites like ARGOS, employ sub-kilovolt arcs with high current between a cathode tip and a diverging conical anode nozzle. AC arcjets are similar but have a shorter lifespan. Pulsed arcjets, characterized by discharge pulses, exhibit lower specific impulse compared to DC arcjets. The configuration of the arcjet is more complex than that of the resistojet, utilizing an electric arc to heat the propellant stream (Jordan 2000).

The arcjet configuration is more intricate than that of the resistojet, employing an electric arc to directly heat the propellant stream. The arcjet, not in direct contact with the wall, can achieve higher propellant temperatures without increasing the wall temperature. The arc forms between a central cathode and an anode, both parts of the divergent nozzle. Achieving uniform heating is crucial, and efficiency ranges from 35% to 54%. The constricted arcjet design, featuring a central cathode upstream of the throat, maximizes heat transfer by arcing between an anode ring downstream of the throat.



2.2.1. DC arcjets

Low-pressure DC-arcjet reactors present attractive sources of chemically reactive gas flows for applications such as spray coating and chemical vapor deposition. These reactors have demonstrated impressive diamond growth rates, reaching up to 1 mm/h, a pace at least ten times faster than observed in alternative reactors. This accelerated growth is attributed to a significant portion of the dissociation of hydrogen feedstock gases within the reactive gas flow generated by the arcjet discharge (Luque et al., 1998).

To assess the impact of various operational parameters on plasma velocity, an optical method was employed to measure the axial velocity of plasma jets produced by a DC plasma spray torch. Systematic examinations of different experimental conditions were conducted, varying the arc current (200-600 A), gas flow rate (30-80 slm), and internal nozzle diameter (6-10 mm). Plasma gases, including an Ar-H₂ mixture or N₂, were used. Clearly defined trends were observed, with arc stability identified as a significant factor influencing velocity fluctuations.

For DC plasma spray torches featuring a stick-type cathode, velocity distributions were measured across different parameters, including arc currents (200-600 A), gas flow rates (30-80 slm), gas composition (Ar-25 vol.% H₂ or N₂), and nozzle diameters (6-10 mm). Velocity was found to be a sensitive parameter, providing insights into jet behaviour and stability. Significant fluctuations in velocity were noted, partly attributed to arc instabilities within the nozzle. Measurements in the plasma core unveiled a noteworthy correlation between velocity fluctuations and arc voltage, especially within the frequency band of the measurement method.

The thermal pinch within the arc column was identified as crucial for confining the plasma jet and shaping the velocity profile near the nozzle exit. The nozzle channel diameter and arc current intensity were identified as the most influential governing parameters, contrasting with the volume flow rate, which exhibited opposing effects that partially compensated for each other, at least within the tested parameter range (Planche et al., 1998).

2.2.2. AC arcjets

Arc jets resulting from high-current fault arcs have the potential to cause damage to surrounding equipment. In a spectroscopic examination of AC arc jets spanning from 10 to 50 kA, iron electrodes with a 40 mm diameter were utilized in a literature study. The study focused on determining the temperature and iron vapor concentration, taking into account the self-absorption of two spectral lines of iron atoms. With an escalation in arc current from 10 to 50 kA, the temperature gradually decreased from 14,000 K to 10,000 K, while the iron vapor concentration in the arc jet sharply rose from 1% to 50%. Interestingly, the energy density of the arc jet showed minimal change ($8 \times 10^3 \text{ J/m}^3$) as the arc current increased from 10 to 50 kA. Additionally, the static and dynamic impedances of the arcjet were measured using two thrusters with nearly identical configurations (Iwata et al., 2005).

A study (Hamley, 1990) investigates the dynamic impedance of arc thrusters in relation to flow rate and DC current levels by superimposing an AC component on the DC arc current. A derived mathematical model reveals that both static and dynamic impedance magnitudes are intricately linked to mass flow rate. Surprisingly, the amplitude of the AC component exhibits minimal influence on dynamic impedance. Noteworthy findings include a substantial change in dynamic impedance magnitude, with no observable phase change, when the DC level is reduced from 10 to 8 amps. The impedance data presented in this study draw favourable comparisons between two distinct thrusters, providing valuable insights into the nuanced interplay of flow rate and DC current levels on the dynamic impedance characteristics of arc thrusters. This research contributes to a deeper understanding of the underlying dynamics, offering implications for the optimization of arc thruster performance.

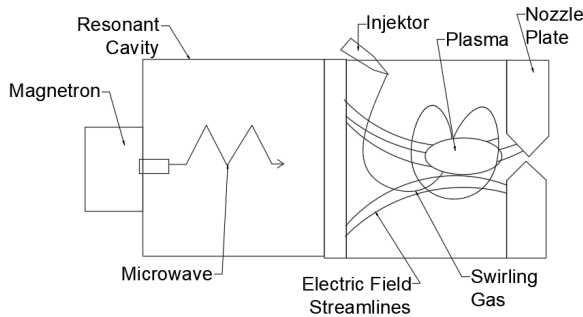
2.3. Microwave Electrothermal

Microwave electrothermal thrusters (METs) make use of standing wave microwave radiation delivered from a waveguide into a plenum chamber through a dielectric window. This electrodeless approach involves the acceleration of electrons in high-field regions by microwave radiation, colliding with injected neutral propellant. The mixing that occurs within the chamber heats the propellant, which is then expelled as exhaust. METs operate in both steady state and pulsed modes, boasting longer lifetimes due to reduced erosion. Achieving specific impulses as high as 1300 sec has been demonstrated using helium. Although the MET concept is currently in the laboratory-testing phase, it offers advantages such as electrodeless operation and high-energy absorption efficiency (Jordan 2000).

The MET utilizes continuous wave microwave energy to initiate and sustain a plasma discharge in a flowing propellant gas. The discharge absorbs the applied microwave energy, converting it into thermal and internal

energy of the propellant. The subsequent expansion and expulsion of the hot propellant through a throat and nozzle result in the conversion of the gas's energy into thrust. Success in the MET concept necessitates high efficiencies in all processes, including the energy conversion process that allows for high energy densities in the discharge volume. METs are particularly well-suited for high-performance propellant gases, such as hydrogen or hydrogen-rich gas mixtures (Power 1992).

A team of researchers (Curran et al., 1993) constructed and tested a cylindrical microwave cavity with internal tuning using a microwave generator equipped with a phase shifter-tuner for continuous variation of microwave power. The test apparatus is also being outfitted with a superconducting magnet for a magnetic nozzle, with the goal of compressing residual plasma, reducing wall heating, and stabilizing the plasma. Analytical results suggest that a specific impulse approaching 2000 s may be achievable using hydrogen as the propellant at chamber pressures of up to 10 atm.



2.4. Solar electric propulsion

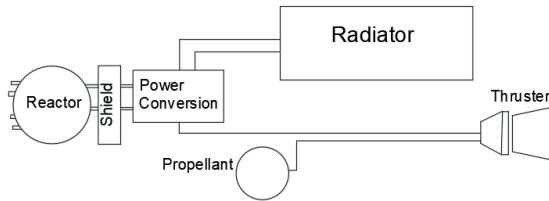
Efficient, affordable, and reliable capabilities are imperative for human and robotic exploration beyond Low Earth Orbit (LEO). Solar Electric Propulsion (SEP) has garnered attention due to its favorable in-space mass transfer efficiency compared to traditional chemical propulsion systems. NASA emphasizes the growing significance of this advantage as missions extend beyond Earth orbit, particularly for human exploration missions, including those involving Near Earth Objects (NEOs). SEP stages emerge as a potentially cost-effective solution for transferring high-mass cargoes beyond LEO in human missions.

Addressing power requirements exceeding 10 times that of current electric propulsion systems, NASA has adopted a progressive approach to identify critical technologies and plan an incremental demonstration mission. The identified 30kW class demonstration mission serves as a meaningful showcase of technologies, operational challenges, and provides the necessary scaling and modularity. Recent studies from NASA's Human Exploration and Operations Mission Directorate highlight SEP's attractiveness, given

its significantly higher specific impulse, versatile propulsion operation, and enhanced operational capability.

SEP introduces the capability for on-the-fly mission redirection or correction. Implementation of SEP in next-generation spacecraft mandates high-power photovoltaic power and propulsion systems. To enable SEP missions at higher power levels, an in-space demonstration of an operational SEP spacecraft exceeding current state-of-the-art power levels is deemed crucial. This demonstration holds direct applicability to a wide range of current and future NASA missions and can be extended to future higher power systems, possibly requiring 100kW of power or more (Smith et al., 2012).

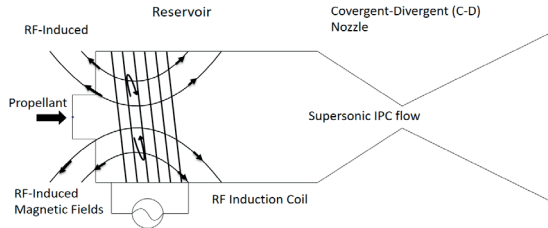
The Jet Propulsion Laboratory (JPL) has been at the forefront of Solar Electric Propulsion (SEP) technology, as evidenced by the Deep Space 1 (DS1) mission in 1996. The NSTAR ion thruster used in DS1 underwent a 30,000 hr Extended Life Test (ELT), leading to the approval and scheduling of the DAWN mission in 2006. However, limitations in NSTAR thruster performance and high system costs impacted potential applications in cost-capped missions. JPL's Advanced Propulsion Group aims to enhance the probability of using electric propulsion in more missions within cost constraints. This involves reducing ion propulsion system (IPS) costs, introducing advanced IPS component technologies, and developing a standardized IPS architecture. In collaboration with NASA centers and industrial partners, JPL is working on developing an Electric Propulsion (EP) Standard Architecture. The goal is to reduce IPS costs by improving thruster service life and performance, eliminating redundant thrusters, standardizing IPS architecture across missions, and introducing new component technologies. The team aims for a 50% reduction in IPS cost, propellant throughput of 400 kg per thruster, thrust of 119 mN, maximum specific impulse (Isp) of 4000 sec, and a more manufacturable, lower-cost Power Processing Unit (PPU) (Goebel et al., 2005).



2.5. Pulsed electrothermal thrusters

Pulsed electrothermal thrusters (PET) expel pulsed plasma through a standard supersonic nozzle, serving as the anode within a propellant chamber. Plasma breakdown in the propellant is induced by discharging a capacitor across the inner electrode, heating the gas introduced into the cylindrical

chamber. Liquid hydrogen is anticipated to have a theoretical specific impulse of approximately 2900 sec, with other propellants scaling inversely with the square root of their molecular mass. The lifespan of the thrusters is constrained by electrode erosion, and as of now, no space tests have been conducted (Jordan 2000).

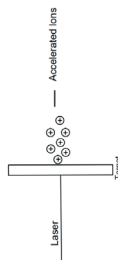


2.6. Laser Thermal Thruster

Laser Ablation Propulsion (LAP) stands as an electric propulsion concept with a history of thirty-five years. In LAP, a concentrated laser beam, whether in pulsed or continuous form, interacts with a condensed matter surface, be it solid or liquid. This interaction generates a jet of vapor or plasma, resulting in a reaction force on the surface that produces thrust, thereby facilitating propulsion for spacecraft and various objects.

LAP presents several advantages compared to chemical and other electric propulsion methods. Its applications span a wide range, from milliwatt-level satellite thrusters to kilowatt-level systems designed for dealing with re-entering near-Earth space debris. LAP is even envisioned for megawatt and gigawatt systems for direct launches to low Earth orbit (Phipps et al., 2010).

In the literature, the experimental setup for LAP typically includes components like a ZnSe condensing lens, ZnSe window, stainless steel chamber, and tungsten throat. Thrust measurement is carried out using a load cell, while the assessment of heat loss to the chamber wall involves measuring the heat film to the cooling water (Tahara & Nishida, 1999).



REFERENCES

- Auweter-Kurtz, M., Glocker, B., Golz, T., et al. (1996). Arcjet thruster development. *Journal of Propulsion and Power*, 12(6), 1077–1083.
- Cassady, R. J., Frisbee, R. H., Gilland, J. H., Houts, M. G., LaPointe, M. R., Maresse-Reading, C. M., ... Sengupta, A. (2008). Recent advances in nuclear powered electric propulsion for space exploration. *Energy Conversion and Management*, 49(3), 412–435. doi:10.1016/j.enconman.2007.10.015
- Chiu, Y.-H., Austin, B. L., Dressler, R. A., Levandier, D., Murray, P. T., Lozano, P., & Martinez-Sanchez, M. (2005). Mass Spectrometric Analysis of colloid thruster ion emission from selected propellants. *Journal of Propulsion and Power*, 21(3), 416–423. doi:10.2514/1.9690
- Curran, F. M., Sovey, J. S., & Myers, R. M. (1993). Electric propulsion: An evolutionary technology. *Acta Astronautica*, 29(9), 651–665. doi:10.1016/0094-5765(93)90084-a
- Goebel, D., Katz, I., Ziemer, J., Brophy, J., Polk, J., Johnson, L., & Sengupta, A. (2005). Electric Propulsion Research and Development at JPL. 41st AIAA/ASME/SAE/ASEE Joint Propulsion Conference & Exhibit. doi:10.2514/6.2005-3535
- Gorshkov, O. (1998). Low-power hall type and ion electric propulsion for the small sized spacecraft. 34th AIAA/ASME/SAE/ASEE Joint Propulsion Conference and Exhibit. doi:10.2514/6.1998-3929
- Hamley, J. (1990). Arcjet load characteristics. 21st International Electric Propulsion Conference. doi:10.2514/6.1990-2579
- Holste, K., Dietz, P., Scharmann, S., Keil, K., Henning, T., Zschätzsch, D., ... Klar, P. J. (2020). Ion thrusters for electric propulsion: Scientific issues developing a niche technology into a game changer. *Review of Scientific Instruments*, 91(6), 061101. doi:10.1063/5.0010134
- Hoskins, W. A., Cassady, R. J., Morgan, O., Myers, R. M., Wilson, F., King, D. Q., & deGrys, K. (2013, October 6–10). 30 Years of Electric Propulsion Flight Experience at Aerojet Rocketdyne. Paper IEPC-2013-439 presented at the 33rd International Electric Propulsion Conference, The George Washington University, Washington, D.C., USA. Aerojet Rocketdyne, Arlington, VA, 22209, USA, and Redmond, WA, 98052, USA.
- Hruby, V., Gamero-Castaño, M., Falkos, P., & Shenoy, S. (2001, October). Micro newton colloid thruster system development. In 27th International Electric Propulsion Conference (pp. 01-281).
- Iwata, M., Tanaka, S. I., Ikeda, K., & Goda, Y. (2005). Temperature, Iron Vapor Concentration and Energy Density for Arc Jets of 10-50kA AC Arcs in a Long Gap. *IEEJ Transactions on Power and Energy*, 125(8), 777-781.
- Jordan, I. J. E. (2000, December 6). Electric Propulsion: Which One For My Spacec-

raft? Submitted to V. Pisacane as part of requirements for 744 Space Systems I course at JHU, Whiting School of Engineering.

- Kokura, H., Yoneda, S., Nakamura, K., Mitsuhiro, N., Nakamura, M., & Sugai, H. (1999a). Diagnostic of surface wave plasma for oxide etching in comparison with inductive RF plasma. *Japanese Journal of Applied Physics*, 38(9R), 5256. doi:10.1143/jjap.38.5256
- Luque, J., Juchmann, W., Brinkman, E. A., & Jeffries, J. B. (1998). Excited state density distributions of H, C, C₂, and CH by spatially resolved optical emission in a diamond depositing DC-Arcjet reactor. *Journal of Vacuum Science & Technology A: Vacuum, Surfaces, and Films*, 16(2), 397–408. doi:10.1116/1.581037
- Mickelsen, W. R. (1967). Auxiliary and primary electric propulsion - present and future. *Journal of Spacecraft and Rockets*, 4(11), 1409–1423. doi:10.2514/3.29107
- Martinez-Sanchez, M., & Pollard, J. E. (1998). Spacecraft Electric Propulsion-an overview. *Journal of Propulsion and Power*, 14(5), 688–699. doi:10.2514/2.5331
- O'Reilly, D., Herdrich, G., & Kavanagh, D. F. (2021). Electric propulsion methods for small satellites: A Review. *Aerospace*, 8(1), 22. doi:10.3390/aerospace8010022
- Phipps, C., Bohn, W., Lippert, T., Sasoh, A., Schall, W., Sinko, J., & Phipps, C. (2010). A review of laser ablation propulsion. *AIP Conference Proceedings*. doi:10.1063/1.3507164
- Planche, M. P., Coudert, J. F., & Fauchais, P. (1998). Plasma Chemistry and Plasma Processing, 18(2), 263–283. doi:10.1023/a:1021606701022
- Power, J. L. (1992). Microwave electrothermal propulsion for space. *IEEE Transactions on Microwave Theory and Techniques*, 40(6), 1179–1191. doi:10.1109/22.141350
- Schmidt, T. D. (2005). Bemannte missionen zum Mars mit kontinuierlichen antrieben (Master's thesis). Institute of Space Systems (IRS), Stuttgart.
- Smith, B. K., Nazario, M. L., & Cunningham, C. C. (2012, May 7). Solar Electric Propulsion Vehicle Demonstration to Support Future Space Exploration Missions. NASA John H. Glenn Research Center, Cleveland, OH 44135. Retrieved August 26, 2013.
- Tahara, H., & Nishida, M. (1999). Overview of electric propulsion activity in Japan. 35th Joint Propulsion Conference and Exhibit. doi:10.2514/6.1999-2159
- Tajmar, M. (2003). Electric Propulsion Systems. *Advanced Space Propulsion Systems*, 73–98. doi:10.1007/978-3-7091-0547-4_6
- Tajmar, M., Genovese, A., & Steiger, W. (2004). Indium field emission electric propulsion Microthruster experimental characterization. *Journal of Propulsion and Power*, 20(2), 211–218. doi:10.2514/1.9247
- Tajmar, M., & Wang, J. (2000). Three-dimensional numerical simulation of field-emission-electric-propulsion neutralization. *Journal of Propulsion and Power*, 16(3), 536–544. doi:10.2514/2.5602
- Wollenhaupt, B. B., Le, Q. H., & Herdrich, G. (2018). Overview of thermal arcjet th-

ruster development. *Aircraft Engineering and Aerospace Technology*, 90(2), 280–301

Xiong, J., Zhou, Z., Ye, X., Wang, X., Feng, Y., & Li, Y. (2002). A colloid micro-thruster System. *Microelectronic Engineering*, 61–62, 1031–1037. doi:10.1016/s0167-9317(02)00466-5

Yeo, S. H., Ogawa, H., Kahnfeld, D., & Schneider, R. (2021a). Miniaturization perspectives of electrostatic propulsion for small spacecraft platforms. *Progress in Aerospace Sciences*, 126, 100742. doi:10.1016/j.paerosci.2021.100742

Yongjie, D., Hong, L., Liqiu, W., Yanlin, H., Yan, S., Hui, L., ... Daren, Y. (2018). Overview of hall electric propulsion in China. *IEEE Transactions on Plasma Science*, 46(2), 263–282. doi:10.1109/tps.2017.2776257



Chapter 7

VALIDATION OF A NUMERICAL METHOD FOR AERODYNAMIC PERFORMANCE ESTIMATION OF WING-IN-GROUND-EFFECT

Yüksel ERASLAN¹

¹ Lect. Dr.

İskenderun Technical University, İskenderun Vocational School, Unmanned Aerial Vehicle Technology and Operatorship Pr.

yuksel.eraslan@iste.edu.tr

ORCID: 0000-0002-5158-5171

1. INTRODUCTION

Aircraft have various flight phases such as takeoff, climbing, cruise, loitering, or landing and the performance of the vehicle depends on many different variables depending on the flight condition. Aerodynamic performance of an aerial vehicle or only its wing is usually mentioned as lift-to-drag ratio (C_L/C_D), which has a great importance on aircraft flight dynamics, stability and performance. Especially in the takeoff and landing phases, as the operation is carried out near the ground, the considerations become different from those at the cruise, climbing, or descending phases. Such cases lead to the forming of a boundary near the wing, and a phenomenon called “ground effect” arises. In Figure 1, the wing-in-ground-effect is illustrated where the chord length is defined as c , and the altitude from the boundary or ground as h , the incidence angle as α and the airspeed or velocity as V .

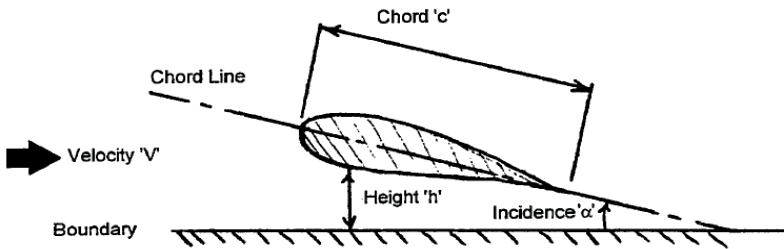


Figure 1. Side view of a wing-in-ground effect (Halloran and O'Meara, 1999)

In the case of the ground effect, the flow under the wing is not allowed to expand likewise it is in free air because of the boundary or ground. Correspondingly, static pressure increment results in an increased lift and affects aerodynamic characteristics of the wing. Moreover, the decrement in downwash angle causes the effective incidence angle to be increased for the same angle of attack, which results in reduction in drag force, increment in lift force and provide improved lift-to-drag ratio (Cui et al., 2010). The effectiveness of the ground effect is known to depend on the ground clearance defined as the ratio between flight altitude and wing chord length (h/c).

Investigation of the impact of ground effect on aerodynamic variables of lift coefficient, drag coefficient, pitching moment coefficient and lift-to-drag ratio has been an attractive topic for scientists for years. In the literature, there are various studies investigating such effects in analytical, numerical or experimental manner. For instance, Bil et al. carried out computational fluid dynamics (CFD) analyses on a wing-in-ground-effect (WIG) aircraft to assess the impact of ground effect on the aerodynamic performance of the vehicle at various angles of attack and flight altitudes. In addition to lift increment and drag reduction, their discussion showed that the ground effect proposed

improved longitudinal stability in terms of pitching moment coefficient (Bil et al., 2015). Lao et al. reported a numerical aerodynamic investigation on a WIG unmanned aerial vehicle using a Navier-Stokes solver and obtained increment in Oswald efficiency and improvement in lift coefficient in ground effect than freestream (Lao et al., 2018). Lee et al. performed experimental investigation on slender reverse delta wing designs with various anhedral angles in a wind tunnel. They found that when h/c is 0.4 and the wing trailing edge is parallel to the ground using an anhedral angle, lift and drag coefficients are increased. Moreover, the lift coefficient was increased with an increment in anhedral angle during the ground effect region (Lee et al., 2019). Deng et al. focused on aerodynamic assessment of complex DLR F6 wing-body design in ground effect. They compared their results obtained from CFD analyses with experimental data and validated their numerical methodology (Deng et al., 2022). Hu et al. focused on the stability challenge of the ground effect and studied on optimization of an airfoil using the free-form deformation technique, where an artificial neural network is also conducted. They aimed to obtain a maximum lift-to-drag ratio and investigated the concluded optimal airfoil geometry by using the CFD method (Hu et al., 2022).

In this study, it is aimed to validate the vortex-lattice method on aerodynamic performance investigation of a wing-in-ground-effect. For that purpose, three wing designs with aspect ratios 1.0, 1.5, and 2.0 are generated on a general public licensed numerical analysis program XFLR5. The designs have the same airfoil sections but differ in wing areas and wing spans as expected from the variation in aspect ratios. Firstly, a grid independence analysis is conducted to ensure the accuracy of the results to be independent of number of the number of panels. Furthermore, the analyses were carried out at various ground clearance conditions and various angles of attack by means of the vortex-lattice method. In conclusion, the discrepancies with experimental results existing in the literature are presented and the success of the methodology is discussed for various conditions.

2. MATERIAL AND NUMERICAL METHOD

In this study, the wing models are prepared the same as the designs that were previously tested in the closed-type wind tunnel at Pusan National University which are presented in (Jung et al., 2008). The models are generated on the general public licensed XFLR5 program using NACA6409 airfoil section and having various aspect ratios (AR) that are presented in Figure 2. Chord length (c) of the designs is 0.2 m, while wing-span (b) and wing area (S) are varied with respect to alteration in wing aspect ratios as given in Table 1. The analysis environment is defined as sea-level conditions where air density is $\rho=1.225 \text{ kg/m}^3$ and kinematic viscosity is $1.5 \times 10^{-5} \text{ m}^2/\text{s}$ and the airspeed defined similar with the experimental data as 25.5 m/s.

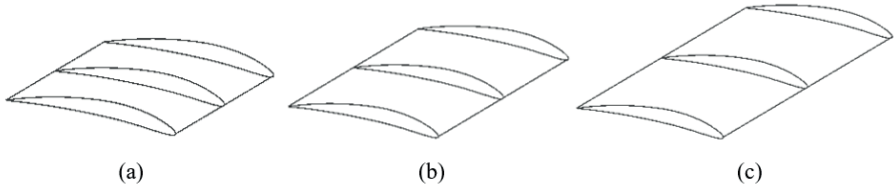


Figure 2. Wing designs with various aspect ratios; a) AR=1.0, b) AR=1.5, c) AR=2.0

Table 1. Geometrical parameters of the wing designs varying with wing aspect ratio

| Wing Aspect Ratio | Chord Length (m) | Wing Span (m) | Wing Area (m ²) |
|-------------------|------------------|---------------|-----------------------------|
| 1.0 | 0.2 | 0.2 | 0.04 |
| 1.5 | 0.2 | 0.3 | 0.06 |
| 2.0 | 0.2 | 0.4 | 0.08 |

2.1. Vortex Lattice Method (VLM)

VLM is a useful tool to investigate the aerodynamic behaviors of a wing design that has a low aspect ratio, sweep angle, or even dihedral angle. XFLR5 proposes two vortex lattice-based solving methods that use only horseshoe vortex or a combination of horseshoe and ring vortices to be located on each elementary panel on the wing. A planform view of a wing design including panel elements and a defined vortex is illustrated in Figure 3.

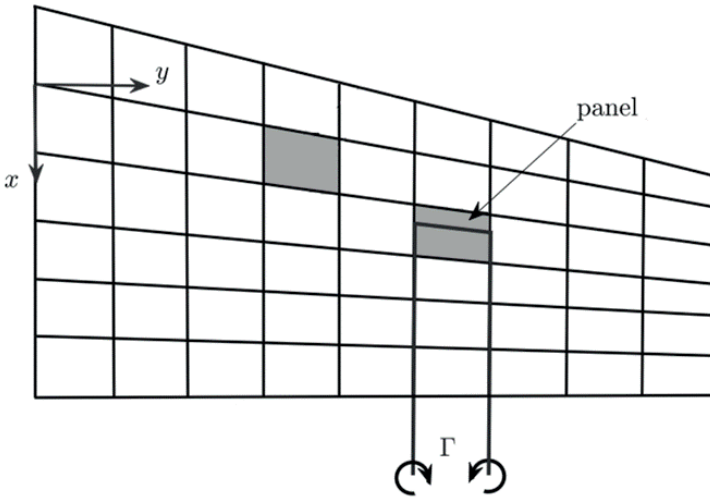


Figure 3. Wing planform divided into panel elements and a vortex formation (Bidar, 2019)

The philosophy behind the method is to model the perturbation generated by the wing with summation of the vortices distributed over the wing

planform (Stempeck et al., 2018). The strength of each vortex is calculated to meet the appropriate boundary conditions on the surface of the panels. For that purpose, a wing planform is divided into a determined number of panel elements. Lift force (F) for each constructed panel is calculated by means of a vector cross product given in Equation 1, where Γ is multiplication of vortex strength and its length, ρ is the fluid density, V is the freestream speed.

$$F = \rho V \times \Gamma \quad (1)$$

The lift coefficient (C_L) is then calculated using Equation 2, where S is the sum of constructed total panel area and F_{wz} is the projection on the vertical wind axis.

$$C_L = \frac{1}{\rho S V^2} \sum_{panels} F_{wz} \quad (2)$$

The formulation is applicable to total wing surface and after the lift coefficient values calculated together with the pitching moment and center of pressure position; the viscous drag coefficient could be interpolated from the airfoil polars. VLM methodology is known not to offer accurate estimations at high angles of attack, especially near the stall region (Deperrois, A., 2010).

2.2. Grid Independence Analysis

In finite element analysis-based engineering applications, grid independence is a usual methodology to ensure the results obtained from the numerical analyses are independent of the number of mesh elements (Şumnu, 2022). In the case of an analysis using the vortex lattice method, the mesh elements are defined as the three-dimensional panels, and the amount of the panels should be optimally determined to provide accurate results independent from the number of elements that also offer minimal computational time. In that context, number of panels have varied from 420 to approximately 14×10^3 on a case wing design with $AR=1$, and the results at 25.5 m/s airspeed, 0-degree angle of attack and ground clearance value of $h/c=0.2$ are presented in terms of the lift coefficient, drag coefficient and lift-to-drag ratio in Figure 4.

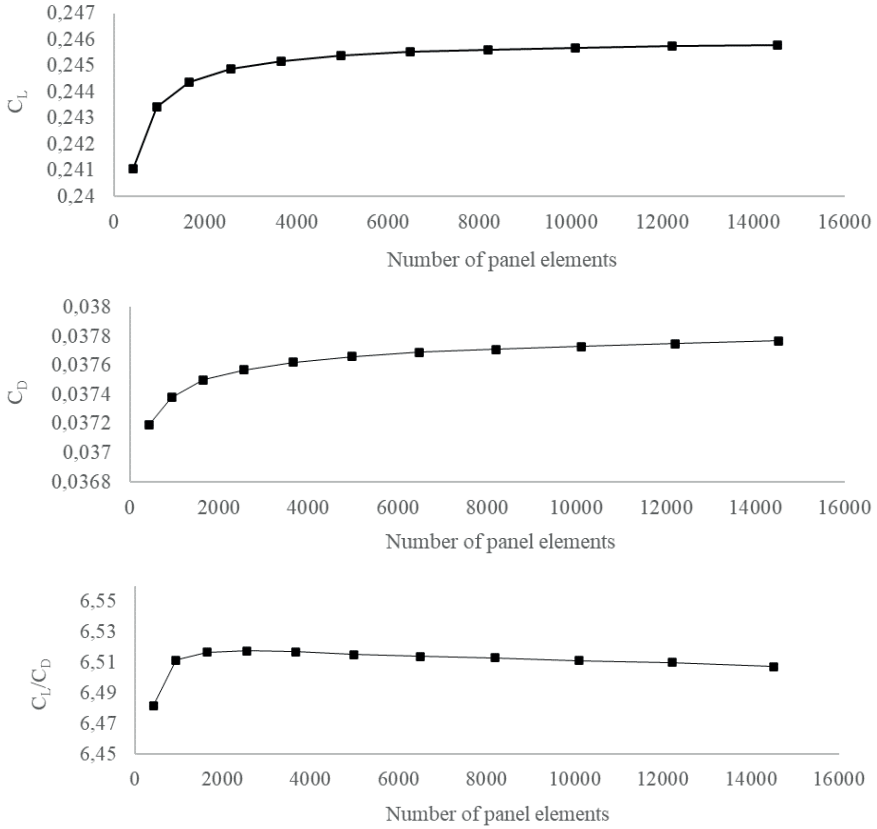


Figure 4. Grid independence analysis results for wing design with $AR=1$ at $h/c=0.2$

It is clear from the figures that the lift coefficient results are converged at approximately 8×10^3 panel elements, while the drag coefficient and the lift-to-drag ratio have continued to their neglectable differentiation. Therefore, it is determined that the number of panel elements around 8×10^3 are adequate to have admissible results for further analyses and distribution of the panel elements are illustrated for the wing design with $AR=1$ in Figure 5.

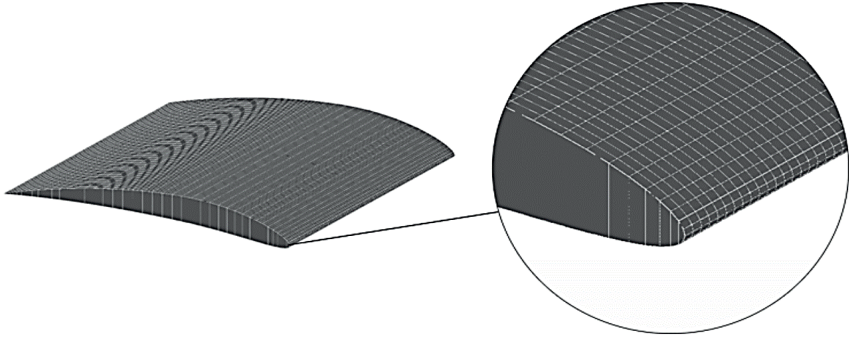


Figure 5. Panel element distribution over the wing surface

As the lifting force is generated considerably by the first quarter chord section of the wing design, the number of panel elements is constructed as increasing beginning from the mid-section of the chordwise location and concentrated to especially leading edge of the design.

3. RESULTS AND DISCUSSION

Aiming for comparison and validation of the used method with experimental results, the wing design with $AR=1$ is analyzed at a ground clearance value of 0.2 at angles of attack varying between 0 degree to 8 degree, and the results at 25.5 m/s airspeed are given in Figure 6. The tendency of lift coefficient, drag coefficient, and lift-to-drag ratio are clearly seen to be similar to experimental results. Lift-coefficient point of view, as expected, a linear variation is obtained, while the lift-curve slope has a slight difference with experimental results. Drag-coefficient estimations are also seen to be satisfactory thanks to the ability of the method to model viscous effects. The aerodynamic performance also has an admissible tendency where the estimated maximum value of the lift-to-drag ratio is at the similar angle of attack to the experimental results.

On the other hand, the discrepancies between numerical analysis and experimental results are given in Table 2, Table 3 and Table 4, where the wing design with $AR=1$ is analyzed at various ground clearance values. Lift-coefficient and lift-to-drag ratio estimation results are found not to be significantly affected by variation in ground clearance values and average discrepancies vary from 7.11% to 8.04%, and from 3.14% to 4.07%, respectively with experimental results. Drag-coefficient estimation results are found to be slightly affected by variation in ground clearance values and average discrepancies are between 7.53% and 9.37% with experimental results.

The analyses are expanded to wing designs generated with aspect ratios 1.5 and 2.0 and results for aerodynamic coefficients are presented in Figure

7 and Figure 8. The discrepancies with experimental and VLM results are found to be lower at low aspect ratio wing designs as expected for vortex-lattice solvers (Chaparro et al., 2017). Nevertheless, the tendencies are similar with experimental results for both of the lift coefficient, drag coefficient and lift-to-drag ratio.

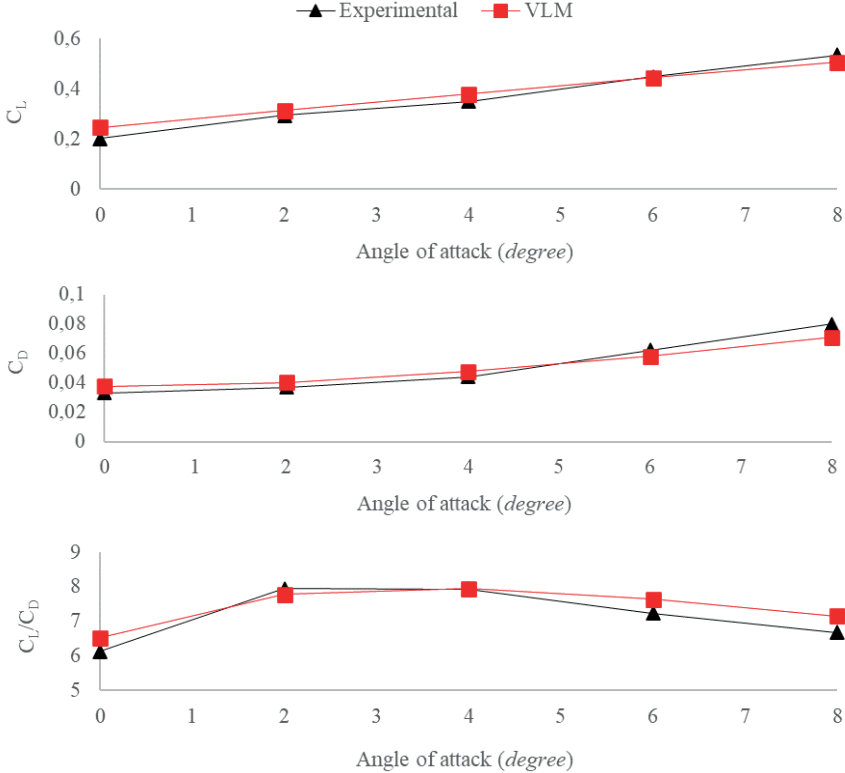


Figure 6. Numerical analysis results in comparison with experimental results with $AR=1$ at $h/c=0.2$

Table 2. Discrepancy between numerical analysis and experimental results with $AR=1$ at $h/c=0.1$

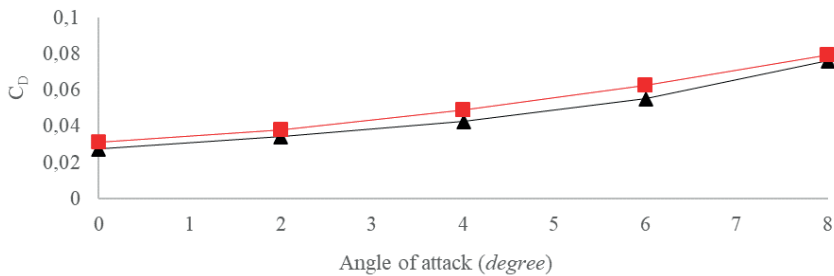
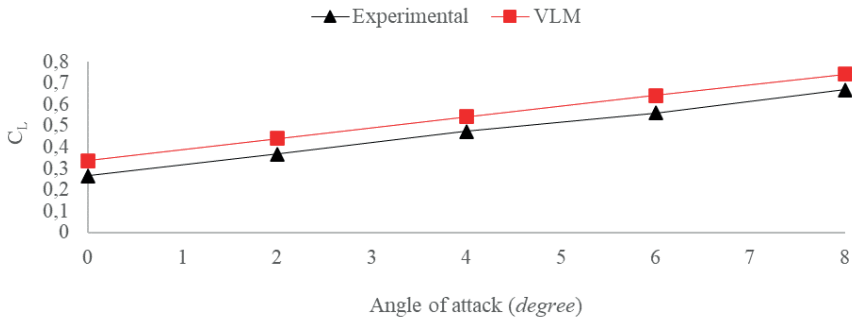
| Angle of attack (degree) | C_L | C_D | C_L/C_D |
|--------------------------|--------------|--------------|--------------|
| 0 | 19.2% | 10.53% | 9.68% |
| 2 | 4.10% | 6.10% | -2.12% |
| 4 | 6.21% | 7.19% | -1.055% |
| 6 | -1.64% | -1.62% | -0.016% |
| 8 | -9.04% | -12.21% | 2.82% |
| Average | 8.04% | 7.53% | 3.14% |

Table 3. Discrepancy between numerical analysis and experimental results with $AR=1$ at $h/c=0.2$

| Angle of attack (degree) | C_l | C_D | C_l/C_D |
|--------------------------|--------------|--------------|--------------|
| 0 | 17.78% | 12.5% | 5.99% |
| 2 | 5.94% | 7.91% | -2.13% |
| 4 | 7.76% | 7.58% | 0.19% |
| 6 | -1.17% | -6.8% | 5.35% |
| 8 | -5.6% | -13.1% | 6.68% |
| Average | 7.65% | 9.62% | 4.07% |

Table 4. Discrepancy between numerical analysis and experimental results with $AR=1$ at $h/c=0.3$

| Angle of attack (degree) | C_l | C_D | C_l/C_D |
|--------------------------|--------------|--------------|--------------|
| 0 | 14.63% | 12.34% | 2.62% |
| 2 | 6.92% | 7.75% | -0.90% |
| 4 | 1.57% | -2.18% | 3.67% |
| 6 | -2.53% | -7.49% | 4.60% |
| 8 | -9.90% | -17.07% | 6.12% |
| Average | 7.11% | 9.37% | 3.58% |



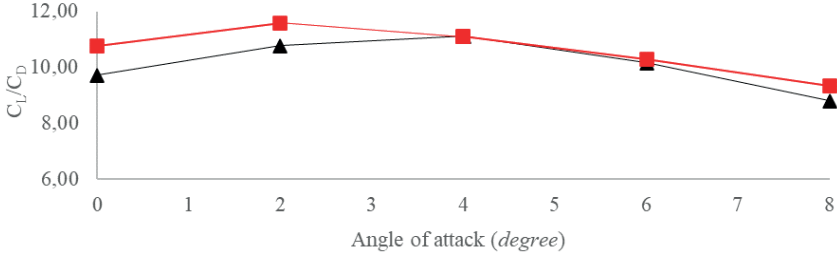


Figure 7. Numerical analysis results in comparison with experimental results with $AR=1.5$ at $h/c=0.2$

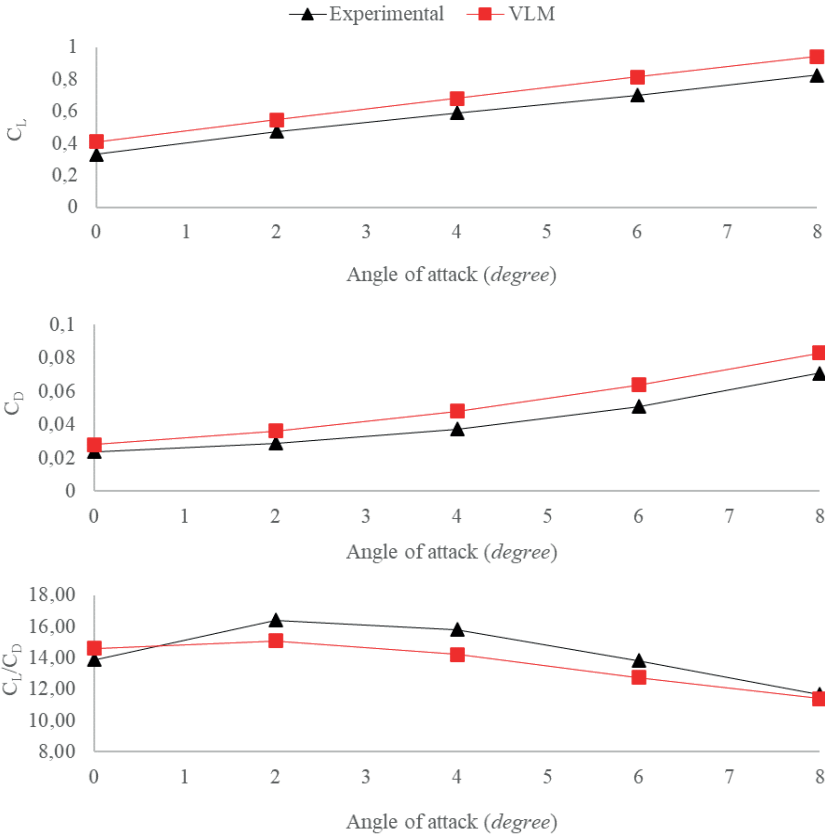


Figure 8. Numerical analysis results in comparison with experimental results with $AR=2.0$ at $h/c=0.2$

The results for wing design with $AR=2$ at various ground clearances are presented in Figure 9. Especially at lower ground clearances, lift coefficient results were found dramatically to differ from experimental results. Lift coefficient results have nearly the same differentiation trend for every ground clearance value. Parallel to the lift coefficient variation, the lift-to-drag ratio

is also estimated more successful at higher ground clearance conditions. The discrepancies between numerical analysis and experimental results are given in Table 5.

Table 5. Discrepancy between numerical analysis and experimental results of AR=2 at various ground clearances at zero angle of attack

| Ground clearance (h/c) | C_l | C_D | C_l/C_D |
|----------------------------|----------------|---------------|----------------|
| 0.1 | -57.7% | -21.9% | -29.3% |
| 0.2 | -24.24% | -17.98% | -5.3% |
| 0.3 | -15.83% | -15.85% | 0.01% |
| Average | -32.59% | -11.5% | -18.58% |

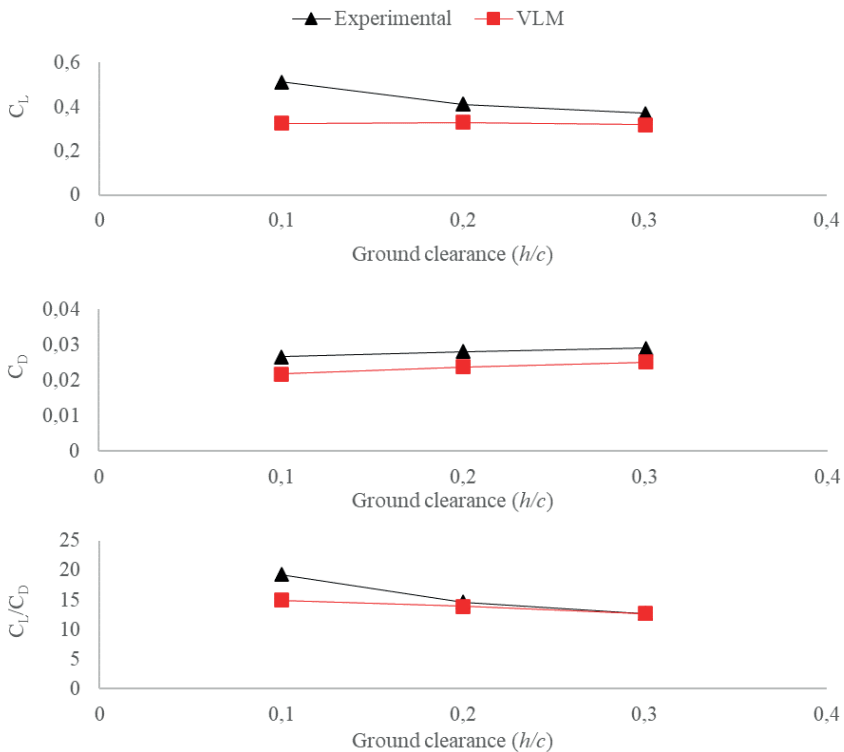


Figure 9. Numerical analysis results in comparison with experimental results with AR=2 at various ground clearances at zero angle of attack

CONCLUSION

In this study, wing designs with various aspect ratios are numerically investigated utilizing a vortex lattice solver for assessment of aerodynamic performances in ground effect. Within the context of the study, the aerodynamic performance (lift-to-drag ratio) of the designs was investigated at

different ground clearances. To ensure the numerical results are independent of the number of panel elements, grid independence analysis was conducted. Moreover, to validate the analysis methodology, each design was analyzed at various ground clearance conditions. In conclusion, the vortex lattice method was found to provide admissible results for especially low aspect ratio designs within the considered ground clearance interval. On the other hand, especially at lower ground clearance regions, aerodynamic variables of higher aspect ratio designs were not found to be estimated successfully when compared with experimental data.

REFERENCES

- Bidar, O. (2019). Aerodynamics and control aspects of formation flight for induced drag savings. <http://dx.doi.org/10.13140/RG.2.2.33983.12962>
- Bil, C., Fung, M. C., Cheung and S. C., Marzocca, P. (2015). CFD analysis of a wing-in-ground-effect (WIGE) vehicle (No. 2015-01-2571). SAE Technical Paper.
- Chaparro, D., Fujiwara, G. E., Ting, E. and Nguyen, N. T. (2017, June). *Transonic and viscous potential flow method applied to flexible wing transport aircraft*. In 35th AIAA Applied Aerodynamics Conference (p. 4221).
- Cui, E. and Zhang, X. (2010). Ground effect aerodynamics. *Encyclopedia of Aerospace Engineering*, 1(Part 3), 245-256.
- Deng, N. and Agarwal, R. K. (2022). Numerical simulation of DLR-F6 wing-body flow field in ground effect. *Computers & Fluids*, 245, 105576.
- Deperrois, A. (2010). Analysis of foils and wings operating at low Reynolds numbers, Guidelines for XFLR5.
- Halloran, M. and O'Meara, S. (1999). *Wing in ground effect craft review*. Australia: DSTO Aeronautical and Maritime Research Laboratory.
- Hu, H., Zhang, G., Li, D., Zhang, Z., Sun and T., Zong, Z. (2022). Shape optimization of airfoil in ground effect based on free-form deformation utilizing sensitivity analysis and surrogate model of artificial neural network. *Ocean Engineering*, 257, 111514.
- Jung, K. H., Chun, H. H. and Kim, H. J. (2008). Experimental investigation of wing-in-ground effect with a NACA6409 section. *Journal of Marine Science and Technology*, 13, 317-327.
- Lao, C. T. and Wong, E. T. T. (2018). CFD simulation of a wing-in-ground-effect UAV. *IOP Conference Series: Materials Science and Engineering*, 370(1), 012006.
- Lee, T., Tremblay-Dionne, V. and Ko, L. S. (2019). Ground effect on a slender reverse delta wing with anhedral. *Proceedings of the Institution of Mechanical Engineers, Part G: Journal of Aerospace Engineering*, 233(4), 1516-1525.
- Stempeck, A., Hassanalian and M., Abdelkefi, A. (2018, June). *Aerodynamic performance of albatross-inspired wing shape for marine unmanned air vehicles*. In 2018 Aviation Technology, Integration, and Operations Conference (p. 3899).
- Şumnu, A. (2022). Investigation of the effect of side devices and crosswind flow on aerodynamic drag of a ground vehicle. *Çukurova University Journal of the Faculty of Engineering*, 37(3), 813-826.



Chapter 8

FUTURE SUSTAINABLE ENERGY IN AUTOMOTIVE: FUEL CELLS

Yasin Furkan GORGULU¹

¹ Assistant Prof. Dr., Isparta University of Applied Sciences, Department of Machinery and Metal Technologies, ORCID: 0000-0002-1828-2849, yasingorgulu@isparta.edu.tr

INTRODUCTION

Today, the automotive industry is on the brink of a significant transformation. Factors such as climate change, limited energy resources, and the preservation of air quality have increased the demand for sustainable and clean energy solutions (Gorgulu, 2022, 2023). In this context, the role and future of the automotive sector in the sustainable energy transformation are examined. Fuel cells, the hydrogen economy, and alternative energy sources hold an important place in the quest of automobile manufacturers for environmentally friendly and energy-efficient solutions. This study explores the potential of these technologies and the innovations they bring to the automotive industry, supporting a vision of sustainable mobility.

FUEL CELLS

A fuel cell is an electrochemical device that works similarly to a battery in that it generates electricity through a chemical reaction. Because batteries are intended to be portable power sources, they must have all of the required ingredients. The battery will run out of power when these substances are exhausted. However, the chemical fuel itself is not present in a fuel cell. All it offers is a reaction chamber, which is where the fuel cell process happens. The real reactants that are needed to produce energy are obtained elsewhere. Power may be produced by the fuel cell as long as there is a chemical fuel supply. Like batteries, some fuel cells are still made to be portable (Breeze, 2017).

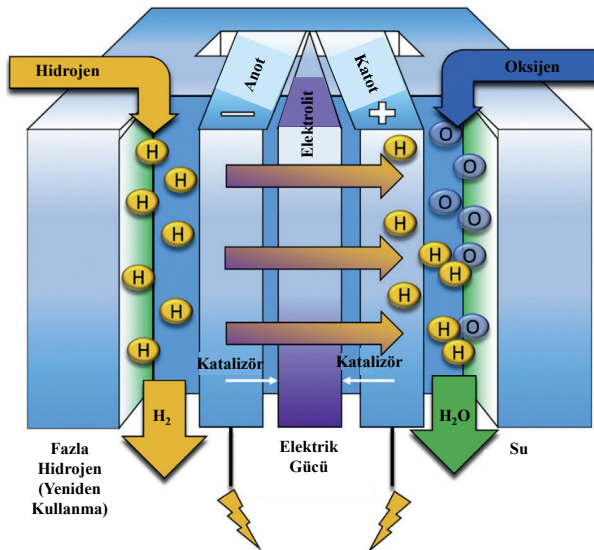
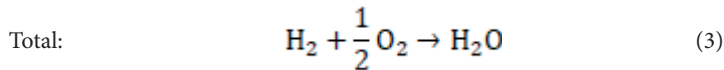
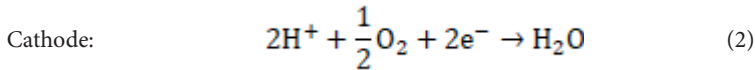
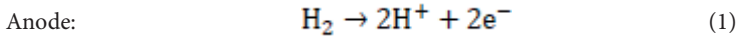


Figure 1. Schematic Representation of a Proton Exchange Membrane Fuel Cell (Sundén, 2019).

Generally speaking, oxygen is the cathode reactant or oxidizing agent and hydrogen is the anode reactant or fuel. Water is the equivalent result of the reaction between hydrogen and oxygen. Ionically conductive electrolyte is necessary for the possibility of an electrochemical reaction. A hydrogen-oxygen electrochemical system with a proton-conducting electrolyte is schematically depicted in Figure 1. Typically, this type of device is referred to as a fuel cell, especially an acidic fuel cell as acids are frequently utilized as electrolytes that carry protons. The following is the course of the electrochemical and overall reactions (Mitsushima et al., 2018):



An external electrical circuit, an electrolyte, a separator, and two electrodes are all present in fuel cells. Every part of the electrochemical system has a certain job to do. The electrodes have a wide electrochemical surface area and are electrically conductive. Despite being electrically insulating, the electrolyte has a high ionic conductivity. In an electrochemical process, these ions—which are typically positively (cation) or negatively (anion) charged atoms or molecules—represent the mobile species. The electrochemical processes that occur at the interface between the electrodes and the electrolyte are frequently complicated, despite the seemingly simple design of such an electrochemical system. We refer to one of the two electrodes as the “anode”. The system’s negative electrode, or anode, is where the fuel—the reactant—is oxidized. Electrons from the reactant are liberated during the electrochemical reaction and used in an external load. The voltage gradient (migration) and concentration gradient (diffusion) in the electrolyte carry the oxidized (anodic) reactant, or cations, away from the anode and toward the second electrode, known as the “cathode.” Even though it is the electrochemical system’s positive electrode, the oxidant is reduced at the cathode.

Proton Exchange Membrane Fuel Cells (PEMFCs)

Operating at about 80°C, the Proton Exchange Membrane Fuel Cell (PEMFC) is a low-temperature device. In general, the energy conversion efficiency—that is, the percentage of hydrogen energy converted to electrical power—ranges from 50% to 60%. Protons flow through a solid polymer called the electrolyte. Because of its tiny size and compact design, this kind of fuel cell has been highly recommended as a power source for land-based vehicles. It also exhibits good start-up performance at low temperatures.

Direct Methanol Fuel Cells (DMFCs)

This is a version of the Proton Exchange Membrane Fuel Cell (PEMFC) that uses methanol instead of a separate reformer upstream of the fuel cell to start the reaction immediately at the anode. The operating temperature spans from 50 to 100°C, and the conversion efficiency is about between 30% and 40%. The reformer's loss is eradicated. It is used in devices like mobile phones and portable PCs.

Phosphoric Acid Fuel Cells (PAFCs)

For a while now, the PAFC (phosphoric acid fuel cell) type has been used in commercial applications. It may be used in a variety of settings, including businesses, hotels, hospitals, airports, and schools. At between 40% and 50%, the conversion efficiency is quite poor. The temperature range in which it operates is 150–200°C. It may generate steam as well as electricity. The electrolyte in this case is phosphoric acid. This kind of fuel cell is especially impervious to contamination when it uses hydrogen fuel and operates at high temperatures. Carbon monoxide can harm the catalyst's platinum layer at lower temperatures. Although this form of fuel cell is acknowledged in technology, the units are often huge and heavy.

Solid Oxide Fuel Cells (SOFCs)

Even in distant locations, the Solid Oxide Fuel Cell (SOFC) type is seen to be a viable option for big units. Applications for it in automobiles include auxiliary power units. The electrolyte is solid and usually composed of zirconium oxide-based hard ceramic material. It operates at a temperature more than 1000°C. High reaction rates can be achieved without the need for costly catalysts because to the high working temperature, and gases like natural gas may be utilized directly or internally converted without the need for an additional unit. It has a conversion efficiency of around 60%. It may also be used with a steam turbine to generate more power. It doesn't need fuel that is only hydrogen.

Molten Carbonate Fuel Cell (MCFC)

Lithium, sodium, and potassium carbonates are melted to create the electrolyte in a Molten Carbonate Fuel Cell (MCFC). The working temperature is around 650°C, and the conversion efficiency is almost 60%. Airborne carbon dioxide is necessary for it to function. Excellent reaction rates may be achieved with nickel, a reasonably priced catalyst that serves as the foundation of the electrode, thanks to the high working temperature. The nature of the electrolyte, a hot and caustic combination of sodium, potassium, and lithium carbonates, counterbalances its simplicity. This kind of fuel cell may produce extra power when paired with a steam turbine, much as other high-temperature fuel cells. In addition to pure hydrogen, it can function with other hydrogen

carriers. Operating at high temperatures can have significant effects on cell components, similar to Solid Oxide Fuel Cells (SOFCs).

Alkaline Fuel Cells (AFCs)

Alkaline Fuel Cells (AFCs) have been used in spacecraft to produce electricity and drinkable water for astronauts. Their conversion efficiency is approximately 70%, and they operate at temperatures ranging from 150 to 200°C. The electrolyte is typically composed of potassium hydroxide (KOH). An advantage of this type of fuel cell is that it does not rely on platinum as a catalyst. Carbon dioxide can affect the conversion and usually requires that the provided air and fuel be free of CO₂, or alternatively, pure oxygen and hydrogen are used. This type of fuel cell has been used in Apollo and Space Shuttle Orbiter spacecraft.

Table 1. provides information on various types of fuel cells, including their operating temperature ranges, materials and catalyst types, electrolytes used, and efficiencies (Sundén, 2019).

Table 1. *Basic Operating Characteristics of Various Fuel Cell Types.*

| Fuel Cell Type | Materials and Catalyst | Operating Temperature (°C) | Electrolyte | Efficiency (%) |
|----------------|----------------------------|----------------------------|---------------------|----------------|
| PEMFC | Carbon and Platinum | 30-100 | Solid Membrane | 40-50 |
| DMFC | Platinum and Ruthenium | 20-90 | Solid Membrane | 20-50 |
| PAFC | H ⁺ | ~200 | Phosphoric Acid | 40-50 |
| AFC | Carbon and Nickel | 50-200 | Potassium Hydroxide | 50-60 |
| MCFC | Stainless Steel and Nickel | ~650 | Metal | >60 |
| SOFC | Ceramic and Perovskites | 500-1000 | Ceramics | 50-60 |

FUELS

A variety of resources, including biomass, water, wind, sun, geothermal, nuclear, coal, and the collection, use, and storage of carbon dioxide, can be used to make hydrogen. Because of the variety of these sources, hydrogen is a viable energy carrier that can be produced practically anywhere in the world. Rather from being a source of energy, hydrogen is a transporter. It must be made from substances containing hydrogen in order to store and transfer energy in a manner that is useful. Fossil fuels like coal and natural gas, non-food biomass cultivated from non-renewable goods, and renewable energy sources like sun, wind, geothermal, and hydroelectric power may all be used to produce hydrogen. One of the main reasons hydrogen is such a promising energy carrier is the multiplicity of these possible supply sources. Large

central facilities, medium-sized semi-central plants, or tiny dispersed units near or at the point of use—like filling stations or stationary power production sites—can all create hydrogen. This flexibility in production scale and location adds to hydrogen’s viability as an integral part of future energy systems (U.S. Department of Energy, 2014, 2022, 2023a, 2023b).

Natural Gas Reforming

Steam methane reforming is a technique that uses high-temperature steam to create hydrogen from natural gas. Approximately 95% of the hydrogen utilized in the US today comes from this technique. Methane is burned in the air using a different process known as partial oxidation to create hydrogen. A “synthesis gas” or “syngas” is produced by both partial oxidation and steam reformation. This gas combines with more steam to create a gas stream that has a greater hydrogen concentration. These methods are key in hydrogen production, especially in regions where natural gas is abundant and readily available.

Renewable Electrolysis

Electrical current is used in electrolysis to separate water into hydrogen and oxygen. There are several ways to produce the necessary amount of power. However, it is preferable to produce electricity using nuclear energy, renewable energy sources (like wind, solar, geothermal, and hydroelectric power), or carbon capture, utilization, and storage in order to reduce greenhouse gas emissions. This approach, known as renewable electrolysis, is increasingly significant in efforts to produce hydrogen in an environmentally sustainable manner. It aligns with global initiatives to reduce carbon footprints and promote clean energy sources.

Gasification

The process of gasification involves heating coal or biomass and converting it into gaseous components when steam, air or oxygen, pressure, and heat are present. Steam is then combined with a succession of subsequent chemical processes to create a gas stream that contains more hydrogen than before. By producing hydrogen straight from coal using carbon capture and storage, greenhouse gas emissions may be cut to almost nothing. Biomass generation, due to its consumption of carbon dioxide from the atmosphere, results in nearly zero net greenhouse gas emissions when hydrogen is produced through biomass gasification. This approach offers a way to produce hydrogen in a more environmentally friendly manner, especially when using biomass as the feedstock.

Renewable Liquid Reforming

Additionally, biomass may be processed to produce transport-friendly, sustainable liquid fuels like bio-oil or ethanol. Hydrogen may then be produced

from these fuels by subjecting them to high-temperature steam. Additionally, aqueous reforming, a variation of this technology, is still under research. This approach represents an innovative way to utilize biomass, not only for direct energy production but also as a precursor for hydrogen generation, thereby contributing to the diversification and sustainability of the energy supply.

Nuclear High-Temperature Electrolysis

Water electrolysis may be made more efficient by using the heat produced by a nuclear reactor. The water may be made to boil for a lower total energy demand since less power is needed to split it into hydrogen and oxygen. This method, known as nuclear high-temperature electrolysis, leverages the substantial heat output of nuclear reactors to make the hydrogen production process more energy-efficient and potentially more cost-effective.

Solar-Assisted Thermochemical Water Splitting

Using the high temperatures produced by nuclear reactors or solar concentrators—mirrors that concentrate and magnify sunlight—is another technique for dividing water. This technique splits water into hydrogen and oxygen using a sequence of chemical processes. The technology recycles and repurposes every intermediate chemical utilized in the process. This approach harnesses solar or nuclear energy to drive thermochemical reactions, providing a potentially efficient and sustainable way to produce hydrogen without direct reliance on electricity.

Biological

Under the influence of sunlight, certain microorganisms, such as cyanobacteria and green algae, may split water into hydrogen and oxygen as a byproduct of their normal metabolic activities. It is possible for other microbes to directly extract hydrogen from biomass.

Photoelectrochemical

With the use of a unique family of semiconductor materials and sunshine, hydrogen may be created straight from water. These particular semiconductors immediately divide water molecules into hydrogen and oxygen by absorbing solar energy.

The diversity in these hydrogen production methods enhances the potential of hydrogen as an energy carrier for the future, offering possibilities for producing hydrogen from various sources. Hydrogen has a wide range of applications, from energy production to transportation, and can meet different needs. This versatility makes it an increasingly important element in global energy strategies, especially in the context of renewable energy and sustainability.

FUEL CELLS AND AUTOMOTIVE

Fuel Cell Vehicles (FCVs) hold significant potential for reducing dependency on external sources, contributing to climate change mitigation, and lowering harmful emissions. FCVs operate using hydrogen gas instead of gasoline and do not emit harmful exhaust emissions. Although there are challenges that FCVs need to overcome to compete with conventional vehicles, the potential benefits are substantial. While FCVs may appear similar to traditional vehicles, they utilize cutting-edge technology. The heart of an FCV is the fuel cell stack, which converts hydrogen gas, carried in the vehicle, and oxygen from the air into electricity to power the electric motor. Figure 2 shows the main components of a typical FCV.

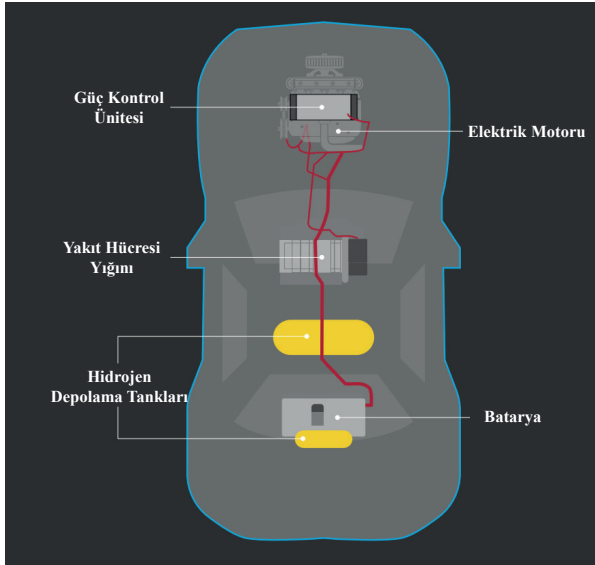


Figure 2. Hydrogen fuel cell electric vehicle system (U.S. Department of Energy, 2022).

Fuel cell vehicles (FCVs) offer several advantages over traditional internal combustion engine vehicles, but they also have some disadvantages.

Advantages

Environmentally Friendly: Fuel cell vehicles (FCVs) can operate with zero emissions as they use hydrogen as fuel. Their only emission is water vapor. As a result, greenhouse gas emissions and air pollution are greatly reduced. Greenhouse gases, especially carbon dioxide (CO₂), are released by gasoline and diesel engines and are linked to climate change. Pure hydrogen fuel cell vehicles (FCVs) solely produce heat and water in their exhaust, releasing no greenhouse gasses. Even yet, compared to conventional gasoline and diesel cars, the creation of hydrogen for fuel cell vehicles (FCVs) can still produce

a significant amount of greenhouse emissions, depending on the technology used.

High Effectiveness: When compared to internal combustion engines, fuel cells have a better energy conversion efficiency. A significant amount of the energy from hydrogen fuel is transformed into electrical energy. Because hydrogen can be generated domestically from fossil fuels like coal and natural gas as well as renewable sources like water, biogas, and agricultural waste, FCVs can lessen reliance on foreign oil. This can reduce economic dependence on other countries and make it less sensitive to the increasingly volatile oil market prices.

Low Noise Levels: Fuel cell vehicles are quiet, as they lack the explosions and vibrations found in internal combustion engines. This is an advantage when used in urban areas and quiet environments.

High Torque: Fuel cell vehicles use electric motors, which means they can produce high torque instantly. This can improve acceleration and driving experience.

Long Range: Fuel cell vehicles have the potential for longer ranges as hydrogen storage technologies advance. This can provide drivers with more travel freedom.

Disadvantages

Fuel Infrastructure: The limited availability of hydrogen fuel restricts the use of fuel cell vehicles (FCVs). The lack of fueling stations impedes the adoption of these vehicles.

High Cost: The production costs of fuel cell vehicles are still high. The use of precious metals like platinum in electrodes increases costs. At the moment, FCVs cost more than conventional and hybrid cars. Still, prices are coming down a lot. Automobile manufacturers may be able to make fuel cell vehicles (FCVs) competitive with conventional cars if they keep cutting prices, especially for the fuel cell stack and hydrogen storage.

Storage and Reliability of Hydrogen: High pressure or liquefied state storage is required for hydrogen. These energy-density storage techniques are not cheap. Fuel cell devices are not as robust as internal combustion engines, particularly in specific temperature and humidity ranges. As of right now, fuel cell stack durability for usage on roads is thought to be around half of what is required for commercialization. In the last few years, durability has been known to range between 47,000 km and 120,000 km, but experts suggest that FCVs need an expected lifespan of about 240,000 km to compete with gasoline vehicles (U.S. Department of Energy, 2023b).




Delivery of Hydrogen to Consumers: The current infrastructure cannot

support the widespread adoption of FCVs. This limits the use and research of FCVs.

Controversial Hydrogen Production: The methods used for hydrogen production are controversial regarding whether hydrogen is produced cleanly and sustainably. The most common production method currently involves natural gas reforming, which can lead to carbon emissions.

Cold Weather Performance: Some fuel cell vehicles may have lower performance in cold weather conditions, as hydrogen storage and cell efficiency can decrease. Table 2 compares three 2022 model Toyota Mirai FCVs, reflecting their fuel consumption. It shows that in urban, intercity, and average values, the amount of hydrogen consumed for the same distance is clearly lower than the amount of fuel consumed.

Table 2. Performance criteria of some fuel cell vehicles.

| | 2022 Toyota Mirai LE | | | 2022 Toyota Mirai Limited | | | 2022 Toyota Mirai XLE | | |
|--------------------------------|---|------|---------|---|------|---------|--|------|---------|
| |  | | |  | | |  | | |
| Fuel Economy | | | | | | | | | |
| km/kg | 28.8 | 29.6 | 28 | 25.6 | 26 | 25.2 | 28.8 | 29.6 | 28 |
| | Avg. | City | Highway | Avg. | City | Highway | Avg. | City | Highway |
| km/lt | 29.6 | 30.4 | 28.4 | 26 | 26.8 | 25.6 | 29.6 | 30.4 | 28.4 |
| | Avg. | City | Highway | Avg. | City | Highway | Avg. | City | Highway |
| Other Estimations | | | | | | | | | |
| Range | 531 | | | 574 | | | 646 | | |
| Vehicle Characteristics | | | | | | | | | |
| Vehicle Class | Compact Car | | | Compact Car | | | Compact Car | | |
| Motor | AC Synchronous (134 kW) | | | AC Synchronous (134 kW) | | | AC Synchronous (134 kW) | | |
| Battery | 311 V Lithium İon | | | 311 V Lithium İon | | | 311 V Lithium İon | | |

*km/kg: Kilograms of hydrogen per kilometer

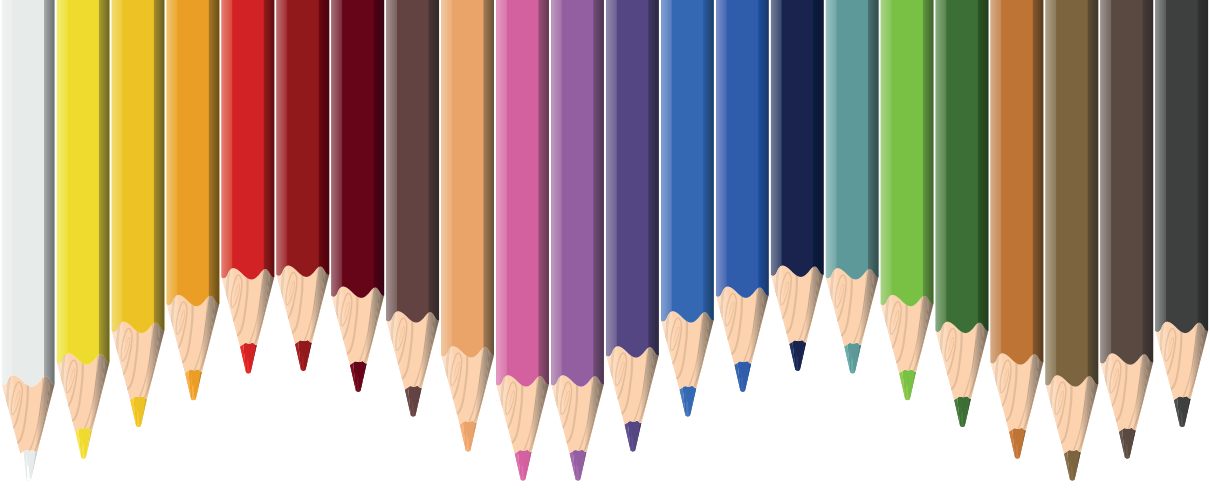
CONCLUSION

The fuel cells, hydrogen economy, and alternative energy sources being considered are shedding light on the sustainable future of the automotive industry. These technologies, offering environmentally friendly and energy-efficient solutions that could replace traditional fossil fuels, provide significant benefits to the automotive industry. Fuel cells operate with low emissions and high efficiency, reducing environmental impact, while the hydrogen economy

presents great potential in energy storage and clean transportation. Additionally, alternative energy sources offer various paths to meet the automotive sector's energy needs, with options like wind, solar, and biofuels. Therefore, the development and adoption of these technologies in the automotive industry will be a crucial step towards achieving more sustainable and environmentally friendly mobility in the future.

REFERENCES

- Breeze, P. (2017). An Introduction to Fuel Cells. In *Fuel Cells* (pp. 1–10). Elsevier. <https://doi.org/10.1016/B978-0-08-101039-6.00001-7>
- Gorgulu, Y. F. (2022). Enerji Krizi ve Yenilenemez Enerji Kaynakları. In C. Karaman (Ed.), *Teknobilim-2022 Enerji Krizi ve Yenilenebilir Enerji* (1st ed., pp. 7–18). Efe Akademi Yayınları. <https://www.efekademi.com/teknobilim-2022-enerji-krizi-ve-yenilenebilir-enerji-ciltli>
- Gorgulu, Y. F. (2023). Renewable Energy Resources and Mitigating the Energy Crisis. In C. Özalp, S. Bardak, & E. Hürdoğan (Eds.), *Sosyal ve Beşeri Bilimlerde Teori ve Araştırmalar-I* (pp. 19–30). Serüven Yayınevi. <https://www.seruvenyayinevi.com/Webkontrol/uploads/Fck/martengineering2023.pdf>
- Mitsushima, S., Gollas, B., & Hacker, V. (2018). Introduction. In *Fuel Cells and Hydrogen* (pp. 1–13). Elsevier. <https://doi.org/10.1016/B978-0-12-811459-9.00001-3>
- Sundén, B. (2019). Fuel cell types - overview. In *Hydrogen, Batteries and Fuel Cells* (pp. 123–144). Elsevier. <https://doi.org/10.1016/B978-0-12-816950-6.00008-7>
- U.S. Department of Energy. (2014). *Hydrogen Production*.
- U.S. Department of Energy. (2022). The Fuel Cell Electric Vehicle (FCEV). In *U.S. Department of Energy*.
- U.S. Department of Energy. (2023a). *Alternative Fuels Data Center: Hydrogen Production and Distribution*. https://afdc.energy.gov/fuels/hydrogen_production.html
- U.S. Department of Energy. (2023b). *Fuel Cell Vehicles*. <https://www.fueleconomy.gov/feg/fuelcell.shtml>



Chapter 9

ANALYSIS AND SIMULATION OF TWO ZVT BOOST CONVERTERS WITH ACTIVE SNUBBER CELL

Hilal Sebnem Gecmez¹

Naim Suleyman Ting²

¹ M.Sc. Student, Erzincan Binali Yildirim University, Institute of Science and Technology, Department of Electrical Electronics Engineering, sbnmgcmz@gmail.com, ORCID: 0009-0005-2820-1490.

² Assoc. Prof. Dr., Erzincan Binali Yildirim University, Faculty of Engineering and Architecture, Department of Electrical Electronics Engineering, nsuleyman@erzincan.edu.tr, ORCID: 0000-0003-3743-0824.

1. INTRODUCTION

The rapidly increasing global population, industrialization, and technological advancements have led to a continuous increase in the energy demand worldwide. This growing demand has caused the excessive use of fossil fuels, such as natural gas, oil, and coal. The realization that fossil fuel resources are limited, together with increasing nature-related apprehension, has triggered a global search for sustainable energy options. Renewable energy sources are important in this context. Resources, such as wind energy, solar energy, and hydroelectric power, offer long-term and environmentally friendly energy solutions. Therefore, promoting the development and utilization of alternative energy sources is a crucial step in reducing dependency on fossil fuels and supporting environmental sustainability. The integration of energy from renewable sources into an electrical grid cannot be achieved without the use of electronic power converters (Sun and Bae, 2022).

DC-DC converters transform the energy obtained from these sources into suitable voltage or current levels that can be connected to storage systems or electrical grids. For instance, wind turbines cannot directly produce electricity at voltages compatible with the electrical grid. Therefore, DC-DC converters are employed to convert the energy acquired from wind turbines into electricity in a suitable format that can be integrated into an electrical grid (Li et al., 2022). Furthermore, these converters play a pivotal role in the charging infrastructure of electric vehicles and have become a significant factor in the rapid growth of the sector (Aslay and Ting, 2022). Soft-switching pulse-width modulation (PWM) DC-DC boost converters, recognized for their high power density and straightforward controllability, are widely utilized across different sectors. Among these applications are electric vehicles and renewable energy sources; commonly, high-frequency switching is preferred in these fields to increase the power density levels. Operating at high frequencies reduces the size of magnetic elements, thereby enabling the use of smaller components. However, operating at high frequencies amplifies both the switching losses and levels of electromagnetic interference (EMI). This presents a potential risk to the overall functionality of the converter, potentially resulting in a decline in its effectiveness.

Soft-switching (SS) techniques involving snubber cells can effectively resolve these issues (Aksoy et al., 2010; Ting et al., 2022). The implementation of these methods ensures a substantial decrease or complete eradication of switching losses. SS techniques are typically categorized into four groups: zero-voltage switching (ZVS), zero-current switching (ZCS), zero-voltage transition (ZVT), and zero-current transition (ZCT) (Bodur et al., 2003). Snubber cells are generally categorized into two types: active and passive (Yeşilyurt and Bodur, 2019). Passive snubber cells do not employ auxiliary switches; instead, a series inductance and parallel capacitor are utilized to reduce switc-

hing losses. Passive snubber cells are simple and cost effective. However, it's important to note that while passive snubber cells offer advantages, they have limitations in recovering parasitic capacitor energy and affecting the switch voltage drop rate (Bodur et al., 2020). One of the main problems of passive snubber cells is that they expose the switching element or the main diode to an additional voltage. By contrast, active snubber cells utilize a minimum of one auxiliary switch (Tseng and Chen, 1998a; Sahin and Ting, 2018). ZVT and ZCT, which are advanced soft-switching techniques, are implemented using active snubber cells. These techniques allow for the recovery of the energy stored in the parasitic capacitance formed during the switching operation. In addition, they allow for the complete elimination of the losses associated with switching (Tseng and Chen, 1998b; Urgan, 2012; Li and Ho, 2016).

In this chapter, exemplary converters belonging to the ZVT PWM DC-DC boost converter types were selected from the literature, and their operating principles are extensively examined. Furthermore, the operating ranges of these exemplary converters are analyzed in detail. Additionally, simulations of these exemplary converters are conducted using PSIM 9.1.1 and emphasizing the advantages and disadvantages of these converters.

2. ZVT BOOST CONVERTERS WITH ACTIVE SNUBBER CELL

The ZVT technique represents an advanced soft-switching method that effectively eradicates losses during power switch turn-on, enabling the recuperation of switching energy. ZVT plays an important role in increasing the performance and efficiency of power converters. In the literature, there are many converter structures that utilize the ZVT technique. The fundamental ZVT PWM DC-DC boost converter proposed by Hua et al. (1994) is the first study in the literature to achieve soft switching utilizing the ZVT technique. The circuit scheme of the converter is illustrated in Figure 1. In this converter, Once the voltage of the main switch reaches zero owing to the active snubber cell, a control signal is given. Thus, it is turned on with ZVT without losses. Additionally, thanks to the presented converter configuration, the discharge energy of the parasitic capacitor is also recovered. However, the converter has some drawbacks. Specifically, in this setup, the auxiliary switch is deactivated using hard switching, whereas the capacitor linked to the main switch terminals is charged with a variable current. Because the charging time is dependent on the load current, the performance of the converter diminishes under lighter loads. Additionally, the level of electromagnetic interference (EMI) noise is quite high.

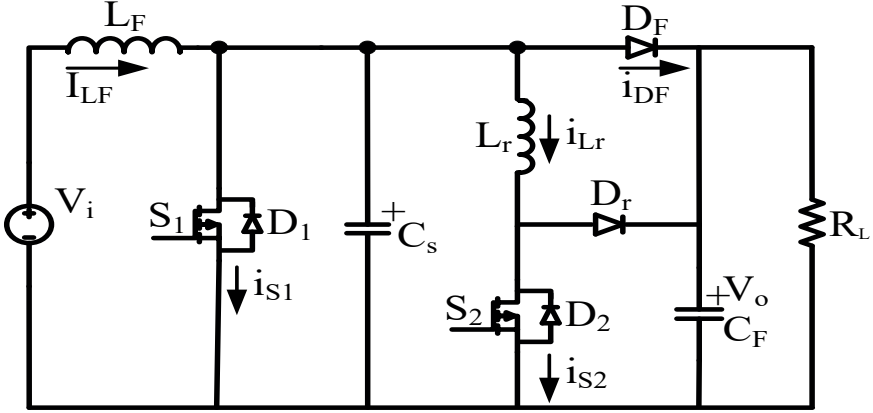


Figure 1. The circuit topology of the converter with fundamental ZVT cell

Numerous studies have been undertaken to improve performance, enhance efficiency, and address the limitations of the fundamental ZVT converter circuit. In this section, detailed theoretical analyses of example two converters with active snubber cells chosen from the family of ZVT PWM DC-DC boost converters in the literature are presented. The theoretical examination of these converters is simplified by the following assumptions:

- Input voltage is constant
- All the semiconductor power devices and passive elements are ideal.
- The C_F filter capacitors are large enough to maintain the V_o output voltages constant.
- The L_F main inductances are large enough to maintain the I_{in} input currents constant
- The voltage drops across the main components are neglected.

2.1. Example ZVT Converter-1

The circuit topology of the converter designed by Lee and Kim (2019) is illustrated in Figure 2. In the proposed converter, V_i represents the input voltage, L_F denotes the main inductance, S_1 signifies the primary switch, D_1 represents the internal diode of the primary switch, D_F refers to the primary diode, C_F denotes the output filter capacitor, and R_L indicates the resistive load. Regarding the snubber cell, S_2 and S_3 represent auxiliary switches, D_2 and D_3 refer to the internal diodes of the auxiliary switches, C_a and C_r represent resonant capacitors and L_r signifies the resonant inductance.

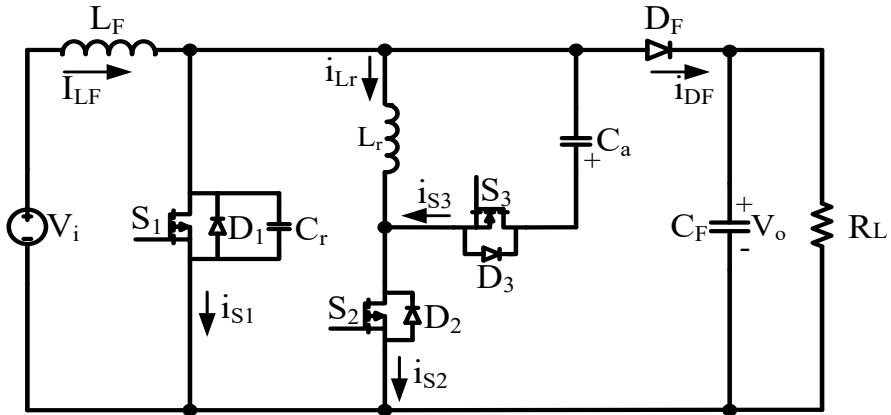


Figure 2. The circuit topology of the example ZVT converter-1

Within a single switching period of the presented converter, there are ten operational intervals. The equivalent circuits for these operational intervals are illustrated in Figure 3.

Interval 1 [Fig. 3(a)]:

During this interval, the power switches are in the off state and the input current I_{LF} is transferred to the output through primary diode D_F . The resonant capacitor C_r is charged to the output voltage V_o and the resonant capacitance C_a is zero. This interval is the off state of the classical boost DC-DC converter.

Interval 2 [Fig. 3(b)]:

At $t = t_1$, the interval begins when a control signal is given to the auxiliary switch S_2 . After turning on the auxiliary switch S_2 , the resonant inductance current i_{Lr} begins to increase linearly from zero. Because the current through S_2 is limited by L_r , auxiliary switch S_2 turns on with ZCS. At the end of this interval, the current of L_r reaches the input current level, and the current through the primary diode D_F decreases to 0. Consequently, the diode D_F turns off with ZCS.

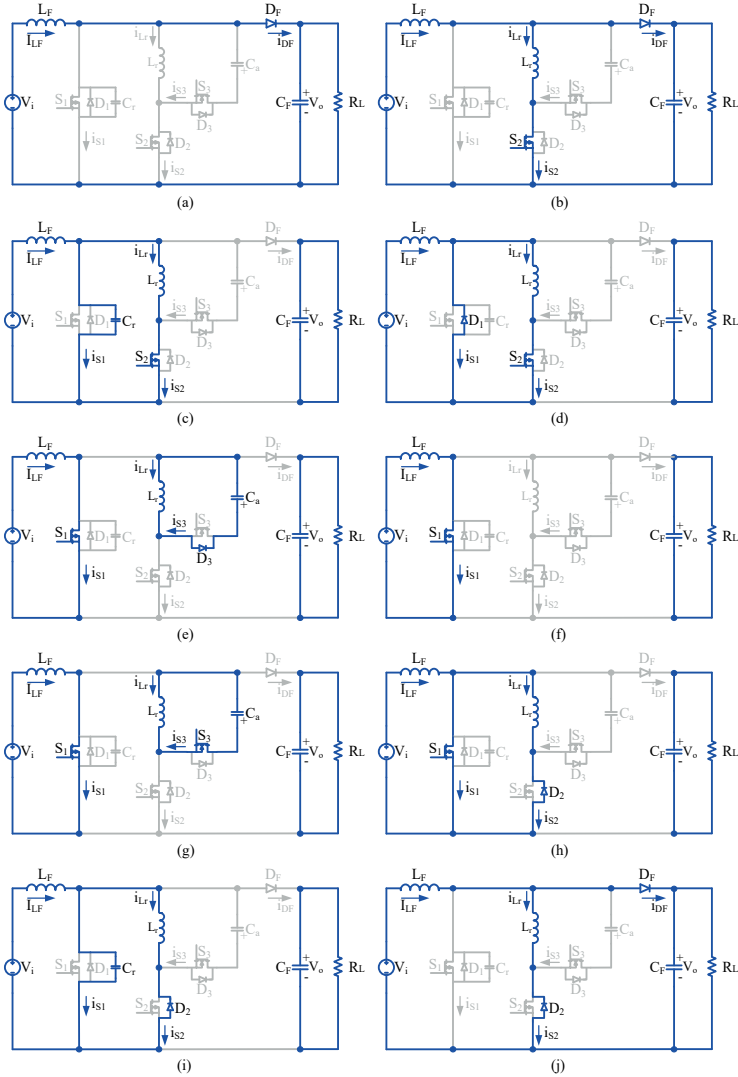


Figure 3. Equivalent circuits of the operating intervals

Interval 3 [Fig. 3(c)]:

At the beginning of this interval, a resonance begins between C_r and L_r . As V_{C_r} reduces, I_{L_r} continues to increase, thereby exceeding the input current level. When V_{C_r} reaches zero, I_{L_r} reaches its maximum level, and this operating interval completes.

Interval 4 [Fig. 3(d)]:

At $t = t_3$, as soon as the V_{C_r} voltage drops to zero, the internal diode D_1 of

the main switch S_1 turns on and conducts the excess of L_r current over the input current. Under these conditions, the control signal is given to the primary switch S_1 , enabling it to turn on with ZVT. At $t = t_4$, the control signal applied to the auxiliary switch S_2 is removed at the conclusion of this interval.

Interval 5 [Fig. 3(e)]:

At the onset of this interval, resonance starts between L_r and C_a via the path $L_r - D_3 - C_a$. In this way, C_a is charged, and the resonant inductance current begins to decrease. In this interval, because of the resonance current charging the C_a capacitor, the auxiliary switch S_2 turns off with ZVS.

Interval 6 [Fig. 3(f)]:

During this interval, the input current I_{in} flows through the primary switch, and all semiconductor devices are in the off state. This interval is the off state of the classical boost DC-DC converter. When auxiliary switch S_3 turns on, this mode ends.

Interval 7 [Fig. 3(g)]:

At $t = t_6$, as soon as S_3 turns on, capacitor C_a resonates with inductance L_r , enabling auxiliary switch S_3 to turn on with ZCS. When the energy stored in C_a is fully transferred to L_r , the control signal applied to S_3 is removed, and the auxiliary switch S_3 is turned off under ZVS conditions.

Interval 8 [Fig. 3(h)]:

At $t = t_7$, when the voltage V_{Ca} drops to zero, the internal diode D_2 of the auxiliary switch S_2 turns on with ZVS. During this interval, the resonant inductance current flows through D_2 and primary switch S_1 , causing a current stress across the primary switch. Upon removal of the control signal for S_1 , this interval is concluded.

Interval 9 [Fig. 3(i)]:

At the beginning of this interval when resonance starts between capacitor C_r and inductance L_r . During this interval, the C_r capacitor charges with the combined current from the L_r main inductance and L_r resonant inductance, enabling the primary switch S_1 to turn on with ZVS. Once the C_r capacitor reaches the V_o output voltage, this interval concludes.

Interval 10 [Fig. 3(j)]:

This mode begins when V_{Cr} voltage reaches the output voltage V_o , the primary diode D_F turns on under the ZVS condition and the current I_{Lr} decreases linearly. By the end of this interval, the I_{Lr} current drops to zero; thus, a single switching cycle is finished and the next switching period begins.

2.2. Example ZVT Converter-2

The circuit scheme of the example ZVT converter-2 designed by Yau et al. (2020) is depicted in Figure 4. In example converter-2, V_i denotes the input voltage, L_F represents the main inductance, S_1 represents the primary switch, D_1 is the internal diode of the primary switch, D_F indicates the primary diode, C_F signifies the output filter capacitor, and R_L represents the resistive load. In the snubber cell, S_2 refers to the auxiliary switch, D_2 signifies the internal diode of the auxiliary switch, D_r is the resonant diode, L_r represents the resonant inductance, and C_r indicates the resonant capacitor.

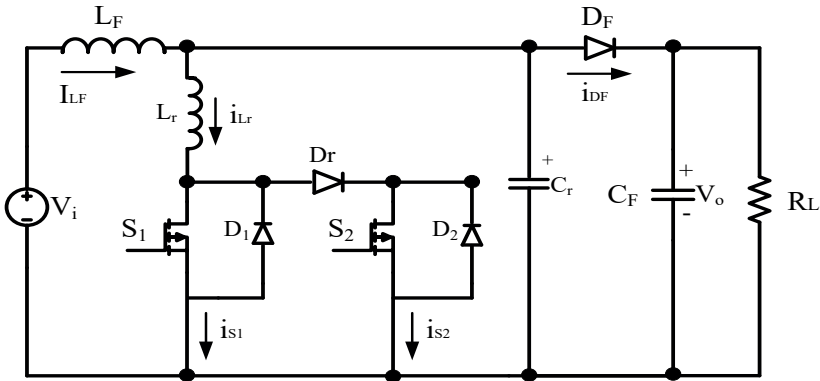


Figure 4. The circuit diagram of ZVT PWM DC-DC converter-2

There are nine operating intervals within a single switching period of the presented converter. The equivalent circuits for these operational intervals are shown in Figure 5.

Interval 1 [Fig. 5(a)]:

In interval $t < t_0$, the power switches are in the off state. During this time, the energy stored in the main inductance L_F is transferred to the output through the primary diode D_F , whereas the voltage across the resonant capacitor C_r is equal to the output voltage V_o . This interval is the off state of the classical boost DC-DC converter. When the control signal is applied to auxiliary switch S_2 , this interval ends.

Interval 2 [Fig. 5(b)]:

This interval begins when the control signal is applied to the auxiliary switch S_2 . Auxiliary switch S_2 and auxiliary diode D_r turns on with ZCS because the rise rate of the auxiliary switch current is limited by the L_r resonant inductance. At the end of this interval, the inductance current I_{Lr} reaches the level of the input current, causing the diode D_F to turn off with ZCS.

Interval 3 [Fig. 5(c)]:

At the beginning of this interval, resonance starts between capacitor C_r and inductance L_r . Owing to the resonance, the resonant inductance current continues to increase, and capacitor C_r starts to discharge. At the end of this interval, at $t = t_2$, capacitor C_r discharges completely, and current I_{Lr} reaches its maximum value.

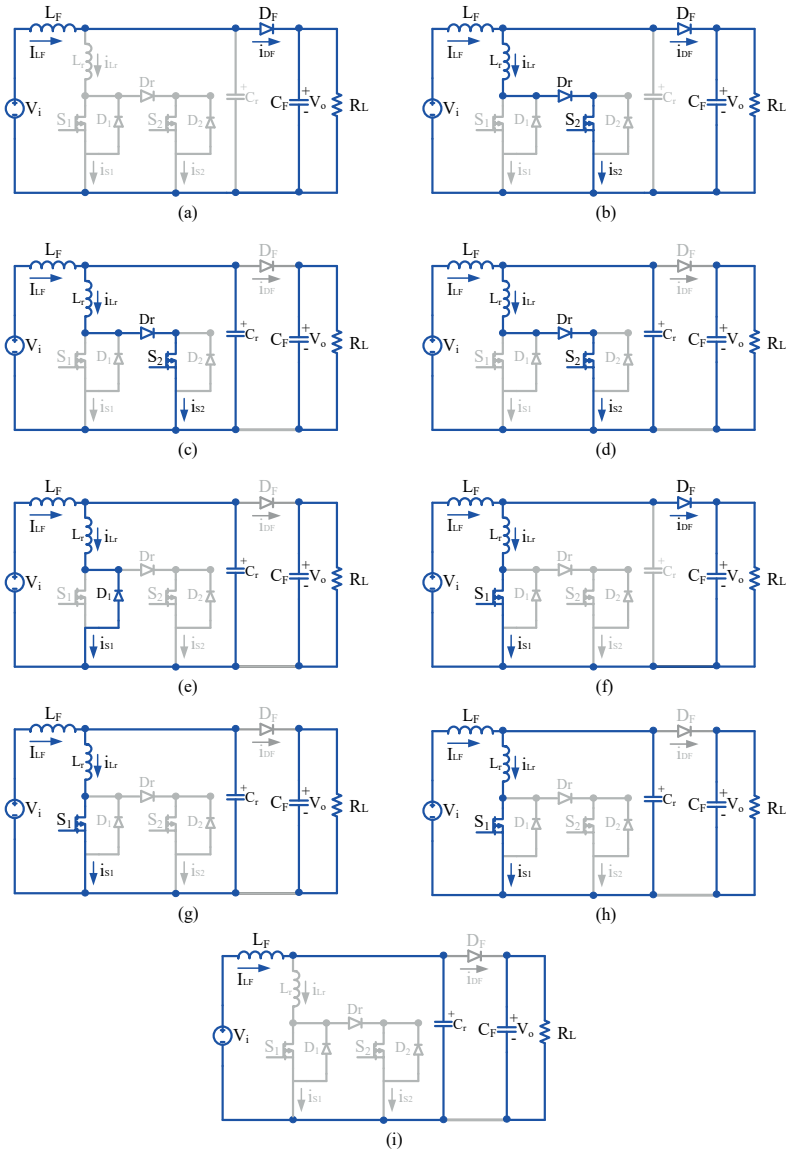


Figure 5. Equivalent circuits of the operating intervals

Interval 4 [Fig. 5(d)]:

The resonance between L_r and C_r occurring in the previous interval continues through the path via $L_r - D_r - S_2 - C_r$ in this interval as well. However, this time, the stored energy of the resonant inductance L_r is transferred to the capacitor C_r . When I_{L_r} decreases to the level of the input current, the voltage across C_r reaches its peak negative value $-V_{C_{rmax}}$. From this moment on, the current I_{L_r} continues to decrease and falls below the input current, and the excess the input current flows into C_r . The resonant capacitor C_r continues to discharge in an increasing direction from the $-V_{C_{rmax}}$ voltage to 0. At the end of this interval, at $t = t_3$, when I_{L_r} drops to zero, and the control signal applied to the auxiliary switch S_2 is removed, it ensures that S_2 and the series-connected diode D_r turn on with ZCS. In this interval, the voltage V_{C_r} drops to the $-V_{C_{rmax}}$ voltage value, resulting in a high voltage stress on the primary diode D_F .

Interval 5 [Fig. 5(e)]:

At $t = t_3$, a negative resonance occurs between C_r and L_r via path $C_r - D_1 - L_r$. While I_{L_r} increases in the negative direction, V_{C_r} decreases in the negative direction. When the C_r voltage reaches zero, the current I_{L_r} reaches its maximum negative value. From this point onwards, I_{L_r} begins to recharge C_r . At any time in this interval, the control signal is applied to S_1 , and the primary switch turns on with ZVT. At the end of this interval, when I_{L_r} reaches zero, the C_r capacitor charges the V_o output voltage, thereby enabling the diode D_F to turn on with ZVS.

Interval 6 [Fig. 5(f)]:

At the beginning of this interval, at $t = t_4$, $V_{C_r} = V_o$, $I_{L_r} = 0$, and the primary diode D_F is in the on state. Because of the constant V_o voltage across L_r , I_{L_r} increases linearly, whereas the current of the diode D_F decreases linearly. At $t = t_5$, once I_{L_r} reaches the level of the input current, diode D_F turns off with ZCS, and this interval is completed. Unlike the classical boost converter, as observed in this converter, the primary diode switches on and off twice, within one operating period. This leads to additional losses.

Interval 7 [Fig. 5(g)]:

At $t = t_5$, a new resonance occurs between the C_r capacitor, charged with the output voltage V_o , and L_r via the $C_r - L_r - S_1$ path. Because the energy stored in C_r is transferred to L_r , the resonant current I_{L_r} increases above the input current level, thereby leading to additional current stress occurs on the switch S_1 . This interval ends when V_{C_r} reaches zero and the current I_{L_r} reaches its maximum value.

Interval 8 [Fig. 5(h)]:

The resonance between L_r and C_r occurred in the previous interval con-

tinues through the path via $C_r - L_r - S_1$ in this interval as well. However, this time, the stored energy of the resonant inductance L_r is transferred to the capacitor C_r . When I_{L_r} decreases to the level of the input current, the voltage across C_r reaches its peak negative value $-V_{Crmax}$. From this moment on, the I_{L_r} current continues to decrease and falls below the input current, and the excess the input current flows into C_r . The resonant capacitor C_r continues to discharge in an increasing direction from the $-V_{Crmax}$ voltage to 0. At the end of this interval, at $t = t_7$, when the current I_{L_r} drops to zero, and the control signal applied to the auxiliary switch S_1 is removed, S_1 is turned on with ZCS. In this interval, the capacitor C_r drops to $-V_{Crmax}$ voltage value as a result a high voltage stress occurs again on the diode D_F .

Interval 9 [Fig. 5(i)]:

At $t = t_7$, when the primary switch S_1 turns off, capacitor C_r begins to charge with a constant input current, causing the voltage V_{Cr} to increase linearly. When the voltage C_r reaches the output voltage V_o , D_F undergoes ZVS during activation; consequently, one switching cycle concludes, initiating the start of the subsequent switching cycle.

3. SIMULATION RESULTS

The examined converters are simulated using PSIM 9.1.1 program to validate their theoretical analyses. The simulation circuit scheme of the example ZVT converter-1 presented by Lee and Kim (2019) is illustrated in Figure 6. The accuracy and validity of the obtained simulation results rely on the accurate definition of the components used in the simulation and the correct determination of their design parameters. The characteristics, capacities, inductances, resistances, and other design parameters of each component used in the simulation process are listed in Table 1. The simulation results are presented in Figures 7–10 for the analysis of the system behavior and the assessment of stability.

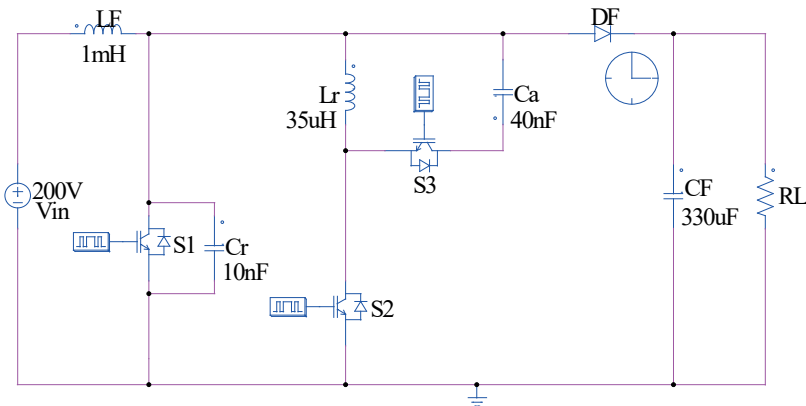


Figure 6. The simulation circuit scheme of the example ZVT converter-1

Table 1. *The design parameters of the components*

| Parameter | Symbol | Value |
|----------------------|----------|--------|
| Input voltage | V_{in} | 200V |
| Output voltage | V_o | 380 V |
| Swithing Frequency | f | 4 kW |
| Output power | P_o | 30 kHz |
| Main inductance | L_F | 1 mH |
| Resonant inductance | L_r | 35 uH |
| Resonant capacitor 1 | C_r | 10 nF |
| Resonant capacitor 2 | C_a | 40 nF |

The waveforms of current and voltage across the primary switch S_1 are depicted in Figure 7. S_1 is activated with ZVT without incurring losses during turn-on and turn-off by utilizing ZVS. The primary switch undergoes high current stress, as shown in Figure 7. This heightened current stress is a notable disadvantage of this converter, as it results in increased conduction losses.

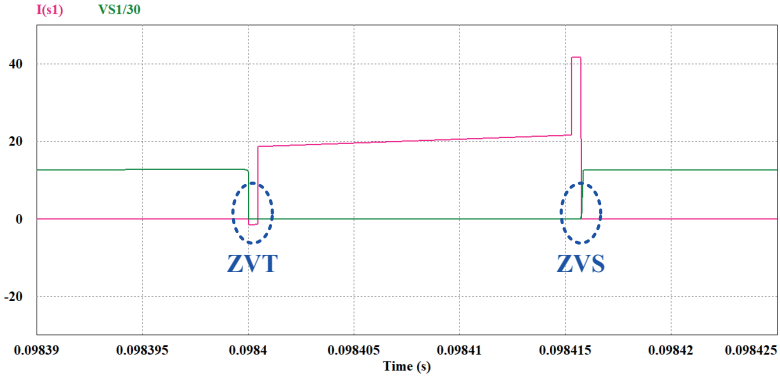


Figure 7. *The waveforms of current and voltage across the primary switch*

The waveforms of the current and voltage across the auxiliary switch S_2 are illustrated in Figure 8, while the waveforms of the current and voltage across the auxiliary switch S_3 are depicted in Figure 9. From these figures, it is evident that auxiliary switches S_2 and S_3 are activated using ZCS and deactivated using ZVS.

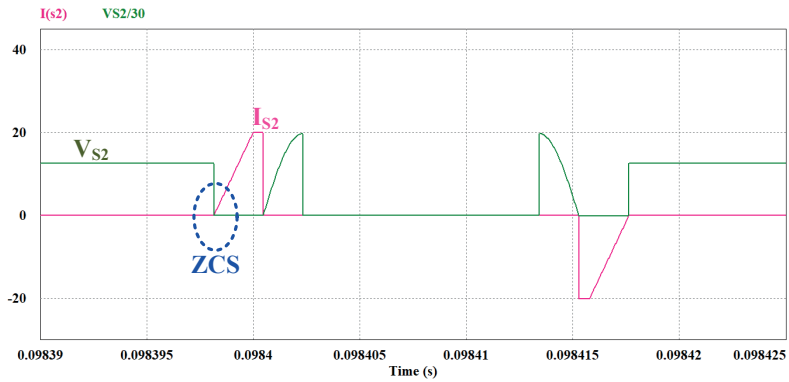


Figure 8. The waveforms of current and voltage across the S_2 auxiliary switch

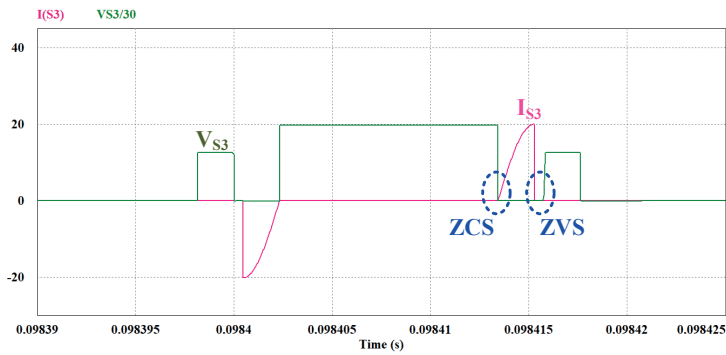


Figure 9. The waveforms of current and voltage across the S_3 auxiliary switch

Figure 10 shows the waveforms of the current and voltage across the primary diode D_F . The DF operates by turning on ZVS and turning off ZCS. However, the diode D_F is subjected to additional current stress.

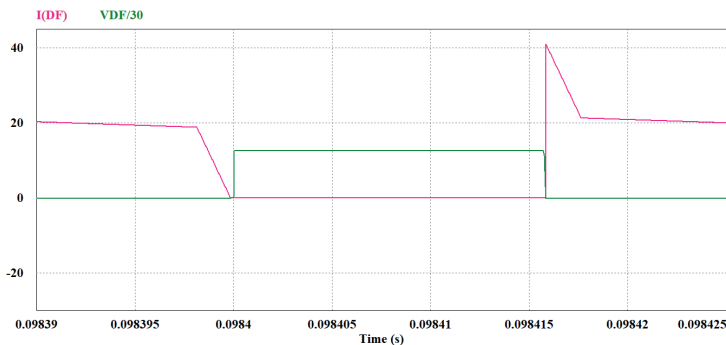


Figure 10. The waveforms of current and voltage across the primary diode

The simulation circuit diagram of the example ZVT converter-2 proposed by Yau et al. (2020) is illustrated in Figure 11. The design parameters of the components utilized in the simulation are presented in Table 2. The simulation outcomes are depicted in Figures 12,13,14 respectively.

Table 1. *The design parameters of the components*

| Parameter | Symbol | Value |
|---------------------|----------|---------|
| Input voltage | V_{in} | 24V |
| Output voltage | V_o | 48 V |
| Swithing Frequency | f | 120 W |
| Output power | P_o | 250 kHz |
| Main inductance | L_F | 100 uH |
| Resonant inductance | L_r | 2 uH |
| Resonant capacitor | C_r | 22 nF |

The waveforms of the current and voltage across primary switch S_1 are depicted in Figure 12, while the waveforms of the current and voltage across the auxiliary switch S_2 are in Figure 13. The primary switch achieves lossless turn-on through ZVT and turns off using ZCS. However, as depicted in the figure, S_1 experienced a high current stress. Meanwhile, auxiliary switch S_2 utilizes ZCS for both activation and deactivation.

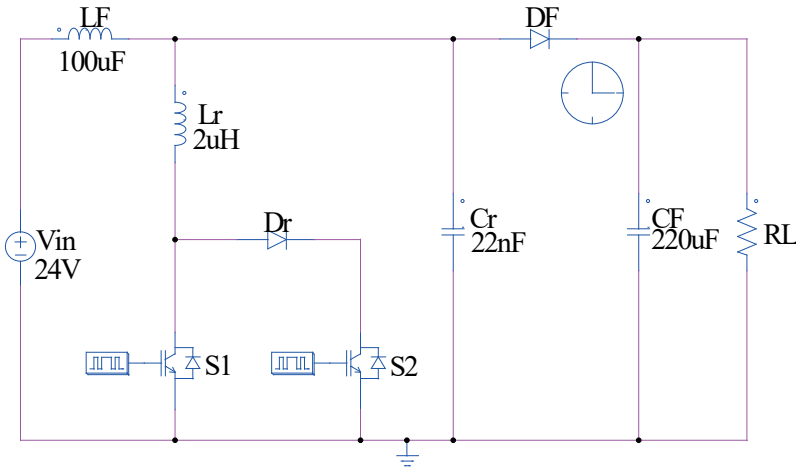


Figure 11. *The simulation circuit scheme of the example ZVT converter-2*

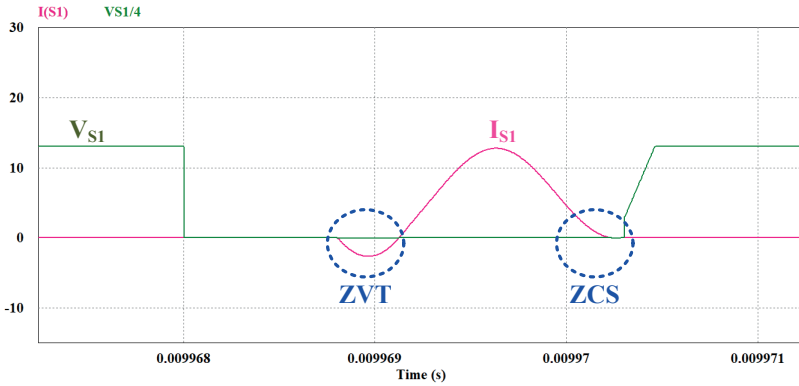


Figure 12. The waveforms of current and voltage across the primary switch

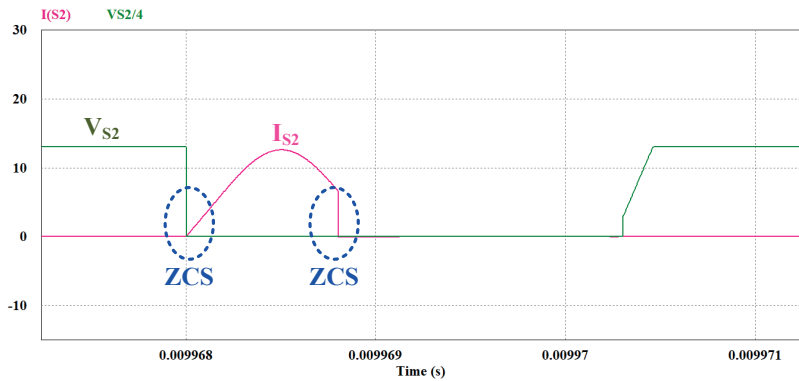


Figure 13. The waveforms of current and voltage across the auxiliary switch

The waveforms of current and voltage across the primary diode, D_F in the converter are illustrated in Figure 14. The diode D_F is turned on with ZVS and turned off with ZCS twice within one cycle. This leads to additional switching losses during conduction and cut-off. Additionally, there are occasional voltage stresses twice per cycle, reaching $-V_{Crmax}$ above the output voltage. This situation poses another significant disadvantage to the converters.

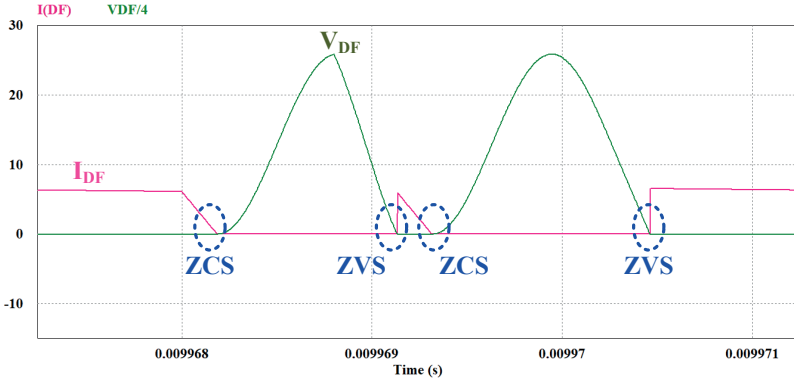


Figure 14. The current and voltage waveforms of the primary diode (10A/div, 40 /div, 1μs/div)

4. CONCLUSION

In this chapter, a detailed examination of two ZVT PWM DC-DC converters with active snubber cells found in the literature is presented. All semiconductor power devices in the proposed converters utilize soft-switching techniques. The primary switch and primary diode in the example ZVT converter-1 experience additional current stress. The S_3 auxiliary switch requires isolation in the driving circuit because it does not have a common emitter connection with other semiconductor power switches, making control of the converter difficult. Additionally, when operated at high frequencies and under high output load conditions, Converter 1 experiences increased losses during turn-on, owing to the use of MOSFETs as switching elements. In the example ZVT converter-2, the snubber cell induces supplementary current stress on the primary switch, resulting in additional conduction losses. Furthermore, using a primary switch with higher current ratings in the converter incurs additional cost. There is also a high-voltage stress on the primary diode, necessitating the use of a diode with higher voltage ratings, consequently increasing the cost. The primary diode switches on and off twice within one period, leading to additional losses. Snubber cells are significant components of DC-DC converters and are utilized to minimize switching losses and reduce electromagnetic interference. However, in some cases, the incorporation of snubber circuits can lead to drawbacks such as energy loss and increased cost. During the design phase, these disadvantages must be balanced with the specific requirements of an application, with the aim of establishing a balance between optimal performance and cost-effectiveness.

REFERENCES

- Aksoy, I., Bodur, H. and Bakan, A. F. (2010) "A new ZVT-ZCT-PWM DC-DC converter", *IEEE Transactions on Power Electronics*, 25(8), 2093-2105.
- Aslay, F. and Ting, N. S. (2022) "Machine Learning-Based Estimation of Output Current Ripple in PFC-IBC Used in Battery Charger of Electrical Vehicles: A Comparison of LR, RF and ANN Techniques", *IEEE Access*, 10, 50078-50086.
- Bodur, H., Bakan, A. and Baysal, M. (2003) "A detailed analytical analysis of a passive resonant snubber cell perfectly constructed for a pulse width modulated dc-dc buck converter", *Electrical Engineering*, 85, 45-52.
- Bodur, H., Yesilyurt, H., and Akboyl, E. (2020) "Passive Lossless Snubber for PFC AC-DC Converters", *Electrica*, 20(1), 97-107.
- Lee, H. J. and Kim, Y. H. (2019) "Analysis and design of a ZVT resonant boost converter using an auxiliary resonant circuit", *Electronics*, 8(4), 466.
- Li, L., Li, B., Wang, Z., Yang, M. and Xu, D. (2022) "Monopolar Symmetrical DC-DC Converter for All DC Offshore Wind Farms", *IEEE transactions on Power Electronics*, 37(4), 4275-4287.
- Li, R. T. H. and Ho, C. N. M. (2016) "An Active Snubber Cell for N-Phase Interleaved DC-DC Converters", *IEEE Journal of Emerging and Selected Topics in Power Electronics*, 4(2), 344-351.
- Sahin, Y. and Ting, N. S. (2018) "Soft switching passive snubber cell for family of PWM DC-DC converters", *Electrical Engineering*, 100(3), 1785-1796.
- Sun, Z. and Bae, S. (2022) "Multiple-Input Soft-Switching DC-DC Converter to Connect Renewable Energy Source in a DC Microgrid", *IEEE Access*, 10, 128380-128391.
- Ting, N. S., Aslay, F. And Sahin, Y. (2022) "A novel zero voltage transition boost converter and artificial neural network-based estimation of converter efficiency", *International Journal of Circuit Theory and Applications*, 50(9), 3251-3265.
- Tseng, C. J. and Chen, C. L. (1998) "A passive lossless snubber cell for nonisolated PWM DC/DC converters", *IEEE Transactions on Industrial Electronics*, 45(4), 593-601.
- Tseng, C. J. and Chen, C. L. (1998) "Novel ZVT-PWM converters with active snubbers", *IEEE transactions on Power Electronics*, 13(5), 861-869.
- Urgun, S. (2012) "Zero-voltage transition-zero-current transition pulsewidth modulation DC-DC buck converter with zero-voltage switching-zero-current switching auxiliary circuit", *IET Power Electronics*, 5(5), 627-634.
- Yau, Y. T., Hwu, K. I. and Shieh, J. J. (2020) "Simple Structure of Soft Switching for Boost Converter", *Energies*, 13(20), 5448.
- Yeşilyurt, H. and Bodur, H. (2019) "New active snubber cell for high power isolated PWM DC-DC converters", *IET Circuits, Devices & Systems*, 13(6), 822-829.



Chapter 10

TREATMENT OF AMOXYCILLIN WASTES USING ADVANCED OXIDATION PROCESSES

M. Fatih ERGİN¹

¹ Associate Prof. Dr., İstanbul University-Cerrahpaşa, Faculty of Engineering, Chemical Engineering, Avcılar Campus, İstanbul, Türkiye, mfergin@iuc.edu.tr, ORCID ID: 0000-0003-4158-368X

1. Introduction

Antibiotics, as fundamental pillars of modern medicine, have been effectively used for the treatment of diseases for many years. Additionally, they are widely employed in veterinary medicine to treat animal diseases and support growth processes. Worldwide, β -lactam antibiotics, with annual sales exceeding 28 billion dollars, constitute a significant economic share, accounting for 3.3% of total drug sales [1]. In this context, the World Health Organization has included 15 β -lactam drugs in the essential medicines list [2]. In Turkey, approximately 24.97% of prescriptions issued by family physicians contain at least one antibiotic. According to 2017 data, Amoxicillin trihydrate holds the top position in terms of cost, with a prescription rate of 29.81% among prescribed antibiotics. The wholesale price of Amoxicillin trihydrate ranges from \$0.02 to \$0.05 per tablet. Continuous production and expansion capacity are necessary to meet the increasing demand and satisfy the demand for essential drugs. The pharmaceutical industry, facing escalating drug development costs and pressure for quality improvement, has focused on enhancing the production efficiency of existing drugs since 2013. The U.S. Food and Drug Administration (FDA) has directed drug manufacturers to take various measures to promote continuous production. These measures include increasing drug availability, shortening production times, improving quality control, and reducing waste production [3].

However, widespread and improper use of pharmaceutical agents, particularly antibiotics, results in a significant amount of antibiotic waste entering water systems and environmental ecosystems. The environmental impacts of these wastes pose potential risks to aquatic organisms, water ecosystems, and human health [4, 5]. Diverse kinds of antibiotics have been found in diverse water settings, from surface waters to groundwater, and from drinking water treatment facilities' input to outflow, at varying concentrations [5-9].

Amoxicillin trihydrate (AMCT), proven to have high solubility, absorption rate, and stability under acidic conditions, is one of the leading β -lactam antibiotics effective against various Gram (+) and Gram (-) bacterial species [10, 11]. This medication is essential for treating a number of illnesses, including tonsillitis, bronchitis, pneumonia, gonorrhoea, ear infections, urinary tract infections, and skin infections. Beta-lactams exhibit bactericidal effects by disrupting cell wall synthesis and activating autolytic enzymes such as autolysins and murein hydrolases. Through inhibition of enzymes involved in the transpeptidation process of peptidoglycan synthesis in the cell wall structure, Amoxicillin causes disruption of cell wall integrity, leading to loss of osmotic resistance and bacterial death [12].

Amoxicillin, introduced in 1972, is generally considered one of the most

effective bactericidal antimicrobials, particularly when effective against bacterial strains susceptible to applied doses. However, the real risk arises with the long-term use of subtherapeutic doses [13]. Antibiotic residues can destroy susceptible bacteria in the human body, making resistant bacteria dominant. This can lead to treatment failure in the use of antimicrobials for disease. The residues of antibiotics in humans and animals, a significant portion of which is excreted through feces, mix with soil, water, and feed substances (grasses, vegetables, fruits) [14].

Amoxicillin trihydrate, being a semi-synthetic antibiotic, can be produced by two main methods: chemical and enzymatic. The chemical process, known as the Dan salt method, achieves high efficiency but involves disadvantages such as low temperatures, the use of solvents such as organochlorides, and additional chemicals. Additionally, this process generates a considerable amount of waste. Therefore, to reduce environmental impact, a transition has been made to an enzymatic process called enzymatic synthesis. This process, carried out with the use of the Penicillin G Acylase (PGA) enzyme, takes place in a watery solution, at neutral pH, and at room temperature. However, PGA's dual nature as a transferase and hydrolase can lead to the formation of side reactions, reducing the efficiency of Amoxicillin trihydrate (Figure 1). Numerous investigations have been carried out to enhance the enzymatic synthesis of amoxicillin trihydrate by optimizing parameters including productivity, selectivity (synthesis-hydrolysis ratio), and efficiency [15, 16]. Given the global intensive production of Amoxicillin

Crystallization, widely employed as a separation and purification technique in processes of crystallization, purification, and separation, is extensively used for the production of specific and active components. This process plays a decisive role in the chemical purity and physical properties of active components through factors such as crystal morphology, size distribution, and crystal structure. The characteristics of crystals can influence factors like the flowability of solids, filterability, tableting behavior, bioavailability, and stability. Crystallization processes are regulated by thermodynamic properties and crystallization kinetics. Understanding these processes is essential for controlling and optimizing existing processes and designing new processes [17-20]

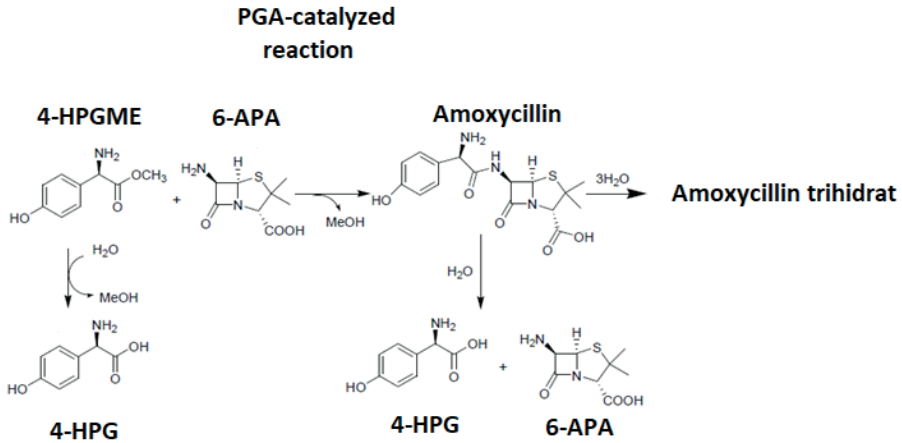


Figure 1. Enzymatic Synthesis of Amoxicillin.

Due to its widespread use in treating bacterial infections, the presence of Amoxicillin in water systems can pose potential risks to the development of resistance and other organisms in the ecosystem. Finding practical ways to eliminate antibiotic residues from water treatment is crucial in this situation. This study focuses on the use of UV (Ultraviolet) and UV-H₂O₂ (Hydrogen Peroxide) techniques to remove amoxicillin. Advanced oxidation techniques, which involve hydrogen peroxide and UV light, have the ability to eliminate antibiotic residues.

2. The Rise of Antibiotic Contamination in Aquatic Ecosystems and Its Environmental Impacts

The incorrect and widespread use of antibiotics has led to a considerable increase in antibiotic residues in water sources, even with modern medicine's enormous improvements. Antibiotics are useful drugs for treating bacterial infections and managing common illnesses. However, the spread of antibiotic residues into water systems is one way that this usage has unintended consequences (Figure 2).

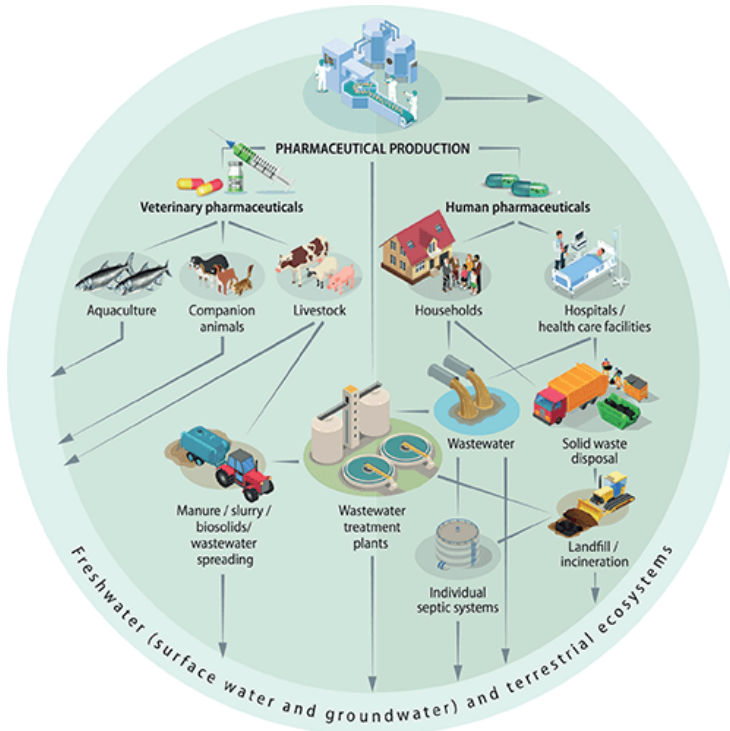


Figure 2. Sources and environmental impacts of medicinal drugs [21].

2.1. Human and Animal Utilization of Antibiotics

Antibiotics are routinely used to treat and manage a wide range of illnesses in both people and animals. These drugs, essential for human health and extensively utilized in animal husbandry, can directly reach water systems through post-use wastewater. With the increasing use of antibiotics, the quantity of waste in these sources also escalates. Antibiotics can infiltrate soil and water systems directly through the use of fertilizers in agricultural fields and medications in animal husbandry. Run offs from agricultural areas and animal waste serve as significant sources transporting antibiotic contamination to water sources. Disposal of antibiotics by users, reaching sewage systems, is another route through which these drugs can enter the environment. Additionally, expired or unused medications may be discarded into the environment through waste disposal, contributing to their presence in water sources.

Antibiotics used in animal agriculture as growth boosters or for veterinary purposes can leach into the soil through manure and even reach groundwater, according to Kümmerer [22]. During antibiotic treatment, residues can reach surface and groundwater in soil or other environmental compartments [22,

23]. Some antibiotics, such as penicillins and ampicillins, easily biodegrade in aquatic environments. However, many antibiotics like tetracyclines, erythromycin, metronidazole, and sulfamethoxazole may not be easily removed through conventional wastewater treatment techniques [23, 24]. Moreover, various antibiotics, such as sulfonamides, strongly bind to sludge, soil, sediment, and manure, displaying a persistent behavior that may hinder further biodegradation. Due to persistent chemical contamination in aquatic environments, bacteria and other microorganisms in aquatic environments may become more resistant to these chemicals. Increased antibiotic resistance and the emergence of hardy organisms in the environment may result from this [23]. Kümmerer [22] emphasized that the biodegradation of persistent antibiotics in sewage treatment plants and other conventional environmental compartments is not a viable option for the reliable removal of these stubborn drug compounds and requires further detailed research [22, 23].

The availability and affordability of drugs and antibiotics, especially those used in veterinary medicine, pose an environmental concern. This situation disrupts the ecological balance by inducing toxicity in organisms within ecosystems and microorganisms in biological treatment systems. The use of drugs, particularly antibiotics, for human and animal health purposes can lead to their presence in the environment through various pathways. The utilization of antibiotics by both humans and in veterinary practices can contribute to their entry into ecosystems.

2.2. Antibiotics Entering the Soil Environment

The physical and chemical characteristics of the soil, the overall climate, and other environmental variables all affect the occurrence of antibiotics in the environment. In environmental chemistry, the behavior and fate of antibiotics in soil are acknowledged as critical subjects. Animal excretion of antibiotics used for veterinary purposes allows them to enter the soil through the use of agricultural fertilizers or farm animal grazing [25]. It is estimated that the loading of antibiotics dumped through fertilization exceeds kilograms per hectare [26, 27]. An estimated 60 million pigs in the United States generate 100,000 million kg of pee and excrement every year, which is subsequently utilized as fertilizer. Additionally, antimicrobial substances used in animals can be released into the environment through agricultural processes. Residues from agricultural operations and resistant bacteria have been reported over the years [26, 28-30]. When sludge is put over fields, substances that have the capacity to retain sludge can have an impact on beneficial organisms and microorganisms. Fertilizers are frequently used in conjunction with medicinal drugs to promote growth in animals housed in barns. These materials may have an impact on soil life [27].

Some antibiotics persist in the environment, especially in soil, for a long

time, while others break down very quickly [26]. The molecular makeup of the medications determines their chemical and physical properties in soil. Thiele-Bruhn has investigated the sorption coefficients in soil, sediment, and sludge as well as the destiny of antibiotic compounds in soil [31]. Antibiotics, depending on their varying structural classes, ionize as amphiphilic or amphoteric, leading to adsorption in soil [26]. The sorption and fixation of materials in soil differ depending on their molecular structure, size, shape, solubility, and hydrophobicity, among other physical and chemical characteristics. Numerous chemicals exhibit polarity, sluggish solubility in water, and hence exhibit severe hindrance in soil [31]. The majority of antibiotics absorb quickly. Antibiotic strength reduction with sorption or fixation does not always imply total antibacterial activity elimination [32]. It has also been shown through experimental investigations that tetracycline and tylosin adsorbed to clay particles in soil have antibacterial action [33]. Tolls [34] presented a thorough analysis of the sorption of veterinary medications in soil. The application of sludge-polluted fertilizer to soil can be expected to increase the degradation rate of antibiotics, resulting in the accumulation of these compounds.

The mobility and modification of antibiotics in soil have been the subject of very few research. According to Alder et al. [35], antibiotics leached from agricultural soils and contaminated surface water. Intensive livestock production and fertilization have resulted in low amounts of antibiotics in groundwater or no antibiotics at all [5, 36]. Distribution coefficients in fertilizer have been determined for oxytetracycline and tylosin, and additionally for sulfachloropyridazine. Since the increasing ratio of fertilizer affects alkaline soil, the distribution coefficient decreases [37]. Hamscher et al. [38] found tetracycline in soil at a depth of 30 centimeters. This data showed that tetracycline was present in soil following liquid fertilizer application, increased in the surrounding environment, and remained [26, 39].

Antibiotics break down due to a variety of circumstances. Although photodegradation of sulfonamides and tetracyclines has been reported [32], it is not a major factor. This is because antibiotics are protected in sludge, reducing the effect of light. Decomposition in soil is primarily related to microbial activity, occurring in the form of enzymatic reactions, hydroxylation, and oxidative decarboxylation processes [40]. Although these reactions are reversible, antibiotics generally break down in soil and fertilizer [41]. Biodegradation in soil increases when microorganisms are added to fertilizer or sludge in large numbers [26, 42].

2.3. Antibiotics Removal in Wastewater Treatment Systems

Cities and industrial facilities often use wastewater treatment systems that may prove insufficient in completely removing antibiotic residues. This can result in untreated water mixing with natural water sources. While the

concentrations of antibiotics in domestic wastewater, measured in ng/L and µg/L levels, do not significantly affect wastewater treatment processes, some studies have indicated substantial impacts at high antibiotic concentrations, affecting microbial activities in wastewater [43-45]. Erythromycin at a dosage of 1 mg/L was demonstrated to lower COD removal efficiency and produce around 5% biogas in anaerobic treatment [45] in a research conducted by Amin et al. [44]. The bio gas and Nitrogen-like gases produced can be used in many fields [46, 47].

Given the prevalence of antibiotic-resistant genes in wastewater treatment facilities, the presence of antibiotics in wastewater is thought to have a role in the emergence and spread of antibiotic-resistant species. The influent and effluent of wastewater treatment facilities contain bacteria including enterococci, *E. coli*, and fecal coliforms that are resistant to antibiotics like vancomycin, ciprofloxacin, trimethoprim, and sulfamethoxazole [48]. In a research conducted with sequential batch reactors, Kim et al. [49] showed that exposure to a concentration of 1 µg/L increased the concentration and rate of tetracycline-resistant bacteria. It is only lately that low antibiotic concentrations in wastewater treatment facilities have been found to have a significant impact on the spread of resistance [50, 51].

The concentration of antibiotics in urban sewage and wastewater treatment facilities is less than 100 times lower than that of hospital wastewater. Anaerobic digestion processes, sewage treatment plant aeration tanks, and urban sewage all include resilient and multidrug-resistant bacteria. Resistance to beta-lactams, quinolones, tetracyclines, sulfamethoxazole/trimethoprim, and other sulfonamides, along with the presence of resistant coding genes, has been identified worldwide in sewage and sludge using classical tools such as processing and resilience. The selective effects of antibiotics on bacterial communities persistently exposed to antibiotics in sewer systems and their role in developing antibiotic resistance on bacterial communities remain to be seen. Sewer system microbial populations may be impacted by antibiotics. Because antibacterial drugs can have a major impact on the breakdown of organic matter, research on their effects on microbial populations—particularly the suppression of sewage bacteria—has received a lot of interest. A decrease in bacterial numbers has been observed in model sewer treatment systems when different antibiotics are applied, accompanying changes in microbial populations.

In order to remove harmful ammonia from sewage, nitrification is an essential stage in the process. Particularly vulnerable is the oxidation of nitrite to nitrate, which is the second step of nitrification. The buildup of particularly harmful nitrite nitrogen at the plant exit might result from uncontrollably inhibiting this cycle. Mild inhibition of methanogens has been demonstrated in several examples pertaining to the propensity of chemicals adsorbed on

anaerobic biomass. In a study focusing on beta-lactams, low $\mu\text{g/L}$ levels were found in the influent and effluent of a domestic wastewater treatment plant [52]. Concentrations of beta-lactams are low compared to their widespread use.

2.4. Pharmaceutical Industry and Production Waste: Environmental Implications of Drug Manufacturing

The pharmaceutical production processes can lead to the infiltration of antibiotic residues into water systems through industrial wastewater discharges. These waste discharges originating from production facilities can contribute to environmental pollution.

A combination of these factors significantly contributes to the increase of antibiotics in water sources. This situation can bring about various environmental issues, including antibiotic resistance and disruptions in ecosystems. Therefore, effective water management strategies and more sustainable antibiotic use are necessary to maintain integrity in combating antibiotic pollution in water systems.

2.4.1. Biological Treatment Methods Applied to Pharmaceutical Industry Wastewaters

In the pharmaceutical sector, biological treatment is a frequently used technique for treating wastewater. Pharmaceutical wastewater is treated using a general treatment system that comprises activated carbon adsorption, primary sedimentation, biological treatment, equalization, and neutralization. Wastewaters initially enter the equalization tank, and then they are directed to the wastewater neutralization tank to achieve a pH level between 6 and 9 [53].

According to Eckenfelder's studies on the biological treatability of wastewater, parameters such as BOD₅, COD, volatile organic carbon, specific pollutants, toxicity, and nitrogen should be examined in addition to the conventional parameters at the effluent. Proper acclimation of biomass during operation is crucial. In case of wastewater toxicity, the necessity of pretreatment or achieving the complete degradation of all separable compounds using extended aeration systems is emphasized. If the toxicity arises from dissolved substances, activated carbon is a highly effective method. Some organic and inorganic substances have an inhibitory effect on the nitrification process used for nitrogen removal. Therefore, the required time for nitrification is crucial. Moreover, considering the importance of volatile emissions in wastewater, scraping should be considered in the design of the activated sludge system [54].

In the study conducted by Kabdaşlı et al. (1999), the characterization of wastewaters originating from the production of three different pharmaceutical

raw materials, namely Paracetamol, Omeprazole, and Mefenoxalon, in a chemical synthesis process was carried out. Experimental studies showed that Paracetamol wastewater exhibited a structure that could be easily biologically degraded. In contrast, for raw Omeprazole wastewater, treatment efficiency was achieved only after chemical oxidation. When Paracetamol and chemically oxidized Omeprazole wastewaters were treated separately or combined and subjected to biological treatment, a COD removal efficiency of around 80% was achieved at F/M ratios of 0.25-0.99 gCOD/gMLSS.day⁻¹. Mefenoxalon exhibited an inert structure and, therefore, could not be treated biologically [55].

The pretreatment of wastewaters from a pharmaceutical firm that mostly employs fermentation for production was investigated in a low-rate anaerobic system by Schlott et al. (1988) before being added to the already-existing extended aeration activated sludge system. In the planned facility, fermentation wastewaters were initially fed into the anaerobic treatment plant, then fermentation wastewaters were combined with chemically synthesized wastewaters and sent to the aerobic treatment plant, achieving 79% COD, 86% BOD, and 83% TSS removal.

Sachs et al. (1978) investigated the treatability of pharmaceutical industry wastewaters containing high COD and low TSS, resulting from organic chemical synthesis, in anaerobic filters (reactor volume = 19 L, T = 35 °C, hydraulic retention time = 36 h). While the initial COD removal in filters fed with 2000 mg/L methanol was 94%, the efficiency decreased when pharmaceutical wastewater, gradually increasing in concentration, was introduced. With diluted concentrations of pharmaceutical wastewater at 2000 mg/L, the efficiency ranged from 70% to 80%. The results of this investigation showed that the anaerobic treatment removed 33% more COD than the real aerobic treatment plant and significantly reduced the amount of dark color in the effluent [56].

2.4.2. Physicochemical Treatment Methods for Pharmaceutical Industry Wastewaters

In the treatment of pharmaceutical industry wastewaters, biological treatment is considered the most suitable treatment alternative. However, due to their inherent composition, these wastewaters cannot be directly subjected to biological treatment and therefore need to undergo a pretreatment. Particularly, antibiotic formulation wastewaters, which contain high concentrations of non-biodegradable substances, do not achieve efficient treatment when directly subjected to biological treatment. This is attributed to the toxic effects on aquatic microorganisms, leading to their inhibition and the formation of resistant bacteria [8, 57, 58]. Consequently, for pharmaceutical wastewaters causing inhibition in biological treatment facilities at high

concentrations, it is necessary to apply a chemical pretreatment process before introducing them to biological treatment.

Gürel et al. (1998) conducted a research whereby they assessed the impact of chemical oxidation on the elimination of organic matter before biological treatment in a pharmaceutical enterprise involved in chemical synthesis, particularly in the manufacturing of Mefenoxalon and Omeprazole. As oxidants, hydrogen peroxide (H_2O_2) and sodium hypochlorite ($NaOCl$) were employed. As a result of chemical oxidation, a 25% total organic carbon (TOC) removal was achieved in the wastewater sample containing Mefenoxalon, and a 30% TOC removal was observed in the wastewater sample containing Omeprazole. Subsequent to biological treatment, a COD removal efficiency of 80% was determined for Paracetamol and pre-oxidized Omeprazole-containing samples. However, it was observed that the Mefenoxalon-containing sample exhibited resistance to biological treatment even after oxidation [59].

Rabosky et al. (1993) conducted a coagulation study on pharmaceutical industry wastewaters, employing three different approaches. In the first approach, weak anionic, weak cationic, medium cationic, and strong cationic polyelectrolytes were used, and the best efficiency was achieved with a weak anionic polyelectrolyte. In the second approach, various types of polyelectrolytes were used without alum and lime, and the best performance was exhibited by a weak cationic polyelectrolyte. In the third approach, the pH was adjusted to 7 using lime, and varying amounts of alum concentration were added with a constant polyelectrolyte concentration of 1 mg/L. The optimum treatment efficiency was achieved with a 15 mg/L alum concentration [60].

Laboratory-scale tests were carried out in different research by Ternes et al. (2002) to look at the removal of certain medications (Diclofenac, Carbamazepine, Clofibrac Acid, and Bezafibrate) from drinking water. The poor sorption qualities of the medications prevented any of them from being removed, as indicated by the results of the Jar test conducted with $FeCl_3$ coagulant. Nonetheless, it was discovered that the ozonation procedure was quite successful in getting rid of these polar substances. Over 90% of Carbamazepine and Diclofenac were removed at an ozone concentration of 5 mg/L, whereas 50% of Bezafibrate was removed at an ozone concentration of 1.5 mg/L. At 3 mg/L ozone concentration, Clofibrac Acid remained stable, but after the ozonation process, effective removal of the selected drugs from water was ensured through granular activated carbon filtration [61].

In recent years, advanced oxidation processes have emerged as significant potential for the treatment of industrial wastewaters containing dissolved pollutants, non-biodegradable toxic, and refractory organic substances.

3. Antibiotic Separation Studies: Comparative Analyses of Treatment Methods in Turkey and Worldwide

Antibiotic removal was shown to be more successful in secondary treatment processes as opposed to primary treatment processes in a research by Gulkowska et al. (2008) carried out at wastewater treatment plants in Hong Kong. Antibiotic concentrations for different antibiotics were assessed in samples taken from four treatment facilities for sewage in Hong Kong and one facility in Shenzhen. The samples from Hong Kong had the greatest quantities of cephalexin, ranging from 670 to 2900 ng/L, whereas samples from Shenzhen showed no detectable levels of the drug. Comparing norfloxacin (5-78%) and tetracycline (7-73%) to other antibiotics, greater clearance efficiencies were often seen. It was determined that traditional therapeutic approaches were insufficient for cephalexin [62].

Li and Zhang (2010) identified the active sludge process as another commonly used method for the removal of cephalexin and ampicillin antibiotic groups. The target antibiotics, namely cephalexin and two sulfonamides, were successfully eliminated using this approach in freshwater and saline sewage systems by biological degradation. Adsorption was the main method used to remove ampicillin. On the other hand, removal efficiencies (30-90%) were reported based on relatively low input concentrations (e.g., 100 µg/L) stated in the study [63].

Bing and Tong (2011) collected composite samples (24 hours) throughout various seasons to study the removal of 20 chosen antibiotics from seven antibiotic classes in two wastewater treatment facilities (WWTPs) in Hong Kong over the course of a year. 52–100% of the antibiotics, including ampicillin, cephalexin, sulfamethoxazole, sulfadiazine, sulfamethazine, chlortetracycline, and vancomycin, were successfully eliminated. Using activated sludge, ampicillin and cephalexin were eliminated with 91–99% efficiency. In a different research, Bing and Tong (2012) methodically investigated the effects of pH on the chlorination behavior of 12 antibiotics in the output matrix of the activated sludge process in Hong Kong. The investigation's findings demonstrated that pH affected both the general response rates of free chlorine species and the three different antibiotic kinds. It was demonstrated that a pH between 5.5 and 8.5 was necessary for the bulk of antibiotics to be eliminated (except from cephalexin and tetracycline). Anionic antibiotic types have a tendency to be more reactive to free chlorine than cationic antibiotic types [64].

Estrada et al. (2012) examined the removal of cephalexin using the electro-Fenton process with RuO₂/Ti anode oxidation, an advanced oxidation method. Although effective COD removal was not achieved, satisfactory COD removal was obtained through a different biological treatment process. Guo

and Chen (2015) evaluated the effect of a combined active sludge-algae system on the removal of cephalosporins, achieving a 94.9% removal efficiency for cephalexin [65]. Kong et al. (2016) investigated the adsorption of cephalexin antibiotic using activated carbon and observed that activated carbon adsorbed approximately 95% of cephalexin at low concentrations [66].

In a study by Kurt and Yonar (2017), the advanced oxidation process was applied to the treatment of wastewater samples containing antibiotics from the β -lactam group (cephalexin, cefazolin, cefoperazone, cefaclor, cefuroxime) and penicillins (ampicillin). Taguchi's Orthogonal Array L9 Experimental Design was used for the design of Fenton processes. Under conditions of $[\text{H}_2\text{O}_2/\text{Fe}^{+2}]$: 6.6 and pH:3, 86.26% COD removal and 67.5% TOC mineralization were achieved. Additionally, under conditions of $[\text{H}_2\text{O}_2/\text{Fe}^{+2}]$: 10 and pH:3.5, 81.6% COD removal and 62.35% TOC mineralization were obtained [67].

However, there are also publications expressing negative views on the biological removal of antibiotics [68, 69]. This is because the concentrations studied in the above publications are relatively low. However, it is not clearly stated in these studies whether an antibiotic at this concentration is actually broken down by biological processes or whether it is biologically retained. Both increasing high concentrations and biological accumulation make the treatment of antibiotics with classical processes very difficult.

4. Advanced Oxidation Processes (AOPs) in Wastewater Treatment: Harnessing Oxidative Power for Environmental Remediation

Advanced Oxidation Processes (AOPs) are recommended as an alternative for the removal of refractory chemicals in wastewater treatment plants that may hinder the operation of facilities or pass through treatment systems without degradation, sometimes causing significant inhibition in ecosystems despite not posing a major hindrance in active sludge reactors [70]. The common and fundamental features of AOPs are based on the formation of free radicals such as hydroxyl ($\bullet\text{OH}$) and peroxy ($\text{HO}_2\bullet$), with very high chemical (combinations of ozone with various oxidants and catalysts) and photochemical (ozone, hydrogen peroxide, and Fenton reagents activated by ultraviolet light) oxidation potentials. When optimized and applied at the correct stage in conventional treatment systems, AOPs have been known to enhance treatment efficiency and significantly contribute to maintaining the water quality standards in receiving environments. In recent years, the effectiveness of AOPs in reducing concentrations of toxic and/or refractory pollutants in conventional biological treatment systems to levels tolerable by microorganisms in wastewater and aquatic organisms in receiving water bodies has been investigated using bacterial growth and substrate removal inhibition tests, biochemical tests, and respirometric methods for respiratory inhibition measurements [71-73]. While conventional methods such as

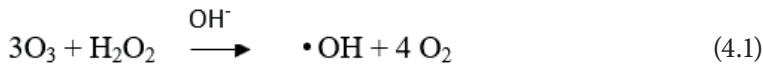
activated carbon adsorption, flocculation, filtration, and biological treatment can remove toxic water pollutants, they fall short in breaking down stable aromatics. AOPs, by generating powerful oxidizing radicals such as $\bullet\text{OH}$ that can effectively degrade many organic pollutants, present a potential solution for the treatment of wastewater containing toxic pollutants. Various advanced oxidation processes, including homogeneous, heterogeneous, and combined systems, are employed in the treatment of wastewaters [74].

4.1. Advanced Oxidation Processes in Homogeneous Photokinetics: Unraveling the Mechanistic Frontiers

In a dark environment and at high pH, it is feasible to generate ozone (O_3/OH^-), ozone with hydrogen peroxide ($\text{O}_3/\text{H}_2\text{O}_2$), and hydroxyl radicals ($\bullet\text{OH}$) through the Fenton reaction. Due to its utilization in this study, detailed information about Fenton processes, whose primary mechanism involves the catalytic decomposition of H_2O_2 with an iron catalyst, is provided under a separate heading.

4.1.1. Ozone Treatment at Elevated pH Levels

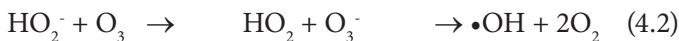
The net reaction of ozone with OH^- results in the formation of $\bullet\text{OH}$ radicals.



It has been shown by Staehelin and Hoigné (1982) that elevated pH alters the ozone process. The capture of $\bullet\text{OH}$ and radical-radical pair reactions might upset the closed-chain reaction started by O_3 and OH^- in the presence of bicarbonate, carbonate, and organic components of humic substances. Furthermore, $\bullet\text{OH}$ can be captured by macroand/or micropollutants in the reaction environment. The carbonate ion is 20 times more effective at trapping radicals than the bicarbonate ion when pH is greater than 10.3 [75].

4.1.2. Ozonation in the Presence of Hydrogen Peroxide

Glaze et al. (1987) demonstrated that the conjugate base of H_2O_2 (HO_2^-) can initiate the ozone decomposition cycle to generate $\bullet\text{OH}$ radicals. Although H_2O_2 reacts with O_3 to produce $\bullet\text{OH}$ radicals, this reaction is quite slow [76]. The reaction rate increases with increasing pH, and the optimum pH is around 7-8.

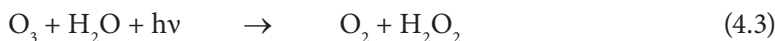


4.2. Photocatalytic Homogeneous Advanced Oxidation Processes

Advanced Oxidation Processes (AOPs) come in a variety of forms, all centered around the production of $\bullet\text{OH}$ radicals in the presence of UV or near-UV (UV-A) light. Comprehensive descriptions of the Photo-Fenton and Photo-Fenton-like advanced oxidation processes are given under a different topic, among the several forms of photocatalytic homogeneous AOPs.

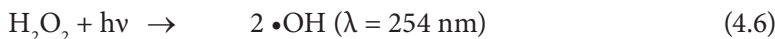
4.2.1. Advanced Oxidation with Ozone and UV-C

This process involves direct ozonation, ozone decomposition, and a photolytic reaction, where O_3 can absorb UV radiation at a maximum wavelength of 253.7 nm in liquid solutions, leading to the accumulation of H_2O_2 throughout this process.



4.2.2. Advanced Oxidation Process with H_2O_2 /UV-C

In this process, H_2O_2 is activated by UV-C to generate $\bullet\text{OH}$ radicals [70].



At a wavelength of 254 nm, the molar extinction coefficient of H_2O_2 ($\epsilon = 19.61$) is much lower than that of ozone ($\epsilon = 3300 \text{ M}^{-1}\cdot\text{cm}^{-1}$). To generate a sufficient amount of $\bullet\text{OH}$ radicals, high concentrations of H_2O_2 are required in the environment [77].

4.3. Application of Advanced Oxidation Processes in the Treatment of Pharmaceutical Industry Wastewaters

Çelebi and Sponza (2008) investigated the chemical pre-treatment of three synthetic wastewater samples containing typical concentrations of cephalosporin, penicillin, and quinolone group antibiotics in order to enhance the biological treatability of formulation wastewaters. They emphasized that ozonation at $\text{pH} = 7$ is an effective method for the efficient removal of active substances in formulation wastewaters. For $\text{COD}_0 = 450 \text{ mg/L}$ and $\text{pH} = 7$, the biological treatability ratio (BOD_5/COD) increased from 0 to 0.07 for cephalosporin, from 0 to 0.28 for penicillin, and from 0.02 to 0.31 for quinolone, partially improving the biological treatability. At an ozone dose of $2960 \text{ mg}/(\text{L}\cdot\text{min})$, COD removal efficiencies were 79%, 81%, and 68% for cephalosporin, quinolone, and penicillin, respectively. When the pH was increased from 7 to 12, COD removal efficiencies for cephalosporin and penicillin increased from

83% and 70% to 89% and 85%, respectively [78].

Özilkiz (2002) investigated the treatability of a synthetic wastewater composed of Amoxicillin Trihydrate and Potassium Clavulanate, a mixture of synthetic penicillins, using $\text{H}_2\text{O}_2/\text{UV-C}$ and $\text{Fe}^{2+}/\text{H}_2\text{O}_2/\text{UV-C}$ processes. For the $\text{H}_2\text{O}_2/\text{UV-C}$ process, a single application of UV-C achieved 6% COD removal at $\text{COD}_0 = 300 \text{ mg/L}$. The effect of pH on the process efficiency was examined, and it was observed that the process efficiency was not affected by pH, with 77% COD removal at $\text{pH} = 3.5$ and 78% COD removal at $\text{pH} = 5.5$. At the selected optimum H_2O_2 concentration (18.75 mM), the BOD5/COD ratio increased from 0.01 to 0.41 after 180 minutes of treatment. At the optimum $\text{H}_2\text{O}_2/\text{Fe}^{2+}$ ratio of 10:1 (9.4 mM H_2O_2 ; 0.98 mM Fe^{2+}), the BOD5/COD ratio increased from 0.01 to 0.58 after 180 minutes. This system was chosen as the most effective method for treating synthetic penicillin formulation wastewater in terms of both efficiency and cost [79].

In a study by Zwiener and Frimmel (2000), pharmaceutical pollutants from domestic wastewater, agricultural areas, and metabolic residues of humans and animals in surface waters were detected. Ibuprofen, Diclofenac (pain relievers), and Clofibric Acid (lipid-lowering) were the most abundant substances in the water, and their sensitivities to oxidation were examined using O_3 and $\text{O}_3/\text{H}_2\text{O}_2$ processes. Applying $\text{O}_3/\text{H}_2\text{O}_2$ at a ratio of 1 mg/L O_3 to 0.4 mg/L H_2O_2 resulted in approximately 50% removal of Clofibric Acid and Ibuprofen concentrations, and complete degradation of Diclofenac was observed. When the $\text{O}_3/\text{H}_2\text{O}_2$ ratio was increased to 3.7 mg/L O_3 to 1.4 mg/L H_2O_2 , a 90% removal was achieved for Clofibric Acid and Ibuprofen concentrations [80].

Vogna et al. (2004) investigated the advanced oxidation of Diclofenac, a commonly used drug, in water. After 90 minutes of reaction time, ozonation achieved 32% mineralization, and $\text{H}_2\text{O}_2/\text{UV}$ processes achieved 39% mineralization. Ternes et al. (2002) demonstrated the effectiveness of the ozonation process in eliminating polar compounds. A concentration of 5 mg/L ozone achieved more than 90% removal of Carbamazepine and Diclofenac, while a concentration of 1.5 mg/L ozone achieved 50% removal of bezafibrate. After the ozonation process, except for Clofibric Acid, the effective removal of selected drugs from water was achieved by subsequent granular activated carbon filtration [81].

References

1. Hamed, R.B., et al., *The enzymes of β -lactam biosynthesis*. Natural product reports, 2013. **30**(1): p. 21-107.
2. Organization, W.H., *WHO model list of essential medicines, 20th list (March 2017, amended August 2017)*. 2017.
3. Lee, S., *Modernizing the way drugs are made: a transition to continuous manufacturing*. FDA website, Published May, 2017. **17**.
4. Kümmerer, K., *The presence of pharmaceuticals in the environment due to human use—present knowledge and future challenges*. Journal of environmental management, 2009. **90**(8): p. 2354-2366.
5. Hirsh, A.V., *The investigation and therapeutic*. A Textbook of In Vitro Fertilization Assisted Reproduction: The Bourn Hall Guide to Clinical Laboratory Practice. 1999. **27**.
6. Heberer, T., *Occurrence, fate, and removal of pharmaceutical residues in the aquatic environment: a review of recent research data*. Toxicology letters, 2002. **131**(1-2): p. 5-17.
7. Kim, S.W., et al., *Functional amino acids and fatty acids for enhancing production performance of sows and piglets*. Asian-Australasian Journal of Animal Sciences, 2007. **20**(2): p. 295-306.
8. Wollenberger, L., B. Halling-Sørensen, and K.O. Kusk, *Acute and chronic toxicity of veterinary antibiotics to *Daphnia magna**. Chemosphere, 2000. **40**(7): p. 723-730.
9. Kümmerer, K. and A. Henninger, *Promoting resistance by the emission of antibiotics from hospitals and households into effluent*. Clinical microbiology infection, 2003. **9**(12): p. 1203-1214.
10. Zayed, M. and S. Abdallah, *Synthesis and structure investigation of the antibiotic amoxicillin complexes of d-block elements*. Spectrochimica Acta Part A: Molecular Biomolecular Spectroscopy, 2005. **61**(9): p. 2231-2238.
11. Ghassempour, A., et al., *Investigation of the solid state properties of amoxicillin trihydrate and the effect of powder pH*. Aaps PharmSciTech, 2007. **8**: p. 91-96.
12. Bernatová, S., et al., *Following the mechanisms of bacteriostatic versus bactericidal action using Raman spectroscopy*. Molecules, 2013. **18**(11): p. 13188-13199.
13. Singh, S., et al., *ANTIBIOTIC RESIDUES: A GLOBAL CHALLENGE*. Pharma Science Monitor, 2014. **5**(3).
14. Şahin, K., *TÜBA-İnsan ve Hayvan Sağlığında Akılcı Antibiyotik Kullanımı ve Antibiyotik Dirençlilik Raporu*. Türkiye Bilimler Akademisi Yayınları, 2017.
15. Bruggink, A., *Synthesis of β -lactam antibiotics*. 2001: Springer Science & Business Media.

16. Giordano, R.C., M.P. Ribeiro, and R.L. Giordano, *Kinetics of β -lactam antibiotics synthesis by penicillin G acylase (PGA) from the viewpoint of the industrial enzymatic reactor optimization*. Biotechnology advances, 2006. **24**(1): p. 27-41.
17. Ergin, M. and H. Yasa, *Determination of amoxicillin trihydrate impurities 4-hydroxyphenylglycine (4-HPG) and 6-Aminopenicylanic acid (6-APA) by means of ultraviolet spectroscopy*. Methods Applications in Fluorescence, 2022. **10**(3): p. 035007.
18. ERGİN, M., *Yıkama Metodu Kullanılarak Saflaştırılan Amoksisilin Trihidratın Taguchi Yöntemi ile Optimizasyonu*. Journal of the Institute of Science Technology, 2022. **12**(2): p. 933-945.
19. Ergin, M., *Purification of amoxicillin trihydrate in the presence of degradation products by different washing methods*. CrystEngComm, 2021. **23**(46): p. 8121-8130.
20. Celik Onar, H., M.F. Ergin, and H. Yasa, *Investigating the Role of Citric Acid as a Natural Acid on the Crystallization of Amoxicillin Trihydrate*. ACS omega, 2023. **8**(39): p. 36344-36354.
21. OECD, *Pharmaceutical Residues in Freshwater*. 2019.
22. Kümmerer, K., *Significance of antibiotics in the environment*. Journal of Antimicrobial Chemotherapy, 2003. **52**(1): p. 5-7.
23. Turkdogan, F.I. and K. Yetilmezsoy, *Appraisal of potential environmental risks associated with human antibiotic consumption in Turkey*. Journal of hazardous materials, 2009. **166**(1): p. 297-308.
24. Halling-Sørensen, B., G. Sengeløv, and J. Tjørnelund, *Toxicity of tetracyclines and tetracycline degradation products to environmentally relevant bacteria, including selected tetracycline-resistant bacteria*. Archives of environmental contamination toxicology letters, 2002. **42**: p. 263-271.
25. Jørgensen, S.E. and B. Halling-Sørensen, *Drugs in the environment*. Chemosphere, 2000. **40**(7): p. 691-699.
26. Kemper, N., *Veterinary antibiotics in the aquatic and terrestrial environment*. Ecological indicators, 2008. **8**(1): p. 1-13.
27. Harms, K. and J. Bauer, *Detection and occurrence of antibiotics and their metabolites in pig manure in Bavaria (Germany)*. RESISTANCE IN THE ENVIRONMENT, 2012: p. 293.
28. Teuber, M., *Spread of antibiotic resistance with food-borne pathogens*. Cellular Molecular Life Sciences CMLS, 1999. **56**: p. 755-763.
29. Rice, L.B., *Emergence of vancomycin-resistant enterococci*. Emerging infectious diseases, 2001. **7**(2): p. 183.
30. Olsen, S.J., et al., *A nosocomial outbreak of fluoroquinolone-resistant Salmonella infection*. New England Journal of Medicine, 2001. **344**(21): p. 1572-1579.
31. Thiele-Bruhn, S., *Pharmaceutical antibiotic compounds in soils—a review*. Jour-

- nal of plant nutrition soil science, 2003. **166**(2): p. 145-167.
32. Sengeløv, G., et al., *Bacterial antibiotic resistance levels in Danish farmland as a result of treatment with pig manure slurry*. Environment international, 2003. **28**(7): p. 587-595.
 33. Chander, Y., et al., *Antibacterial activity of soil-bound antibiotics*. Journal of environmental quality, 2005. **34**(6): p. 1952-1957.
 34. Tolls, J., *Sorption of veterinary pharmaceuticals in soils: a review*. Environmental science technology, 2001. **35**(17): p. 3397-3406.
 35. Alder, A.C., et al., *Occurrence and fate of fluoroquinolone, macrolide, and sulfonamide antibiotics during wastewater treatment and in ambient waters in Switzerland*. 2001, ACS Publications.
 36. Kemper, N., et al. *Determination of antibiotic residues in leachate of conventional and organic dairy farms*. in *Proceedings of the XIIIth International Congress in Animal Hygiene, Tartu, Estland, June*. 2007.
 37. Boxall, A.B., et al., *The sorption and transport of a sulphonamide antibiotic in soil systems*. Toxicology letters, 2002. **131**(1-2): p. 19-28.
 38. Hamscher, G., et al., *Determination of persistent tetracycline residues in soil fertilized with liquid manure by high-performance liquid chromatography with electrospray ionization tandem mass spectrometry*. Analytical chemistry, 2002. **74**(7): p. 1509-1518.
 39. Samuelsen, O.B., V. Torsvik, and A. Ervik, *Long-range changes in oxytetracycline concentration and bacterial resistance towards oxytetracycline in a fish farm sediment after medication*. Science of the Total Environment, 1992. **114**: p. 25-36.
 40. Al-Ahmad, A., F. Daschner, and K. Kümmerer, *Biodegradability of cefotiam, ciprofloxacin, meropenem, penicillin G, and sulfamethoxazole and inhibition of waste water bacteria*. Archives of environmental contamination toxicology letters, 1999. **37**: p. 158-163.
 41. Ingerslev, F. and B. Halling-Sørensen, *Biodegradability properties of sulfonamides in activated sludge*. Environmental Toxicology Chemistry: An International Journal, 2000. **19**(10): p. 2467-2473.
 42. Nwosu, V.C., *Antibiotic resistance with particular reference to soil microorganisms*. Research in Microbiology, 2001. **152**(5): p. 421-430.
 43. Ingerslev, F. and B.I. Halling-Sørensen, *Biodegradability properties of sulfonamides in activated sludge*. %J Environmental Toxicology Chemistry: An International Journal, 2000. **19**(10): p. 2467-2473.
 44. Amin, M.M., et al., *Influence of the antibiotic erythromycin on anaerobic treatment of a pharmaceutical wastewater*. Environmental science technology, 2006. **40**(12): p. 3971-3977.
 45. Gartiser, S., et al., *Anaerobic inhibition and biodegradation of antibiotics in ISO test schemes*. Chemosphere, 2007. **66**(10): p. 1839-1848.

46. YAŞA, H., et al., *Importance of inert gases for chemical transportation*. Proceedings Book, 2016: p. 825.
47. ERGİN, A. and M.F. ERGİN, *Reduction of ship based CO2 emissions from container transportation*. %J International Journal of Computational Experimental Science Engineering, 2018. **4**(3): p. 1-4.
48. Nagulapally, S.R., et al., *Occurrence of ciprofloxacin-, trimethoprim-sulfamet-hoxazole-, and vancomycin-resistant bacteria in a municipal wastewater treatment plant*. Water Environment Research, 2009. **81**(1): p. 82-90.
49. Kim, S., et al., *Removal of antibiotics in wastewater: effect of hydraulic and solid retention times on the fate of tetracycline in the activated sludge process*. Environmental science technology, 2005. **39**(15): p. 5816-5823.
50. Le-Minh, N., et al., *Fate of antibiotics during municipal water recycling treatment processes*. Water research, 2010. **44**(15): p. 4295-4323.
51. Jury, K.L., et al., *Are sewage treatment plants promoting antibiotic resistance?* Critical Reviews in Environmental Science Technology, 2011. **41**(3): p. 243-270.
52. Christian, T., et al., *Determination of antibiotic residues in manure, soil, and surface waters*. Acta hydrochimica et hydrobiologica, 2003. **31**(1): p. 36-44.
53. Rabosky, J. and W. Schuliger. *Water and wastewater survey for the Brazilian Merck, Sharp and Dohme chemical and pharmaceutical plant*. in *Proceedings 37 th Industrial Waste Conference, West Lafayette, IN, May 11-13, 1982*. Purdue Univ., 1983. p 259-270. 3. 1983.
54. Eckenfelder Jr, W.W., *Biological treatability studies: new regulations require a new approach*. Environmental progress, 1995. **14**(3): p. 172-175.
55. Kabdaşlı, I., M. Gürel, and O. Tünay, *Pollution prevention and waste treatment in chemical synthesis processes for pharmaceutical industry*. Water science technology, 1999. **39**(10-11): p. 265-271.
56. Sachs, E.F., J.C. Jennett, and M. Rand. *Anaerobic treatment of synthesized organic chemical pharmaceutical wastes*. in *Proceedings 33rd Annual Industrial Waste Conference*. 1978. Purdue University Lafayette.
57. Kümmerer, K., A. Al-Ahmad, and V. Mersch-Sundermann, *Biodegradability of some antibiotics, elimination of the genotoxicity and affection of wastewater bacteria in a simple test*. Chemosphere, 2000. **40**(7): p. 701-710.
58. Ferrari, B.t., et al., *Ecotoxicological impact of pharmaceuticals found in treated wastewaters: study of carbamazepine, clofibric acid, and diclofenac*. Ecotoxicology environmental safety, 2003. **55**(3): p. 359-370.
59. Gürel, M., I. Kabdaşlı, and O. Tünay, *Kimyasal sentez ile üretim yapan bir ilaç endüstrisi atıksularının karakterizasyonu ve arıtılabilirliği*, İTÜ 6. Endüstriyel Kirlenme Kontrolü Sempozyumu, 1998: p. 3-5.
60. Rabosky, J. and W. Schuliger. *Water and wastewater survey for the Brazilian Merck, Sharp and Dohme chemical and pharmaceutical plant*. in *Proceedings 37*

- th Industrial Waste Conference, West Lafayette, IN, May 11-13, 1982. Purdue Univ., 1983. p 259-270. 3 Fig, 5 Tab. 1983.*
61. Ternes, T.A., et al., *Removal of pharmaceuticals during drinking water treatment.* Environmental science technology, 2002. **36**(17): p. 3855-3863.
 62. Gulkowska, A., et al., *Removal of antibiotics from wastewater by sewage treatment facilities in Hong Kong and Shenzhen, China.* Water research, 2008. **42**(1-2): p. 395-403.
 63. Li, B. and T. Zhang, *Biodegradation and adsorption of antibiotics in the activated sludge process.* Environmental science technology, 2010. **44**(9): p. 3468-3473.
 64. Li, B. and T. Zhang, *Mass flows and removal of antibiotics in two municipal wastewater treatment plants.* Chemosphere, 2011. **83**(9): p. 1284-1289.
 65. Estrada, A.L., Y.-Y. Li, and A. Wang, *Biodegradability enhancement of wastewater containing cefalexin by means of the electro-Fenton oxidation process.* Journal of hazardous materials, 2012. **227**: p. 41-48.
 66. Kong, Q., et al., *Isotherm, kinetic, and thermodynamic equations for cefalexin removal from liquids using activated carbon synthesized from loofah sponge.* Desalination Water Treatment, 2016. **57**(17): p. 7933-7942.
 67. Kurt, A., et al., *Treatment of antibiotics in wastewater using advanced oxidation processes (AOPs).* Physico-chemical wastewater treatment resource recovery, 2017. **175**.
 68. Sukul, P. and M. Spiteller, *Fluoroquinolone antibiotics in the environment.* Reviews of environmental contamination toxicology letters, 2007: p. 131-162.
 69. Kim, S. and D.S. Aga, *Potential ecological and human health impacts of antibiotics and antibiotic-resistant bacteria from wastewater treatment plants.* Journal of Toxicology Environmental Health, Part B, 2007. **10**(8): p. 559-573.
 70. Legrini, O., E. Oliveros, and A. Braun, *Photochemical processes for water treatment.* Chemical reviews, 1993. **93**(2): p. 671-698.
 71. Gutierrez, M., J. Etxebarria, and L. De Las Fuentes, *Evaluation of wastewater toxicity: comparative study between Microtox® and activated sludge oxygen uptake inhibition.* Water Research, 2002. **36**(4): p. 919-924.
 72. Ho, T.-F.L. and J.R. Bolton, *Toxicity changes during the UV treatment of pentachlorophenol in dilute aqueous solution.* Water Research, 1998. **32**(2): p. 489-497.
 73. Chang-Won, K., et al., *Continuous and early detection of toxicity in industrial wastewater using an on-line respiration meter.* Water Science Technology, 1994. **30**(3): p. 11.
 74. Oppenländer, T. and F. Xu, *Temperature effects on the vacuum-UV (VUV)-initiated oxidation and mineralization of organic compounds in aqueous solution using a xenon excimer flow-through photoreactor at 172 nm.* Ozone: Science Engineering, 2008. **30**(1): p. 99-104.
 75. Staehelin, J., J.J.E.S. Hoigne, and Technology, *Decomposition of ozone in water:*

- rate of initiation by hydroxide ions and hydrogen peroxide*. 1982. **16**(10): p. 676-681.
76. Staehelin, J. and J. Hoigne, *Decomposition of ozone in water: rate of initiation by hydroxide ions and hydrogen peroxide*. Environmental Science Technology, 1982. **16**(10): p. 676-681.
77. Glaze, W.H., J.-W. Kang, and D.H. Chapin, *The chemistry of water treatment processes involving ozone, hydrogen peroxide and ultraviolet radiation*. 1987.
78. ÇELEBİ, H. and D. SPONZA, *Antibiyotiklerin Anaerobik Ayrışabilirlikleri*. Biyoloji Bilimleri Araştırma Dergisi, 2008. **1**(2): p. 01-08.
79. Özkiz, G., *Treatability of pharmaceutical process effluents by advanced oxidation*. 2002, Çevre Bilimleri Enstitüsü.
80. Zwiener, C. and F. Frimmel, *Oxidative treatment of pharmaceuticals in water*. Water Research, 2000. **34**(6): p. 1881-1885.
81. Vogna, D., et al., *Advanced oxidation of the pharmaceutical drug diclofenac with UV/H₂O₂ and ozone*. Water research, 2004. **38**(2): p. 414-422.



Chapter 11

MODELING AND MANUFACTURING OF MINI PRUNING ROBOT PROTOTYPE

Faruk GÜNER¹

Hilmi ZENK²

¹ Ph.D., Assoc.Prof., Giresun University, 0000-0002-3438-0553

² Hilmi ZENK, Ph.D., Assoc.Prof. Giresun University, 0000-0002-1653-8580

1. Introduction

There are significant populations of trees around the world. The low branches of these trees are pruned by the relevant institutions due to industrial and safety requirements. A machine that can perform this type of pruning is manufactured according to the requirements of the forestry industry. The current application is by people climbing the tree or by users carrying saws supported by platform cranes with baskets. A prototype attached to the boot of the tree climbs up spirally thanks to its stepped tyres and cuts the low branches with the saw on it. This study presents the basic support system for the production of this prototype up to a certain tree diameter.

Pruning is a method of tree and plant care in which certain parts of a plant, such as branches, roots, etc., are cut and removed in a controlled manner. Pruning is a factor that has an important impact on the health and structure of the tree. Well-pruned trees require less maintenance as they provide a safe environment and an aesthetic appearance. (Badrulhisham & Othman, 2016). Pruning makes forests better and healthier and produces high-quality, branch-free forest products. It also has a positive impact on the development of biodiversity (Ishigure, Kachi, Mori, & Kawasaki, 2010).

Despite all these positive effects, pruning trees is a dangerous job that relies on human labour, so the decrease in the number of workers and the demands of forestry have paved the way for the emergence of robots for pruning. The presence of robots leads to a decrease in product efficiency and a decrease in employment due to the decrease in the number of workers, but ensures that the sector remains vibrant by making a large contribution to the forestry industry. In terms of employment, it is becoming increasingly difficult and costly to find qualified personnel to work in forestry.

On the other hand, there is an important need for climbing and pruning work on power transmission lines. Pruning is required to protect these lines from trees. More detailed prototypes, such as drones, have been produced for use in such harsh environments.

Although tree-climbing and pruning robots are now mainly used in countries such as Japan, India, the USA, Germany, and China, they are still in the early stages and are forestry equipment that has yet to be developed (Ishigure et al., 2010; Wang, Zheng, Zhang, & Meng, 2021).

Studies on pruning were first carried out in countries with good economies, such as Europe, America, and Japan. The main idea of this study is based on the difficulties encountered by the Directorate General of Forestry in Turkey in carrying out pruning activities. Maintenance measures are carried out in order to convert the existing forest potential into quality products in the long term. One of these maintenance measures is to ensure

the long and healthy growth of the tree by pruning the low branches of the tree. By growing long and neatly, these trees achieve first quality in the classification of trees, which means that high sales figures can be achieved. In the existing forest areas, pruning is almost negligible as it is based on labour and the risk of occupational safety. Currently, for pruning in forested areas, a belt tied around the waist and holding hooks attached to the feet are used to climb the tree and prune the branches with a hand-held saw. Although this method is very difficult in forest areas, it poses great risks in terms of work and personnel safety.

Currently, pruning in wooded areas is done by climbing the tree with a belt tied around the waist and grappling hooks attached to the feet and pruning the branches with a hand-held saw. Although this procedure is very difficult in the forest, it carries great risks in terms of work and personnel safety. If the pruning is not carried out, the timber yield decreases as the smaller trees below and next to the trees do not receive enough daylight due to the proximity of the trees to each other. To increase this yield, a pruning machine is needed that can be easily deployed on the forest site.

Another problem is that the branches of the trees on the roadside, which are up to six metres high, pose a danger to the passage of vehicles up to four metres high. To eliminate this danger, the low branches should be pruned. It turns out that, unlike forests, the maintenance of roadside trees is never interrupted because it carries a safety risk. This activity, which cannot be interrupted, is a slow and costly maintenance activity that requires a crane and at least three to four workers. The production of the mini-prototype to be designed will minimise manpower requirements in forest areas, work safety, and disruption to traffic flow during roadside work. (Engür & Kaya, 2023).

Today, robots have made a name for themselves in almost all areas. They have increased the comfort of human life in many areas, including in our homes, especially in industry, and they have begun to replace humans in production through their skills.

Favouring robots and machines in dangerous situations that can endanger human lives is considered one of the most logical solutions. The activity of climbing over long distances, which can lead to death, shows the importance of robots in this area. They are also a good alternative to reduce costs and time losses. (Bogue, 2019).

Climbing trees for pruning or other purposes is one of the actions that endanger people's lives. In forested areas, the height of trees can easily reach up to 10 metres, which helps us to understand the dimensions of the risk. For all these reasons, it is necessary to have a robot that can climb trees and do this work instead of humans.

The studies in the literature can be divided into two groups. These can be classified as tree climbers for forestry purposes and other utility robots. A new generation vertical climbing robot called RiSE, developed by Boston Dynamics, is one of the best examples of payload robots. It is designed for military surveillance and inspection for security purposes. Similar to reptiles, its six-legged structure gives it a good grip on the surface it climbs. There are 2 motors on each leg. One set of three legs of the robot allows it to move forward and the other set of three legs allows it to hold on to a tree. The tail of the RiSE robot in Figure 1, which is also shaped like a reptile, makes it easier for it to hold on to the tree. (Saunders, Goldman, Full, & Buehler, 2006).



Figure 1. RiSE surveillance robot (Saunders et al., 2006)

Another robot inspired by the snake, a reptile in nature, has been developed in China for use in rescue operations. This robot has successfully overcome the challenges of flexibility and easy adaptation in covering long

distances. Thanks to its small, interconnected, rotatable modules and its locomotive structure, the robot can successfully overcome obstacles on the surface. This autonomously controlled robot can perform the climbing task with a spike-like movement. The snake robot shown in Figure 2 consists of 16 equivalent modules. The connection points of these modules form the climbing route thanks to its ability to rotate laterally and vertically. (Zhen, Gong, & Choset, 2015).

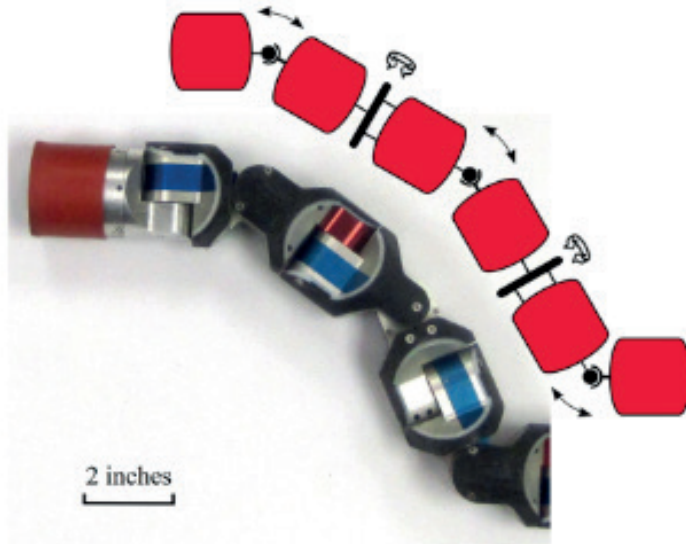


Figure 2. Snake Robot (Zhen et al., 2015)

In another study inspired by Kraken, Figure 3 shows an autonomous robot that can be controlled and used for different purposes and is able to climb vertical objects such as trees, pipes, etc. Thanks to its flexibility, it can move without the need for a robot. Thanks to its flexibility, it can hold on to different surfaces without the help of a sensor. The robot consists of six legs that are designed to move freely on the surface. Each leg contains two servomotors that move the robot up and down. In addition, rubber bands are used to press the body against the surface. With these features, the robot can be used for various controls and purposes. (Ito, Aoyagi, & Homma, 2019).

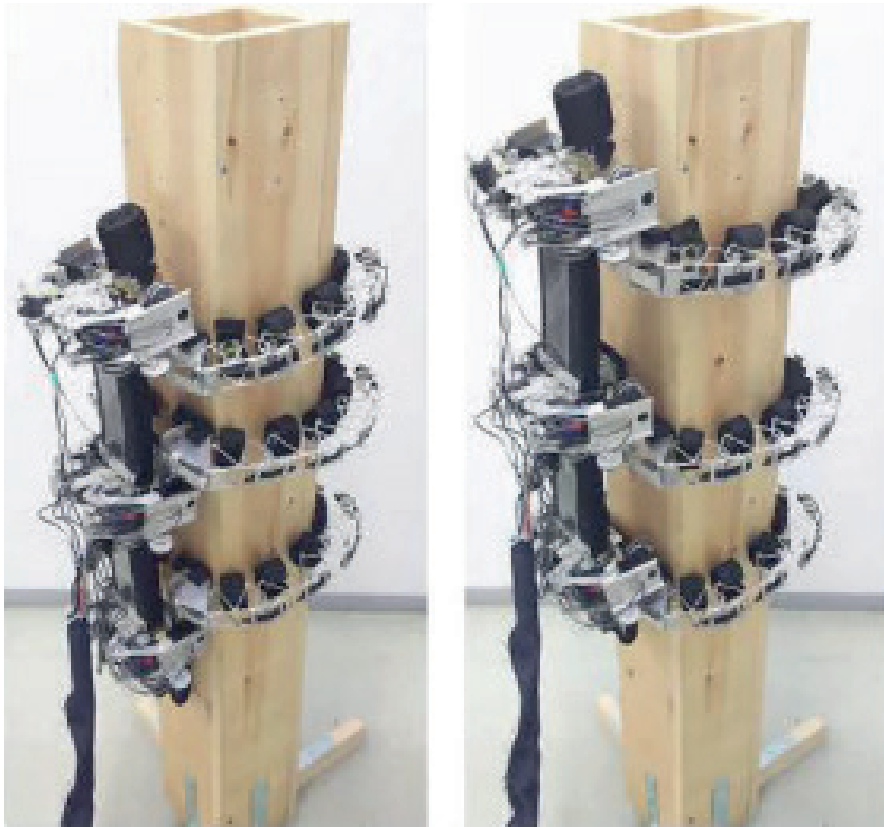


Figure 3 TAOYAKA-III: A Six-Legged Robot (Ito et al., 2019)

A design realised in Switzerland includes a wheeled prototype capable of climbing structural elements such as palm trees, telephone poles and lampposts. Images of this powerful robot can be found in Figure 4. Inspired by humans climbing with rope clamps, this new climbing approach allows climbing with a high preload. Depending on the motor power, a preload of 100 kg was achieved. The prototype can climb on tree trunks with a wide diameter range (20-50 cm) and move at a speed of 2 m/s despite a mass of 20 kg, taking wet ground conditions into account.

The body of the robot is made of aluminium to make it light and easy to manufacture. By using a planetary gear motor and a worm gear, 2 kW of power and 250 Nm of torque were achieved. These features allow the robot to work effectively in different environmental conditions.(Fischer & Siegwart, 2010).

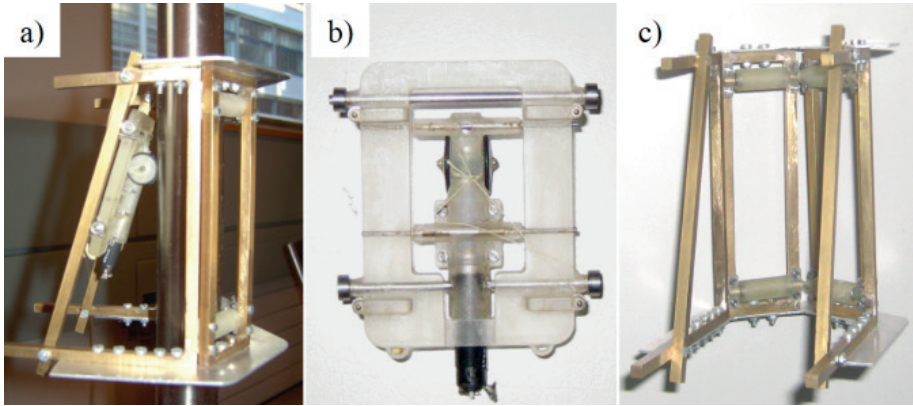


Figure 4. Climbing Robot with High Preload Capacity (Fischer & Siegart, 2010)

The University of Gifu has been working on a robot that is capable of pruning trees with a new generation of climbing techniques. This robot is able to climb quickly thanks to its light weight. In this study, which was inspired by human climbing methods, the robot's centre of gravity is outside the tree so that it can hold itself by applying pressure to the boot. No holding mechanism was developed for the body. Four wheels are mounted at regular intervals, two at the bottom and two at the top. Thanks to this wheel-driven structure, the robot can climb the tree quickly. (Kawasaki, Murakami, Kachi, & Ueki, 2008). In the second prototype, the spiral climbing ability was added to the straight climbing ability. This made both straight and spiral climbing an adjustable option. With the power of a 24 V battery and a chainsaw, it can trim target branches with a diameter of 1 cm. (Ueki, Kawasaki, Ishigure, Koganemaru, & Mori, 2011).



Figure 5. Kawasaki Straight and Spiral Climbing Tree Pruning Robot (Ueki et al., 2011)

Three different prototypes were developed as part of the WOODY project, which was initiated at Waseda University in Japan. Like the Kawasaki robot, the main aim of this study was to protect forests. Another aim of the project was to prevent the excessive number of branches on the trees in the forests from blocking the passage of sunlight and causing the fruit on the ground to

rot. In addition, the risk that trees could topple and fall on people and workers during heavy rainfall due to an excessive number of branches was also taken into account. To avoid endangering human lives, the researchers launched the WOODY project.

WOODY is designed as a robot that can be controlled manually. It can be clamped to the tree with its arms and can perform opening and closing movements in the robot body thanks to the gear shaft in its structure. At the top there is a cutting device for pruning. The wheels inside each arm rotate on the tree boot and start the pruning process. Its design is limited by its ability to climb flat trees such as cedars and cypresses (Lam & Xu, 2012).



Figure 6 WOODY Pruning Robot (Gennert, 2013)

AB232R is an automatic pruning robot manufactured by Seirei, a commercial product. The robot is driven by wheels and has a certain spiral climbing angle because the wheel angles are fixed. Thanks to this fixed angle, the robot's saw can cut off almost any branch on the tree trunk. The robot climbs up the tree at a constant speed and the branches are cut with a saw mounted on the top of the robot. It can be easily controlled and moved up and down in a spiral.

The robot can close and hold on to the tree using the pressure exerted on the body by the pre-tensioned springs. The ability to close is limited to certain areas and this area varies in direct proportion to the size of the robot. Seirei offers two types of models for different diameter ranges. These models appear as AB232R for diameters between 70-230 mm and AB351R for diameters between 150-350 mm. These features ensure that the robot can be used for different tree diameters (Gui, 2018; Lam & Xu, 2012).



Figure 7 AB232R Pruning Robot manufactured by Seirei (Gui, 2018)

This global need has been addressed in different ways, but no absolute solution has been found. The only commercially available product is a German-made pruning shear. It is a machine with a hydraulic feed. The hydraulic feed uses a unit that supplies the necessary pressurized oil and can only be used on a tractor or on flat terrain. The whole system consists of two main parts. The drive unit, which is connected to a small, standardized tractor, and the cutting unit, which climbs the tree. The required climbing speed is achieved by a hydraulically driven rubber belt. This ensures minimal pressure on the bark and a better grip on the tree. The blade in the cutting section cuts all branches of the tree safely and cleanly. This machine is highly efficient. It can prune 40 trees per hour. It can easily reach distances between 12-15 meters. However, with a weight of 50 kg, the cutting unit is quite heavy. As Germany is located on the Central European plateau, most of its land is flat sloping land. As Germany lies on the Central European plateau, a large part of its surface is flat sloping land. However, a significant part of the forest potential in Germany is larch forests, which were planted in a controlled manner after the Second World War and in which transportation facilities were created. Of course, not all forest areas in Germany are flat and covered with larch forests, but there

is enough of a market for the commercial use of these loppers. The German pruning shears are fast, but work on the basis of cutting dry branches with a maximum thickness of 4 cm. The maintenance and repair of a hydraulic system under field conditions is a costly and long-term process. (Jordan, 2019; “Leaf-nosed bat,” 2009; “Mechanical High Delimiting Systems,” 2023).



Figure 8. Advaligno PATAS Pruning Robot (“Leaf-nosed bat,” 2009)

In China, a study was conducted on pruning robots for the care of tall and fast-growing trees. In the study, a semi-autonomous robot was developed that can prune with an electric saw connected to a mechanical arm. Depending on the environmental conditions, the electric saw can be adjusted with the mechanical arm and the desired cut can be performed. The robot, which climbs with a fixed spiral climbing angle, consists of drive wheels, idle wheels and a docking mechanism. The drive wheels are connected to the motor via a chain and a gear wheel. There are two types of docking mechanisms: active and passive. Active docking works by pressing the robot against the tree trunk with two electric drive pistons when pruning the branches. Passive docking ensures that the wheels can always hold on to the trunk when climbing with the signal from the force sensor. (Yang, Wang, Yan, & Fan, 2021).

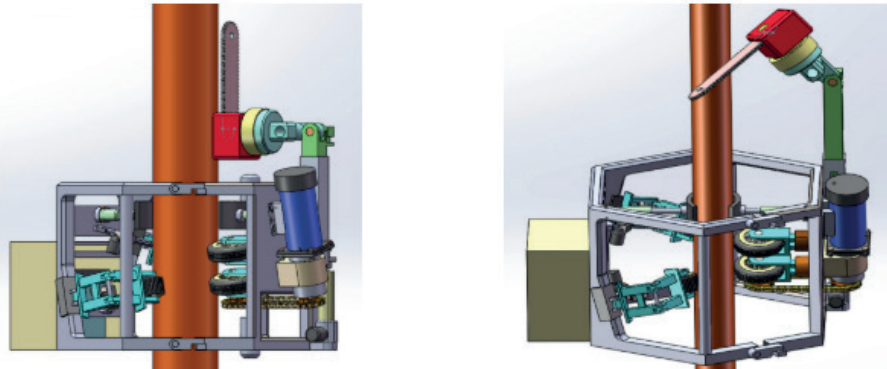


Figure 9. Electrical powered ChainSaw Pruning Robot (Yang et al., 2021)

A free-moving robot has been developed for pruning trees in wooded areas and parks. This robot walks on the tree trunk with its four claws and cuts the branches with its motorized circular saw. Mechanical components such as the motor, worm gear and threaded screws in the claws have made the design complex. While one of the lower claws holds on to the tree, the upper claw, which is at an angle to it, is released. The claws that end their movement in this way can move, while the other claws remain free and the climbing cycle continues in this way. Thanks to its sharp, pointed claws, it has a firm grip on the tree. This design offers an interesting solution for the development of an efficient and flexible mobile robot for tree maintenance (Polishchuk, Tkach, Parkhomey, Boiko, & Eromenko, 2020).

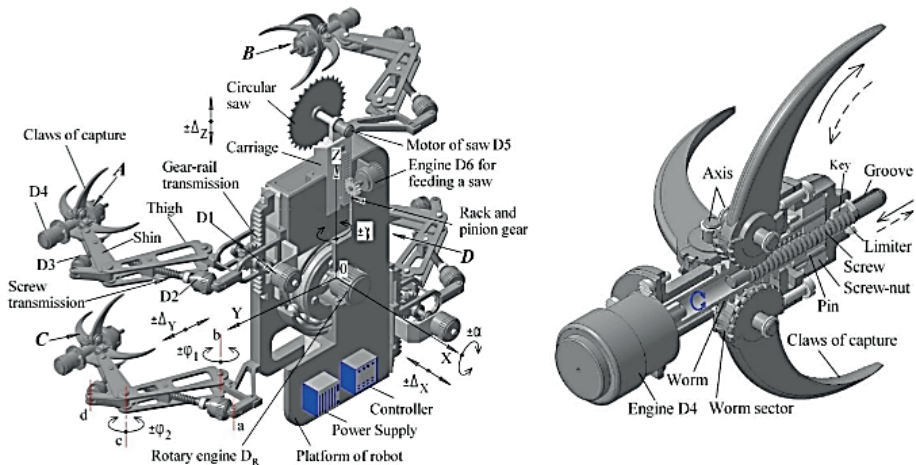


Figure 9. Pençe tutunmalı Mobil Budama Robotu (Polishchuk et al., 2020)

Due to the difficulties and risks of pruning trees near high-voltage power lines in cities, a flying, drone-like tree trimming robot has been developed in Japan. The robot holds the branches and prunes them. Its structure includes a DC motor with a gearbox, a lithium battery, and servomotors. The servomotors are connected to the grippers and set in the appropriate position for the robot to hang on the branch. Thanks to its grippers, it can also provide a very good grip on uneven branches. Tree pruning can be carried out with the circular saw connected to the DC motor. The main table of the robot is made of aluminium to make it light. (Molina & Hirai, 2017).



Figure 10. Drone Ağaç Budama Robotu (Molina & Hirai, 2017)

2. Material and Method

2.1. Model Guidelines

Pruning is one of the most important activities in tree and plant cultivation (Clark & Matheny, 2010). Pruning is the cutting of branches, etc., from the plant with the aim of ensuring healthy and controlled plant growth, influencing fruit yield, and beautifying the appearance of the plant. For appropriate and correct pruning, it is important to analyse the plant's growth habit, structure, and garden layout in detail. With the right pruning, young trees can grow long-lived, healthy, and in the desired order. Pruning young trees also helps to achieve the necessary spacing and regular order between the branches and increase the strength of the tree (Meade & Hensley, 1998).

Pruning is a frequently used method to increase the value of the wood and the wood species. It also makes it possible to obtain knot-free and clean wood. Tree branches and knots not only affect the quality of the wood but can also pose a risk of rotten branches falling over time, which shows how important pruning is from a safety point of view. From an economic point of view, the effort and costs involved in pruning are negligible compared to the

increase in wood diversity (Danilović, Sarić, Cirović, & Pudja, 2022).

There has long been a debate in forestry about suitable methods of pruning. After pruning, certain processes take place on the surface of the tree. The wounds in the pruned area heal over time, forming a cambium layer and new growth rings at the branch root. It is important to reduce the injured area on the tree trunk as much as possible using the correct pruning techniques. The intensity and duration of pruning influence the size of the wound. Early and careful pruning techniques reduce the size of the wound and enable the production of new and healthy wood products. In contrast, incorrect practices can slow down the growth of trees and have negative consequences.(O'Hara, 2007).

Regardless of the pruning method, the following goals should be pursued:

- Each pruning cut should be able to significantly change the shape of the tree.
- The pruned branches should be able to influence the tree's ability to absorb sunlight efficiently.
- The pruning of large branches should make a significant contribution to the shape and appearance of the tree.
- For safety reasons, pruning that tends to fall over should be carried out.

There are three basic pruning methods. The first is reduction pruning, in which side branches and stems of sufficient length are shortened. Another method, head pruning, is the cutting of branches and trunks to a certain height according to a predetermined plan. Removal pruning, which was used in this study, refers to the removal of side stems and branches attached to the trunk of the tree by removing them from the trunk. With this technique, the pruning of other branches to be removed from the main trunk must be carried out properly and carefully(Gilman, 2011).

2.2. Modelling of Prototype

The four wheels of the designed mini-prototype are to be moved by magnetic, self-propelled wheels and 4 idle wheels. To simplify operation, the speed of movement is ensured by a radio remote control that is controlled by the user or by software that can be operated from a cell phone. Since the part of the system that is not part of the saw is powered by the prototype's batteries, the system can also be used smoothly and fully in field conditions.

Since the forest areas are usually located in steep terrain, the system is carried by only two people into areas that cannot be traveled by vehicles and can be operated without drive vehicles.

Apart from this, it was found that there are models in the literature with electric or combustion engine drive connected to the tree trunk, but these have not yet been implemented in industrial products. The main problems of systems with internal combustion engines are the weight of the machine, the need for time or mechanically adapted gears for reverse motion. In the case of electric systems, designs that depend on the electricity grid to cover the power requirements and extend the operating time cause problems. In the current project proposal, the advantages of these models are exploited to the maximum and the negative characteristics are addressed in the best possible way through technical solutions.

Not all tree species are pruned in forests, and the bark structure of the different tree species to be pruned also complicates the pruning process. Pruning in forests plays an important role in tree planting. The planting of trees depends on various factors such as season, region and nursery. In forestry, seedlings are planted in the forest about 2 to 4 years before felling. This is done to ensure that the sapling, which grows under harsh winter conditions, is not damaged by pruning the branches of the large trees next to it and not to prevent the growth of the large trees next to it as it grows. In addition, this pruning will adjust the amount of sunlight during the summer months.

Not all tree species are pruned in forests, and the bark structure of the various tree species to be pruned also complicates the pruning process. Pruning in forests plays an important role in the planting of trees. The planting of trees depends on various factors such as season, region and nursery. In forestry, seedlings are planted in the forest about 2 to 4 years before felling. This is done to ensure that the sapling, which grows in harsh winter conditions, is not damaged by pruning the branches of the large trees next to it and to prevent the growth of the large trees next to it as it grows. In addition, this pruning also adjusts the amount of sunlight in the summer.

When lift pruning, you should ensure that the bark overhang on the main trunk of the branches to be pruned is not exceeded. In some cases, you can make a very deep cut by cutting off this projection, which can be an incorrect practice. Another common mistake is to cut branches away from the main trunk. A correct cut should be made as close to the trunk as possible without touching it (Bedker, 1995).

This study investigates the kinematic analysis of a new generation asymmetric gripper robot designed for pruning branches near power lines. The robot is driven by a multi-rotor helicopter and grasps asymmetrically with two grippers connected to a pair of servomotors. This gripping is achieved by aligning the shafts of the servomotors to the same axis of rotation. Shafts rotating in opposite directions make it possible to hold on to branches. Trimming is achieved by rotating the base plate around the servomotor shafts.

Asymmetrical grippers are designed for gripping and pruning and are controlled by servomotors. They are designed to avoid contact with the servo motor shafts. The trimming mechanism also includes a DC motor with a circular saw. This motor performs the trimming process by rotating the base plate. The kinematic and geometric analysis of the robot focuses on its ability to effectively grip straight and uneven branches thanks to the large gripping surface and volume of the grippers.



Figure 11 3D Model of mini pruning robot

3. Discussion and Results

The felling of trees near high-voltage power lines can be dangerous for people in the vicinity and poses a potential risk to the power supply. Therefore, the development and use of this robot aims to prune the branches of trees in a safe and effective way. It is intended to provide a safer and more effective

alternative to conventional pruning methods.

The mechanism of the robot consists of a helicopter mechanism, asymmetrical grippers, a DC motor with a circular saw and other parts. This mechanism is designed to perform gripping and pruning operations. It also includes subsystems such as the robot's ascent and descent mechanism, motor and drive mechanism. The robot's chassis is connected to a pair of gear shafts consisting of two parts and is made of aluminium. The movement of the robot is ensured by six motors and can be controlled remotely for easy operation.

This robot was specially developed for the safe pruning of branches near high-voltage power lines. Its components, such as the helicopter mechanism, the asymmetrical grippers and the DC motor with circular saw, are integrated in such a way that they enable effective gripping and pruning of branches. The robot has been designed with safety, efficiency and ease of use in mind, which may offer advantages over conventional pruning methods.

This study describes the gripping mechanism and climbing method, which enable the robot to climb on uneven surfaces. The upper and lower gripping mechanism is connected to the piston pair and can be adjusted with the gear shaft nut. This mechanism provides the linear motion required for the robot to climb. The entire mechanical frame is made of L-profile aluminium, which reduces the weight.

The holding mechanism consists of two structures formed by the motor gear shafts. The motor gear shafts are connected to one part of the gripping mechanism and the other part has a properly aligned nut. While the motor gear shafts move together, small wheels on an irregular surface ensure uniform movement on the bark. The vertical movement is realised by the gear shaft and the nut and 2 motors are used for this movement.

There are two pistons in the structure of the robot, which reduce vibration by adjustment and provide strong support. The symmetrical structure ensures that the robot's centre of gravity remains in the middle and prevents it from tipping over when climbing. At the moment of climbing, the upper and lower parts close and the robot holds on to the tree. When the lower part opens, the motor's gear shafts reverse, causing vertical movement. Then the lower part closes and the upper part opens. The geared motor rotates clockwise to provide vertical movement. All these steps form a single motion of the climbing process.

The effector of the robot has 3 degrees of freedom and is made of a hollow steel tube. The vertical arm is rotated by a high torque DC motor and is connected to a bevel gear. The speed of the motor used for cutting is quite high. The climbing mechanism consists of wheels mounted at an oblique angle and a structure that enables spiral movement. The pruning mechanism

consists of a mechanical arm and a saw blade and can change the pruning method according to the work requirement.

Pruning is an important operation in forestry and has a significant impact on the growth of trees and the quality of the harvest. A good pruning robot can increase economic profit by reducing the number of workers and providing an automated and versatile solution for forestry.

Assuming a tree height of 20 m and a robot weight of 60 kg, the total potential energy required is calculated as 11772 joules and 15303.6 joules, taking into account an energy loss of 30%. Dividing this value by 60 results in a required power of 255.6 W.

In the control unit of the designed robot, forward and backward controls with brushless DC motor, a DC motor for voltage control, a linear DC motor for machete angle control and sensor limitation control were made. Portable wheel motors with a two-stage transmission ratio of 10:1 and 22:1, 24V, 150 W, 3000 rpm and a braking torque of 3 Nm were selected for the movement. Industrial type 6-36 VDC sensors were used for the detection of metal objects at a distance of 4 mm.

Other features of the sensor, diameter 12mm, detection distance 4mm, output current 300mA, response frequency 0.5KHz, material type iron, operating temperature -25°C to +55°C, 6.2 x 2cm/2.4" x 0.8", weight 46 g

The 12V high power DC motor for machete movement is used as a windshield wiper motor for various automobiles as well as for various off-road vehicles and various projects that require high power. The motor speed is 55 rpm and the front bearing is equipped with ball bearings, making it suitable for long-term operation. There are three 6 mm diameter screw holes on the motor that can be used for mounting. Motor no-load current 2A, drive current 10A, drive torque 45 kg-cm, motor power 120W, shaft diameter 10mm, shaft length 29mm, weight 1280gr

4. Conclusion

This pruning robot was developed to automatically prune and maintain tall and long-lived trees. It is able to process trees with a height of 20-30 meters and a trunk thickness of 10-30 cm. Compared to manual pruning, the automatic and semi-automatic functions of this robot offer a faster, less labor-intensive and more efficient solution. In addition, working on tall trees can be dangerous, so the robot offers a safe solution by reducing these risks.

The main features of the robot are:

Climbing and gripping mechanism: Thank you to the spiral climbing mechanism and four clamps, the robot can hold on to the tree and climb up to a certain distance. The climbing speed is specified as 1-2 m/min.

Pruning systems: It is equipped with an electric saw and a mechanical arm pruning mechanism. The robot has two different pruning systems: Side branch pruning and top pruning.

Climbing steps: The working principle takes place in four phases: Preparation phase, climbing phase, pruning phase and return phase.

Environmentally Friendly Design: An electrically powered robot has been designed to avoid the negative impacts caused by internal combustion engines. This provides an environmentally friendly maintenance solution.

Climbing Speed and Safety: The robot's design aims to climb trees safely thanks to its high climbing speed and gravity-independent grapples.

Remote Control: The mobile robot can be controlled remotely and is powered by a battery unit. This allows the operator to control the robot from a safe distance.

This design aims to optimize tree care and pruning operations in the forestry industry.

References

- Badrulhisham, N., & Othman, N. (2016). Knowledge in Tree Pruning for Sustainable Practices in Urban Setting: Improving Our Quality of Life. *Procedia - Social and Behavioral Sciences*, 234, 210-217. doi:<https://doi.org/10.1016/j.sbspro.2016.10.236>
- Bedker, P. J. (1995). *How to prune trees* (Vol. 1): US Department of Agriculture, Forest Service, Northeastern Area, State
- Bogue, R. (2019). Climbing robots: recent research and emerging applications. *Industrial Robot: the international journal of robotics research and application*, 46(6), 721-727.
- Clark, J. R., & Matheny, N. (2010). The research foundation to tree pruning: a review of the literature. *Arboriculture & Urban Forestry*, 36(3), 110-120.
- Danilović, M., Sarić, R., Cirović, V., & Pudja, V. (2022). The impact of pruning on tree development in poplar *Populus× canadensis* "I-214" plantations. *iForest-Bioengineering and Forestry*, 15(1), 33.
- Engür, M. O., & Kaya, Ö. (2023). *Teleskopik Platformlu Araçlarla Yapılan Budama İşlerinde Tehlikeler Ve Güvenlik Önlemleri*. Paper presented at the 29.Ulusal Ergonomi Konferansı.
- Fischer, W., & Siegart, R. (2010, Aug 31-Sep 03). *WHEELED POLE-CLIMBING-ROBOT WITH HIGH PAYLOAD CAPABILITY, USING A CLAMPING MECHANISM WHICH IS INSPIRED BY THE ROPE-CLAMPS IN HUMAN CLIMBING*. Paper presented at the 13th International Conference on Climbing and Walking Robots and the Support Technologies for Mobile Machines, Nagoya Inst Technol, Nagoya, JAPAN.
- Gennert, M. A. (2013). Design and Construction of a Tree-Climbing Robot. *Diss. WORCESTER POLYTECHNIC INSTITUTE*.
- Gilman, E. F. (2011). *An illustrated guide to pruning*: Cengage Learning.
- Gui, P. (2018). *Tree pruning/inspection robot climbing mechanism design, kinematics study and intelligent control: a thesis presented in partial fulfilment of the requirements for the degree of Doctor of Philosophy in Mechatronics at Massey University, Manawatu Campus, New Zealand*. Massey University,
- Ishigure, Y., Kachi, H., Mori, Y., & Kawasaki, H. (2010). *Pruning machine with a mechanism for preventing branch bite*. Paper presented at the Proc. of Forest Engineering: Meeting the Needs of the Society and the Environment (FORMEC 2010).
- Ito, K., Aoyagi, R., & Homma, Y. (2019). TAOYAKA-III: A Six-Legged Robot Capable of Climbing Various Columnar Objects. *Journal of Robotics and Mechatronics*, 31(1), 78-87. doi:10.20965/jrm.2019.p0078
- Jordan, E. (2019). Machine for debranching living trees. In: Google Patents.

- Kawasaki, H., Murakami, S., Kachi, H., & Ueki, S. (2008). *Novel climbing method of pruning robot*. Paper presented at the 2008 SICE Annual Conference.
- Lam, T. L., & Xu, Y. (2012). *Tree climbing robot: Design, kinematics and motion planning* (Vol. 78): Springer.
- Leaf-nosed bat. (2009). In *Encyclopædia Britannica*: Encyclopædia Britannica Online.
- Meade, G., & Hensley, D. L. (1998). Pruning landscape trees and shrubs.
- Mechanical High Delimiting Systems. (2023). Retrieved from <https://advaligno.com/en/>
- Molina, J., & Hirai, S. (2017). *Kinematic analysis of a novel skew-gripper for aerial pruning tasks*. Paper presented at the Proceedings of the 3rd International Conference on Mechatronics and Robotics Engineering.
- O'Hara, K. L. (2007). Pruning wounds and occlusion: A long-standing conundrum in forestry. *Journal of Forestry*, 105(3), 131-138.
- Polishchuk, M., Tkach, M., Parkhomey, I., Boiko, J., & Eromenko, O. (2020). Walking mobile robot for trimming trees: design and modeling. *International J Control & Autom*, 13(2), 1760-1772.
- Saunders, A., Goldman, D. I., Full, R. J., & Buehler, M. (2006). *The rise climbing robot: body and leg design*. Paper presented at the Unmanned Systems Technology VIII.
- Ueki, S., Kawasaki, H., Ishigure, Y., Koganemaru, K., & Mori, Y. (2011). Development and experimental study of a novel pruning robot. *Artificial Life and Robotics*, 16(1), 86-89.
- Wang, J., Zheng, H., Zhang, C., & Meng, C. (2021). *Analysis and Research on Tree-climbing and Pruning Robots*. Paper presented at the Journal of Physics: Conference Series.
- Yang, X., Wang, J., Yan, M., & Fan, S. (2021). *Structure Design of Surrounding Tree-climbing and Pruning Robot*. Paper presented at the Journal of Physics: Conference Series.
- Zhen, W., Gong, C., & Choset, H. (2015). *Modeling rolling gaits of a snake robot*. Paper presented at the 2015 IEEE international conference on robotics and automation (ICRA).



Chapter 12

FOOD WASTE MANAGEMENT IN THE FOOD SUPPLY CHAIN AND SUSTAINABILITY

Fatma Zehra YAKUT¹

Mukaddes KILIÇ BAYRAKTAR²

Cengiz ÇETİN³

¹ Master Student, Karabuk University, Faculty of Health Sciences, Food Toxicology Master Programme, Student No: 2328310502

² Associate Professor Dr., Karabuk University, Faculty of Health Sciences, Department of Nutrition and Dietetics, ORCID No: 0000-0002-8871-8820

³ Lecturer, Karabuk University, Eflani Vocational School, Hotel Restaurant and Catering Services, Cookery Programme, ORCID No: 0000-0003-0511-6304

1. Introduction

The World's population is growing and, with it, consumption is increasing daily, requiring ever more efficient use of natural resources. Food is wasted and lost throughout the entire life cycle, from harvesting to production, processing and consumption (Drewitt, 2013). This means the loss of food and the waste of resources, time, energy, and water. To protect food from contamination, ensure consistent delivery to consumers, and extend food shelf life, edible films applied as a coating on or between food ingredients have recently become increasingly popular. By using edible coatings and biodegradable films, contamination can be minimized (Oğuzhan et al., 2016, Benbettaieb et al., 2016). Blockchain technology can potentially be used to ensure food safety and monitoring. Blockchain technology makes it possible to track the life cycle of an agricultural product virtually and transparently, from production to consumer and marketing (Kshetri and Loukoianova, 2019). As technology advances, 3D food printing technology has emerged as a technology that enables a new food design that can provide the desired characteristics in terms of shape, size, texture, and taste in the production of food for particular purposes, as energy can be saved by minimizing waste and labor costs (Aday and Aday, 2020). Promoting sustainable food production should benefit all stakeholders by avoiding excessive waste, financial expenditure, the environment and food safety. The topics of waste, waste management, and sustainability in food production are covered in this section. The causes of food waste, potential food losses in the food supply chain, blockchain technology, edible packaging, and 3D printing are also covered.

2. Food Loss and Waste

In general, food waste and losses are investigated throughout the food supply chain. Food losses happen when consumable food is inadvertently lost in the supply chain at different stages (Ozkan et al., 2022; Lipinski et al., 2013). Food losses have adverse effects on the environment and society in addition to excessive resource depletion (FAO, 2011). Food loss during sale and consumption is referred to as food waste. According to Lipinski et al. (2013), the definition of food waste is that it is purchased by customers, restaurants, and food producers but is not consumed by customers in establishments or by individuals at home. Figure 1 (FAO, 2020) summarizes the food lost and wasted globally along the food supply chain.

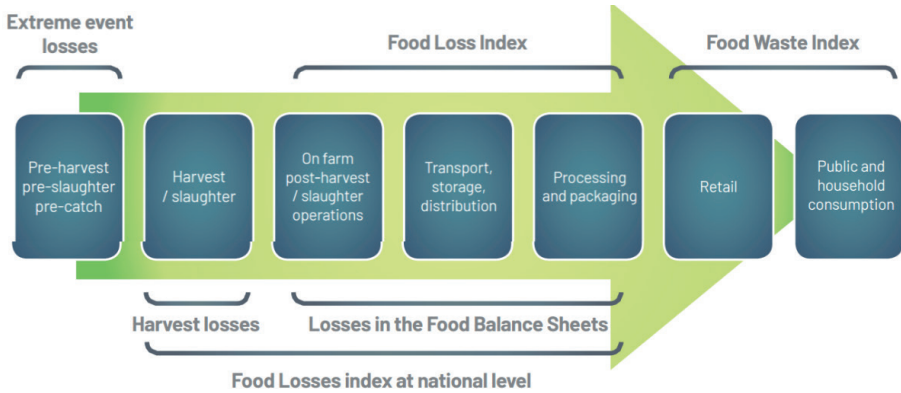


Figure 1: Global food loss and waste throughout the food supply chain (FAO, 2020)

Food waste is food that spoils or is wasted in producing, distributing, storing, and ultimately consuming food. Food loss and food waste are thus included in the definition of “waste” (FAO, 2013). When food is lost at any point in the food supply chain, it is called waste, from the producer to the processor to the retailer or consumer. According to the Waste Management Regulation, it is defined as “any substance or material which is or has to be disposed of or released into the environment by the producer or the natural or legal person who possesses it” (Waste Management Regulation, 2015, Bellemare et al., 2017).

There are two categories of food waste: edible waste and non-edible waste. Edible food waste results from uncontrolled purchasing, inadequate preparation, improper storage, and large portion sizes and is defined as unused, damaged products that can be eaten before being thrown away. Inedible food loss is the portion of food unsuitable for human consumption and therefore thrown away, as well as waste generated during the preparation phase in the food sector. Examples of inedible food waste include bones, egg shells, fruit and vegetable peelings, fat, and tendons from meat (Bagherzadeh et al., 2014; Lipinski et al., 2013).

Food waste affects many areas of the economy, agriculture, soil fertility, natural resources, global warming and climate, social justice, and economic distribution, making it one of the global problems that urgently needs to be solved (Türkiye Ministry of Trade, 2018; TISVA, 2019). The Food and Agriculture Organization of the United Nations (FAO, 2019) reported that every year, roughly 1.3 billion tons (or one-third) of food are wasted worldwide, costing the world economy 990 billion dollars. In underdeveloped countries, insufficient development of agricultural techniques, various infrastructure problems, lack of adequate and appropriate storage, and an unfavorable climate contribute to food waste, while in nations with mature economies,

food waste is a result of consumer behavior (Bräutigam et al., 2014; Tefera et al., 2011). In industrialized countries, the extent of food waste in households is significantly higher than in developing and underdeveloped countries (Buzby and Hyman, 2012; Jörissen et al., 2015).

Food waste has consequences connected to global hunger, obesity in developed nations, environmental damage, and economic disruption. Besides the substantial financial losses resulting from food waste, it also leads to the overuse of other resources that contribute to global climate issues, including labor, productive farmland, water, fertilizer, and energy (Buzby and Hyman, 2012). Food waste happens at several points in the food chain, including harvesting, production, transportation, and consumption, as can be observed through studies on the topic in the literature (Braeutigam et al., 2014).

3. The Current State in the World and Türkiye

3.1. Food Waste and Loss in the World

While over 800 million individuals worldwide are suffering from hunger due to population growth, food waste is one of the most critical concerns the globe has examined in the last thirty years. It is estimated that the World's finite resources will eventually be unable to sustain the equilibrium between supply and demand since a third of produced food is thrown away before it is consumed (Drewitt, 2013). The FAO Food Waste Index Report estimates that 17% of the food production globally in 2019 was thrown away, amounting to 1.3 billion tons of food valued at 990 billion dollars (FAO, 2019).

Different nations experience different losses in the food chain. The FAO 2019 states that a survey conducted in 152 other regions in 54 countries found that 569 million tons of food (61%) is wasted annually by households, 224 million tons (26%) by food service establishments, and 118 million tons (13%) by retailers. The proportion of food waste and loss is 5-6% in Australia and New Zealand, 20-21% in Central and South East Asia, and 16% in Europe and North America. Food waste in households is 40 million tons in the U.S., 47 million tons in the E.U., 4.5 million tons in the U.K., 7.3 million tons in Australia, and 18 million tons in China (U.N. Food Waste Index, 2021). Annual food waste from producers to consumers is around 100 million tons in Europe and approximately 35 million tons in the USA (U.S. Environmental Protection Agency, 2016).

The amount of food waste produced annually per person in North America and Europe is between 95-115 kg, while it is estimated at 6-11 kg in Africa, South and Southeast Asia. Within emerging nations, 40% of food waste is generated during pre-harvest, harvest, and processing, while in industrialized countries, it is generated in retail chains and during consumption (Sputnik, 2019; ISRAF, 2019).

3.2. Food Waste and Loss in Türkiye

According to Türkiye's waste report, 26 million tons of food are wasted every year. As a result of the research, it was found that the most wasted product group is fruits and vegetables, and 25-40% of the produced fruits and vegetables are thrown away. It is stated that these losses correspond to 15% of the country's economy and amount to 555 billion T.L. These losses mean that food is wasted and natural resources can be destroyed (T.C. Ticaret Bakanlığı, 2018). Although Türkiye belongs to the group of high- and middle-income countries, it falls into the Middle Eastern and North African countries category according to the Global Food Security Index (GFSI). This assessment shows Türkiye's food security score is 63.9, indicating a good situation. At the same time, according to the latest UNEP 2021, Türkiye is in third place globally, after the Democratic Republic of the Congo and Mexico, with an annual food waste per inhabitant of 92.3 kg (Dağdur and Olhan, 2015; UNEP, 2021).

When the characterization of household waste in Türkiye is examined, it is found that biodegradable organic waste ranks first at 55.54% compared to other wastes. According to TUIK, it can be assumed that with a generation of 32.3 million tons of household waste in 2020, around 18 million tons of biodegradable waste will be generated (TUIK, 2021). The Federation of Food and Beverage Industry Associations of Türkiye (TGDF) states that 4.9 million pieces of bread are wasted every day in Türkiye (1.7 billion pieces annually) (TGDF, 2020). It is reported that 3 million of these are found in bakeries (62%), 1.4 million in private households (28%), and 0.5 million in staff and student canteens, restaurants, and hotels (10%). The study on stale bread found that 71% was used to prepare meals and desserts, 49% was given to stray animals and pet owners, and 14% was stored in freezers. Only 11% of respondents stated that they throw bread directly into the trash (T.C. Ticaret Bakanlığı, 2018).

It was found that 80 hospitals and 500 schools could be built with the cost of the bread wasted annually (1.7 billion), and the seriousness of the bread waste situation is better understood. As a result, the research has determined that studies on food waste in our country have increased in some foods, such as bread, while other food groups have not received enough attention. In addition to bread, it has been determined that the highest waste rate of 20% is vegetables and that they produce food waste due to their rapid deterioration (Tatlıdil et al., 2013).

4. Food Supply Chain and Causes of Food Waste Along the Chain

When transporting food to consumers, it is necessary to establish a comprehensive supply chain. The food distribution chain begins with the provision of raw materials and continues with the procedures that the food

goes through, the logistics of intermediate and final products, and information on every step of the process up to the consumer. By coordinating the many phases of the business to ensure product sustainability and an error-free flow of information, food supply chain management seeks to maintain food safety and quality. The prerequisites for proper food supply chain management are effective communication between units, the chain's ability to adapt to advances in technology and standards, and an efficient logistics system (Mahalik and Kim, 2016).

The supply chain, which establishes the circumstances for a healthy relationship between producers and consumers, is the sum of all relationships and connections of products and services from the producer to the customer (Kehoe et al., 2017; Özdemir, 2004). An example of all these connections, consisting of supplier, producer, distributor, retailer, and customer, is shown in **Figure 2**.

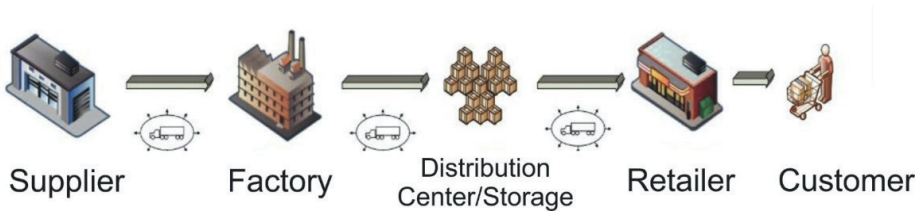


Figure 2: Supply chain example (Yıldızbaşı and Üstünyer, 2019)

As the food industry is linked to many suppliers and customers, the supply chain is diversified, and food production differs from other sectors in its risks related to food safety, short shelf life, sensitive quality parameters, etc. Maintaining the integrity of the chain is crucial, as various parties have an impact on the chain as a whole, reducing product quality and jeopardizing food safety (Sezen, 2011). Accordingly, players have turned to new forms of supply chains by utilizing emerging technologies to meet consumer demands, adapt to competitive conditions, and achieve more effective and efficient outcomes (Kehoe et al., 2017). Some of these technologies used in the supply chain are electronic data interchange (EDI), internet, enterprise resource planning (ERP), radio frequency identification (RFID), supply chain management and planning (SCM/SCP) software (Özdemir and Doğan, 2010).

Approximately 49 million tons of fruits and vegetables are produced annually in Türkiye. However, only 52% of the fruits and vegetables produced reach consumers. It is estimated that between 25% and 40% of fruits and vegetables are wasted due to exposure to poor conditions along the food supply chain (Çirişoğlu and Akoğlu, 2021).

It has been reported that the most wasted foods in the world are,

respectively, root and tuber crops (such as potatoes and onions) with 40-50%, cereals with 30% (half of the World's annual cereal production), oilseeds (such as corn and sunflower), fruits and vegetables, meat and animal products with 20% (Ozkan et al., 2022). In Türkiye, it is reported that vegetables have the highest rate (20%) among all food groups due to their perishability (Tatlıdil et al., 2013). In another study conducted in China, vegetables (29%), rice (14%), seafood (11%), wheat (10%), and meat (8%) were the food groups that caused the most losses in restaurants (Tatlıdil et al., 2013, Wang et al., 2017). Marketplaces, which provide citizens with daily or weekly access to fresh fruits and vegetables in many cities, are also a considerable source of biodegradable food loss (Ouadi et al., 2019).

5. Environmental Impact of Food Waste

Food waste is the loss of resources — labor, water, land, and energy — used in the production of food (Buzby and Hyman 2012). From this perspective, the effects of food loss and waste on the world is more severe than previously thought. On the other hand, increased food production can adversely affect biodiversity, clean water resources, soil fertility, and erosion. In addition, food production leads to a demand for fertilizers, water and energy resources, and the emission of greenhouse gasses that contribute to climate change (Meyer et al., 2017).

The loss or waste of food causes 10% of greenhouse gas emissions in the universe. Greenhouse gases are thought to cause the most damage from food loss and waste. From food production to consumption, greenhouse gas emissions can occur at various stages. The disposal of food that is not consumed also generates large quantities of greenhouse gas emissions. For example, in the U.K., greenhouse gas emissions from food waste disposal account for 30% of all consumption-related emissions (Liegeard and Manning, 2020). Greenhouse gases are the leading cause of global warming. For these reasons, eliminating food loss and waste to ensure food security is one of the worldwide goals aimed at relieving the strain on natural resources (Lundqvist et al., 2008; Smith, 2013; FAO, 2013).

6. Food Waste Management: Conventional and Innovative Methods

The food business produces large volumes of solid and liquid waste at every stage of the production chain, right up to the consumer. Because these wastes include valuable components like food ingredients and biomass, it is not optimal to dispose of them (Deniz et al., 2015; Kanmaz and Saral, 2017). Food waste is utilized in creative and traditional ways.

There are some conventional techniques used for food waste management such as composting, incineration, landfill and animal feeding. These methods have their own advantages and disadvantages (Al-Obadi et al., 2022).

Conventional methods of composting studies have been carried out to reduce the negative impact of food and greenhouse waste on the environment and ensure recycling. In Türkiye, composting plants are mainly located in the Marmara and Mediterranean regions, while compost production is lower in Eastern Anatolia and the Black Sea region (Çerçioğlu, 2019). To reduce the problem of solid waste, the production of biodegradable materials plays an important role, as it creates compostable organic residues. The use of bio-based (biodegradable) packaging materials is a possible alternative to replace petroleum-based (synthetic) polymers. This reduces demand for petroleum-based products, releasing fewer gases into the atmosphere and reducing dependence on renewable resources to produce plastics (Väisänen et al., 2016; Berthet et al., 2016).

One of the most significant sources of waste is the fruit and vegetable sector. Fresh fruit and vegetables and vegetables processed into juice, jam, or preserves account for 25–40% of waste. Waste products from all these processes include fruit pulp, peel, and seeds, which have a high concentration of proteins, lipids and polysaccharides. This organic waste can be reused through several techniques as raw materials in various industries, including the chemical, pharmaceutical, cosmetics and food industries. In particular, waste from the fruit and vegetable industry has a high pectin content and contains various essential oils. The biodegradable films produced from these organic waste products are also used to improve the mechanical properties and barrier function of packaging materials (Yılmaz et al., 2017; Wikiera et al., 2016; Pereira et al., 2016; Oliveira et al., 2016).

In terms of innovative techniques of food waste management, there are quite new technologies such as blockchain technology, edible and biodegradable packaging, intelligent trashcans and 3D printing technologies can be mentioned (Al-Obadi et al., 2022).

6.1. Blockchain Technology

The innovative method of blockchain solves many problems in the supply chain, as it offers transparency and traceability. Thanks to this technology, all transfers and transactions within the supply chain can be recorded so that they can be observed by the parties involved (Kshetri and Loukoianova, 2019). Barcodes and blockchain technology sensors are frequently used in today's supply chain. Therefore, applying blockchain technology in the supply chain is more economical than other applications (Kshetri and Loukoianova, 2019). The use of smart contracts in the transactions of this technology widely used in the supply chain will provide an advantage, and the certification process makes it more secure, economical, and faster (Morkunas et al., 2019). At the same time, it is a widely used technology as the parties can view the terms and details of the contract as there is no trust issue (Kırbaş, 2018). Figure 3 shows the key features of blockchain technology and Figure 4 shows the advantages of blockchain technology in the food supply chain.

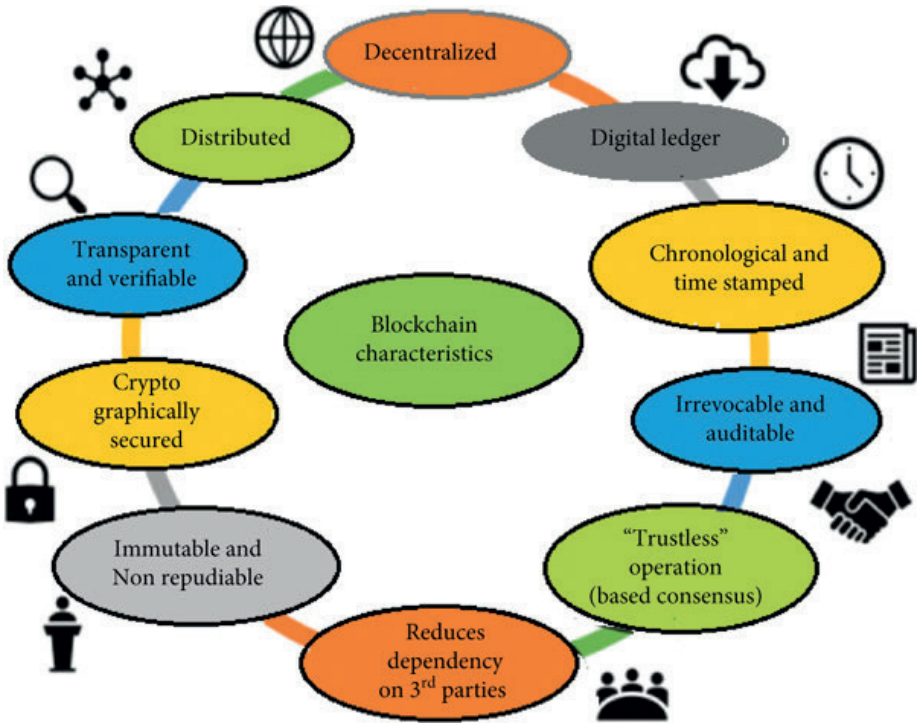


Figure 3: Key Characteristics of Blockchain Technology (Puthal et al., 2018)

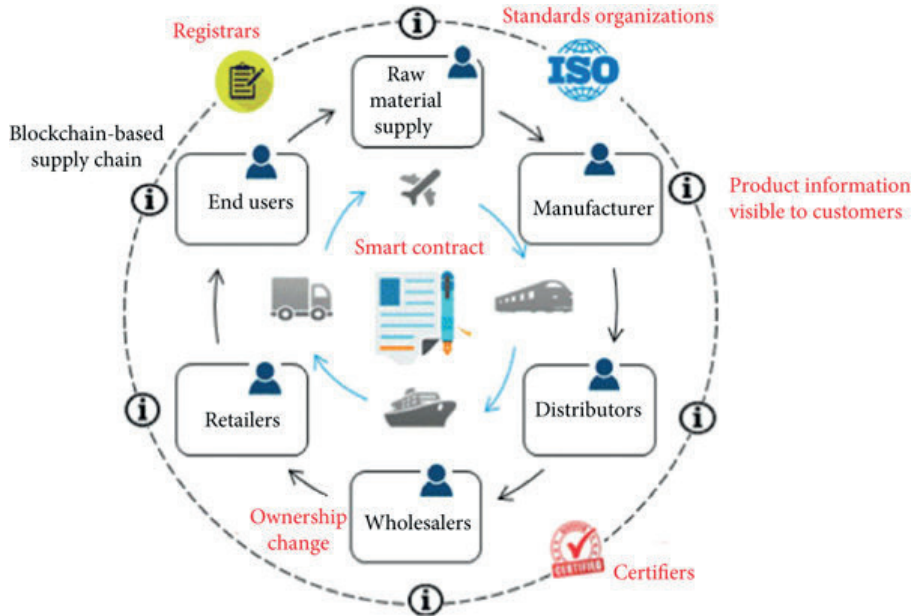


Figure 4: Advantages of Blockchain Technology in Food Supply Chain (Puthal et al., 2018)

6.2. 3D Printing

Compared to traditional methods of food production, 3D printing technology has become an attractive alternative due to its advantages such as less waste, more appealing products due to the desired structure and shape, time and energy savings in production, thus reducing the ecological footprint, and a simple production process (Yang et al., 2015). Since 3D printing technology in the food industry can combine many operations in a single step, it reduces the amount of waste generated. Since food production is only done on demand, it is one of the energy-saving technologies as it uses less water and energy, which plays an essential role in its widespread use in this sector (Shahbazi and Jäger, 2020). The general use of 3D printing technology has been found to reduce around 19 million tons of food waste annually in Europe alone, saving water and energy (Boissonneault, 2019).

3D food printing is also crucial for consumer groups requiring special diets. With this new technology, soft and easy-to-swallow foods can be produced for the elderly, children, pregnant women, athletes, and people with swallowing difficulties. Children can be encouraged to eat fruit and vegetables, and the amount of waste can be reduced (Godoi et al., 2016; Aday and Aday, 2020, Yang et al., 2015; Kouzani et al., 2017).

Upprinting food in the Netherlands has shown that food waste can be avoided by producing snack products from old bread, damaged or unsaleable fruit and vegetables, and leftover food in restaurants using 3D printing technology (Boissonneault, 2019). The Netherlands Organization for Applied Scientific Research has developed delicious and nutritious new food products with proteins derived from algae, insects, mushrooms, or lupine seeds as alternative ingredients instead of the usual food. In this context, 3D printing technology offers raw materials that are difficult to consume (Peppel, 2015; Sun et al., 2015; Izdebska and Zolek, 2016).

3D printer technology is based on layered deposition of the material placed in the printer cartridge using digital data on the computer (Yang et al., 2015). Depending on the nature of the food to be printed, different printing technologies are used in 3D food design. Factors such as the variety of food to be published, ease of use, and low cost affect the preferability of the printer. Selective laser sintering, binder jetting, ink jetting, and extrusion are commonly used in 3D food printing (Izdebska and Zolek-Tryznowska, 2016).

People's concerns about food safety and a negative view of laser technology limit food production with 3D printers (Liu et al., 2019). Selective laser and hot air sintering processes provide the advantage of quickly producing foods with a high production process. These technologies generally suit sugar and fat-based products with low melting points. The system is complex as many parameters are involved in production (Sun et al., 2015). While binder spraying

technology has benefits such as fast manufacturing and low material cost, it also has handicaps such as the product's rough surface and high machine costs. Binder spray technology can be used to produce visually appealing foods. Still, the low nutritional value and high sugar content are harmful to health, as they are associated with diabetes, obesity, and heart disease (Sun et al., 2015).

6.3. Edible Packaging

Food packaging ensures that the food reaches the consumer reliably, protects the product from microorganisms and chemicals to extend its shelf life, prevents external effects such as oxygen, moisture, and light, and protects the product during storage and transportation (Rhim et al., 2013).

Today's commonly used packaging materials are not biodegradable, which causes environmental concerns due to using petroleum-based synthetic polymers. For this reason, there is a growing interest in developing new biopolymer-based packaging materials to replace petroleum-based synthetic polymers. Biopolymers can be used as food packaging materials because of their environmental friendliness, low cost, and edible film/coating properties (Demir, 2015; Chaichi et al., 2017).

According to Oğuzhan and Yangılar (2016) and Benbettaïeb et al. (2016), edible films and coatings are described as edible films that are applied as a coating on food or between food components. Edible coatings extend the shelf life of food, reduce the risk of developing pathogens and provide the consumer with a helpful product with health benefits as they are carriers of bioactive chemicals (Lopez et al., 2013, Piñeros-Hernandez et al., 2017).

Edible polysaccharide-based coverings protect fresh and processed fruits and vegetables from oxidative deterioration, quality loss, and dehydration. When fruits and vegetables with edible films are stored, their shelf life is prolonged, and ripening is postponed due to the decreased respiration rate (Hassan et al., 2018; Işık et al., 2013; Kerch, 2015). Applying edible films to cheese prevents undesirable microbial development on the surface of the cheese while offering semi-permeable qualities for oxygen, carbon dioxide, and water vapor. Therefore, edible films help to regulate food quality, water loss, and the ripening rate. (Artiga et al., 2017; Costa et al., 2018).

Edible films and coatings on chocolate products help prevent fat release, browning reactions, and discoloration, such as moisture/fat migration, and harbor bacteria that rely on low water activity (Mchung and Avena, 2012; Dias et al., 2018). Since microbial spoilage starts on the surface of bakery products, edible films and coatings are alternative methods to prevent microbial spoilage, preserve dough properties, and extend shelf life (Quezada-Gallo, 2009). As edible packaging is readily biodegradable and made from natural,

biodegradable materials, it contributes to a more sustainable solution to the problem of environmental pollution. As the food and packaging industries search for sustainable and eco-friendly solutions, edible packaging presents a promising option.

7. Sustainability

The necessity of sustainable waste management to prevent and reduce waste that cannot be prevented is obvious. Sustainable waste management is essential for less cost, a cleaner environment, less waste of resources, preserving the future food supply-demand balance, and the tracklements of hunger problems (Çirişoğlu and Akoğlu, 2021)

Sustainable food production aims to ensure everyone can access sufficient, balanced, and healthy food without depleting or polluting existing natural resources or exacerbating the climate crisis (McClements, 2020).

One of the most important motivations for sustainable food production is that the needs of future generations should not be ignored while meeting the needs of today's environmentally friendly food production. However, this sustainability system's planning, transformation, and implementation processes, which are ideal in theory, can be pretty challenging (Gheewala et al., 2020).

In addition to the need for food to be accessible, safe, and nutritious (in terms of macro- and micronutrients), it should also be affordable by communities, the amount of clean water used in its production, and its global warming potential (in kg CO₂). The related values such as ozone depletion effect, toxin emission, fossil fuel consumption, total energy requirement, and total acid emission (based on kg SO₂) should be just as low, and the disposal of the wastes generated should be carefully monitored in consideration of the mentioned environmental factors (McClements, 2020).

Realizing holistic, sustainable food production can only be possible by transforming and adapting traditional production stages towards this goal. This transformation can only be realized if stakeholders involved in each stage of food/raw material procurement, production, consumption, and integrated waste management adopt and fulfill their respective roles. The concept of "digital transformation," developed for this purpose, has been one of the most prominent academic and industrial research areas in recent years (De Bernardi and Azucar, 2020; Herrero et al., 2020), meaning the use of technologies and innovations such as artificial intelligence for intelligent agriculture, projection, and urban agriculture, data science/management for less waste generation, and blockchain for supply chain traceability and auditability within the most up-to-date possibilities. Artificial intelligence technology holds great promise in the transformation required for sustainable food practices (Camaréna, 2020).

Developing next-generation packaging materials that do not pose a risk to climate change (biodegradable) and designing these products for industrial-scale use is one of the essential contributions that academia/industry collaboration can make to sustainable food production, regardless of geographical location (Mendes and Pedersen, 2021).

As another striking example, sterilizing packaged food products, especially by non-thermal physical methods such as high hydrostatic pressure and cold plasma, allows for lower energy consumption and reduced chemical additives/preservatives (Bourke et al., 2018). Although such methods are initially known as technologies that require high investment costs and are not very easy to adapt to the industry, thanks to the decrease in equipment production costs with advancing technology, investment costs have decreased, and the widespread use of equipment has increased (Kusmayadi et al., 2021).

This judgment is confirmed by the significant increase in scientific publications in recent years on investigating non-thermal food processing methods on a wide range of food ingredients using laboratory and semi-industrial scale equipment. As another example, microalgae can be a sustainable and up-and-coming source of nutrients/proteins for human and animal nutrition using biotechnology tools, which is a current and promising topic being studied by many researchers around the World. Microalgae can be an essential environmental alternative in sustainable food production thanks to their high-yielding production potential and rich nutrient content, which requires little energy consumption and does not increase the risk of climate crisis (Kusmayadi et al., 2021). The growing awareness of the climate crisis and the shift towards sustainable resources all over the World is a vital reality for the food industry. The opportunities offered by technology and innovation are essential tools for transforming sustainable food production (Ozkan et al., 2022)

8. Conclusion

This study provides general information on food loss and waste in Türkiye and worldwide. At every stage of the food supply chain, corrective and preventive actions should be implemented to lower food waste, increase public awareness of cost, environmental, and food safety issues, and promote sustainable food production. Innovative technologies can be used in this context. In accordance with the research conducted, it is seen that the studies with 3D food printers are progressing rapidly, the production of personalized food, the extension of the shelf life of food, the production of functional products with new texture and content, and the potential for the future use of this technology is relatively high. Recent research on the subject of edible films and coatings has focused on limiting the chemical, physical, and sensory deterioration of food during storage, prolonging shelf life, and improving

the mechanical integrity of the edible film and coating. Blockchain can create data that cannot be altered, so stakeholders can trust each other for smart agricultural management. Researchers should consider the benefits of blockchain technology for food safety.

References

- Al-Obadi, M., Ayad, H., Pokharel, S., & Ayari, M. A. (2022). Perspectives on food waste management: Prevention and social innovations. *Sustainable Production and Consumption*, 31, 190-208.
- Aday, S., & Aday, M.S. (2020). 3 Boyutlu yazıcıların gıda endüstrisinde kullanımı. Türkiye 13. Gıda Kongresi, 21-23 Ekim 2020, Çanakkale, Türkiye, 444 s.
- Artiga-Artigas, M., Acevedo-Fani, A., & Martín-Belloso, O. (2017). Improving the shelf life of low-fat cut cheese using nanoemulsion based edible coatings containing oregano essential oil and mandarin fiber. *Food Control*, 76, 1-12.
- Bagherzadeh, M., Inamura M., & Jeong H. (2014). Food waste along the food chain. *OECD Food, Agriculture and Fisheries Papers*, 71. OECD Publishing, Paris. <http://dx.doi.org/10.1787/5jxrcmftzj36-en>
- Bellemare, M.F., Çakır, M., Peterson, H.H., Novak, L. & Jeta, R. (2017). On the Measurement of Food Waste. *Journal of Agricultural Economics*, 99, Issue 5, 1148-1158.
- Benbettaieb, N., Chambin, O., Karbowski, T., & Debeaufort, F. (2016). Release behavior of quercetin from chitosan-fish gelatin edible films influenced by electron beam irradiation. *Food Control*, 66, 315-319.
- Berthet, M.A., Angellier-Coussy, H., Guillard, V., & Gontard, N. (2016). Vegetal fiber-based biocomposites: Which stakes for food packaging applications. *Journal of Applied Polymer Science*, 133, 42528-42546.
- Bräutigam, K. R., Jörissen, J., & Priefer, C. (2014). The extent of food waste generation across E.U. 27: Different calculation methods and the reliability of their results. *Waste Management & Research*, 32(8), 683-694.
- Boissonneault, T. (2019). Upprinting food transforms food waste into edible 3D printed snacks. Retrieved from <https://www.voxelmatters.com/upprinting-food-food-waste-edible-3d-printed-snacks/>
- Bourke, P., Ziuzina, D., Boehm, D., Cullen, P. J., & Keener, K. (2018). The Potential of Cold Plasma for Safe and Sustainable Food Production. *Trends in Biotechnology*, 36(6), 615-626.
- Buzby, J. C., & Hyman, J. (2012). Total and per capita value of food loss in the United States. *Food policy*, 37(5), 561-570.
- Camaréna, S. (2020). Artificial intelligence in the design of the transitions to sustainable food systems. *Journal of Cleaner Production*, 271, 122574.
- Chaichi, M., Hashemi, M., Badii, F., & Mohammadi, A. (2017). Preparation and characterization of a novel bionanocomposite ediblefilm based on pectin and crystalline nanocellulose. *Carbohydrate Polymers*, 157, 167-175.
- Costa, M.J., Maciel, L.C., Teixeira, J.A., Vicente, A.A., & Cerqueira, M.A. (2018). Use of edible films and coatings in cheese preservation: Opportunities and challenges.

Food Research International, 107, 84-92.

- Çerçioğlu, M. (2019). Sürdürülebilir Atık Yönetiminde Sera Atıklarının Kompost Olarak Değerlendirilmesi. *Bursa Uludağ Üniv. Ziraat Fak. Derg.*, 33 (1), 167-177.
- Çirişoğlu, E., & Akoğlu, A. (2021). Restoranlarda Oluşan Gıda Atıkları ve Yönetimi: İstanbul İli Örneği. *Akademik Gıda*, 19(1) 38-48.
- Dağdur, E., & Olhan, E. (2015). Küresel Gıda Güvencesi Endeksi Kapsamında Türkiye'nin Değerlendirilmesi. *Turkish Journal of Agricultural Economics*, 21(2), 49- 61.
- De Bernardi, P., & Azucar, D. (2020). *Innovative and Sustainable Food Business Models*. In: *Innovation in Food Ecosystems*. Contributions to Management Science. Springer, Cham. https://doi.org/10.1007/978-3-030-33502-1_7.
- Demir, S.S. (2015). *Modifiye Atmosferde Paketlemenin Tyty F1 Kokteyl Domatesinin Kalite ve Raf Ömrü Üzerine Etkisi* (Yüksek Lisans Tezi). Mustafa Kemal Üniversitesi, Fen Bilimleri Enstitüsü.
- Deniz, E., Yeşilören, G., & İşçi, N.Ö. (2015). Türkiye'de Gıda Endüstrisi Kaynaklı Biyokütle ve Biyoyakıt Potansiyeli. *Gıda*, 40(1), 47-54, doi: 10.15237/gida.GD14037.
- Dias, J., Coelho, P., Alvarenga, N.B., Duarted, R.V., & Saraiva, J.A. (2018). Evaluation of the impact of high pressure on the storage of filled traditional chocolates. *Innovative Food Science and Emerging Technologies*, 45, 36-41.
- Drewitt, T. (2013). *Food Waste Prevention in Quick Service Restaurants*. MSc Thesis. Lund University Master of Science in Environmental Management and Policy, Sweden.
- FAO (2011), Food and Agriculture Organization of the United Nations. *Global food losses and food waste – Extent, causes and prevention*. Rome.
- FAO (2013), Food and Agriculture Organization of the United Nations. *Food wastage footprint: impacts on natural resources*. Retrieved from <https://www.fao.org/3/i3347e/i3347e.pdf>
- FAO (2019). *The State of Food and Agriculture 2019. Moving forward on food loss and waste reduction*. Rome
- FAO (2020). Türkiye's National Strategy Document On Prevention, Reduction And Monitoring of Food Loss And Waste And Its Action Plan. Ankara.
- Gheewala, S. H., Jungbluth, N., Notarnicola, B., Ridoutt, B., & van der Werf, H. (2020). No simple menu for sustainable food production and consumption. *The International Journal of Life Cycle Assessment*, 25(7), 1175–11 82.
- Godoi, F.C., Prakash, S., & Bhandari, B.R. (2016). 3D printing technologies applied for food design: Status and prospects. *Journal of Food Engineering*, 179, 44–54.
- Hassan, B., Chatha, S.A.S., Hussain, A.I., Zia, K.M., & Akhtar, N. (2018). Recent advances on polysaccharides, lipids and protein based edible films and coatings: A review. *International Journal of Biological Macromolecules*, 109,1095-1107.
- Herrero, M., Thornton, P. K., Mason-D'Croz, D. et al. (45 more authors) (2020). Inno-

- vation can accelerate the transition towards a sustainable food system. *Nature Food*, 1 (5), 266- 272.
- Işık, H., Dağhan, Ş., & Gökmen, S. (2013). Gıda Endüstrisinde Kullanılan Yenilebilir Kaplamalar Üzerine Bir Araştırma. *Gıda Teknolojileri Elektronik Dergisi*, 8 (1), 26-35.
- Izdebska, J., & Zolek-Tryznowska, Z. (2016). 3D food printing – facts and future. *Agro Food Industry Hi-Tech*, 27(2), 33-36.
- İSRAF. (2019). 2018 Rakamları ile Türk Ekonomisinin Kara Deliği-1. Retrieved from <http://israf.org/sayfa/2018-RAKAMLARI-ILE-TURK-EKONOMISININ-KARA-DELIGI-ISRAF-1/557>
- Jörissen, J., Priefer, C., & Bräutigam, K. R. (2015). Food waste generation at household level: results of a survey among employees of two European research centers in Italy and Germany. *Sustainability*, 7(3), 2695-2715.
- Kanmaz, E.Ö., & Saral, Ö. (2017). Portakal kabuğundan elde edilen kritik altı su ekstraksiyonlarında antioksidan aktivite değerleri ile fenolik bileşikler arasındaki ilişki. *Gıda The Journal of Food*, 42(5), 485-493.
- Kehoe L, O'Connell N, Andrzejewski D, Gindner K, & Dalal D (2017). When two chains combine: Supply chain meets blockchain. *Deloitte*, 2–15.
- Kerch, G. (2015). Chitosan films and coatings prevent losses of fresh fruit nutritional quality: A review. *Trends in Food Science & Technology*, 2015, 46,159-166.
- Kırbaş, İ. (2018). Blokzinciri teknolojisi ve yakın gelecekteki uygulama alanları. *Mehmet Akif Ersoy Üniversitesi Fen Bilimleri Enstitüsü Dergisi*, 9(1), 75–82.
- Kouzani, A.Z., Adams, S., J. Whyte, D., Oliver, R., Hemsley, B., Palmer, S., & Balandin, S. (2017). 3D Printing of food for people with swallowing difficulties. *The International Conference on Design and Technology*, 23–29.
- Kshetri N., & Loukoianova E. (2019). Blockchain adoption in supply chain networks in Asia. *I.T. Professional*, 21(1), 11–15.
- Kusmayadi, A., Leong, Y. K., Yen, H.-W., Huang, C.-Y., & Chang, J.-S. (2021). Microalgae as sustainable food and feed sources for animals and humans – Biotechnological and environmental aspects. *Chemosphere*, 271, 129800.
- Liegeard, J., & Manning, L. (2020). Use of intelligent applications to reduce household food waste. *Critical reviews in food science and nutrition*, 60(6), 1048-1061.
- Lipinski B., Hanson C., Lomax J., Kitinoja L., Waite R. & Searchinger T. (2013). Reducing food loss and waste. working paper, Installment 2 of Creating a Sustainable Food Future, World Resources Institute, Washington, DC.
- Lipinski, B., Hanson, C., Lomax, J., Kitinoja, L., Waite, R., & Searchinger, T. (2016). *Toward a sustainable food system Reducing food loss and waste*. World Resource Institute, June,1–40. Retrieved from http://pdf.wri.org/reducing_food_loss_and_waste.pdf <https://ebrary.ifpri.org/digital/collection/p15738coll2/id/130211>

- Liu, Y., Zhang, W., Wang, K., Bao, Y., Renstein, J. M., & Zhou, P. (2019). Fabrication of gel-like emulsions with whey protein isolate using microfluidization: Rheological properties and 3D printing performance. *Food and Bioprocess Technology*, 12, 1967- 1979.
- Lopez, D., Marquez, A., Gutierrez-Cutino, M., Venegas-Yazigi, D., & Bustos, R., Matia- cevich, S. (2013). Edible film with antioxidant capacity based on salmon gelatin and boldine. *LWT- Food Science and Technology*, 77, 160-169.
- Lundqvist, J., Fraiture, C. de, Molden, & D. (2008). *Saving Water: From Field to Fork – Curbing Losses and Wastage in the Food Chain*. SIWI Policy Brief.
- Mahalik N, & Kim K (2016) The Role of Information Technology Developments in Food Supply Chain Integration and Monitoring. *Innovation and Future Trends in Food Manufacturing and Supply Chain Technologies*, 21-37
- McClements, D. J. (2020). Future foods: Is it possible to design a healthier and more sustainable food supply? *Nutrition Bulletin*, 45(3), 341–354.
- McHung, T.H., & Avena-Bustillos, R.J. (2012). *Applications of edible films and coatings to processed foods. Edible Coatings and Films to Improve Food Quality*, CRC Press, New York.
- Mendes, A. C., & Pedersen, G. A. (2021). Perspectives on sustainable food packaging: – is bio-based plastics a solution? *Trends in Food Science & Technology*, 112, 839–846.
- Meyer, H.C., Frieling, D., Hamer, M., & Oertzen G. (2017). Food Losses in Supply Chains for Fruits, Vegetables and Potatoes Between Field and Retail Shelf in North-Rhine Westphalia, Germany, *International Journal on Food System Dynamics*, Available online at www.centmapress.org .
- Morkunas, V. J., Paschen, J., & Boon E (2019). How blockchain technologies impact your business model. *Business Horizons*, 62(3), 295-306
- Oliveira, T.Í.S., Rosa, M.F, Ridout, M.J., Cross, K., Brito, E.S., Silva, L.M., & Azeredo, H.M. (2017). Bionanocomposite films based on polysaccharides from banana peels. *International Journal of Biological Macromolecules*, 101: 1-8.
- Oğuzhan-Yıldız, P., & Yangılar, F. (2016). Yenilebilir Film ve Kaplamaların Gıda Endüstrisinde Kullanımı. *BEÜ Fen Bilimleri Dergisi*, 5 (1):27-35.
- Ozkan G., Subaşı B.G, Kamiloğlu S., & Capanoğlu S. (2022). Sürdürülebilir Gıda ve Tarımsal Atık Yönetimi, *Çevre, İklim ve Sürdürülebilirlik*, 23(2):145-160.
- Özdemir A.İ. (2004). Tedarik zinciri yönetiminin gelişimi, süreçleri ve yararları. *Erciyes Üniversitesi İktisadi ve İdari Bilimler Fakültesi Dergisi*, 23, 87–96.
- Özdemir, A.İ., & Doğan, N.Ö. (2010). Tedarik zinciri entegrasyonu ve bilgi teknolojileri. *Sosyal Bilimler Enstitüsü Dergisi*, 28(1): 19–41.
- Pereira, P.H.F., Oliveirai T.Í.S., Rosa, M.F., Cavalcante, F.L., Moates, G.K., Wellner, N., & Azeredo, H.M. (2016). Pectin extraction from pomegranate peels with citric acid.

- Pineros-Hernandez, D., Medina-Jaramillo, C., Lopez-Cordoba, A., Goyanes, S., "Edible cassava starch films carrying rosemary antioxidant extracts for potential use as active food packaging", *Food Hydrocolloids*, 2017, 63:488-495
- Piñeros-Hernandez, D., Medina-Jaramillo, C., López-Córdoba, A., & Goyanes, S. (2017). Edible cassava starch films carrying rosemary antioxidant extracts for potential use as active food packaging. *Food Hydrocolloids*. 63, 488-495
- Puthal, D., Malik, N., Mohanty, S.P., Kougianos, E., Yang, C. (2018). The blockchain as a decentralized security framework (future directions). *IEEE Consumer Electronics Magazine*, 7, 18-21.
- Ouadi, M., Bashir, M. A., Speranza, L. G., Jahangiri, H. & Hornung, A. (2019). Food and market waste—a pathway to sustainable fuels and waste valorization. *Energy & Fuel*, 33 (10), 9843-9850.
- Quezada-Gallo, J.A. (2009). Delivery of Food Additives and Antimicrobials Using Edible Films and Coatings. *Edible Films and Coatings for Food Applications*, Springer, Science+Business Media, New York.
- Rhim, J-W., Park, H-M., & Hac, C-S. (2013). Bio-nanocomposites for food packaging applications. *Progress in Polymer Science*, 38, 1629-1652.
- Sezen, G. (2011). *Gıda Zincirlerinde Dağıtım Ağı Tasarımı: Hollanda'da Bir Uygulama*. Yüksek Lisans Tezi, Adnan Menderes Üniversitesi Sosyal Bilimler Enstitüsü, Aydın.
- Shahbazi, M., & Jäger, H. (2020). Current status in the utilization of biobased polymers for 3D printing process: a systematic review of the materials, processes, and challenges. *ACS Applied Bio Materials*, 4(1), 325-369.
- Smith, P. (2013). Delivering food security without increasing pressure on land. *Global Food Security*, 2(1), 18-23.
- Sputnik. (2019). Türkiye yılda 214 milyar liralık gıda israf ediyor. Retrieved from <https://tr.sputniknews.com/ekonomi/201909291040278150-turkiye-yilda-214-milyar-liralik-gida-israf- ediyor/>
- Sun, J., Zhou, W., Huang, D., Fuh, J.Y.H., & Hong, G.S. (2015). An overview of 3D printing technologies for food fabrication. *Food and Bioprocess Technology*, 8(8), 1605-1615.
- Tatlıdil, F.F., Dellal, İ., & Bayramoğlu, Z. (2013). Food Losses And Waste in Türkiye. Country Report, FAO Publication, www.fao.org/3/a-au824e.pdf
- T.C. Ticaret Bakanlığı, (2018). Türkiye İsraf Raporu. Tüketicinin Korunması ve Piyasa Gözetimi Genel Müdürlüğü, ISBN: 978-605-5254-31-5, Ankara.
- Tefera, T., Kanampiu, F., De Groote, H., Hellin, J., Mugo, S., Kimenju, S., & Banziger, M. (2011). The metal silo: An effective grain storage technology for reducing post-harvest insect and pathogen losses in maize while improving smallholder farmers' food security in developing countries. *Crop protection*, 30(3), 240-245.
- TGDF (2020), Türkiye Gıda ve İçecek Sanayii Dernekleri Federasyonu. 2020 Dış Ticaret Verileri. Retrieved from <https://www.tgdf.org.tr/wp-content/uploa->

ds/2021/04/2020-Dis-Ticaret-Verileri-HD.pdf

- TİSVA (2019). Dünyada Analizi. Gıda İsrafının Karşılaştırılması. Retrieved from https://israf.org/public/admin/filemanager/uploaded/kitapciklar/dunyada_gida_israfi_karsilastirma.pdf
- TÜİK (2021), Türkiye İstatistik Kurumu. Atık İstatistikleri 2020 Bülteni, yayımlanma tarihi 23 Aralık 2021, sayı: 37198.
- UNEP (2021), United Nations Environment Programme. UNEP Food Waste Index Report. Retrieved from <https://www.unep.org/resources/report/unep-food-waste-index-report-2021>.
- U.S. Environmental Protection Agency. (2016). United States 2030 Food Loss and Waste Reduction Goal. Washington DC. Retrieved from <https://www.epa.gov/sustainable-management-food/united-states-food-loss-and-waste-2030-champions>
- Väisänen, T., Haapala, A., Lappalainen, R., & Tomppo, L. (2016). Utilization of agricultural and forest industry waste and residues in natural fiberpolymer composites: A review. *Waste Management*, 54, 62-73,
- Wang, L.E., Liu, Gç, Liu, X,Liu,Y., Gao, J., Zhou, B., Gao, S., & Cheng, S. (2017). The weight of unfinished plate: a survey based characterization of restaurant food waste in Chinese cities. *Waste Management*, 66, 3-12
- Wikiera, A., Mika, M., Starzyńska-Janiszewska, A., & Stodolak, B. (2016). Endo-xylanase and endocellulase-assisted extraction of pectin from apple pomace. *Carbohydrate Polymers*, 142, 199-205.
- Yang, F., Zhang, M., & Bhandari, B. (2015). Recent development in 3D food printing. *Critical Reviews in Food Science and Nutrition*, 57(14): 31.
- Yıldızbaşı A, & Üstünyer P. (2019). Tarımsal Gıda Tedarik Zincirinde Blokzincir Tasarımı: Türkiye’de Hal Yasası Örneği. *Bartın Orman Fakültesi Dergisi*, 21(21): 458-465.
- Yılmaz, M.T., Muslu, A., Karasu, S., Bozkurt, F., Dertli, E. (2017). Portakal Posasından Modifiye Pektin Eldesi ve Optimizasyonu, Kompozisyonel ve Yatışkan Faz Özelliklerinin Karakterizasyonu. *Tekirdağ Ziraat Fakültesi Dergisi*, 14(2), 71-80.



Chapter 13

PREDICTIVE MODELING OF R&D EXPENDITURES FOR TURKEY: SVR KERNEL VARIATIONS

Didem GULERYUZ¹

Pelin AKIN²

¹ Doç.Dr., Bayburt Üniversitesi, Uygulamalı Bilimler Fakültesi, Yönetim Bilişim Sistemleri, dguleryuz@bayburt.edu.tr, ORCID: 0000-0003-4198-9997

² Arş.Gör.Dr., Çankırı Karatekin Üniversitesi, Fen Fakültesi, İstatistik Bölümü, pelinakin@karatekin.edu.tr, ORCID: 0000-0003-3798-4827.

1. Introduction

Research and Development (R&D) activities have gained strategic importance with the rapid advancement of technology. The advancement of science and technology affects economic growth and development and changes social and cultural dynamics. In this context, technological developments can be sustainable, and competitive advantages can be achieved through increased R&D activities. High-technology-intensive economies aim to open to new markets and increase their R&D expenditures to maintain competitiveness. This situation enables scientific discoveries and technological innovations to emerge rapidly and companies to gain competitive advantage and keep their leading positions at the global level. R&D activities are critical for understanding the complexity of today's world and finding practical solutions to future challenges. Countries' investments in R&D are essential to gain a competitive advantage.

Therefore, R&D expenditures fundamentally shape international competitiveness by contributing to global scientific and technological progress (Edler et al., 2023). These expenditures have significant environmental and social impacts by supporting efforts to achieve sustainable development goals. Since R&D activities are based on providing solutions to global problems, they can make considerable contributions in critical areas such as energy, health, environment, and security (Shahsavari and Akbari, 2018). Moreover, its effects on strengthening international cooperation are also significant regarding its potential to increase knowledge transfer and support the knowledge economy. Increasing R&D expenditures produces more effective solutions by supporting technology transfer globally. Therefore, R&D activities are a priority step to increasing international knowledge sharing, expanding the impact of R&D, and finding solutions to global problems (Davies et al., 2023). As a result, increasing R&D expenditures can be considered as a strategic step towards a more sustainable, innovative, and equitable future, as they both stimulate innovation by accelerating progress in science and technology and have the potential to provide solutions to significant problems.

R&D investments are vital for Turkey's competitiveness in the global economic arena. Such assets are critical in ensuring sustainable economic growth, technological development, and international competitiveness in the country. Innovative studies and technological advancements strengthen the

position of Turkish companies in world markets and simultaneously increase new business opportunities and sectoral diversification (Ekinci, Koçak, and Benli, 2023). R&D investments are expected to increase globally and in Turkey because these investments aim to provide a technological competitive advantage, encourage innovation, and support economic growth. At the same time, R&D activities are important to achieve sustainable development goals, solve environmental problems, and strengthen international reputation. These increases aim to improve countries' scientific and technological capacities by creating a qualified labor force. Figure 1 shows the increase in R&D expenditures in the last 25 years for Turkey, worldwide, and OECD countries (OECD, 2020).

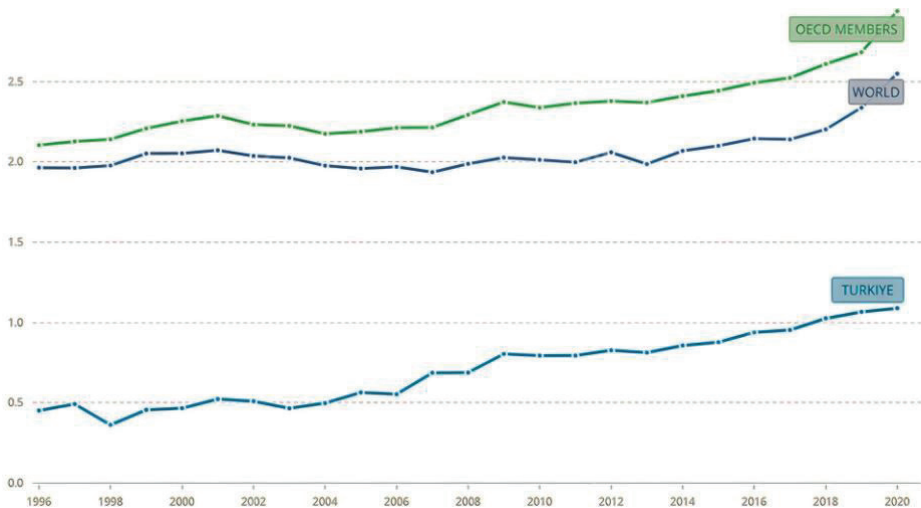


Figure 1. Research and development expenditure (% of GDP) - Turkiye, OECD members, world

According to Figure 1, although the ratio of R&D investments to GDP in Turkey has increased from past to present, it has remained far behind the averages of the world and OECD countries. Economic growth can be supported by allocating more resources to R&D, thus contributing more effectively to development targets. The development of technological infrastructure and efforts to produce advanced technology products and sustainable energy solutions will accelerate digital transformation. At the same time, by increasing the need for qualified human resources, it will be possible

to contribute to the training of science and technology experts, thus supporting Turkey's progress in the knowledge economy (Yantur, 2023).

Increasing the innovation capacity of Turkish companies will provide a competitive advantage both in the domestic market and internationally so that R&D efforts in areas such as accelerating industrial transformation, designing more efficient production processes, sustainable energy solutions, and smart manufacturing systems will make Turkish industry more competitive (Jahanshahi, Adiguzel, and Cakir 2023) In conclusion, increasing R&D expenditures for Turkey to achieve its long-term development targets will contribute to a sustainable future by placing its economic foundations on more solid ground. Since the increase in R&D expenditures will contribute to the acceleration of technological progress, the promotion of innovation, and the maintenance of competitive advantages, forecasting R&D expenditures will facilitate the formulation of a sustainable strategy, the effective use of resources, and the achievement of long-term scientific and economic goals. The fact that R&D expenditures accelerate industrial transformation and work in more efficient production processes, sustainable energy solutions, and smart production systems provide an opportunity to make the Turkish industry more competitive. Therefore, increasing R&D expenditures to achieve Turkey's long-term development goals is essential, as this will contribute to a sustainable future by consolidating the country's economic foundations. This increase in R&D expenditures is a strategic step for accelerating technological progress, fostering innovation, and maintaining competitive advantages. Therefore, forecasting R&D expenditures is important for Turkey regarding efficient use of resources and establishing a critical strategy to achieve long-term scientific and economic goals. At the global level, forecasting R&D expenditures can offer the potential to support continuous and high-quality scientific and technological progress. This will lead to the rapid emergence of discoveries and innovative solutions, contribute significantly to the overall body of knowledge, and play a critical role in gaining competitive advantage. According to the development levels of countries, accurate estimation of R&D expenditures for developed countries is crucial in maintaining their technological leadership and preserving their competitive advantage. This is because these estimates strengthen strategic planning and can help to ensure a strong competitive advantage in science and technology-oriented sectors. Forecasting R&D expenditures in developing countries is important to provide effective strategic guidance on economic

transformation, local innovation, and global competitiveness. In less developed countries, R&D forecasts play a key role in sustainable development by supporting the development of solutions to basic needs, increasing productivity in sectors, and focusing on development goals. As a result, the estimation of R&D expenditures will provide positive effects in a wide range of areas, from strategic planning of the business world to scientific progress, from economic development to competitive advantage. Therefore, accurate and reliable forecasts are the basis of a successful and sustainable R&D strategy.

Moreover, the ability of the government to manage R&D expenditures depends on identifying the main factors affecting expenditures and selecting suitable forecasting models. Forecasting studies in the literature generally use traditional statistical models. These models can give good results when the correlation between variables is strong. However, with the development of machine learning methods, non-linear relations among inputs and outputs can be modeled quickly, and variables that are not correlated with the output variable can also be included in the model. Especially recently, with the development of data science and machine learning techniques, machine learning-based forecasting models have been used in many fields (Samastı & Küçükdeniz, 2023; Zhao et al., 2018) For this reason, an artificial intelligence model to be developed to estimate R&D expenditures is predicted to provide effective results (Güteryüz and Özden 2020). When previous studies are analyzed, the studies conducted to estimate R&D expenditures can be classified as statistical and artificial intelligence-based methods (Koçak and Ulucak, 2019; Tümer and Akkuş, 2018a; Wang, Khalid, and Mahmood, 2023). For this reason, some previous studies are given below.

Akar (2023) examined the effects of economic complexity and R&D expenditures on economic growth in highly competitive countries. The study used the panel cointegration method to evaluate long-term mutual relations using the data set covering 1995-2019. The panel cointegration tests reveal a long-term cointegration relationship between overall gross domestic product (GDP) per capita, economic complexity index, and R&D expenditures. The economic complexity index, R&D expenditures, and GDP per capita variables positively correlate with the selected countries.

Wang et al. (2023) aimed to analyze the long-term effects of economic policy uncertainty on R&D activities in Asian countries. The panel cointegration method was used for the data set covering 2003-2018, and variables such as technological expertise and economic activities were examined for the countries identified in the study. The study results show that increased economic policy uncertainty reduces R&D expenditures. In addition, it is observed that when economic growth accelerates, the tendency of countries to invest in R&D increases, and international trade also encourages R&D.

Nasir and Zhang (2024) examined the relationship between innovation inputs, outputs, and productivity is analyzed in detail. In this context, the emphasis is on how the factors can be separated according to a country's income level. Within the scope of quantitative research, a data set for 105 countries was prepared, and regression and panel regression techniques were used to obtain long-term forecasts. The study's results were evaluated by considering the comparison of these methods. The findings emphasized that it is important to develop customized innovation strategies, considering that the economic situation of the countries included in this study constantly changes.

Koçak ve Ulucak (2019) examined the impact of energy research and development (R&D) expenditures, which contribute to energy innovations, on CO₂ emissions using the dynamic panel data method for 19 high-income OECD countries between 2003-2015. According to the results of the analysis, it is observed that R&D expenditures for energy efficiency and fossil energy have an increasing effect on CO₂ emissions. However, contrary to the predictions, a significant relationship was not found between renewable energy R&D expenditures and CO₂ emissions.

Tümer ve Akkuş (2018) developed an artificial neural network algorithm that uses R&D expenditures as input to predict Turkey's GDP per capita. In this context, models with different neural network architectures were designed. Other input variables are education level, number of academic articles published per capita, number of researchers per employment, and number of patents per capita. The comparison between the model results and real data showed a high correlation coefficient (0.96), indicating that the developed model can be used for GDP per capita estimation with non-economic input variables.

In the existing body of research, few studies have utilized artificial neural networks (ANN) for predicting R&D spending. Surprisingly, the literature has a noticeable gap as the Support Vector Regression (SVR) model is not commonly employed for R&D expenditure estimation. This study aims to fill this gap by utilizing various input variables such as GDP per capita, researchers in R&D, patent applications, labor force, females (% of total labor force), and medium and high-tech exports to R&D expenditure (% of GDP) in Turkey. These variables have been previously used in R&D spending estimation literature (Akar, 2023; Ekinçi et al., 2023; Griffith, Redding, and Reenen, 2004; Wang et al., 2023). This study employs SVR with different kernels to estimate R&D spending using the selected indicators as input features. This research aims to make a distinctive contribution to the existing literature by introducing forecasting models based on machine learning methodologies, specifically Support Vector Regression (SVR) with diverse kernels. The study employs SVR models with various kernels to predict the Research and Development (R&D) spending in Turkey. Notably, to the authors' knowledge, the application of SVR models with different kernels for modeling R&D spending has yet to be explored in previous research endeavors. This novel approach seeks to enhance the understanding and accuracy of forecasting R&D expenditure by leveraging the versatility offered by SVR models with diverse kernels.

The manuscript is organized into four sections. The second section encompasses the materials and methods employed in the study, along with the evaluation of model accuracy and the structural details of the developed models. Subsequently, the third and fourth sections present the outcomes derived from the developed models and the concluding remarks, respectively. This structured framework facilitates a comprehensive understanding of the study's methodology, outcomes, and overall conclusion.

2. Material and Method

2.1. Data Collection Process

Estimating R&D expenditure (% of GDP) in Turkey involves the utilization of diverse indicators, including GDP per capita, researchers in R&D, patent applications, female labor force (% of total labor force), and medium and high-tech exports. The dataset spans 1990 to 2019 and has been compiled from various sources. Table 1 provides a detailed elucidation of variable definitions,

abbreviations, units, and corresponding data sources, enhancing the clarity and transparency of the utilized variables in the analysis.

Table 1. Explanation of Variable Definitions

| Variable | Abbr. | Unit | Sources |
|--------------------------------------|-------|------------------------|------------------|
| Research and development expenditure | RDE | % of GDP | (OECD 2020) |
| GDP per capita | GDP | Constant 2015 US\$ | (OECD 2021) |
| Researchers in R&D | RRD | per million people | (OECD 2020) |
| Patent applications | PA | number | (OECD 2020) |
| Labor force, female | LFF | % of total labor force | (Worldbank 2021) |
| Medium and high-tech exports | MHE | % manufactured exports | (Worldbank 2021) |

Table 2 provides the descriptive statistics of both input and output variables, offering a comprehensive overview of their key statistical measures.

Table 2. The basic statistics

| | GDP | RRD | PA | LFF | MHE | RDE |
|-----------------|----------|---------|---------|-------|-------|------|
| Mean | 7989.10 | 715.40 | 3307.74 | 28.45 | 35.36 | 0.63 |
| Std | 2247.79 | 472.47 | 2388.00 | 2.13 | 9.10 | 0.24 |
| Min | 5256.93 | 181.88 | 837.00 | 24.94 | 19.65 | 0.28 |
| Mak | 12072.40 | 1775.35 | 8555.00 | 32.47 | 45.54 | 1.09 |
| Kurtosis | -1.10 | -0.75 | -0.27 | -0.80 | -1.31 | 1.17 |
| Skew | 0.55 | 0.69 | 0.97 | 0.06 | -0.63 | 0.33 |

The selection of input indicators was guided by thoroughly examining existing literature on R&D expenditure prediction studies. Gross domestic product per capita is an indicator obtained by dividing the total economic production in a country by the number of populations. The relationship between GDP per capita and R&D expenditures reflects the interaction between a country's economic size and innovation capacity (Ozden and Guleryuz, 2021). The general tendency is that countries with higher gross domestic product per capita tend to increase their R&D expenditures. This is because more prosperous economies generally invest more in technological development and innovation. However, this relationship may vary depending on several factors, such as sectoral distribution, economic policies, cultural factors, and country-specific characteristics. For example, a country's economic policies

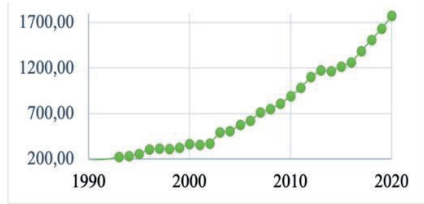
and R&D promotion strategies may affect R&D expenditures regardless of economic size. Therefore, analyses that consider the specific conditions of each country will produce more effective results (Gumus and Celikay, 2015). There is a strong link between patent applications and R&D expenditures. Increased R&D expenditures in a country generally result in discoveries, technological innovations, and inventions and lead to an increase in patent applications. This is because companies need to protect new technologies that emerge because of R&D activities. Patent applications can be an important indicator of a country's innovation capacity and competitive advantage. Therefore, high R&D expenditures in a country are usually parallel to the increase in patent applications because new inventions that emerge as a product of these expenditures enable companies to maintain their competitive advantage and, at the same time, support economic growth (Meliciani 2000). Considering the proportion of the female labour force in the total labour force, greater participation of women in the labour force generally encourages innovation by increasing diversity and different perspectives. This allows for various skills and perspectives to be brought to R&D activities, resulting in more comprehensive and innovative results (Singh and Kumar, 2022). When analyzed regarding exports of medium and high technology products, R&D expenditures can increase the production of medium and high technology products by supporting technological innovations in a country's industrial sectors. Thus, competitive, on the other hand, the increase in medium and high technology advantage in international markets can be achieved, and economic development can be encouraged (Ozden, 2022b). Exports are an indicator of a country's technological competitiveness. It is essential for sustainable economic growth and global competitiveness because of R&D-oriented strategies (Aldakhil et al., 2019; Ozden, 2022a). It can be decided whether to use feature selection according to the prediction performance of the selected input variables. When previous studies are analyzed, the principal component analysis method is frequently used for feature selection (Gıdık 2021).

In light of all these indicators, in this study, GDP per capita, researchers in R&D, patent applications, female labor force (% of total labor force), and medium and high-tech exports variables are used as inputs to estimate Turkey's R&D expenditure. Figure 2 illustrates the yearly fluctuations in the input indicators.

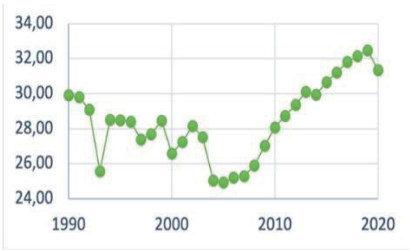
GDP Per Capita (constant 2015 US)



Researchers in R&D (per million people)



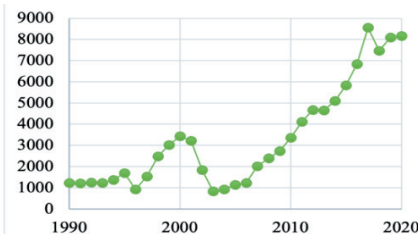
**Labor force, female
(% of total labor force)**



**Medium and high-tech exports
(% manufactured exports)**



Patent applications



R&D expenditure (% of GDP)

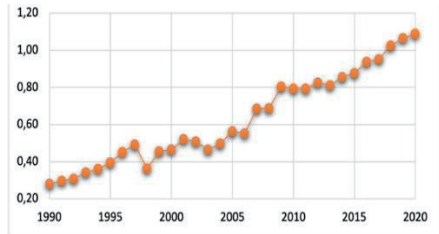


Figure 2. Trends in Variables from 1990 to 2020

Data normalization has been applied because input and output variables are in different units. The entire dataset has been normalized within the range of 0.05 to 0.95. It is recognized that normalizing input data before the training phase in machine learning applications serves to mitigate estimation errors and reduce algorithmic computation time. This normalization not only impacts the precision of predictions but also aids in overcoming limitations in model

learning. Consequently, the gradient descent is facilitated to converge more expeditiously.

2.2. Support Vector Regression (SVR)

Support Vector Regression (SVR) is a support vector machine (SVM) algorithm used especially in regression analysis. In addition, when the literature is examined, it is seen that SVM is frequently used for classification problems. This basic structure developed for SVM can be adapted to regression problems. C and ϵ are the two most important parameters in the structure of SVR. C controls the margin around a hyperplane, and ϵ is the error tolerance (Candelieri et al. 2019).

Kernel functions, which play an essential role in the success of SVR, allow data points to be transformed into high-dimensional spaces. This transformation is used to handle non-linear relationships that pose difficulties in problem-solving. In this study, new prediction models will be developed using different kernel functions for the SVR model. Different kernel functions may provide different advantages depending on the data set. Some of the capabilities and advantages of using different kernel functions are listed below (Candan and Şahin, 2023; Colkesen, Sahin, and Kavzoglu, 2016).

- Kernel functions can be used to capture complex structures that other models cannot analyze by transforming the data used into high-dimensional spaces, providing the benefit of being able to analyze non-linear relationships.
- Kernel functions enable SVM and SVR to be successful for data sets that a linear hyperplane cannot separate.
- Kernel functions provide a flexible modeling capability by transforming the data into different dimensional spaces. Thus, creating more complex and generally valid models in regression or classification problems is possible.
- Kernel functions offer the flexibility to adjust the model's hyperparameters, allowing different kernel functions to suit different data structures and problems. This gives the user more options to optimize the performance of the model.

The choice of kernel functions should be determined based on a specific problem. The most appropriate kernel function should be selected depending on the data set's characteristics, the problem's complexity, and the user's performance targets. When the previous studies are examined, there is no

frequently used optimization method for kernel function selection. Therefore, developing optimization models and designing experiment methods to be applied to select the appropriate kernel function may help determine the optimum kernel function. In many interdisciplinary studies in the literature, design experiment methods are commonly used to determine the optimum variables (Kutlu, Kamiloglu, and Elbir, 2022; Uçurum et al., 2018). These methods can also be used to select the optimum kernel function.

The kernel functions used in this study are the linear kernel, Gaussian kernel, quadratic kernel, and cubic kernel. The SVR equations are below via Eq. (1) (Guleryuz 2022).

$$\text{maximize} \begin{cases} \frac{1}{2} \sum_{i=1}^l (\vartheta_i - \vartheta_i^*) (\vartheta_i - \vartheta_i^*) K(x_i, x_j) \\ -\epsilon \sum_{i=1}^l (\vartheta_i + \vartheta_i^*) + \sum_{i=1}^l y_i (\vartheta_i - \vartheta_i^*) \end{cases} \quad (1)$$

$$\text{s. t} \begin{cases} \sum_{i=1}^l (\vartheta_i - \vartheta_i^*) = 0 \text{ and } \vartheta_i, \vartheta_i^* \in [0, C] \\ 0 \leq \vartheta_i, \vartheta_i^* \leq \frac{C}{l} \\ i = 1, 2, \dots, l \end{cases}$$

In Equation (1), the symbols ϑ_i and ϑ_i^* represent nonnegative multipliers associated with each observation. Here, x_i denotes the current data, and l denotes the size of the data set. The penalty coefficient is denoted by C , while ϵ signifies the penalty dimension. The kernel function is also represented as $K(x_i, x_j)$. The optimization process involves adjusting the vector ϑ , expressed as $[\vartheta_1, \vartheta_1^*, \dots, \vartheta_l, \vartheta_l^*]^T$, to attain the optimal solution. The formulation of the regression equation is presented in Equation (2).

$$f(x) = \sum_{i=1}^l (\vartheta_i - \vartheta_i^*) K(x_i - x_j) + b^* \quad (2)$$

The kernel function transforms the data into a higher-dimensional space, representing the non-linear function as a linear function within the input space. Consequently, kernel functions provide a convenient means of

addressing non-linear problems (Akin and Koc, 2021; Kouziokas, 2020). Various types of kernel functions, as detailed in Table 3, contribute to this capability.

Table 3. SVR Kernel Functions

| Kernel Function | Expression |
|------------------------|--|
| Linear | $K(x_i, x_j) = (x_i, x_j)$ |
| Polynomial | $K(x_i, x_j) = (\langle x_i, x_j \rangle + 1)^d$ |
| Gaussian | $K(x_i, x_j) = e^{-\frac{\ x_i - x_j\ ^2}{2\gamma^2}}$ |
| Sigmoid | $K(x_i, x_j) = \tanh(\gamma \langle x_i, x_j \rangle + 1)^d$ |

2.3. Performance evaluation criteria

Using performance evaluation criteria to compare Support Vector Regression (SVR) models with different kernel functions is critical. These criteria help to assess the estimation ability of the model objectively. The evaluation of the model's accuracy was conducted through the utilization of key metrics, namely the root mean square error (RMSE), the coefficient of determination (R^2), and the mean absolute error (MAE). It is imperative to undertake a comparative analysis of these metrics to facilitate meaningful interpretations (Akin and Koc, 2022; Atalan, Şahin, and Atalan, 2022; Ozden, 2022a). The mathematical expressions defining the performance criteria are provided in Equations (3) through (5), delineating the quantitative measures for assessing the model's predictive accuracy and efficacy.

$$MAE = \frac{1}{n} \sum_{t=1}^n |RDE_i^{observed} - RDE_i^{predicted}| \quad (3)$$

$$RMSE = \sqrt{\frac{1}{n} \sum_{t=1}^n (RDE_i^{observed} - RDE_i^{predicted})^2} \quad (4)$$

$$R^2 = \left(\frac{\sum_{i=1}^n (RDE_i^{observed} - \overline{RDE_i^{observed}}) (RDE_i^{predicted} - \overline{RDE_i^{predicted}})}{\sqrt{\sum_{i=1}^n (RDE_i^{observed} - \overline{RDE_i^{observed}})^2 (RDE_i^{predicted} - \overline{RDE_i^{predicted}})^2}} \right)^2 \quad (5)$$

In the context of the given information, 'n' signifies the total number of observations. $RDE_i^{observed}$ represents a variable's actual or observed value denoted as RDE at a specific time point 'i', while $RDE_i^{predicted}$ corresponds to the anticipated or estimated value of the same variable RDE at that time 'i'.

3. Results and Discussion

Support Vector Regression (SVR) models with different kernels have been constructed to delineate the association between five input variables and the R&D spending variable. The results of performance metrics for all models are presented in Table 4. Consequently, the developed models are prioritized based on the coefficient of determination (R^2) values.

Table 4. Evaluation metrics for the created models

| | Model Type | RMSE | RSquared | MAE | Rank |
|-----------------------|----------------------|------------|----------|-------|-------|
| Training Phase | Linear SVR | 0,074 | 0,938 | 0,052 | 1 |
| | Quadratic SVR | 0,086 | 0,915 | 0,060 | 3 |
| | Cubic SVR | 0,088 | 0,913 | 0,058 | 4 |
| | Fine Gaussian SVR | 0,175 | 0,654 | 0,148 | 6 |
| | Medium Gaussian SVR | 0,091 | 0,905 | 0,070 | 5 |
| | Coarse Gaussian SVR | 0,080 | 0,927 | 0,067 | 2 |
| | Testing Phase | Linear SVR | 0,069 | 0,872 | 0,057 |
| Quadratic SVR | | 0,068 | 0,876 | 0,055 | 2 |
| Cubic SVR | | 0,079 | 0,831 | 0,063 | 5 |
| Fine Gaussian SVR | | 0,096 | 0,750 | 0,075 | 6 |
| Medium Gaussian SVR | | 0,065 | 0,888 | 0,057 | 1 |
| Coarse Gaussian SVR | | 0,073 | 0,855 | 0,060 | 4 |

All models effectively predict R&D spending based on identified indicators. The R^2 values for these six models range from 0,938 to 0,654 during the training phase, affirming the robust predictive capability of the developed models. The predictive efficacy of the models hinges on the accurate representation of relationships between inputs and outputs established during the training phase. Correct modelling of this relationship indicates the machine learning algorithm yielding satisfactory results during the subsequent test phase. To assess generalization performance, 30% of the data was reserved for testing. The predictive ability of the developed models in the testing phase is detailed in Table 4. Notably, the R^2 value of the Support Vector Regression with linear kernel model is 0,938 during training and 0,872 during testing, respectively. However, another model with a substantially higher R^2 value during the testing phase, indicating superior predictive performance, deserves attention. This model is the Medium Gaussian SVR, which attains an R^2 value of 0,888. High accuracy in the testing phase is anticipated for machine learning prediction models.

Consequently, among the six different models developed, the Medium Gaussian SVR model has been identified as the most suitable for predicting R&D expenditures. Nevertheless, scrutinizing the R^2 values of the other models, they range between 0,888 and 0,750. Consequently, all developed models have yielded acceptable results for estimating R&D expenditures in Turkey. Figure 3 illustrates a comparative analysis of the developed models, evaluating their performance using R^2 metrics in both the training and testing phases.

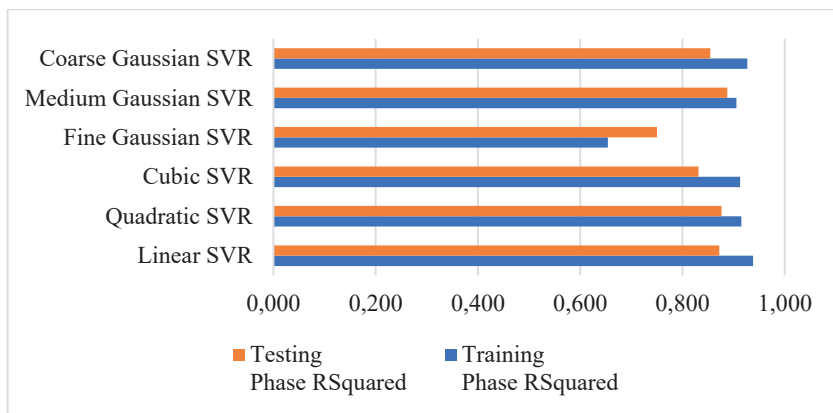


Figure 3. The comparative analysis of the constructed models.

Figure 4 presents scatter plots that intricately delineate the comparative analysis between the actual values of R&D expenditure and the prognostications derived from the Medium Gaussian Support Vector Regression (SVR) model across the corresponding years.

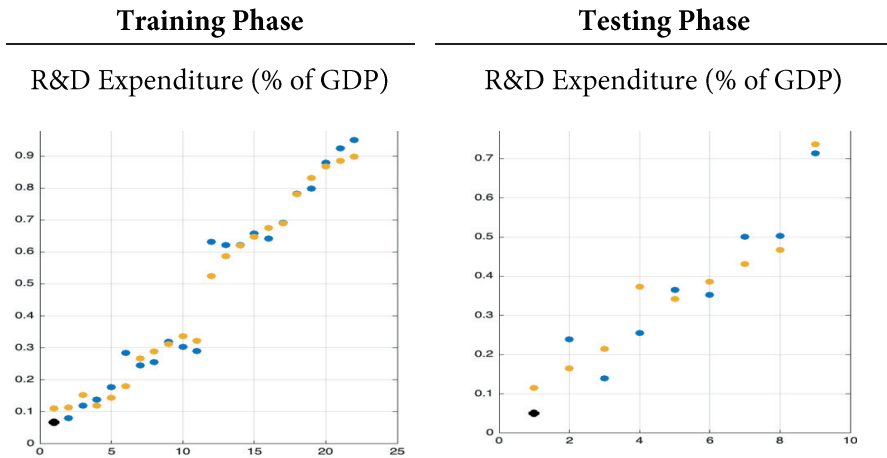


Figure 4. Scatter plots of medium Gaussian model for both phases.

4. Conclusion

Economic development is a tool for measuring the growth and development of a country. Technological innovations and information technologies are vital factors in economic growth today, contributing to the development and renewal of production methods. Investing in research, development, and innovation supports countries' competitiveness and progress in the world market. At the same time, by ensuring the development of employees, it creates new products and is instrumental in increasing the welfare of countries. Therefore, innovation is one of the most critical factors contributing to the growth and welfare of a nation. It is accepted that economically strong governments can allocate more money to research and development. Sustainable economic growth will ensure economic and social development and the transfer of technological wealth to future generations. In this study, a machine learning-based forecasting model is developed to estimate Turkey's R&D expenditures using five different input variables. In the model development phase, Support Vector Regression (SVR) algorithm is designed using different kernel functions. According to the study results, the algorithm using the medium gaussian kernel function for the data set covering 1990-2021 has superior forecasting ability compared to other developed algorithms. This

study can serve as a decision support system for decision-makers to determine Turkey's economic development strategies, optimize R&D policies, promote industrial innovation, increase its international reputation, and contribute to sustainable development goals. In future studies, the kernel function and some parameters the developer determines for SVR can be determined using optimization algorithms and contribute to the prediction performance.

References

- Akar, Tuba. 2023. "Ekonomik Karmaşıklık, Ar-Ge Harcamaları ve Ekonomik Büyüme İlişkisi." *Pamukkale Üniversitesi Sosyal Bilimler Enstitüsü Dergisi* (55):315–29. doi: 10.30794/pausbed.1117645.
- Akın, Pelin, and Tuba Koc. 2021. "Comparison of Kernel Functions in Geographically Weighted Regression Model: Suicide Data as an Application." *Acta Infologica* 5(2):333–40. doi: 10.26650/acin.914952.
- Akın, Pelin, and Tuba Koc. 2022. "Estimation of High School Entrance Examination Success Rates Using Machine Learning and Beta Regression Models." *Journal of Intelligent Systems: Theory and Applications* 5(1):9–15. doi: 10.38016/jista.922663.
- Aldakhil, Abdullah Mohammed, Adyia Zaheer, Sobia Younas, Abdelmohsen A. Nassani, Muhammad Moinuddin Qazi Abro, and Khalid Zaman. 2019. "Efficiently Managing Green Information and Communication Technologies, High-Technology Exports, and Research and Development Expenditures: A Case Study." *Journal of Cleaner Production* 240:118164. doi: <https://doi.org/10.1016/j.jclepro.2019.118164>.
- Atalan, Abdulkadir, Hasan Şahin, and Yasemin Ayaz Atalan. 2022. "Integration of Machine Learning Algorithms and Discrete-Event Simulation for the Cost of Healthcare Resources." *Healthcare* 10(10). doi: 10.3390/healthcare10101920.
- Candan, Hasibe, and Hasan Şahin. 2023. "Breast Cancer Prediction with Artificial Intelligence Based Clinical Decision Support System." *Electronic Letters on Science and Engineering* 19(1):29–35.
- Candelieri, Antonio, Ilaria Giordani, Francesco Archetti, Konstantin Barkalov, Iosif Meyerov, Alexey Polovinkin, Alexander Sysoyev, and Nikolai Zolotykh. 2019. "Tuning Hyperparameters of a SVM-Based Water Demand Forecasting System through Parallel Global Optimization." *Computers & Operations Research* 106:202–9. doi: <https://doi.org/10.1016/j.cor.2018.01.013>.
- Colkesen, Ismail, Emrehan Kutlug Sahin, and Taskin Kavzoglu. 2016. "Susceptibility Mapping of Shallow Landslides Using Kernel-Based Gaussian Process, Support Vector Machines and Logistic Regression." *Journal of African Earth Sciences* 118:53–64. doi: 10.1016/j.jafrearsci.2016.02.019.
- Davies, Samuel, Fabian Jintae Froese, Daniel Han Ming Chng, and Fedor Portniagin. 2023. "Improving Subsidiary Performance via Inpatriate Assignments: The Role of Host Country National Subsidiary CEOs' Social Ties and Motivational Cultural Intelligence." *Journal of World Business* 58(5):101460. doi: <https://doi.org/10.1016/j.jwb.2023.101460>.
- Edler, Jakob, Knut Blind, Henning Kroll, and Torben Schubert. 2023. "Technology Sovereignty as an Emerging Frame for Innovation Policy. Defining Rationales,

- Ends and Means.” *Research Policy* 52(6):104765. doi: <https://doi.org/10.1016/j.respol.2023.104765>.
- Ekinci, Aykut, Zeynep Koçak, and Muhammed Benli. 2023. “OECD ÜLKELERİ ÖRNEĞİNDE AR-GE HARCAMALARININ EKONOMİK BÜYÜME ÜZERİNDEKİ ETKİSİ.” *Sakarya İktisat Dergisi* 12(2):241–52.
- Gıdık, Betül. 2021. “Antioxidant, Antimicrobial Activities and Fatty Acid Compositions of Wild Berberis Spp. by Different Techniques Combined with Chemometrics (PCA and HCA).” *Molecules* 26(24). doi: [10.3390/molecules26247448](https://doi.org/10.3390/molecules26247448).
- Griffith, Rachel, Stephen Redding, and John Van Reenen. 2004. “Mapping the Two Faces of R&D: Productivity Growth in a Panel of OECD Industries.” *The Review of Economics and Statistics* 86(4):883–95.
- Guleryuz, Didem. 2022. “Estimation of Soil Temperatures with Machine Learning Algorithms—Giresun and Bayburt Stations in Turkey.” *Theoretical and Applied Climatology* 147(1):109–25. doi: [10.1007/s00704-021-03819-2](https://doi.org/10.1007/s00704-021-03819-2).
- Güleryüz, Didem, and Erdemalp Özden. 2020. “Büyük Veri Ile Gelen Değişim: Finans Sektöründe Yapay Zeka.” Pp. 155–71 in *Finans Alanında Spesifik Konular*, edited by Ü. Gülhan and A. Ağ. Ankara: Gazi Kitabevi.
- Gumus, Erdal, and Ferdi Celikay. 2015. “R&D Expenditure and Economic Growth: New Empirical Evidence.” *Margin: The Journal of Applied Economic Research* 9(3):205–17. doi: [10.1177/0973801015579753](https://doi.org/10.1177/0973801015579753).
- Jahanshahi, A. A., Z. Adiguzel, and F. S. Cakir. 2023. “Knowledge Management Strategy as the Key Factor for Turkish Firms’ Innovation in the Digital Era.” *IEEE Engineering Management Review* 51(2):166–81. doi: [10.1109/EMR.2023.3265570](https://doi.org/10.1109/EMR.2023.3265570).
- Koçak, Emrah, and Zübeyde Şentürk Ulucak. 2019. “The Effect of Energy R&D Expenditures on CO2 Emission Reduction: Estimation of the STIRPAT Model for OECD Countries.” *Environmental Science and Pollution Research* 26(14):14328–38. doi: [10.1007/s11356-019-04712-2](https://doi.org/10.1007/s11356-019-04712-2).
- Kouziokas, Georgios N. 2020. “A New W-SVM Kernel Combining PSO-Neural Network Transformed Vector and Bayesian Optimized SVM in GDP Forecasting.” *Engineering Applications of Artificial Intelligence* 92(December 2019):103650. doi: [10.1016/j.engappai.2020.103650](https://doi.org/10.1016/j.engappai.2020.103650).
- Kutlu, Naciye, Aybike Kamiloglu, and Tugba Elbir. 2022. “Optimization of Ultrasound Extraction of Phenolic Compounds from Tarragon (*Artemisia Dracunculus* L.) Using Box–Behnken Design.” *Biomass Conversion and Biorefinery* 12(11):5397–5408. doi: [10.1007/s13399-022-02594-y](https://doi.org/10.1007/s13399-022-02594-y).
- Meliciani, Valentina. 2000. “The Relationship between R&D, Investment and Patents: A Panel Data Analysis.” *Applied Economics* 32(11):1429–37. doi: [10.1080/00036840050151502](https://doi.org/10.1080/00036840050151502).

- Nasir, Muhammad Hamid, and Sen Zhang. 2024. "Evaluating Innovative Factors of the Global Innovation Index: A Panel Data Approach." *Innovation and Green Development* 3(1):100096. doi: <https://doi.org/10.1016/j.igd.2023.100096>.
- OECD. 2020. *OECD Science, Technology and Innovation Outlook 2020*.
- OECD. 2021. "OECD." *Health Spending (Indicator)*. Retrieved February 9, 2021 (doi: 10.1787/8643de7e-en).
- Ozden, Erdemalp. 2022a. "Forecasting of Export Volume Using Artificial Intelligence Based Algorithms." *Bitlis Eren Üniversitesi Fen Bilimleri Dergisi* 11(2):715–26. doi: 10.17798/bitlisfen.1107311.
- Ozden, Erdemalp. 2022b. "The Dynamics Affecting the Export-Import Ratio in Turkey: A Hybrid Model Proposal with Econometrics and Machine Learning Approach." *Journal of Economic Policy Researches* 9(2):265–91. doi: 10.26650/JEPR1088322.
- Ozden, Erdemalp, and Didem Guleryuz. 2021. "Optimized Machine Learning Algorithms for Investigating the Relationship Between Economic Development and Human Capital." *Computational Economics*. doi: 10.1007/s10614-021-10194-7.
- SAMASTI, Mesut, and Tarık KÜÇÜKDENİZ. 2023. "Precipitation Forecast with Logistics Regression Methods for Harvest Optimization." *International Journal of Agriculture Environment and Food Sciences* 7(1):213–22. doi: 10.31015/jaefs.2023.1.26.
- Shahsavari, Amir, and Morteza Akbari. 2018. "Potential of Solar Energy in Developing Countries for Reducing Energy-Related Emissions." *Renewable and Sustainable Energy Reviews* 90:275–91. doi: <https://doi.org/10.1016/j.rser.2018.03.065>.
- Singh, Ajay K., and Sanjeev Kumar. 2022. "Exploring the Impact of Sustainable Development on Social-Economic, and Science and Technological Development in Selected Countries." *Society & Sustainability* 4(1):55–83. doi: 10.38157/ss.v4i1.405.
- Tümer, Abdullah Erdal, and Aytekin Akkuş. 2018a. "Forecasting Gross Domestic Product per Capita Using Artificial Neural Networks with Non-Economical Parameters." *Physica A: Statistical Mechanics and Its Applications* 512:468–73. doi: <https://doi.org/10.1016/j.physa.2018.08.047>.
- Tümer, Abdullah Erdal, and Aytekin Akkuş. 2018b. "Forecasting Gross Domestic Product per Capita Using Artificial Neural Networks with Non-Economical Parameters." *Physica A: Statistical Mechanics and Its Applications* 512:468–73. doi: <https://doi.org/10.1016/j.physa.2018.08.047>.
- Uçurum, Metin, Akın Özdemir, Çağatay Teke, Hüseyin Serencam, and Mümtaz İpek. 2018. "Optimization of Adsorption Parameters for Ultra-Fine Calcite Using a Box-Behnken Experimental Design." 16(1):992–1000. doi: doi:10.1515/chem-2018-0114.

- Wang, Bin, Samia Khalid, and Hamid Mahmood. 2023. "R&D Spending and Economic Policy Uncertainty in Asian Countries: An Advanced Panel Data Estimation Study." *Journal of the Knowledge Economy*. doi: 10.1007/s13132-023-01285-x.
- Worldbank. 2021. "World Bank Open Data." Retrieved (<https://data.worldbank.org/>).
- Yantur, Pelin. 2023. "Arge Harcamaları ve Dış Ticaret Haddinin Ekonomik Büyüme Üzerindeki Etkileri: Türkiye Örneği." *Marmara Üniversitesi İktisadi ve İdari Bilimler Dergisi* 45(2):141–59. doi: 10.14780/muiibd.1367980.
- Zhao, Changyu, Haishan Chen, and Shanlei Sun. 2018. "Evaluating the Capabilities of Soil Enthalpy, Soil Moisture and Soil Temperature in Predicting Seasonal Precipitation." *Advances in Atmospheric Sciences* 35(4):445–56. doi: 10.1007/s00376-017-7006-5.



Chapter 14

APPLICATION OF ANFIS AND ANNS MODEL IN THE PREDICTION OF DRYING KINETICS OF FIRE HOSE IN A MICROWAVE DRYER

Halil Nusret BULUŞ¹

Aytaç MORALAR²

Soner ÇELEN³

1 Dr. Halil Nusret BULUŞ: Tekirdağ Namık Kemal University, Çorlu Faculty of Engineering, Tekirdağ, Türkiye, ORCID ID: 0000-0003-1844-6484

2 Dr. Aytaç MORALAR: Tekirdağ Namık Kemal University, Çorlu Faculty of Engineering, Tekirdağ, Türkiye, ORCID ID: 0000-0002-3964-4909

3 Assoc. Prof. Soner ÇELEN: Tekirdağ Namık Kemal University, Çorlu Faculty of Engineering, Tekirdağ, Türkiye, ORCID ID: 0000-0001-5254-4411

1. INTRODUCTION

The optimization of drying parameters holds paramount significance in the production of high-quality goods. Mathematical modeling serves as an exceptional tool for process simulation and optimization. It is extensively employed for the prediction of product drying times and the generalization of drying behavior (Tarafdar et al., 2021).

Soft computing techniques, also known as the black-box modeling method, have recently garnered significant attention, owing to their notable precision and ease of use. These methods are particularly well-suited for scenarios where the construction of precise mathematical models or understanding of system dynamics proves to be challenging. In the domain of soft computing, diverse methodologies are employed, encompassing the Adaptive Neuro-Fuzzy Inference System, Artificial Neural Networks, Fuzzy Inference System, and Genetic Algorithms, among others (Omari et al., 2018).

Soft computing denotes the use of artificial intelligent techniques that are implemented to control or execute seemingly intricate tasks. Given the limitations of the human brain in efficiently managing the exponentially growing information, machine intelligence has become imperative in the modern context. While the integration of artificial intelligence methods in the field of drying is still in its nascent stage, ongoing progress is anticipated to address emerging demands and offer innovative solutions. Consequently, research in this domain retains its relevance (Ojediran et al., 2020).

When dealing with the modeling of drying behaviors and the determination of drying kinetics, it is important to recognize the highly nonlinear nature of this process, which poses challenges for modeling, simulation, and prediction. In addressing such complexities, the use of artificial intelligence methods, particularly neural networks, proves to be beneficial. While the utilization of existing empirical correlations based on a large volume of experimental data is the simplest means to predict the drying characteristics of a food product, these correlations often fall short as they fail to encompass the entirety of the drying system's characteristics under examination (Fabani et al., 2021).

During the system design phase, the application of algorithmic analysis offers valuable insights into the appropriate selection of components and application techniques, exerting a substantial influence on operational expenses and energy conservation. ANN and Adaptive ANFIS models represent machine learning-based approaches that are employed for the prediction of complex system outcomes, including those related to drying technology. In recent years, robust models have emerged under the category of ANFIS-based fuzzy inference systems across various engineering domains. These systems effectively analyze intricate drying processes by leveraging the training capabilities of neural networks and the interpretive nature of linguistic

fuzzy systems. At present, adaptive fuzzy systems stand out as one of the most practical methods for prediction and modeling purposes (Kaveh et al., 2021).

Artificial Neural Networks, in conjunction with various mathematical and semi-experimental models, represent an advanced computational approach employed for modeling intricate relationships between input and output parameters. The analysis facilitated by ANNs enables the attainment of predictions that are more realistic and accurate (Tarafdard et al., 2021).

Alternatively, ANNs offer an enticing option. The learning process of the network necessitates a minimal number of training sets, relying on a limited set of experiments, rendering it remarkably efficient. With a properly trained ANN, the accurate prediction of a new drying curve can be swiftly achieved within a matter of seconds, circumventing the need for time-consuming additional experiments (Fabani et al., 2021).

ANNs serve as an artificial intelligence tool with a flexible structural relationship set between interconnected nodes and layers to fulfill the function of system or process modeling. The structure of the ANN model is established using the relevant experimental data, thus enabling it to represent and predict the data with high accuracy (Okonkwo et al., 2022). Artificial Neural Networks (ANNs) stand as a firmly established instrument for modeling intricate systems and addressing intricate nonlinear issues. Moreover, these networks exhibit efficacy in managing partial datasets and tasks characterized by fuzzy and/or insufficient information. They possess the capacity to forecast multiple outputs based on multiple inputs, even in scenarios where prior information about process relationships is lacking. (Beigi et al., 2017).

ANNs possess the capability to autonomously acquire meaningful relationships between input and output materials through their neural network system. The advantages associated with the utilization of ANNs include self-learning, adaptation to non-linear variables, and real-time learning (Rahman and Al-Ameri, 2023).

ANFIS, a subdivision of artificial intelligence, amalgamates the learning capabilities of artificial neural networks with the reasoning proficiency of fuzzy systems. As a result, it integrates the strengths of both models within a unified methodology. By combining fuzzy systems and artificial neural networks, ANFIS establishes an effective approach for various engineering applications. Notably, ANFIS serves as a potent instrument for modeling, mapping, forecasting, problem-solving, and data mining in order to elucidate the relationship between input and output values and describe the nonlinear behavior within complex systems (Dolatabadi et al., 2018).

ANFIS, as a soft computing technique, finds application in resolving intricate and nonlinear problems. It demonstrates the ability to generate

and predict a single output (Kaveh et al., 2018). The Adaptive Neuro-Fuzzy Inference System (ANFIS) is a form of multilayer neural network rooted in the Sugeno fuzzy inference system, employing fuzzy rules to discern system outputs. The integration of neural network principles and fuzzy logic in ANFIS enhances its decision-making ability in uncertain scenarios, thereby improving accuracy in handling uncertainty. ANFIS operates in a manner akin to a fuzzy inference system, mitigating system errors through a post-publication model (Abdi et al., 2023).

In recent years, the prominence of new models founded on the Adaptive Neuro-Fuzzy Inference System (ANFIS) has escalated, as they serve as universal approximators for highly nonlinear functions. Their learning capabilities facilitate adaptation to system alterations. Notably, in fuzzy inference systems, human knowledge or experimental data and the process of inference can be depicted and qualitatively analyzed through fuzzy if-then rules (Akkaya, 2016).

In a precedent investigation into the application of artificial intelligence methodologies, Aktas et al. (2015) conducted experiments focusing on the drying of thin layers of bay leaves within a closed-loop heat pump dryer. In order to forecast the moisture content as well as the overall energy usage, they utilized an Artificial Neural Network model. Within the network, the researchers applied the Levenberg-Marquardt and Fermi transfer functions back-propagation learning algorithm. Zalnezhad et al. (2013) achieved commendable approximations through the application of fuzzy logic for forecasting the surface hardness of alloy coatings.

Yousefi (2017) applied Adaptive Neuro-Fuzzy Inference System (ANFIS) and genetic algorithm-based artificial neural networks to model the drying kinetics of papaw slices in a hot air dryer. Notably, ANFIS demonstrated superior predictive capabilities based on statistical root mean square error values. During the combined hot air-infrared drying of rough rice, Zare et al. (2012) used a variety of ANNs to forecast the drying time, moisture content fluctuation, percentage of cracked kernels, and the necessary failure force. They identified training techniques, transfer functions, and ideal network topologies. In contrast, Rahman et al. (2012) discovered that ANFIS exhibited superior predictive abilities compared to ANN and multivariable regression in forecasting the thermal conductivity of foods.

Artificial neural networks were effectively used by Kaveh and Amiri Chayjan (2014) to forecast particular drying characteristics of terebinth fruit during an infrared fluidized bed drying process. Similar to this, ANFIS showed the most accurate predictions when Kaveh et al. (2018) compared its predictive performance with that of ANN and eleven other mathematical models in calculating the moisture ratio of an almond kernel in a convection drier.

Buluş et al. (2023a) investigated the prediction of moisture change and

drying rate of zucchini slices using the ANN and ANFIS methods. The ANFIS-based prediction model outperformed the ANN model in terms of drying rate performance, while the ANN model excelled in predicting moisture content values, demonstrating the suitability of both methods for estimating the behavior of zucchini slices.

Currently, natural drying methods are employed for drying fire hoses used in fire stations for firefighting, water extraction, and similar operations. To ensure their longevity and facilitate efficient post-use cleaning and maintenance, the fire hoses need to be dried and stored after use. The aim is to delay hose deterioration, reduce the weight by eliminating the trapped water, and enable the rapid deployment of hoses during emergencies through the practice of specific techniques such as the deployment and retrieval method. However, the current natural drying process is both susceptible to weather conditions and relatively slow, necessitating the exploration of alternative methods (Dağlı, 2020).

This study investigates alternative drying methods to natural drying, aiming to conserve energy, reduce operational inefficiencies, and save time during unproductive working hours. To achieve this goal, ANN/ANFIS methods were employed for predicting the moisture content of fire hoses dried in a microwave dryer.

2.MATERIALS AND METHODS

2.1Fire Hose and Dryer

Fire hoses, standard in fire stations, consist of a fabric exterior and a rubber interior. Untreated hose samples were employed in this study, with no prior usage. The microwave dryer shown in Figure 1 was used for the experiments (Dağlı et al., 2020).

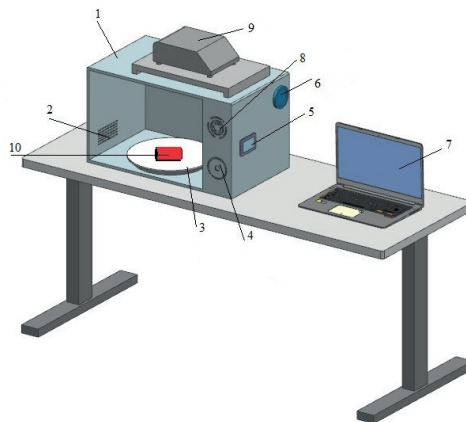


Figure 1. Schematic of the Microwave Dryer (1: oven, 2: ventilation, 3: tray, 4: timer, 5: magnetron, 6: fan; 7: computer, 8: power control button, 9: precision scale, 10: firehose sample)

2.2 Method

A commercially available 20 m long fire hose was used for this study. Prior to the experiments, the couplings at the ends of the hoses were removed, and the study was conducted solely on the hose segment. Samples of 20 cm in length were cut from the 20 m hose for the experiments. The soaking process in a water bath is carried out as a preprocess and is applied for 30 - 60 minutes in the experiments. Microwave drying was performed at power levels of 120 W, 350 W, and 460 W, with a frequency of 2450 Hz.

During the experiments, the moisture content with respect to the wet basis was calculated for the samples according to Equation 1 (Tınmaz Köse, E., 2019; Çelen et al., 2018).

$$m_y = \frac{M_y - M_k}{M_y} \quad (1)$$

In these equations, m_y represents the moisture content with respect to the wet basis, M_k denotes the product's dry mass (g), M_y denotes the product's wet mass (g) (Çelen ve Kuş, 2016).

2.2.1 ANN model

In this research, MATLAB was employed as the computational tool. The feed-forward neural network was configured with preprocessing time (min), microwave power (W), and drying time (min) as input variables, while moisture content was designated as the output variable in the output layer. The input layer and the 20-neuron hidden layer made up the model architecture. The input layer did not utilize any transfer function, while the hidden layer utilized the tan-sig transfer function and the output layer applied the purelin transfer function. Using the Levenberg-Marquardt learning method, a feed-forward back-propagation mechanism made training the network easier.

A dataset of 100 instances was utilized for constructing the ANN prediction model. Of these datasets, 70% (70 instances) were allocated for the training phase, while the remaining 30% of the datasets were evenly divided for testing and validation purposes. It is a customary practice to employ a single test set for both validation and testing, especially with smaller datasets. Therefore, in this study, the entirety of the 20% subset (24 instances) was employed as the test set to facilitate result comparison with both experimental and ANFIS model-predicted outcomes. Additionally, it is worth noting that the datasets chosen for testing the model were randomly selected, ensuring the robustness

of the ANN prediction model. Figure 2 illustrates the ANN architecture used in this research. An important factor influencing the performance of the ANN is the choice of transfer functions. In the output layer of the generated ANN, a linear transfer function was applied, while the tangent sigmoid function was used in the hidden layer (Lertworasirikul and Tipsuwan, 2008; Buluş et al., 2023b).

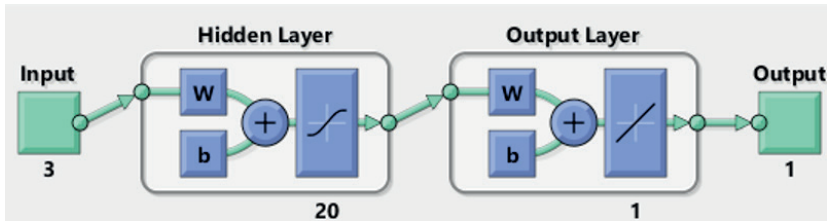


Figure 2. *The Utilized ANN Structure.*

2.2.2 ANFIS model

The fuzzy inference method enables the representation of ambiguous circumstances through a decision-making process employing rules. The architecture of the ANFIS comprises five layers: the fuzzy layer, product layer, normalized layer, de-fuzzy layer, and total output layer, as illustrated in Figure 3. The fuzzy inference method is characterized by three inputs and one output. In the ANFIS modeling process, MATLAB was employed for data modeling. Input parameters included preprocessing time (min), microwave power (W), and drying time (min), with moisture content serving as the sole output parameter.

The ANFIS model was trained over a total of 500 training epochs. For the input side, the linear type of membership function (MF) was selected, and for the output side, the trimf type MF. Out of the 124 datasets, 80% (100 datasets) were dedicated to training the model, leaving the remaining 20% (24 datasets) for testing the model. Notably, the datasets for testing the model were randomly selected from the overall dataset pool.

The ANFIS model is composed of 5 layers (Tao et al., 2016; Taşova et al., 2020). In the first layer of this model, the input values are preprocessing time, drying time, and microwave power. These inputs acquire their membership degrees through a membership function and exit the layer. In the second layer, the inputs are multiplied and exit a node. The third layer normalizes the m_y values. Following the fourth layer, the Sugeno model is applied. Finally, the total output values are obtained from the model in the fifth layer. ANFIS model was created to conduct my predictions. Identical training and test sets were employed for these two models, resulting in the creation of 27 rules.

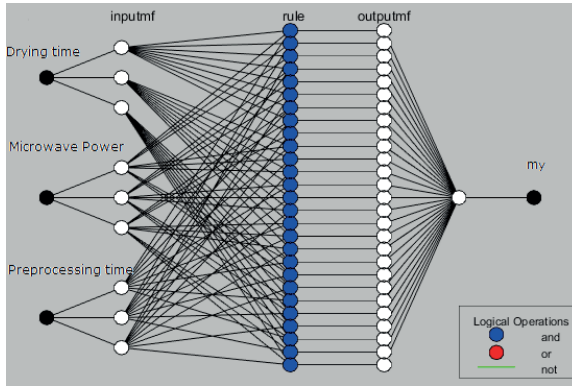


Figure 3. ANFIS Model Structure.

2.3 Statistical analysis

After assessing the performance of the ANFIS and ANN models, a comparative analysis was carried out using MATLAB software. The prediction errors considered in this study encompassed the root mean square error (RMSE), mean absolute percentage error (MAPE), and coefficient of determination (R^2) (Çelen et al., 2015; Tınmaz Köse ve ark. 2019).

3. ANALYSIS RESULTS

The moisture content of the fire hose obtained for different drying times with 2 preprocessing time applications and 3 different microwave power levels is shown in Figure 4 and Figure 5. As the drying time increased, the moisture of the hose rapidly decreased. Similarly, an increase in microwave power resulted in a faster drying process.

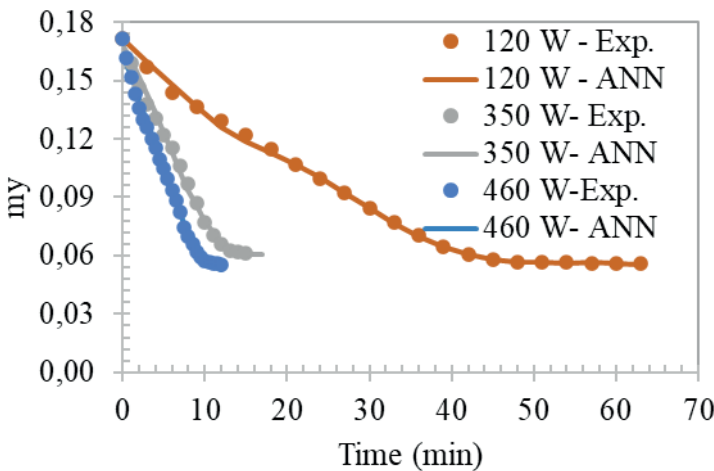


Figure 4. The ANN Curve of a Fire hose Soaked in a 30-Minute Preprocessing Phase

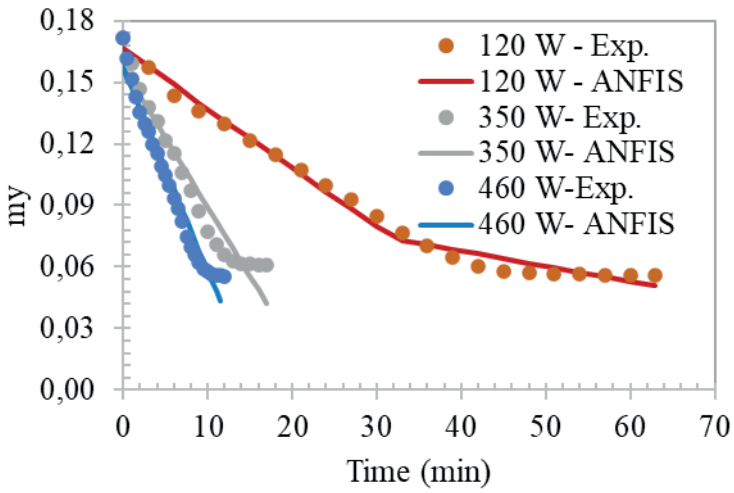


Figure 5. The ANFIS Curve of a Fire hose Soaked in a 30-Minute Preprocessing Phase

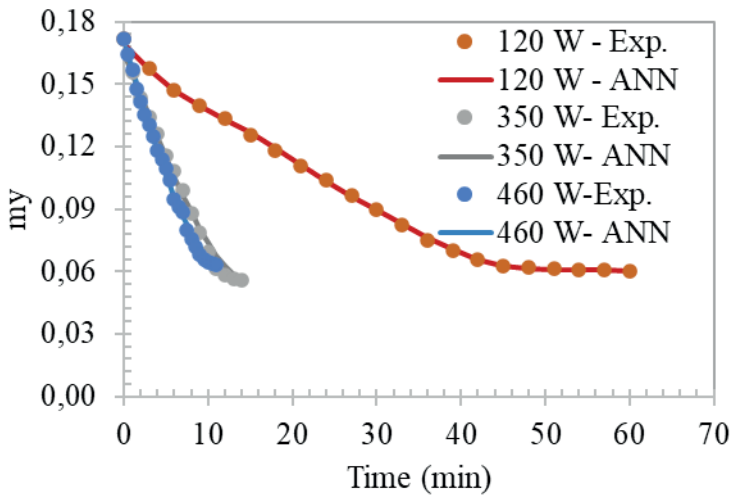


Figure 6. The ANN Curve of a Fire hose Soaked in a 60-Minute Preprocessing Phase

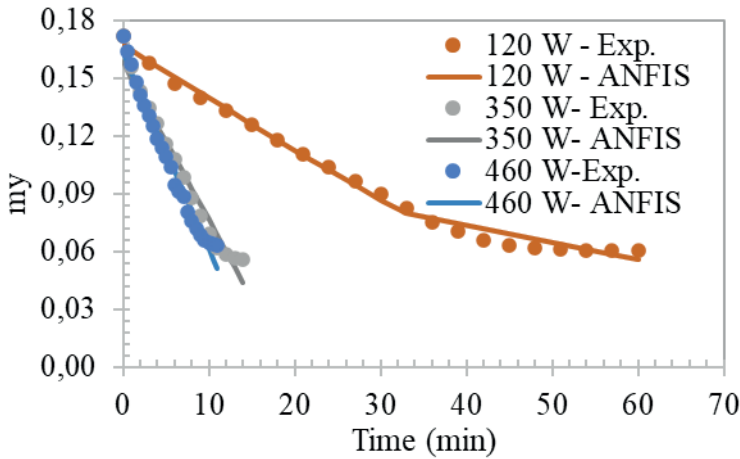


Figure 7. *The ANFIS Curve of a Fire hose Soaked in a 60-Minute Preprocessing Phase*

The drying data were applied to the ANN model created in the MATLAB program. This model constituted a single-hidden-layer neural network model with 3 inputs and 1 outputs. The input data for the network comprised drying time, microwave power, and two pretreatments, while the output data encompassed moisture content.

The system was found to be fully efficient in predicting the moisture content values obtained under all experimental conditions. While creating the ANN architecture, different numbers of neurons were tested and it was seen that using 20 neurons in the hidden layer gave good results in predicting humidity values. It has been observed that the ANFIS model predictions and experimental measurements show similar trends and overlap. When examined, it is clear that the reported moisture content values as a function of drying time are in good agreement with the experimental results as well as the predictions obtained from ANN and ANFIS.

In creating the models, 70% of the 100 available experimental data were used for training, 15% for testing and 15% for validation. These data were randomly distributed to create training, validation and test sets. When establishing the ANN model, 3 inputs (drying time, microwave power and preprocessing time) were selected, and moisture were selected as outputs. In the single hidden layer ANN model, a tangent sigmoid was used as the hidden layer function, a linear transfer function was used as the transfer function, and the Levenberg-Marquardt algorithm (`trainlm`) was used as the learning algorithm. According to the results obtained from various experiments, the number of neurons in the hidden layer was determined as 20.

Figure 8 presents the validation performance of the most successful ANN training. Regression plots for training, testing, and validation are shown in Figure 9 along with all data for the created ANN model.

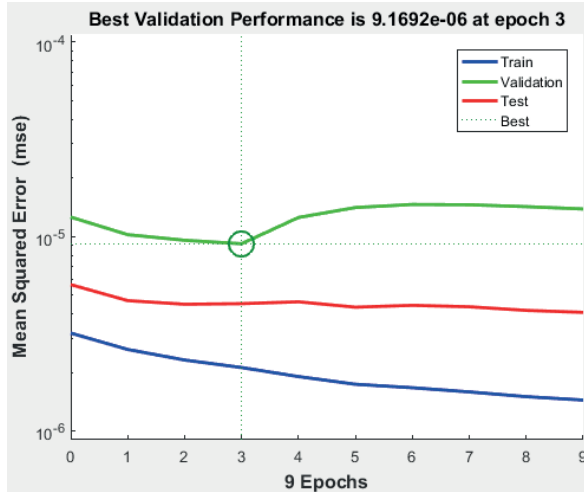


Figure 8. ANN model validation performance providing the highest prediction performance.

Drying data was applied to the ANN model created in the MATLAB program. This model created a neural network sensor model with 3 inputs and 1 outputs, a single hidden layer. The input data of the network consisted of drying time, microwave power and two preprocessing times, while the output data included moisture content.

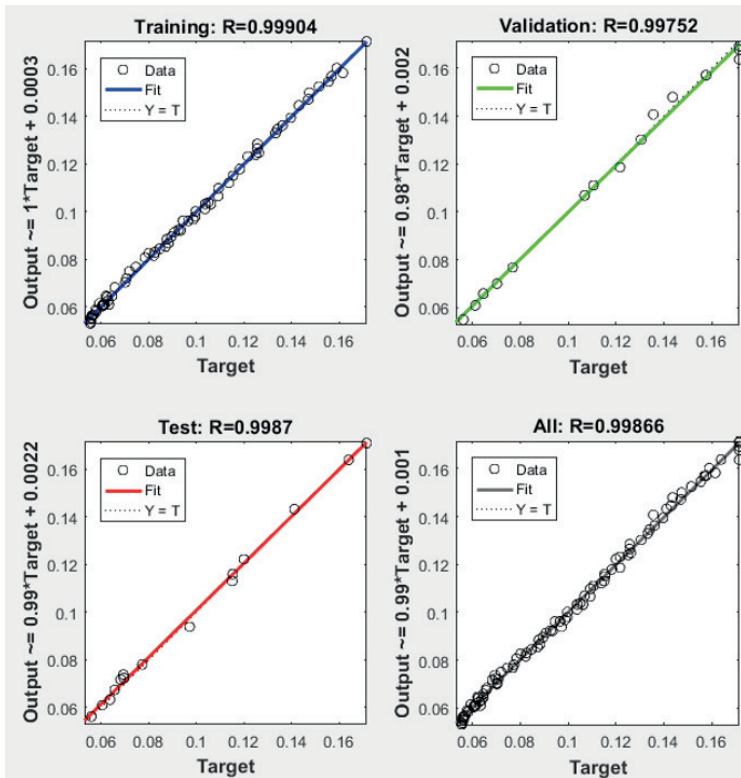


Figure 9. Regression plots for (a) training, (b) validation, (c) testing, and (d) all data.

In this study, an ANN model was developed for the estimation of the m_y parameters in fire hose. A model that enables the construction of drying curves under different drying conditions in a microwave dryer was successfully implemented. Accordingly, the m_y parameters can be successfully predicted at different microwave power and preprocessing duration values. This facilitates the easy prediction of the system's behavior at different power levels, enabling both time and energy savings. This method can also be applied by creating a prediction model for other products or different drying powers.

The study employed 100 data points obtained from experimental results in the application of ANFIS, consisting of 100 (80%) training data and 24 (20%) test data. The model was implemented using the ANFIS toolbox in MATLAB software.

The training and test data sets created from the specified proportion of experimentally obtained data for both ANFIS models are provided in Figure 10. The training cycle number for the two models, each having 3 inputs and

1 output generated from the given sets, was set to 500, and the training error graph resulting from this training was obtained. This training error graph is presented in Figure 11.

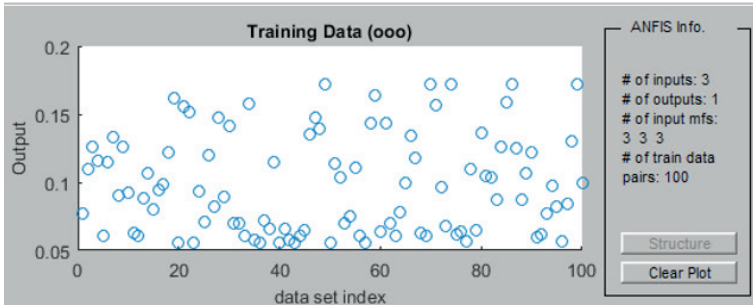


Figure 10. Training and Test data for m_y

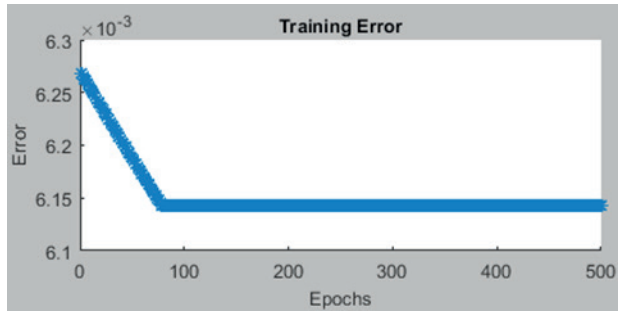


Figure 11. Prediction error rate for 100 training rounds.

ANFIS rules were created by training the developed models. Figure 12 shows these rules. 27 rules emerged in this model and were later used to make predictions.

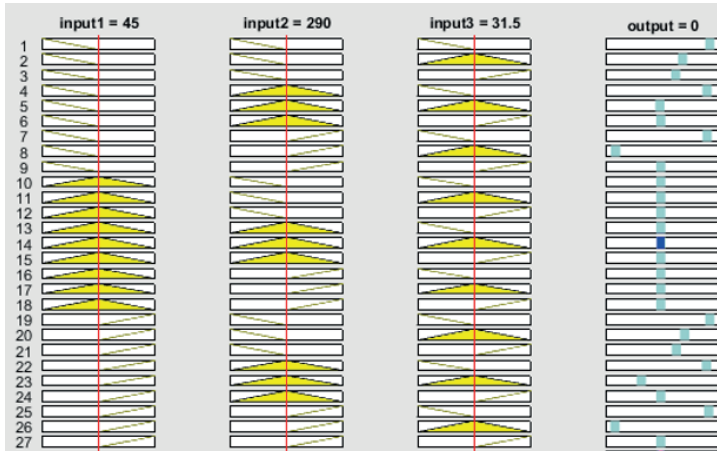


Figure 12. Rules created for ANFIS Models.

The ANFIS model more closely approximated the experimental data for m_y values compared to the ANN model. Mango slices were used to predict effective diffusivity using a Takagi-Sugeno fuzzy model, with similar results (Vaquiro et al., 2008).

The difference between the experimental and analytical model prediction results is indicated by the error parameters. The model error parameters, indicating low RMSE and MAPE values and an R^2 value close to 1, demonstrate the accuracy of the model. Upon reviewing the literature, it is evident that R^2 values are commonly used to evaluate model performance.

CONCLUSION

In this study, the moisture content of a fire hose sample was calculated through drying, and predictive models were employed using ANFIS and ANN. The ANN model was selected as a single-hidden-layer model with 20 neurons in the hidden layer. Similar to the ANFIS model, 20% of the experimental data was chosen as test data within the training dataset. The ANFIS model, configured with 124 data inputs and a segmentation of 85% for training and 20% for testing, established the most successful network with 27 rules. Both the ANN and ANFIS models demonstrated good predictive capabilities, both statistically and graphically. These prediction models aim to minimize the number of tests for future drying processes. Moreover, this methodology can be applied by developing prediction models for different products and microwave power levels.

REFERENCES

- Abdi, R., Shahgholi, G., Sharabiani, V.R., Fanaei, A.R. and Szymanek, M. (2023). Prediction compost criteria of organic wastes with Biochar additive in in-vessel composting machine using ANFIS and ANN methods, *Energy Reports*, 9, 1684-1695.
- Aghbashlo M, Mobli H, Rafiee S, Madadlou A. An artificial neural network for predicting the physicochemical properties of fish oil microcapsules obtained by spray drying. *Food Sci Biotechnol* 2013; 22:677e85.
- Akkaya, E. (2016). ANFIS based prediction model for biomass heating value using proximate analysis components, *Fuel*, 180, 687-693.
- Aktas, M., Sevik S, Ozdemir MB, Gonen E. Performance analysis and modeling of a closed-loop heat pump dryer for bay leaves using artificial neural network. *Appl Therm Eng* 2015;87:714e23.
- Beigi, M., Torki-Harchegani, M. and Tohidi, M. (2017). Experimental and ANN modeling investigations of energy traits for rough rice drying, *Energy*, 141(15), 2196-2205.
- Buluş, H.N., Moralar, A. and Çelen, S., (2023a). Modeling Of The Moisture Content And Drying Rate Of The Zucchini (*Cucurbita Pepo L.*) In A Solar Hybrid Dryer With Ann And Anfis Methods, *The Philippine Agricultural Scientist (PAS)*, Vol. 106 No. 3, 293-305.
- Levent, M., Buluş, H.N., Çelen, S. and Moralar, A., (2023b). Comparison of Artificial Neural Networks and Fuzzy Logic Methods in the Hazelnut Shell Drying Process, *European J. Eng. App. Sci.*, 6(2), 50-55.
- Ceylan I. Determination of drying characteristics of timber by using artificial neural networks and mathematical models. *Dry Technol* 2008;26:1469e76.
- Çakmak G, Yildiz C. The prediction of seedy grape drying rate using a neural network method. *Comput Electron Agric* 2011;75:132e8.
- Çelen, S., Aktaş, T., Karabeyoğlu, S.S. Akyıldız, A. (2015). Drying of prina using microwave energy and determination of appropriate thin layer drying model. *Tekirdağ Ziraat Fakültesi Dergisi* 12(2): 21–31.
- Çelen, S. and Kuş, S. Effect Of Microwave Energy To The Drying Of Quince Slices, *Electronic Journal of Vocational Colleges*, 6(3), 30-40, 2016.
- Çelen S, Arda S. O. ve Karataşer M. A., Güneş Enerji Destekli Mikrodalga Konveyör Kurutucu Kullanılarak Kuruma Davranışının Modellenmesi, *El-Cezeri Fen ve Mühendislik Dergisi Cilt: 5, No: 1, 2018 (267-271)*.
- Dağlı, M. (2020). İtfaiye Hortumunun Kurutma Parametreleri Ve Uygun Kurutucu Seçimi, *Yüksek Lisans Tezi, Tekirdağ Namık Kemal Üniversitesi, Tekirdağ*.
- Dağlı, M., Çelen, S. and Moralar, A. (2020). Yangın Müdahale Hortumunun İçyapı Ve Termal Analizi, *Mühendislik Ve Mimarlık Bilimleri: Teori, Güncel Araştır-*

malar ve Yeni Eğilimler, Eds: Can ÇİVİ and Tuncay YILMAZ, IVPE yayınevi, Vetinje, KARADAĞ.

- Dolatabadi, M., Mehrabpour, M., Esfandyari, M., Alidadi, H. and Davoudi, M. (2018). Modeling of simultaneous adsorption of dye and metal ion by sawdust from aqueous solution using of ANN and ANFIS, *Chemometrics and Intelligent Laboratory Systems*, 181, 72-78.
- Fabani, M.P., Capossio, J.P., Roman, M.C., Zhu, W., Rodriguez, R. And Mazza, G. (2021). Producing non-traditional flour from watermelon rind pomace: Artificial neural network (ANN) modeling of the drying process, *Journal of Environmental Management*, 281, 111915.
- Igwilo, C.N., Ude, N.C., Onoh, I.M., Eneke, C.B. and Alieze, B.A. (2022). RSM, ANN and ANFIS applications in modeling fermentable sugar production from enzymatic hydrolysis of *Colocynthis Vulgaris* Shrad seeds Shell, *Bioresource Technology Reports*, 18, 101056.
- Kardani, N., Bardhan, A., Samui, P., Nazem, M. and Asteris, P.G. (2022). Predicting the thermal conductivity of soils using integrated approach of ANN and PSO with adaptive and time-varying acceleration coefficients, *International Journal of Thermal Sciences*, 173, 107427.
- Kaveh M, Amiri Chayjan R. Prediction of some physical and drying properties of terebinth fruit (*Pistacia atlantica* L.) using artificial neural networks. *Acta Sci Technol Aliment* 2014;13:65e78.
- Kaveh, M, Sharabiani, V.R., Chayjan, R.A., Taghinezhad, E., Bbaspour-Gilandeh, Y., Golpour, I., (2018). ANFIS and ANNs Model For Prediction Of Moisture Diffusivity And Specific Energy Consumption Potato, Garlic And Cantaloupe Drying Under Convective Hotair Dryer. *Inf Process Agr.* 5 (3):372–387. doi:10.1016/j.inpa.2018.05.003.
- Kaveh, M., Chayjan, R.A., Golpour, I., Poncet, S., Seirafi, F. And Khezri, B. (2021). Evaluation of exergy performance and onion drying properties in a multi-stage semi-industrial continuous dryer: Artificial neural networks (ANNs) and ANFIS models, *Food and Bioproducts Processing*, 127, 58-76.
- Krishna, S.H.V., Santosh, B.S. and Prasanth, B.H.S.S. (2024). Prediction of UCS and CBR of a stabilized Black-cotton soil using artificial intelligence approach: ANN, *Materials Today: Proceedings*, (in press).
- Ojediran, J.O., Okonkwo, C.E., Adeyi, A.J., Adeyi, O., Olaniran, A.F., George, N.E. and Olayanju, A.T. (2020) Drying characteristics of yam slices (*Dioscorea rotundata*) in a convective hot air dryer: application of ANFIS in the prediction of drying kinetics. *Heliyon.* 6(3), e03555.
- Okonkwo, C.E., Moses, O.I., Nwonuma, C., Abiola, T., Benjamin, B.O., Folorunsho, J.O., Olaniran, A.F. and Pan, Z. (2022). Infrared and Microwave as a dry blanching tool for Irish potato: Product quality, cell integrity, and artificial neural networks (ANNs) modeling of enzyme inactivation kinetic, *Innovative Food Science and Emerging Technologies*, 78, 103010.

- Omari, A., Behrooz-Khazaei, N., Sharifian, F. (2018). Drying kinetics and artificial neural network modeling of the mushroom drying process in a microwave-hot air dryer. *Journal of Food Process Engineering* 41: 1–10.
- Rahman, S.K. and Al-Ameri, R. (2023). Structural assessment of Basalt FRP reinforced self-compacting geopolymer concrete using artificial neural network (ANN) modelling. *Construction and Building Materials*, 397, 132-464.
- Sarkar, J., Prottoy, Z.H., Bari, M.T. Faruque, M.A.A. (2021). Comparison of ANFIS and ANN modeling for predicting the water absorption behavior of polyurethane treated polyester fabric, *Heliyon*, e08000.
- Tarafdar, A., Jothi, N. And Kaur, B.P. (2021). Mathematical and artificial neural network modeling for vacuum drying kinetics of *Moringa olifera* leaves followed by determination of energy consumption and mass transfer parameters, *Journal of Applied Research on Medicinal and Aromatic Plants*, 24, 100306.
- Tınmaz Köse, E., Çelen, S., Çelik S. Ö., Akın, G. and Akyıldız, A. Drying Of Drilling Sludge: Conventional And Microwave Drying, *Hittite Journal Of Science & Engineering*, 6(2), 119-122, 2019.
- Vaquiro, H.A., Bon, J. and Diez, J.L. Fuzzy logic application to drying kinetics modeling, *Proceedings of the 17th World Congress The International Federation of Automatic Control Seoul, Korea, July 6-11, 2008*.
- Yousefi, A.R., 2017. Estimation of papaw (*Carica papaw* L.) moisture content using adaptive neuro-fuzzy inference system (ANFIS) and genetic algorithm-artificial neural network (GA-ANN). *Iran. Food Sci. Technol. Res. J.* 12, 767–779.
- Zalnezhad, E., Sarhan, A.A.D., Hamdi, M., 2013. A fuzzy logic-based model to predict surface hardness of thin-film TiN coating on aerospace AL7075-T6 alloy. *Int. J. Adv. Manuf. Technol.* 68, 415–423.
- Zare, D., Naderi, H. And Jafari, A. (2012). Experimental and Theoretical Investigation of Rough Rice Drying in Infrared-assisted Hot Air Dryer using Artificial Neural Network, *World Academy of Science, Engineering and Technology*, 69.



Chapter 15

INVESTIGATION OF THE PERFORMANCE OF A PCM-BASED PASSIVE BATTERY THERMAL MANAGEMENT SYSTEM UNDER DIFFERENT GEOMETRICAL, AMBIENT AND MATERIAL CONDITIONS

Bariř KAVASOĐULLARI¹

Mücahit Emin KARAGÖZ²

Mehmet Nurullah ÖNEL³

1 Assist. Prof. Dr./Sivas University of Science and Technology/ORCID: 0000-0002-6086-8923

2 Res. Assist./Sivas University of Science and Technology/ORCID: 0000-0002-6503-9518

3 Res. Assist./Sivas University of Science and Technology/ORCID: 0000-0002-4109-7860

1. Introduction

Whereat the advancing technology, the plea for energy has also increased. The depletion of fossil fuels and growing environmental concerns propel researchers to explore alternative solutions. In response to these challenges, the utilization of batteries as a power source stands out as a promising alternative. Over the last few decades, electric vehicles and hybrid electric vehicles have become very popular. However, the power batteries in electric vehicles require precise operating conditions to ensure their quality and prevent potential hazards such as fires or explosions. Addressing this challenge, researchers are actively investigating various battery thermal management systems to enhance cooling performance and reduce costs. Youssef et al. (2022) introduce a novel design optimization aimed at improving environmental sustainability and reducing the weight of the cooling system. In this innovative approach, jute fibers, an economical and lightweight material readily available, were integrated with PCM-based BTMS. This research explores the thermal behavior of large lithium-ion batteries (LIBs) in various load scenarios, such as genuine driving cycles, periodic loads, and fast discharge. In their work, El Idi et al (2021) developed an effective PCM-metal foam composite heat management system for Li-ion battery cells. The study evaluated a PCM and PCM-metal foam composite's capacity to absorb the heat produced by the LIB using a mathematical and numerical model. The numerical analysis made use of both COMSOL Multiphysics and MATLAB. The outcomes showed that adding aluminum foam to the cell allows for more effective heat control. The optimization analysis also showed that high temperatures were caused by underestimating the thickness (needed PCM mass). In their investigation, Vermaa et al. (2019) focused on passive cooling methods utilizing capric acid as a Phase Change Material (PCM) placed around the battery pack. The PCM layer's thicknesses of 3 mm, 7 mm, 9 mm, and 12 mm were taken into consideration. Capric acid's performance as a PCM was evaluated and contrasted with paraffins that are typically utilized. The findings showed that the 3 mm PCM layer worked best, causing the battery's maximum temperature to drop significantly to 305 K. A hybrid BTMS was investigated by Safdari et al. in 2020. Three different vessel cross-sections with identical volumes-circular, rectangular, and hexagonal-encapsulated the PCM around the battery cell. A single-pack holder holds 12 Sony 18650 batteries, which are used in each BTMS. The battery pack's thermal management under various charge and discharge rates was investigated in the study. The results show that the thermal

performance of PCM containers that are hexagonal and circular is comparable. The utilization of latent heat as a passive heat sink in battery thermal management proves effective, with the circular PCM configuration identified as the optimal choice. In their study, Goli et al. (2014) demonstrated a substantial enhancement in Li-ion batteries' thermal management and reliability using graphene-filled hybrid PCMs. The graphene-enhanced hybrid PCM, with its latent heat storage capability, exhibits double the thermal conductivity. The application of this hybrid PCM leads to a significant reduction in temperature rise within battery packs, as evidenced under realistic conditions. To evaluate the thermal management capabilities of two PCMs in a 20-cell LIB pack operating at $-5\text{ }^{\circ}\text{C}$ and $-10\text{ }^{\circ}\text{C}$, Ling et al. (2018) carried out the research. Two composites were investigated: one with a low thermal conductivity of 60 weight percent RT44HC/fumed silica and another with a high thermal conductivity of 60 weight percent RT44HC/expanded graphite (EG). During single discharge experiments at 0.5C, 1C, 1.5C, and 2C, more than 20 charge-discharge cycles that replicated the behavior of electric car batteries, temperature and voltage distributions were recorded. The results showed that the PCMs successfully prevented the heated battery pack from cooling down too quickly. In comparison to the RT44HC/EG composite, which has a higher thermal conductivity, the RT44HC/fumed silica composite, which has a lower thermal conductivity, showed a longer cooling time. An experimental study of the thermal management of battery modules with PCMs was carried out by Duan and Naterer (2010). To replicate a battery cell, the study used a heat source. Two different PCM designs were studied: one with the heater surrounded by a PCM cylinder and the other with the heater covered by PCM jackets. The heater operated effectively in both setups, staying within the intended temperature range. A three-dimensional numerical model was developed by Peng et al. (2022) to analyze the discharge process at different discharge rates (0.5C, 1C, and 2C). The investigation revealed a non-uniform distribution of the PCM liquid fraction during discharge, with the outer layer and top of the PCM melting first. Temperature differences between batteries emerged due to different heat transfer rates at higher discharges. The study showed that composites of PCM (paraffin wax) and expanded graphite (EG) exhibited superior heat dissipation performance compared to pure PCM. Chen et al. (2021) investigated the performance of a BTMS incorporating PCM and a heat pipe (HP). The study used numerical methods to investigate the effect of environmental, HP, and PCM parameters on system performance. The maximum temperature in the battery was found to be reduced by reducing

PCM thickness or ambient temperature, increasing the environment's convective heat transfer coefficient (h), and increasing the latent heat of PCM. To minimize temperature differences in the battery pack, the BTMS's PCM was designed with varying thickness distribution while maintaining a constant PCM volume. An optimization strategy was proposed to adjust the thickness distribution of the PCM, with results showing that optimal distribution was achieved with just a few tuning steps. Li et al. (2018) introduced a method for optimizing the thermal performance of BTMS incorporating PCM. The optimization objective is to minimize PCM mass while achieving the desired runtime and maximum temperature difference. During the optimization phase, the research considered four different types of BTMS with single, dual, triple, and quad batteries. The impacts of several variables on the minimal PCM mass were examined, including battery radius, the separation between nearby batteries, battery heat generation, and top and bottom PCM thickness. The limited thermal conductivity of traditional pure PCM was addressed by creating an EG/PA composite PCM, which was then used in the BTMS. The results showed how well the suggested optimization strategy for BTMS with PCM worked, and they also gave engineers helpful pointers for creating systems comparable to this one.

In the present work, a passive Battery Thermal Management System (BTMS) involving 8 battery cells is filled with Phase Change Material (PCM). The modeled 3D BTMS was analyzed in COMSOL Multiphysics software for different parameters. The surface temperature of battery cells at the end of the process was investigated. Analyses were conducted for three different S_T^* values (1.25, 1.5, and 2.0) and three different PCM types with thermal conductivities of $0.2 \text{ Wm}^{-1}\text{K}^{-1}$, $1 \text{ Wm}^{-1}\text{K}^{-1}$, and $5 \text{ Wm}^{-1}\text{K}^{-1}$ at various discharge rates (3C, 5C, and 7C) and ambient temperatures (20°C , 30°C , and 40°C).

2. Material and Method

The battery thermal management system (BTMS) analyzed in this study is shown in Figure 1. As can be seen in the figure, the BTMS consists of 8 18650 type (diameter $D=18 \text{ mm}$, length $H=65 \text{ mm}$) Li-ion battery cells and a PCM layer applied around the cells. In the calculations, the horizontal and vertical distance between the battery cells is S_T and will be found by $S_T=S_T^* \cdot D$. The distance of the first battery cell to the starting point is determined as $S_T/2$, as

can be seen in the figure. Accordingly, the width of the battery pack formed with the PCM layer will be $W=S_T$ and the length will be $L=8S_T$.

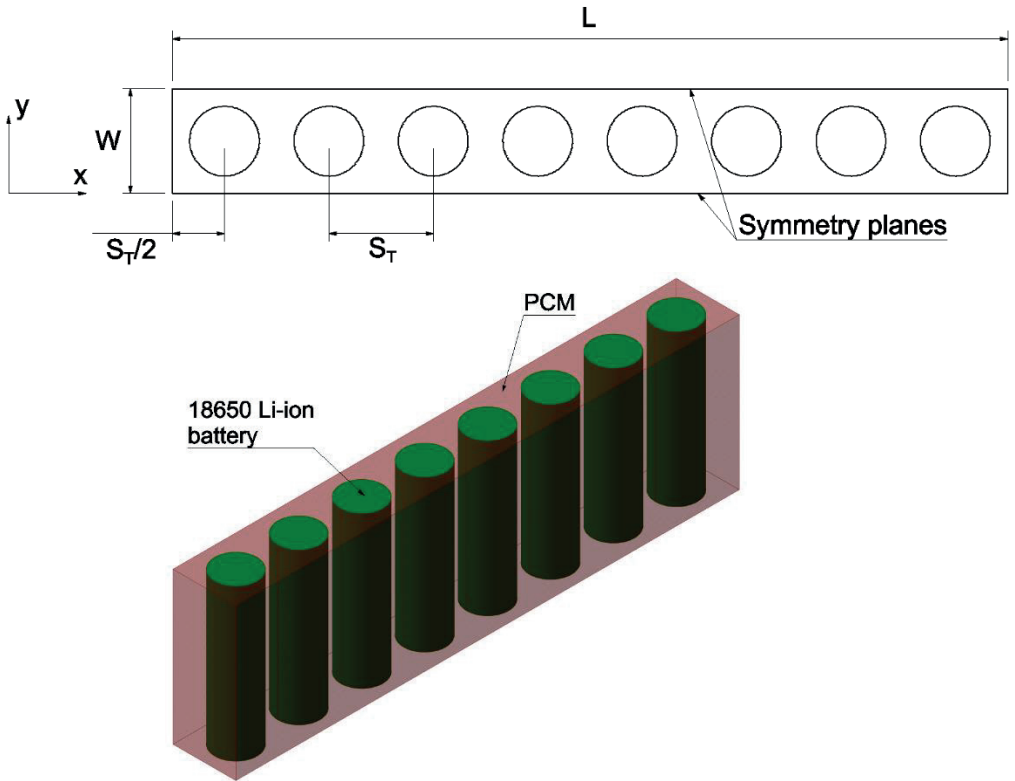


Figure 1. The BTMS analyzed in the study

The physical properties of the battery cells and PCM used in the designed system are given in Table 1 (Choudhari et al. 2020). Paraffin, which has low thermal conductivity and is frequently used in PCM-based BTMSs due to its cost and availability, was preferred as PCM in the study (Putra et al. 2020; Zhang et al. 2021). In the calculations, it was assumed that the physical properties of the PCM used do not change in the solid and liquid phases. Other assumptions made to simplify the analysis are listed below:

- Due to the high viscosity of the PCM, its movement in the liquid phase is neglected. Accordingly, it is assumed that conduction heat transfer occurs between the PCM and the battery both in the solid phase and in the liquid phase.
- Heat transfer by radiation is neglected.
- Ambient conditions are constant.

- It is assumed that the internal resistance of the battery cells does not change with temperature or charge/discharge conditions.

Table 1. Physical properties of the materials used in the system

| Property | Li-ion battery | Paraffin |
|--------------------------------------|----------------|----------|
| $k_s, \text{Wm}^{-1}\text{K}^{-1}$ | 3 | 0.2 |
| $k_b, \text{Wm}^{-1}\text{K}^{-1}$ | - | 0.2 |
| $Cp_s, \text{Jkg}^{-1}\text{K}^{-1}$ | 300 | 2000 |
| $Cp_b, \text{Jkg}^{-1}\text{K}^{-1}$ | - | 2000 |
| ρ_s, kgm^{-3} | 2720 | 820 |
| ρ_b, kgm^{-3} | - | 820 |
| LH, Jkg^{-1} | - | 165000 |
| $T_m, ^\circ\text{C}$ | - | 43 |
| $R_i, \text{m}\Omega$ | 30 | - |
| Capacity, Ah | 2.4 | - |

The energy equation for the battery cell in the system is given in Equation (1):

$$\rho_b C p_b \frac{\partial T_b}{\partial t} = k_b \nabla^2 T + q_b \quad (1)$$

Here, q_b is the amount of heat released in the battery and can be calculated by Equation (2) (Bernardi et al. 1985):

$$q_{gen} = q_{irr} + q_{rev} \quad (2)$$

In Equation (2), q_{irr} and q_{rev} represent the heat released due to irreversible and reversible reactions in the battery, respectively. Here, q_{rev} can be neglected since it is considerably smaller than q_{irr} (Son et al. 2023; Liu et al. 2022). q_{irr} can be calculated by the following equation:

$$q_{irr} = I^2 \cdot R_i \quad (3)$$

Where I (Ampere-A) is the current value drawn from the battery, R_i is the internal resistance of the battery and is given in Table 1. The energy equation for PCM is given in Equation (4).

$$\rho_{FDM} \frac{\partial H_{FDM}}{\partial t} = k_{FDM} \nabla^2 T \quad (4)$$

In Equation (4), H_{PCM} is the total enthalpy of PCM material and can be found by the following equation:

$$H_{PCM} = h_{PCM} + \Delta H_{PCM} \quad (5)$$

In the above equation, h_{PCM} and ΔH_{PCM} are the amount of sensible and latent heat of PCM respectively and are calculated by the following equations:

$$h_{PCM} = \int_{T_0}^{T_{PCM}} C_{p,PCM} dT_{PCM} \quad (6)$$

$$\Delta H_{PCM} = F \cdot LH_{PCM} \quad (7)$$

In the above equations, T_0 , F and LH represent the initial temperature, liquefaction rate and latent heat of PCM, respectively. F value is determined by the following relation:

$$F = \begin{cases} 0, & T_{PCM} < T_m \\ 1, & T_{PCM} > T_m \end{cases} \quad (8)$$

In Equation (8), T_m is the melting temperature of PCM and is given in Table 1. To solve the energy equations presented in Equations (1) and (4), some boundary conditions must be defined. The heat transfer between the battery cell and PCM is by conduction and the related boundary condition is given in Equation (9).

$$k_b \frac{\partial T}{\partial n} = k_{PCM} \frac{\partial T}{\partial n} \quad (9)$$

Heat transfer will occur by convection between the ambient air and the PCM. The relevant boundary condition is defined by Equation (10).

$$k_{PCM} \frac{\partial T}{\partial n} = h(T_{PCM} - T_a) \quad (10)$$

Where h and T_a represent the outdoor convection coefficient and temperature, respectively. Initially, PCM, battery and ambient air temperatures are assumed to be equal to each other. The relevant initial condition is defined by Equation (11):

$$t = 0, \quad T_b(x, y, z) = T_{PCM}(x, y, z) = T_a = T_0 \quad (11)$$

The solution procedure and validation

In this study, a numerical analysis of a PCM-based BTMS according to different parameters was carried out using COMSOL Multiphysics software (Kavasogullari et al. 2023). The PCM is modeled in 3-dimensional form in COMSOL software. To obtain the temperature and phase change in the system, the time-dependent solution of the energy equations given in the previous section was performed. In the finite element analysis performed in COMSOL software, PARDISO was used as a solver and the relative tolerance was set as 0.01. In the parametric study, the T_a value was changed to 20, 30, and 40 °C to see the effect of ambient conditions on the system performance; S_T^* value was changed to 1.25, 1.5, and 2.0 to see the effect of geometric properties; k_{PCM} was changed to 0.2, 1 and 5 $Wm^{-1}K^{-1}$ to see the effect of PCM properties. The ambient convection heat transfer coefficient h was determined as 5 $Wm^{-2}K^{-1}$ (Lazrak et al. 2018). In the numerical calculations, the discharge rate of the battery cells was determined as 3C, 5C, and 7C and it was assumed that the battery cells can be discharged at these speeds. According to the battery specifications given in Table 1, the current values drawn from the cells at the determined discharge rates will be 7.2A, 12A, and 16.8A, respectively; and the heat generated in the cells will be 1.56W, 4.32W, and 8.47W, respectively. The discharge times corresponding to these discharge rates will be 1200, 720, and 515 seconds, respectively.

For the mesh structure used in the numerical analysis of the study, the independence analysis from the number of mesh elements was performed. The variation of temperature in the system is given in Figure 2 for four different mesh element numbers: 25296, 41590, 69420, and 145809. As can be seen in the figure, almost the same temperature values are obtained for four different numbers of mesh elements. Therefore, for saving time and power, the network structure with 25296 elements was preferred. The preferred mesh structure is shown in Figure 3.

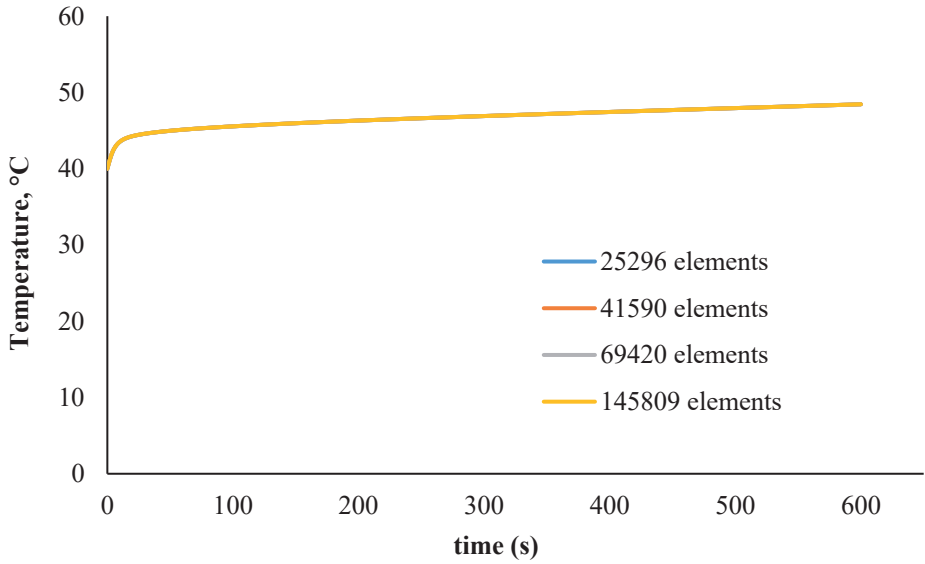


Figure 2. The results of the grid independence analysis

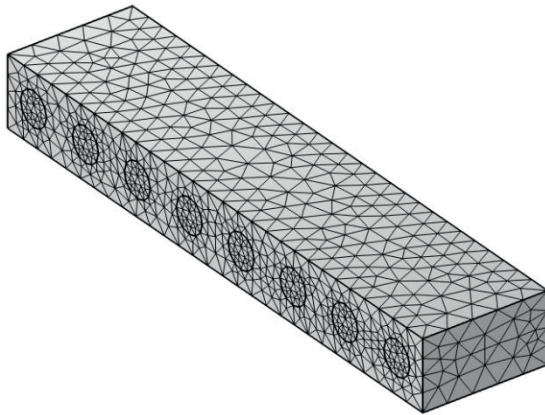


Figure 3. The preferred mesh structure in numerical analysis

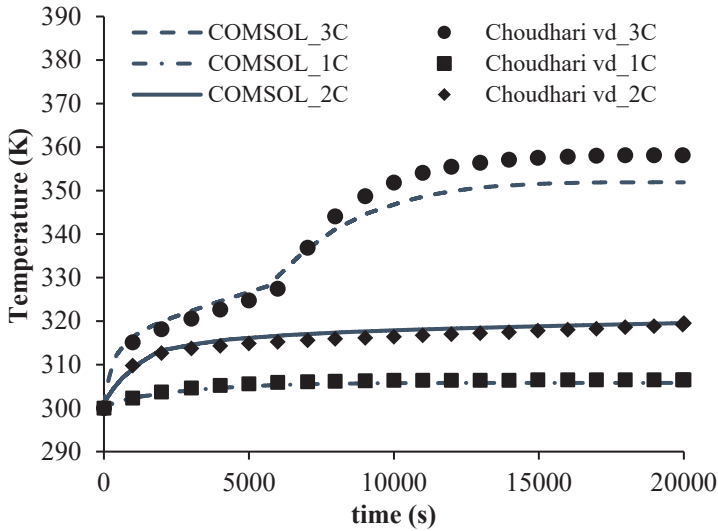


Figure 4. The comparison of numerical analysis with the literature

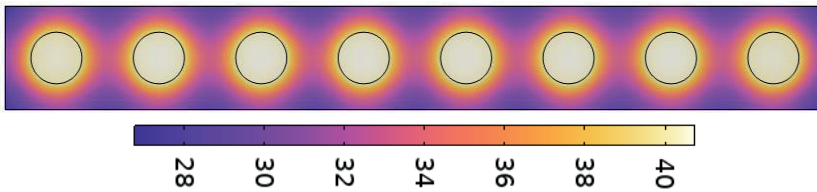
The verification of the model prepared for analysis in COMSOL software was carried out by comparing it with the study previously conducted by Choudhari et al. (2020) in the literature. Accordingly, the literature study was re-modeled in COMSOL software in 3D with the same geometry and material properties. The analysis of the modeled previous study was carried out at three different discharge velocities, 1C, 2C, and 3C, by applying the same modules used in this study in the software. The comparison results are given in Figure 4. As can be seen in the figure, there is almost no difference between the presented study and the literature results at 1C and 2C discharge rates. Only at the 3C discharge rate, there is a difference of 5 K. The comparison results show that the results obtained in the study are in agreement with the literature.

3. Results and Discussion

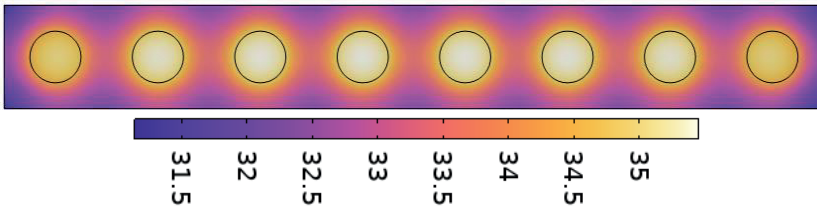
As mentioned before, the effects of ambient temperature (T_a), intercellular dimensionless distance (S_T^*), and PCM thermal conductivity coefficient value (k_{PCM}) on the cooling performance of BTMS were investigated at different discharge rates of 3C, 5C, and 7C. Accordingly, T_a was determined as 20, 30, and 40 °C; S_T^* as 1.25, 1.5 and 2.0; k_{PCM} as 0.2, 1 and 5 $Wm^{-1}K^{-1}$. Figure 5 shows the temperature distributions in the battery pack according to the determined conditions. As can be seen in the figure, due to the temperature interaction between the cells, the 4th and 5th battery cells have the highest temperature in

the eight-cell battery pack. Since the increase in k_{PCM} value increases the temperature interaction between the cells, the temperature difference between the cells has become more pronounced in cases where high heat conduction PCM is preferred. For this reason, the temperature of the 4th battery cell is considered in the results.

$k_{PCM}=0.2 \text{ Wm}^{-1}\text{K}^{-1}$



$k_{PCM}=1 \text{ Wm}^{-1}\text{K}^{-1}$



$k_{PCM}=5 \text{ Wm}^{-1}\text{K}^{-1}$

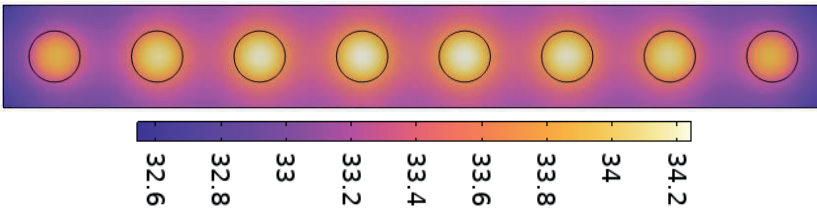
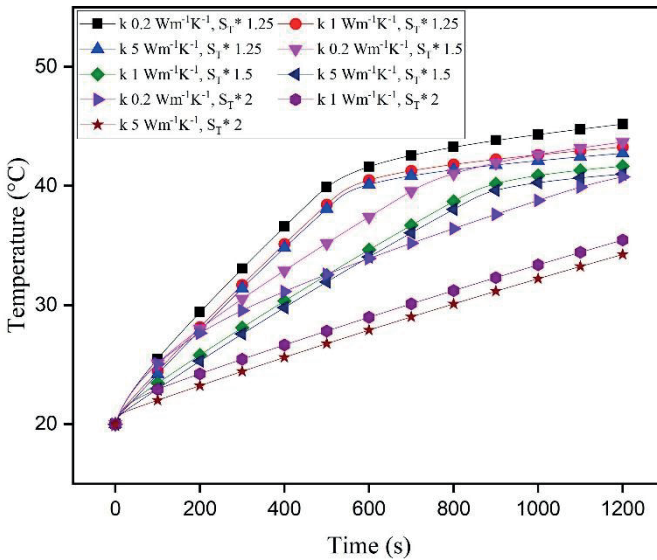


Figure 5. The battery pack temperature distributions obtained for the specified cases
($3C$, $S_T^*=2.0$, $T_a=20 \text{ }^\circ\text{C}$)

Figure 6 shows the time variation of the 4th battery cell according to different parameters at a $3C$ discharge rate. As can be seen from the figures, at the determined discharge rate, the temperature was below the critical temperature in all cases considering the discharge time. As expected, increasing the k_{PCM} value decreased the temperature values since it increased the amount of heat dissipated to the external environment. For example, in the case where $T_a=20 \text{ }^\circ\text{C}$, the temperature obtained at the end of the unloading period was about $45 \text{ }^\circ\text{C}$.

°C for $k_{PCM}=0.2 \text{ Wm}^{-1}\text{K}^{-1}$ at $S_T^*=1.25$, while it was calculated as about 42 °C for $k_{PCM}=5 \text{ Wm}^{-1}\text{K}^{-1}$. The lowest temperatures were found at $S_T^*=2.0$ and $k_{PCM}=5 \text{ Wm}^{-1}\text{K}^{-1}$ values as approximately 34, 40, and 42 °C for ambient temperatures of 20, 30 and 40 °C, respectively. Figure 7 shows the variation of the temperature with time according to the determined parameters at different ambient temperatures at a 5C discharge rate. As can be seen from the graphs given, at the end of 720 seconds discharge time, the cell temperature was found to be very close to the critical temperature when $S_T^*=1.25$, $T_a=20$ °C, and $k_{PCM}=0.2 \text{ Wm}^{-1}\text{K}^{-1}$. At 30 and 40 °C ambient temperatures, it was observed that the cell temperature exceeded the critical temperature at the same S_T^* and k_{PCM} values. In these cases, at the end of the unloading period, the temperature reached approximately 61 and 70 °C, respectively. Since increasing the S_T^* value both reduces the heat interaction between the cells and increases the thermal capacity of the PCM, the cell temperature could be kept below the critical temperature at all T_a and k_{PCM} values at S_T^* values of 1.5 and 2.0.



$T_a=20$ °C

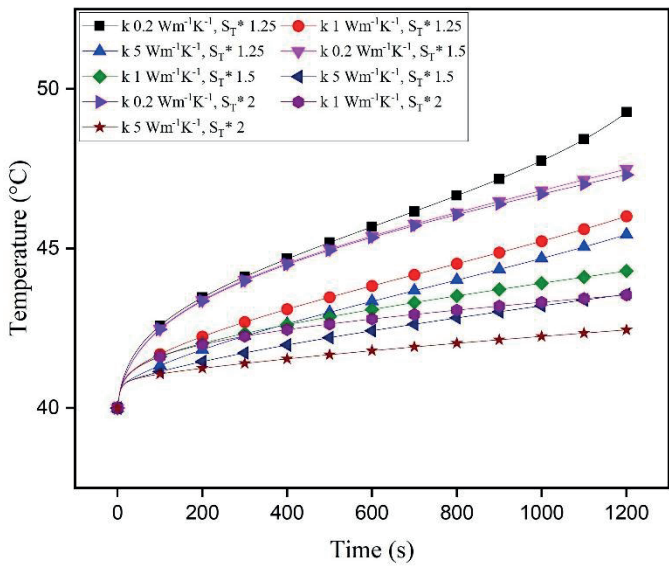
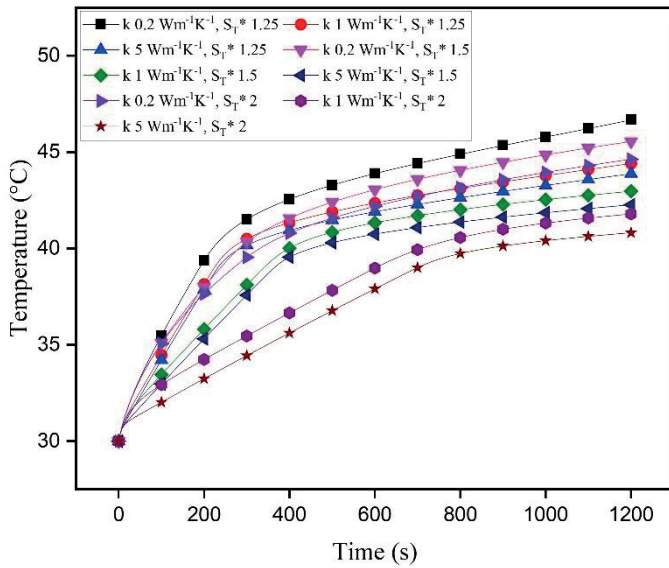
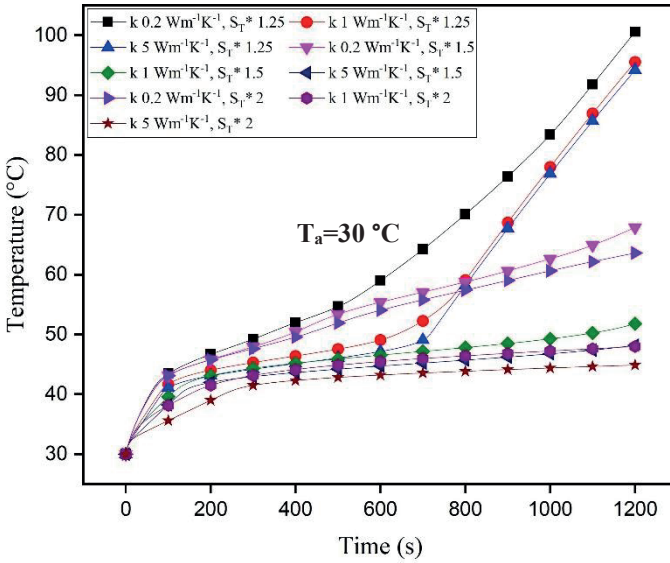
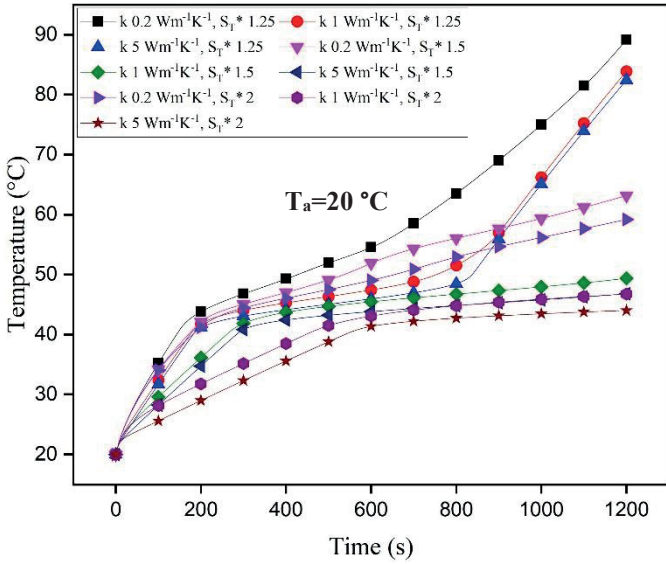


Figure 6. The variation of temperature for different parameters at a 3C discharge rate



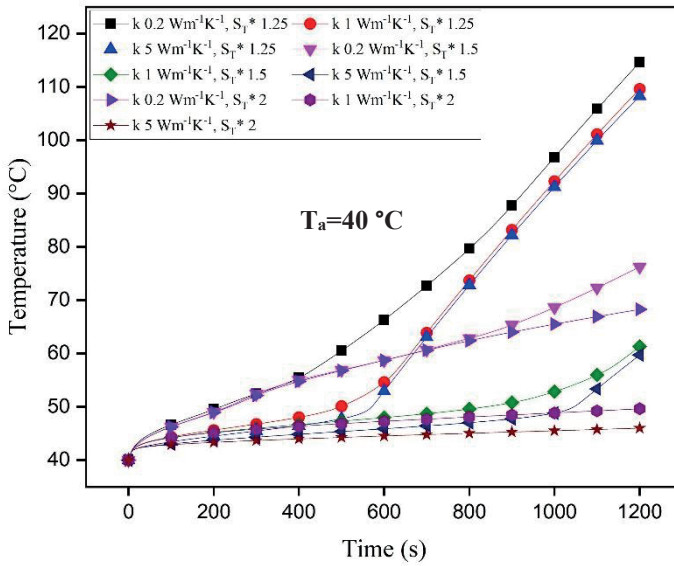
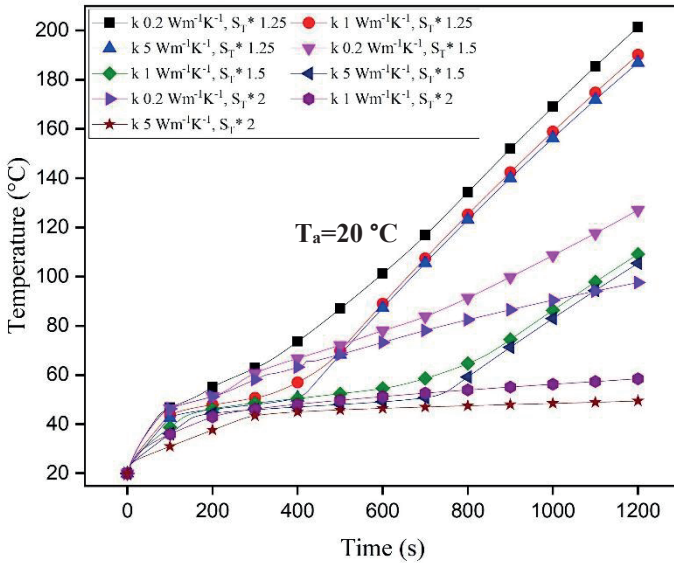


Figure 7. The variation of temperature for different parameters at a 5C discharge rate



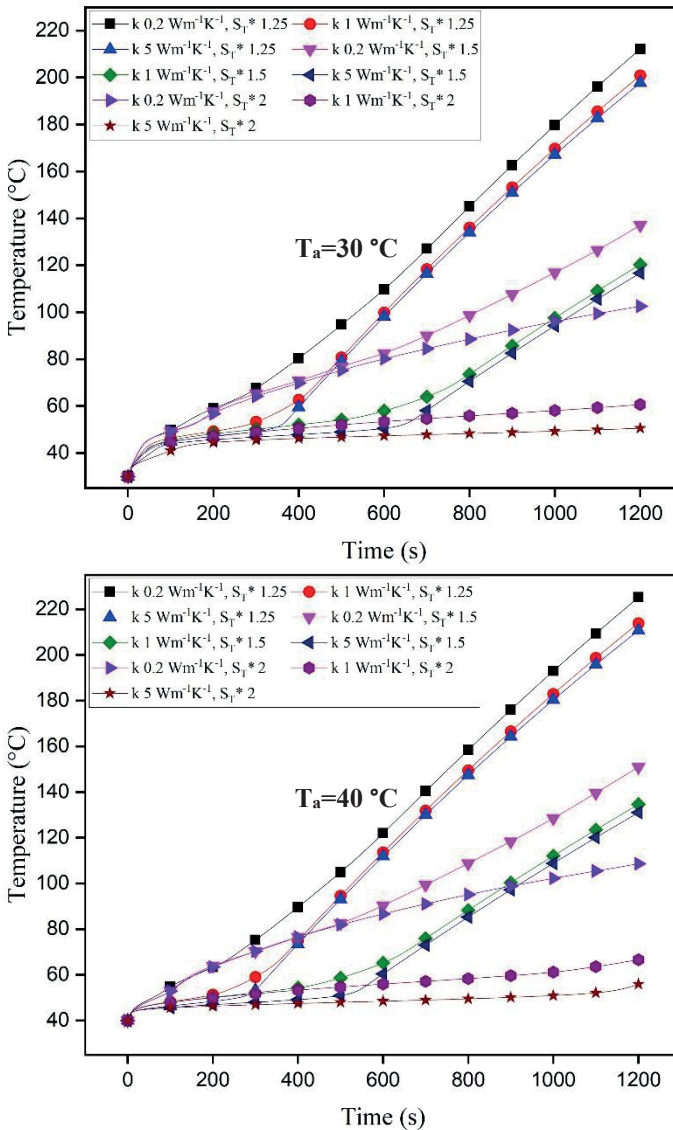
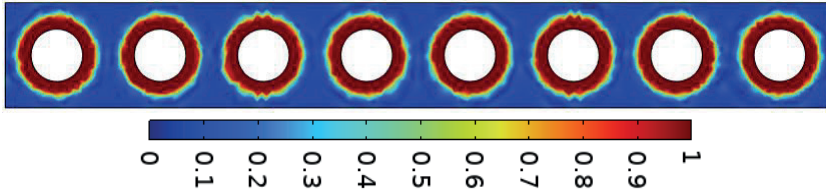


Figure 8. The variation of temperature for different parameters at a 7C discharge rate

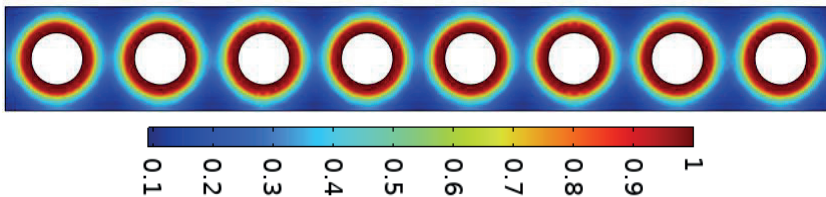
Figure 8 shows the variation of the cell temperature at a 7C discharge rate according to different ambient temperatures. The high amount of heat generated in the battery at a 7C discharge rate caused the cell temperature to rise further in all cases. Considering 515 seconds discharge time, the temperature could not be kept below 60 °C in any case for $S_i^* = 1.25$. At the

determined ambient temperatures, it was observed that a safe discharging process could be realized with an S_T^* of at least 1.5 and a k_{PCM} of $1 \text{ Wm}^{-1}\text{K}^{-1}$.

$k_{PCM}=0.2 \text{ Wm}^{-1}\text{K}^{-1}$



$k_{PCM}=1 \text{ Wm}^{-1}\text{K}^{-1}$



$k_{PCM}=5 \text{ Wm}^{-1}\text{K}^{-1}$

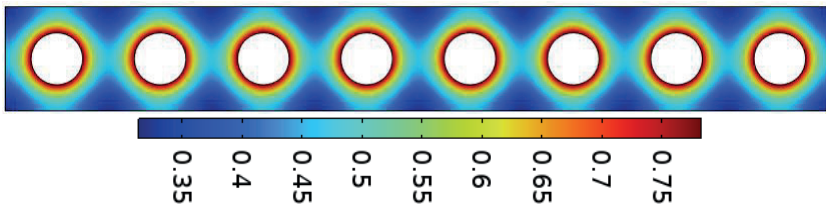


Figure 9. The liquid phase contours formed in the battery pack in the specified cases ($7C$, $S_T^*=2.0$, $T_a=40^\circ\text{C}$)

At low k_{PCM} values, the heat generated in the battery could not be transmitted well through the PCM layer, resulting in heat accumulation in the vicinity of the battery. Due to this accumulated heat, the battery temperature increased even more and the phase change in the PCM layer became irregular. As can be seen in the contour obtained for $k_{PCM}=0.2 \text{ Wm}^{-1}\text{K}^{-1}$, the PCM layer in the vicinity of the battery is completely melted, while the other regions are almost not melted. The other contours show that at higher k_{PCM} values, the difference in the melting rate between the parts of the PCM layer near and far from the battery decreases. The obtained temperature and phase change results show that PCMs with high k_{PCM} values should be preferred to obtain both good temperature control and a more regular phase change in the system. However,

since materials with high k_{PCM} values are relatively more expensive, this may increase the system cost. In addition, the results obtained in the study revealed that increasing the S_T^* value improves the temperature control performance of the system. However, increasing the S_T^* value will increase the size of the battery pack and accordingly, the amount of PCM used. This situation may again increase the system cost.

4. Conclusion

In the present study, the effect of different PCM types and S_T^* values on the cooling performance of a passive BTMS was investigated. Analyses were conducted for three different S_T^* values (1.25, 1.5, and 2.0) and three different PCM types with thermal conductivities of $0.2 \text{ Wm}^{-1}\text{K}^{-1}$, $1 \text{ Wm}^{-1}\text{K}^{-1}$, and $5 \text{ Wm}^{-1}\text{K}^{-1}$ at various discharge rates (3C, 5C, and 7C) and ambient temperatures (20°C , 30°C , and 40°C). The modeled 3D BTMS was analyzed in COMSOL Multiphysics software for different parameters. The study revealed the following results:

- At a discharge rate of 3C, the lowest temperatures were observed at $S_T^*=2.0$ and $k_{PCM}=5 \text{ Wm}^{-1}\text{K}^{-1}$ values as approximately 34 , 40 , and 42°C for ambient temperatures of 20 , 30 , and 40°C , respectively.
- At a discharge rate of 3C, the increase in S_T^* from 1.25 to 2.0 resulted in a decrease in temperature at the end of discharge 20.37%, 8.88%, and 7.48% for ambient temperatures of 20 , 30 , and 40°C , respectively.
- At a discharge rate of 5C, the lowest temperatures were observed at $S_T^*=2.0$ and $k_{PCM}=5 \text{ Wm}^{-1}\text{K}^{-1}$ values as approximately 42.3 , 43.6 , and 44.9°C for ambient temperatures of 20 , 30 , and 40°C , respectively.
- At a discharge rate of 5C, the increase in S_T^* from 1.25 to 2.0 resulted in a decrease in temperature at the end of discharge 10.38%, 13.32%, and 30.92% for ambient temperatures of 20 , 30 , and 40°C , respectively.
- At a discharge rate of 7C, the lowest temperatures were observed at $S_T^*=2.0$ and $k_{PCM}=5 \text{ Wm}^{-1}\text{K}^{-1}$ values as approximately 45.9 , 46.9 , and 48°C for ambient temperatures of 20 , 30 , and 40°C , respectively.
- At a discharge rate of 7C, the increase in S_T^* from 1.25 to 2.0 resulted in a decrease in temperature at the end of discharge 35.53%, 42.87%, and 39.52% for ambient temperatures of 20 , 30 , and 40°C , respectively.

- The PCM with a thermal conductivity of $0.2 \text{ Wm}^{-1}\text{K}^{-1}$ is determined to be adequate only for the discharge rate of 3C.

The increase in the S_T^* value resulted in a significant decrease in the temperature at the end of discharge for all cases. However, considering that the use of more PCM will increase the cost, it was deemed appropriate to choose the S_T^* value as 1.25 and 1.5 for discharge rates of 3C and 5C, respectively.

References

Bernardi, D., Pawlikowski, E., & Newman, J. (1985). A general energy balance for battery systems. *Journal of the Electrochemical Society*, 132(1), 5.

Chen, K., Hou, J., Song, M., Wang, S., Wu, W., & Zhang, Y. (2021). Design of battery thermal management system based on phase change material and heat pipe. *Applied Thermal Engineering*, 188, 116665.

Choudhari, V. G., Dhoble, A. S., & Panchal, S. (2020). Numerical analysis of different fin structures in phase change material module for battery thermal management system and its optimization. *International Journal of Heat and Mass Transfer*, 163, 120434.

Duan, X., & Naterer, G. F. (2010). Heat transfer in phase change materials for thermal management of electric vehicle battery modules. *International Journal of Heat and Mass Transfer*, 53(23-24), 5176-5182.

El Idi, M. M., Karkri, M., & Tankari, M. A. (2021). A passive thermal management system of Li-ion batteries using PCM composites: Experimental and numerical investigations. *International Journal of Heat and Mass Transfer*, 169, 120894.

Goli, P., Legedza, S., Dhar, A., Salgado, R., Renteria, J., & Balandin, A. A. (2014). Graphene-enhanced hybrid phase change materials for thermal management of Li-ion batteries. *Journal of Power Sources*, 248, 37-43.

Kavasogullari, B., Karagöz, M. E., Yildiz, A. S., & Biçer, E. (2023). Numerical investigation of the performance of a hybrid battery thermal management system at high discharge rates. *Journal of Energy Storage*, 73, 108982.

Lazrak, A., Fourmigué, J. F., & Robin, J. F. (2018). An innovative practical battery thermal management system based on phase change materials: Numerical and experimental investigations. *Applied Thermal Engineering*, 128, 20-32.

Li, Y., Du, Y., Xu, T., Wu, H., Zhou, X., Ling, Z., & Zhang, Z. (2018). Optimization of thermal management system for Li-ion batteries using phase change material. *Applied Thermal Engineering*, 131, 766-778.

Ling, Z., Wen, X., Zhang, Z., Fang, X., & Gao, X. (2018). Thermal management performance of phase change materials with different thermal conductivities for Li-ion battery packs operated at low temperatures. *Energy*, 144, 977-983.

Liu, X., Zhang, C. F., Zhou, J. G., Xiong, X., & Wang, Y. P. (2022). Thermal performance of battery thermal management system using fins to enhance the combination of thermoelectric cooler and phase change material. *Applied Energy*, 322, 119503.

Peng, P., Wang, Y., & Jiang, F. (2022). Numerical study of PCM thermal behavior of a novel PCM-heat pipe combined system for Li-ion battery thermal management. *Applied Thermal Engineering*, 209, 118293.

Putra, N., Sandi, A. F., Ariantara, B., Abdullah, N., & Mahlia, T. M. I. (2020). Performance of beeswax phase change material (PCM) and heat pipe as passive battery cooling system for electric vehicles. *Case Studies in Thermal Engineering*, 21, 100655.

Safdari, M., Ahmadi, R., & Sadeghzadeh, S. (2020). Numerical investigation on PCM encapsulation shape used in the passive-active battery thermal management. *Energy*, 193, 116840.

Son, Y. W., Kang, D., & Kim, J. (2023). Passive battery thermal management system for an unmanned aerial vehicle using a tetrahedral lattice porous plate. *Applied Thermal Engineering*, 225, 120186.

Verma, A., Shashidhara, S., & Rakshit, D. (2019). A comparative study on battery thermal management using phase change material (PCM). *Thermal Science and Engineering Progress*, 11, 74-83.

Youssef, R., Hosen, M. S., He, J., Mohammed, A. S., Van Mierlo, J., & Berecibar, M. (2022). Novel design optimization for passive cooling PCM assisted battery thermal management system in electric vehicles. *Case Studies in Thermal Engineering*, 32, 101896.

Zhang, W., Liang, Z., Wu, W., Ling, G., & Ma, R. (2021). Design and optimization of a hybrid battery thermal management system for electric vehicle based on surrogate model. *International Journal of Heat and Mass Transfer*, 174, 121318.



Chapter 16

MOTH-FLAME OPTIMIZATION ALGORITHM FOR DISASSEMBLY LINE BALANCING PROBLEM UNDER THE TRUNCATED LEARNING EFFECT

Halime SOMTÜRK¹

Mehmet Duran TOKSARI²

¹ Arş Gör., Tokat Gaziosmanpaşa Üniversitesi, Mühendislik ve Mimarlık Fakültesi, Endüstri Mühendisliği Bölümü, halime.somturk@gop.edu.tr, Orcid ID:0000-0001-7329-495X

² Prof. Dr., Erciyes Üniversitesi, Mühendislik Fakültesi, Endüstri Mühendisliği Bölümü, dtoksari@erciyes.edu.tr, Orcid ID:0000-0001-9577-1956

1. INTRODUCTION

When a product's useful life is up or a new version is introduced due to advancements in technology, it becomes waste (McGovern & Gupta, 2007; K. Wang, Li, & Gao, 2019b). Increasing waste materials in recent years cause environmental problems. Therefore, it has become important to properly recycle these waste products through both government environmental regulations and public awareness. Waste materials can be recycled or remanufactured. At this stage, disassembly becomes important in terms of separating the products into parts. Disassembly lines need to be set up successfully and efficiently in order for the products to be disassembled as best they can. This phenomenon is called disassembly line balance in the literature.

After being first studied by Güngör and Gupta (1999) and Güngör and Gupta (2001), DLB problem has been widely solved using different purposes and methods. It was shown by McGovern and Gupta (2007) that DLB problems are NP-hard.

DLB problems are single-objective (Li & Janardhanan, 2021; Z. Zhang, Wang, Zhu, & Wang, 2017) or multi-objective (Liang, Zhang, Yin, Zhang, & Wu, 2023; Yin, Zhang, & Jiang, 2021a) optimization problems that involve appropriately assigning many disassembly operations to stations. The objective functions used in studies in the DLB literature can be listed as follows: minimization number of workstations (Altekin, 2017; Askiner Güngör & Gupta, 2001; Liang et al., 2023; Xiao, Wang, Yu, & Nie, 2017), minimization of idle time of Workstation (Güngör & Gupta, 2002; Liu & Wang, 2017), minimization hazardous index (Ren et al., 2018; Xiao et al., 2017; Y. Zhang, Zhang, Guan, & Xu, 2022), minimization of the number of direction changes required for disassembly (Aşkiner Güngör & Gupta, 2002; Z. Zhang et al., 2017), profit maximization (Kalaycılar, Azizoğlu, & Yeralan, 2016; K. Wang, Li, Gao, Li, & Sutherland, 2022). In DLB problems, task failure (Güngör & Gupta, 2001), swap out the tools (Saif, Guan, Liu, Zhang, & Wang, 2014), task relationships that depend on sequence (K. Wang et al., 2022), etc. many factors such as can affect optimal solutions. Solution methods for solving DLB problems may vary depending on the size of the problem. Linear programming (Altekin, 2017), nonlinear programming (Bentaha, Battaia,

Dolgui, & Hu, 2015), mixed integer programming(Edis, Ilgin, & Edis, 2019; Yin, Zhang, Zhang, Wu, & Liang, 2022a) and stochastic programming(Bentaha, Dolgui, Battaïa, Riggs, & Hu, 2018; Kalaycılar et al., 2016) techniques are applied to get the best answer for small-sized problems. (Yin et al., 2023).

In the problem's solution stage, there are two main constraints: cycle time and priority relations. The limitation on cycle time guarantees that the time it takes to complete the disassembly process of workstations does not exceed the maximum value known as cycle time. The precedence relations constraint ensures that the work that needs to be disassembled before is assigned to the queues in front of the job that will be dismantled later, according to the connections between the tasks during the disassembly phase.

The disassembly process is carried out completely (Liu & Wang, 2017; Ren et al., 2020; Z. Zhang et al., 2017) or partially(Liang et al., 2023; Ren et al., 2017; Yin et al., 2021, 2023). Zhu et al. (2018), studied the disassembly process of a refrigerator, which included twenty-five tasks, that is, they carried out a complete disassembly process by removing all twenty-five parts. On the other hand, Yin et al. (2021a) studied the partial disassembly of a laptop consisting of forty-seven parts. Hazardous parts were separated and forty-two parts were successfully disassembled (Liang et al., 2023).

Disassembly lines are divided into five groups according to their layout: Straight, two-sided layout, U-shaped, parallel layout and multi-parallel layout. The straight layout is the layout type that has been studied the most in the DLB literature (Ren et al., 2020; Yin, Zhang, Zhang, Wu, & Liang, 2022b; Zhou & Bian, 2022). The second most frequently worked layout is the two-sided layout (Kucukkoc, Li, & Li, 2020; K. Wang, Li, & Gao, 2019a; Y. Zhang et al., 2022). The third layout type, U-shaped layout, has been studied in many articles(Guo et al., 2022; Li & Janardhanan, 2021; Li, Kucukkoc, Tang, & Zhang, 2023; K. Wang, Gao, & Li, 2020). Parallel (Qin et al., 2023; Zhu, Zhang, & Guan, 2020) and multi-parallel (Liang et al., 2023) layout have been seen in recent studies in the DLB literature. In solving DLB problems, precedence relationships between tasks should be taken into account when assigning jobs to stations. The products to be disassembled may have attached parts that need to be removed before some parts can be removed. Therefore, when assigning jobs

to stations, precedence relationships impose a constraint, making DLB problems difficult. While small-sized DLB problems can be solved with optimization methods, metaheuristic methods are used to reach the optimum result or the closest result to the optimum in large-sized problems. Some of them are: Genetic algorithm(Kalayci et al., 2016; McGovern & Gupta, 2007), artificial bee colony algorithm(Liu & Wang, 2017), hummingbird algorithm(Yin et al., 2021), firefly algorithm(Zhu et al., 2018), hybrid driving algorithm(Yin et al., 2022b), whale optimization algorithm(Y. Zhang et al., 2022), flower pollination algorithm(K. Wang et al., 2019a) and Cuckoo search algorithm(Li & Janardhanan, 2021).

In this study, for a straight disassembly line where the products are completely disassembled, the effect of truncated position-based learning on the minimum number of stations to be opened was studied. The truncated position-based learning effect is a phenomenon that has been studied in the scheduling literature. The position-based learning effect was first introduced to the literature by Biskup (1999). It was thought that workers learned by doing a job over and over again. The work learned is also completed in a shorter time. As far as we have examined in the DLB literature, Jobs have fixed processing times. The sequence in which a work is completed at the station has no impact on how long it takes to process. However, in real life, tasks are learned as they are done, and if the order of operations at the station is larger, the processing time decreases. Workers become increasingly proficient at their jobs when they perform them repeatedly. Therefore, if it is placed further up in a workstation, processing time will be shorter (X. Y. Wang et al.,2013).

In the position-based learning model proposed by Biskup (1999), as the learning effect increases, The job's processing time is continuously declining and getting closer to zero. Thereupon, Wu et al. (2013) state that a job's processing time is dependent on both its position and a control parameter in their truncated position-based learning effect model. Learning is thought to be limited to a point where it cannot continue continuously.

We can summarize the contribution of this study as follows;

- The effects of truncated position-based learning were investigated on DLB problems for the first time in this work. In the literature, task processing times for DLB problems are constant in the literature. Due to the truncated position based learning effect, it has been observed that depending on the positions they are assigned to, job processing times vary during the process.
- To prove the accuracy of the model proposed for the most well-known small-sized DLB problem, the optimum result was found with the Lingo.11 optimization program.
- The Moth-Flame optimization technique has been used to provide a solution approach for large-sized problems. The generated code is coded in C# software language. The MFO algorithm was used for the first time in the DLB problem.

2. MATERIAL AND METHOD

The process of assigning disassembly tasks to a number of workstations optimally to achieve different disassembly objectives while meeting the workstation cycle time limitation and precedence relationships between jobs is known as the DLB issue, which is a difficult optimization problem. The aim of this work is to determine, under the truncated position-based learning effect, the number of minimum workstation for DLB problems that satisfy the cycle constraint and precedence relations requirements.

The processing time of a task in position-based learning decreases as a function of the task's position at the station. However, in the position-based learning model proposed by Biskup (1999), The processing times of jobs in subsequent positions soon approach zero as the number of jobs at stations increases. Due to this situation, Wu et al. (2013), presented a new study proving that a job's position and a control parameter determine the job's actual processing time. This learning is known as truncated position-based learning in the literature.

The truncated position-based learning model is defined as:

$$P_{ir} = p_i \times \max(r^a, \rho) \quad (1)$$

Here, p_{ir} is the normal processing time of job i , $a \leq 0$ is the learning index, ρ is the control parameter ($0 < \rho < 1$). Learning index is the logarithmic base 2 value of the learning rate. For example, if the learning rate is 0.80, the learning index is -0.322 ($\log_2 0.80$).

Learning cannot continue continuously and, like other human characteristics, is limited (X. Y. Wang et al., 2013). In this study, learning rates were taken as 3 different values as 0.70, 0.80 and 0.90, and the control parameters were taken as 0.80 and 0.70 (Wu et al., 2013). The objective function values found for different combinations of learning rates and control parameters were examined.

Table 1. Task definitions and processing times of 8-tasks DLB problem

| Task no | Task Definition | Task Time(sec) |
|---------|---|----------------|
| 1 | Removal of the top cover of the PC (TC) | 14 |
| 2 | Removal of the hard drive (HD) | 10 |
| 3 | Removal of the back plane (BP) | 12 |
| 4 | Removal of PCI cards (PCI) | 18 |
| 5 | Removal of PCI cards (PCI) | 23 |
| 6 | Removal of two RAM modules (RAM) | 16 |
| 7 | Removal of the power unit (PU) | 20 |
| 8 | Removal of the motherboard (MB) | 36 |

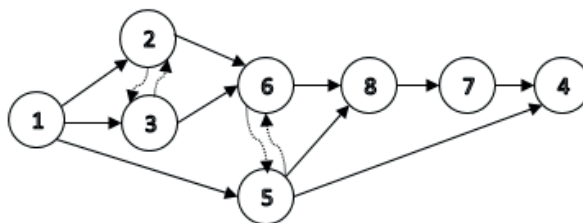


Figure 1. Precedence relationships between tasks

The task definitions of the DLB problem, which consists of 8 tasks (Güngör & Gupta, 2001), which is the simplest and most common example of the DLB

literature, are shown in Table 1. The precedence relationships between the works to be dismantled are shown in Figure 1. In the problem, the cycle time of the stations is considered as 40. In line with the precedence relationships in Figure 1, part 1 should be removed before parts 2 and 3, and likewise, part 5 should be removed before parts 8 and 4.

Some of the assumptions considered when creating the mathematical model of the DLB problem can be listed as follows: assigning each task to only one station, assigning a task to only one row in the station, completing the jobs of the stations not to exceed the cycle time, completely disassembling the products, ensuring precedence relationships between the jobs. The notations used in the model are seen in Table 2.

Table 2. Notation List

| Notations |
|--|
| $I, k \in N$ tasks set |
| $(i, k) \in SP$ set of interactive tasks |
| $j \in M$ workstations set |
| $r \in N$ position of the task on the station |
| a : learning index, |
| ρ : control parameter, |
| K : big number, |
| ct : cycle time, |
| y_{ij} : If task i is assigned to station j , 1; otherwise 0, |
| z_j : if station j is open, 1; otherwise 0, |
| x_{ijr} : if task i is assigned to position r at station j , 1; otherwise 0, |
| b_{jr} : if sequence r is used in the station j , 1; otherwise 0, |
| t_{jr} : task time of task at the sequence r in the station j , |
| c_{jr} : completion time of task at the sequence r in the station j , |

Mathematical Model:

$$f = \text{Min} \sum_{j=1}^n z_j \quad (2)$$

Constraints:

$$\sum_{j=1}^n y_{ij} = 1 \quad \text{for } \forall i \in n \quad (3)$$

$$\sum_{j=1}^n y_{ij} \leq z_j \times ct \quad \text{for } \forall i \in n \quad (4)$$

$$\sum_{r=1}^n c_{jr} \times x_{ajr} \times b_{jr} - \sum_{R=1}^n c_{jR} \times x_{k_jR} \times b_{jR} \leq 0 \quad \text{for}\{a, k\} \quad (5)$$

$$\sum_{i=1}^n x_{ijr} \leq 1 \quad \text{for } \forall j \in M, r \in N \quad (6)$$

$$\sum_{r=1}^n x_{ijr} = y_{ij} \quad \text{for } \forall j \in M, i \in N \quad (7)$$

$$\sum_{i=1}^n (g_i \times \max(r^a, \rho) \times x_{ijr}) = t_{jr} \quad \text{for } \forall j \in M, r \in N \text{ and } r \neq 1 \quad (8)$$

$$\sum_{i=1}^n g_i \times x_{ijr} = t_{jr} \quad \text{for } \forall i \in N, r = 1 \quad (9)$$

$$c_{jr} = c_{j(r-1)} + t_{jr} \quad \text{for } \forall j \in M, r \in N \text{ and } r \neq 1 \quad (10)$$

$$t_{jr} \times b_{jr} \leq t_{j(r-1)} \times b_{j(r-1)} \times M \quad \text{for } \forall j \in M, r \in N \text{ and } r \neq 1 \quad (11)$$

$$c_{jr} \times b_{jr} \leq c_{j(r-1)} \times b_{j(r-1)} \times M \quad \text{for } \forall j \in M, r \in N \text{ and } r \neq 1 \quad (12)$$

$$c_{jr} = t_{jr} \quad \text{for } \forall j \in M \text{ and } r = 1 \quad (13)$$

$$x_{Ij(r-1)} \leq \sum_{i=1}^n x_{ijr} \quad (I \neq i), (I = 1, \dots, N) \quad (14)$$

$$x_{ijr}, y_{ij}, b_{jr}, z_j \in \{0, 1\} \quad (15)$$

In Eq. (2), the goal is to minimize the number of stations that are opened.. Constraints (3) and (7) ensure that every task is assigned to just one position at only one station. Eq. (4) makes ensuring that each station's job completion time doesn't exceed the cycle time. Eq. (5) ensures that the priority relationships between jobs are complied with when assigning to stations. Eq. (6) assigns a job to only one position at the station. Eq. (8) computes, under the truncated position-based learning effect, the processing times of work assigned to positions other than the first order. Eq. (9) determines how long the task assigned to the first position at the station will take to process. Eq. (10) calculates the work completion times of the stations. Eq. (11) provides the relationship between the processing times of jobs assigned to any station j . Eq. (12) and (13) provide the relationship between the processing completion times of jobs assigned to successive positions at any station. Eq. (14) ensures that only one job can be assigned to each position at any station. Eq. (15) completes the binary variables.

Lingo.11 optimization program was used to solve the 8-tasks DLB problem. For the basic case of the problem, that is, when the truncated position-based learning effect is not considered, the number of stations found is 4 in the

literature. Using the Lingo.11 optimization program, we found that the basic version of the problem had a value of 4. According to the results obtained; Task5 and Task1 were assigned to station 1, Task 2-4-3 were assigned to station 2, respectively; Tasks 7-6 were assigned to station 3, and finally task 8 was assigned to station 4. The job completion times of the stations are calculated as 39-40-36 and 36, respectively, and the job completion times of the stations are shorter than the cycle time.

DLB problems were solved under the truncated position based learning effect in this study. Truncated position-based learning has two parameters: learning index and control parameter. The learning index in this study was computed using three different learning rates: 0.9, 0.8 and 0.7. In addition, 0.8 and 0.7 were accepted as control parameters. The results obtained with Lingo.11 using the mentioned parameters for the 8-tasks DLB problem under the effect of truncated position based learning are as seen in Table 3. For this dataset, the objective function value was found to be the same for all combinations of learning rate and control parameter.

Table 3. Results for 8-parts DLB problem under the truncated position based learning effect

| learning rate & control parameter | lr=0.9 & p=0.8 | lr=0.9 & p=0.7 | lr=0.8 & p=0.8 | lr=0.8 & p=0.7 | lr=0.7 & p=0.8 | lr=0.7 & p=0.7 |
|---|----------------------|-------------------|-------------------|-------------------|-------------------|----------------------|
| workstation number | 4 | 4 | 4 | 4 | 4 | 3 |

*lr=learning rate

The optimum workstation assignment found for the case where the learning rate is 0.70 and the control parameter value is 0.70 is shown in Table 4. While the learning rate is 0.70, the learning index is calculated as $\log_2 0.70$. Tasks 3-7 and 4 were assigned to the 1st station respectively, tasks 1 and 8 were assigned to the 2nd station respectively, finally tasks 2,6 and 5 were assigned to the 3rd station respectively. The processing completion times for each station are 38.6056, 39.21 and 37.3 respectively (see Table 4).

Table 4. Calculating the processing times of tasks when the learning rate is 0.7 and the control parameter is 0.7

| Task assignment (task,station,position) | Calculation of task processing time | Completion time of tasks |
|--|-------------------------------------|-----------------------------|
| (3,1,1) | 12 | 12 |

| | | |
|---------|--|----------------------------|
| (7,1,2) | $20 * \max(2^{(-0.514)}, 0.7) = 14.0056$ | $12 + 14.0056 = 26.0056$ |
| (4,1,3) | $18 * \max(3^{(-0.514)}, 0.7) = 12.6$ | $26.0056 + 12.6 = 38.6056$ |
| (1,2,1) | 14 | 14 |
| (8,2,2) | $36 * \max(2^{(-0.514)}, 0.7) = 25.21$ | $14 + 25.21 = 39.21$ |
| (2,3,1) | 10 | 10 |
| (6,3,2) | $16 * \max(2^{(-0.514)}, 0.7) = 11.2$ | $23 + 11.2 = 21.2$ |
| (5,3,3) | $23 * \max(3^{(-0.514)}, 0.7) = 16.1$ | $21.2 + 16.1 = 37.3$ |

2.1. Moth-Flame Optimizer (MFO)

MFO is a method introduced into the literature by Mirjalili (2015), inspired by the flying and navigation movements of moths. Moths are candidate solutions in the MFO algorithm. The moths' locations inside the space are the variables in the problems. In MFO, which is a position-based algorithm, the set that gives the position of the moths can be represented as:

$$M = \begin{bmatrix} m_{1,1} & m_{1,2} & m_{1,3} & \dots & m_{1,d} \\ m_{2,1} & m_{2,2} & m_{2,3} & \dots & m_{2,d} \\ \vdots & \vdots & \vdots & \vdots & \vdots \\ m_{n,1} & m_{n,2} & m_{n,3} & \dots & m_{n,d} \end{bmatrix} \tag{16}$$

where, n is the population size and d is the size of the problem. The fitness function of each solution candidate is calculated. The matrix that holds the fitness function values of each element of the matrix M , which is a set of randomly generated candidate solutions, can be defined as follows:

$$OM = \begin{bmatrix} OM_1 \\ OM_2 \\ \vdots \\ OM_n \end{bmatrix} \tag{17}$$

where, OM_1 represents the fitness function value of the first solution candidate.

Flames are another significant set in the MFO algorithm. It is similar to the M matrix that forms moths.

$$F = \begin{bmatrix} F_{1,1} & F_{1,2} & F_{1,3} & \dots & F_{1,d} \\ F_{2,1} & F_{2,2} & F_{2,3} & \dots & F_{2,d} \\ \vdots & \vdots & \vdots & \vdots & \vdots \\ F_{n,1} & F_{n,2} & F_{n,3} & \dots & F_{n,d} \end{bmatrix} \tag{18}$$

Where, d is the size of the problem and n is the size of the population. M and F matrices are equal in size (see in Eq 16 and 18). The matrix that holds the fitness values of the flames is as follows:

$$OF = \begin{bmatrix} OF_1 \\ OF_2 \\ \vdots \\ OF_n \end{bmatrix} \quad (19)$$

Flames and moths are the problem's solutions. But the difference between them is that moths are actual search agents in the search space. Flames are the moth's position that has produced the best results so far. The flames array is updated when there is a moth that achieves better results in the search space. Because of this, the moth never loses its optimal location or solution.

MFO algorithm is an algorithm containing 3 elements (I, P, T) that aims to approach optimum in optimization problems. The random initial population and fitness values, which include the moths' positions in the search space, are represented by Element I, Element P allows moths to move in the search space and update their positions. Element T represents the stopping constraint of the algorithm, it stops the search when the maximum iteration is reached.

$$MFO = (I, P, T) \quad (20)$$

The spiral flight path of moths is found with Eq. 20. Each moth's position is updated by a flame that represents the moth's best position so far. The location update of each moth is done as follows:

$$S(M_i, F_j) = D_i \times e^{bt} \times \cos(2\pi t) + F_j \quad (21)$$

Where, $M_i = (m_{i1}, m_{i2}, \dots, m_{iD})$ and, $F_j = (F_{j1}, F_{j2}, \dots, F_{jD})$, D_i calculated in Eq. 22, gives the distance between moth i and flame j representing this moth. t is a random number generated in the range $[-1, 1]$. b is a constant number that determines the shape of the logarithmic spiral. D_i is determined in this way:

$$D_i = |F_j - M_i| \quad (22)$$

$$t = (\varphi - 1) \times rand[0,1] + 1 \quad (23)$$

$$\varphi = -1 + k \left(-\frac{1}{K} \right) \quad (24)$$

According to the coefficient φ , the moth path is obtained in a spiral shape towards the flame. In Eq 24, while the k value represents the current iteration, the K value represents the maximum number of iterations.

The procedure of the MFO algorithm is as seen in Fig. 2

```

Initialize MFO parameters
    d=problem dimension
    n=number of moth
    itermax=maximum iteration
Generate initial moth position,  $M_i$  ( $i = 1,2, \dots, n$ )
while  $iter < itermax$ 
     $iter = iter + 1$ 
    Evaluate fitness,  $OM_i = f(M_i)$ 
    Update flame position,  $F_j$  ( $j = 1,2, \dots, n$ )
    if  $iter = 1$ 
         $F_j = sort M_i$ 
         $OF_j = sort OM_i$ 
    else
        if sort  $(OM_i) < (OF_j)$ 
             $OF_j = sort (OM_i)$ 
             $F_j = sort M_i$ 
        Endif
    Endif
    Update moth position,  $M_i$  using Eq. (20)
End

```

Figure 2. MFO algorithm procedure

In the application of the MFO algorithm, the problem parameters are first determined. Then, according to the parameters, an initial population was created containing the positions of the moths that were solution candidates. The OM fitness array was created by calculating the fitness function values of the initial population. The flame set and the set of fitness function values of the

flames were created. Then, the distances between the moths and the flames were calculated using Eq 22, and the positions of the moths were updated using Eq 21. Fitness function values are obtained for the new moth array. If the result obtained is better than the fitness value of the flame representing this moth, the position vector and fitness function vector of the flame are updated. The moths' positions are updated and the process carries on until the maximum number of iterations is achieved. Upon reaching the maximum number of iterations, the program stops and the optimum or closest to optimum result is obtained.

3. Computational Results

In this study, the change in the number of stations opened in DLB problems under the effect of truncated position-based learning was examined. The processing times of jobs are taken to be constant during the process in classical DLB problems. However, processing times of tasks can be affected positively or negatively for different reasons. DLB problems that under the truncated position-based learning effect, jobs are learned by workers over time and can be done in a shorter time. In this learning model, it is argued that learning cannot be endless and, like other human behaviors, learning can stop at a certain level (Wu et al., 2013). In this study, results were obtained with different combinations of three different learning rates and two different control parameters, and comparisons were made. Changes in the number of stations opened were examined in percentage terms.

3.1. Truncated position-based learning effect on Cellular Phone Disassembly Example

At this stage, the cellular phone disassembly example, which is most frequently used in the DLB literature, was examined under the effect of truncated position-based learning. Task definitions and precedence relationships of the sample problem consisting of 25 tasks are shown in Table 5. The cycle time is 18. For the most basic version of the problem, the objective function value is 9 (Duta, Caciula, & Patric, 2016; Edis, 2021; Kalayci et al., 2016). In this study, with the MFO algorithm, the number of stations opened for the situation where the truncated position-based learning effect was not considered was found to be 9 as a result of 200 iterations, while the population size was 50.

Current DLB problem under the effect of learning, improvements are seen in the objective function values. It was deemed necessary to open 9 stations when the learning rate was 0.9 and the control parameters were 0.8 and 0.7. When

the learning rate was 0.8, it was found necessary to open 8 stations with both control parameter values. However, when the learning rate is 0.7, 8 stations must be opened when the control parameter is 0.8, while 7 stations must be opened when the control parameter is 0.7. Therefore, while the learning rate was 0.7, an increase in the objective function value was observed as the control parameter value increased. While the control parameter is constant, the objective function value improves as the learning rate decreases.

Tablo 5. Task definitions, processing times, and precedence relationships for the 25-parts cellular telephone DLB problem.

| Görev | Parça ismi | İşlem süresi | Öncelik ilişkisi |
|-------|----------------|--------------|------------------|
| 1 | Antenna | 3 | |
| 2 | Battery | 2 | |
| 3 | Antenna guide | 3 | 1,2 |
| 4 | Bolt(Type 1) A | 10 | |
| 5 | Bolt(Type 1) B | 10 | |
| 6 | Bolt(Type 2) 1 | 15 | 2 |
| 7 | Bolt(Type 2) 2 | 15 | 2 |
| 8 | Bolt(Type 2) 3 | 15 | 2 |
| 9 | Bolt(Type 2) 4 | 15 | 3 |
| 10 | Clip | 2 | 4,5 |
| 11 | Rubber seal | 2 | 10 |
| 12 | Speaker | 2 | 11 |
| 13 | White cable | 2 | 6,7,8,9 |
| 14 | Red/blue cable | 2 | 6,7,8,9 |
| 15 | Orange cable | 2 | 6,7,8,9 |
| 16 | Metal top | 2 | 6,7,8,9 |
| 17 | Front cover | 2 | 13,14 |
| 18 | Back cover | 3 | 15 |
| 19 | Curciut board | 18 | 13,14,16,18 |
| 20 | Plastic screen | 5 | 17 |
| 21 | Keyboard | 1 | 17 |
| 22 | LCD | 5 | 21 |
| 23 | Sub-keyboard | 15 | 16,21 |

| | | | |
|----|-------------------|---|-------|
| 24 | Internal IC Board | 2 | 19,23 |
| 25 | Microphone | 2 | 21 |

In the truncated position-based learning model, the control parameter puts a limit on the learning of the task. In a situation where the control parameter is not taken into account, it is assumed that the job is learned continuously. Thus, the processing times of jobs assigned to subsequent positions in the station are rapidly approaching zero. Therefore, in truncated position-based learning, the learning rates of jobs are limited and the processing times of jobs assigned to the next positions from a certain position are considered equally affected by the learning effect.

For example, when the learning rate is 0.9 and the control parameter is 0.8, 7 different jobs are assigned to the 6th station. 5 different jobs (15-24-14-11-13) with equal processing times of 2 were assigned consecutively. While the processing time of job 15, assigned to the 3rd row, decreased from 2 to 1.69 with the effect of learning, the processing time of job 24, assigned to the 4th row, decreased to 1.62. The processing time of job 14, which was assigned to the 5th row, decreased to 1.6. In this station, while the processing times of all jobs up to the 5th row decreased continuously, the processing times of the jobs assigned to the 6th and 7th rows did not decrease further and remained at 1.6 after the control parameter introduced the limitation(see in table 6).

With the truncated position-based learning effect, a decrease was observed in the processing times of the jobs assigned to the stations in the 25-part DLB problem. Thanks to the decrease in the processing times of the jobs, there has been an increase in the number of jobs assigned to the stations. Work intensity has increased at stations.

Table 6. Number of stations opened with different learning rates for the 25-tasks DLB problem under the effect of truncated position-based learning

| Learning rate | İstasyona İşlerin Atanma Sırası | İşlem Süreleri | İş Tamamlama Süresi | Açılan İstasyon Sayısı |
|----------------------------------|---------------------------------|--------------------------------|---------------------|------------------------|
| Learning rate=0 & $\rho=0$ | | | | |
| | 20-13-11-3-18-14 | 5-2-2-3-3-2 | 17 | |
| | 6-10 | 15-2 | 17 | |
| | 17-9 | 2-15 | 17 | |
| | 4-12-16-1-21 | 10-2-2-3-1 | 18 | |
| | 24-23 | 2-15 | 17 | 9 |
| | 19 | 18 | 18 | |
| | 5-22-15 | 10-5-2 | 17 | |
| | 25-7 | 2-15 | 17 | |
| | 8-2 | 15-2 | 18 | |
| Learning rate: 0.90 & $\rho=0.8$ | | | | |
| | 16-18-2-4-25-12 | 2-2,7-1,6-8,1-1,6-1,6 | | 17,7 |
| | 1-9 | 3-4,5 | 7,5 | |
| | 17-21-3-23 | 2-0,9-2,53-12,15 | 17,58 | |
| | 7 | 15 | 15 | |
| | 8 | 15 | 15 | |
| | 22-20-15-24-14-11-13 | 5-4,5-1,69-1,62-1,6-1,6-1,6 | 17,61 | 9 |
| | 5 | 10 | 10 | |
| | 19 | 18 | 18 | |
| | 6-10 | 15-1,8 | 16,8 | |
| Learning rate=0.90 & $\rho=0.7$ | | | | |
| | 8 | 15 | 15 | |
| | 7-1 | 15- 2,7 | 17,7 | |
| | 14-23-2 | 2- 13,5- 1,69 | 17,19 | |
| | 17-6 | 2- 13,5 | 15,5 | |
| | 19 | 18 | 18 | 9 |
| | 5-10 | 10- 1,8 | 11,8 | |
| | 9-13-21 | 15- 1,8- 0,85 | 17,65 | |
| | 4-18-25-24-11 | 10- 2,7- 1,69- 1,62- 1,56 | 17,57 | |
| | 12-22-3-16-20-15 | 2- 4,5- 2,54- 1,62- 3,91- 1,52 | 16,09 | |
| Learning rate=0.80 & $\rho=0.8$ | | | | |
| | 12-9-18-16 | 2-12-2,4-1,6 | 18 | |
| | 7-3 | 15-2,4 | 17,4 | |
| | 22-8 | 5-12 | 17 | |
| | 14-19 | 2-14,4 | 16,4 | 8 |
| | 20-25-5-11 | 5-1,6-8-1,6 | 16,2 | |
| | 10-1-24-6 | 2-2,4-1,6-12 | 18 | |
| | 21-13-23-2-15 | 1-1,6-12-1,6-1,6 | 17,8 | |
| | 4-17 | 10-1,6 | 11,6 | |
| Learning rate=0.80 & $\rho=0.7$ | | | | |
| | 15-23 | 2-11,99 | 13,99 | |
| | 21.08.2024 | 1-12-1,4 | 14,4 | |
| | 19 | 18 | 18 | |
| | 25-6-14-11 | 2-12-1,4-1,4 | 16,8 | |
| | 9 | 15 | 15 | 8 |
| | 4-5 | 10-7,99 | 17,99 | |
| | 18-13-22-20-2-3-10 | 3-1,6-3,5-3,5-1,4-2,1-1,4 | 16,5 | |
| | 17-1-12-7-16 | 2-2,4-1,4-10,5-1,4 | 17,7 | |
| Learning rate=0.70 & $\rho=0.8$ | | | | |
| | 24-12-9-14 | 2-1,6-12-1,6 | 17,2 | |
| | 6-1 | 15-2,4 | 17,4 | |
| | 13-17-25-11-4-3 | 2-1,6-1,6-1,6-8-2,4 | 17,2 | |
| | 10-7-20 | 2-12,4 | 18 | |
| | 21-2-23 | 1-1,6-12 | 14,6 | 8 |
| | 22-8 | 5-12 | 17 | |
| | 19 | 18 | 18 | |
| | 15-18-16-5 | 2-2,4-1,6-8 | 14 | |
| Learning rate=0.70 & $\rho=0.7$ | | | | |
| | 21-16-19-11 | 1-1,4-12,6-1,4 | 16,4 | |
| | 22-17-23 | 5-1,4-10,5 | 16,9 | |
| | 2-7-20-13 | 2-10,5-3,5-1,4 | 17,4 | |
| | 25-18-1-6 | 2-2,1-2,1-10,5 | 16,7 | 7 |
| | 12-09-15 | 2-10,5-1,4 | 13,9 | |
| | 3-24-8-14-10 | 3-1,4-10,5-1,4-1,4 | 17,7 | |
| | 4-5 | 10-7 | 17 | |

When the learning rate was 0.9, the average work intensity of the stations was 2.72, and when both the learning rate and control parameter values were 0.7, the average work intensity of the stations was 3.57. While there was a 22%

decrease in the number of stations opened, the average workload at the stations increased by 28.8% (Table 6).

3.2. Comparison of the Results of Different Sizes DLB Problems Under the Truncated Position-Based Learning Effect

The number of stations opened under the effect of truncated position-based learning was calculated for different sizes DLB problems in the literature (Scholl, 1995). Objective function values in the literature were obtained for the basic version of the problems. While the algorithm could achieve the optimum result in 200 iterations for small-sized problems, it might need to run 5000 iterations or more for large-sized problems. Learning rates are considered as 0.9, 0.8, 0.7 and control parameter values are 0.8 and 0.7. The results calculated for different sizes DLB problems under the effect of truncated position-based learning are shown in Table 7.

Table 7. Number of stations opened for DLB problems under the truncated position-based learning effect

| Yazar | n | Ct | *Optimum Sonuç | MFO | | | | | | |
|------------------|-----|------|-------------------|----------------|-----------------------|-----------------------|-----------------------|--------------------------|--------------------------|-----------------------|
| | | | | lr=0 ρ =0 | lr=0.9 ρ =0.8 | lr=0.9 ρ =0.7 | lr=0.8 ρ =0.8 | lr=0.8 ρ =0.7 | lr=0.7 ρ =0.8 | lr=0.7 ρ =0.7 |
| Gungor and Gupta | 8 | 40 | 4 | 4 | 4 | 4 | 4 | 4 | 4 | 3 |
| Gupta et al. | 25 | 18 | 9 | 9 | 9 | 9 | 8 | 8 | 8 | 7 |
| Heskiaoff | 28 | 138 | 8 | 8 | 7 | 7 | 7 | 6 | 7 | 6 |
| Lutz-1 | 32 | 1414 | 11 | 11 | 10 | 10 | 9 | 9 | 9 | 8 |
| Kilbrid | 45 | 56 | 10 | 10 | 9 | 9 | 9 | 8 | 9 | 8 |
| Hahn | 53 | 2806 | 6 | 6 | 5 | 5 | 5 | 4 | 5 | 4 |
| Tonge | 70 | 364 | 10 | 10 | 9 | 8 | 9 | 8 | 9 | 8 |
| Wee-Mag | 75 | 49 | 32 | 32 | 31 | 32 | 30 | 30 | 30 | 30 |
| Arcus-1 | 83 | 5048 | 16 | 16 | 14 | 13 | 13 | 12 | 13 | 12 |
| Lutz-3 | 89 | 79 | 22 | 22 | 20 | 20 | 19 | 17 | 19 | 17 |
| Mukherjee | 94 | 222 | 20 | 20 | 18 | 18 | 17 | 16 | 17 | 15 |
| Arcus-2 | 111 | 5785 | 27 | 28 | 26 | 25 | 25 | 23 | 25 | 23 |

*lr=learning rate, ρ =control parameter

Thanks to learning, a decrease was observed in the number of stations opened in all DLB problems. The change in objective function values varies depending on the learning rate and control parameter. When the learning rate was 0.9

and the control parameter was 0.8, the number of stations opened in four different DLB problems did not change (Güngör and Gupta, Kilbrid, Hahn and Tonge). When the control parameter decreases to 0.7, the number of data sets whose number of stations does not change decreases to two (See in Table 7). The control parameter is the most important part of the truncated position-based learning model, which assumes that learning is limited. It applies the thesis that learning can occur up to a certain level and then remains static.

In all cases where the control parameter was 0.8 and the learning rate was 0.8 and 0.7, the objective function values were found to be the same for all DLB problems. Especially in large-sized DLB problems, the value of the learning rate remained insignificant because the control parameter limited the learning effect after a certain order. However, when the learning rate is 0.9, the number of stations opened is higher than other learning rates. This shows that when the learning rate is 0.9, learning tasks progresses much slower.

When the control parameter is 0.7 and the learning rates are 0.8 and 0.7, the number of DLB problems with an equal number of opened stations is 8. In 33% of the DLB problems studied, as the learning rate decreased, the number of stations opened also decreased. A learning rate of 0.7 means that the work done in 1 unit of time can be done in 0.7 units of time.

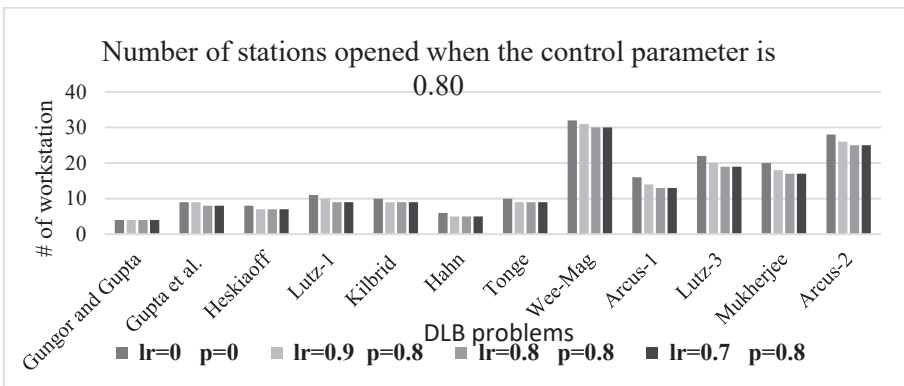


Figure 3. Number of stations opened for when the control parameter is 0.8

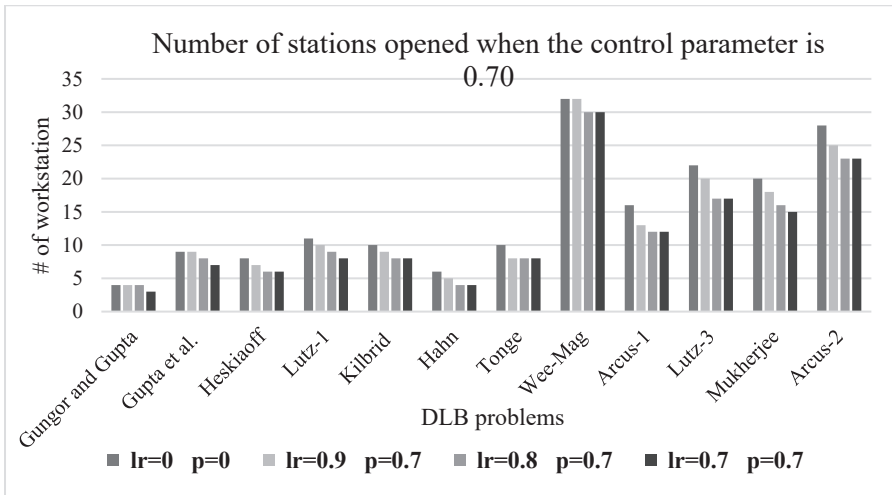


Figure 4. Number of stations opened for when the control parameter is 0.70

4. Results

In this study, the effect of truncated position-based learning on the number of opened stations, which is the objective function, in DLB problems was studied. Workers learn as they repeat the work they do and do the learned work in a shorter time. In line with our research, in DLB problems, the processing times of jobs are considered constant throughout the process. However, thanks to learning, the processing times of jobs can be shortened. Truncated position-based learning model includes two parameters: learning rate and control parameter. The control parameter provides limitation of learning. Because, like people's other behaviors, their learning should also be limited. In this study, various problems in the DLB literature are solved under the effect of truncated position-based learning. The change in the value of the number of stations opened, which is the objective function, was examined. The objective function values found with the learning model created using different combinations of three different learning rates and two different control parameters were compared. In DLB problems, as the control parameter value and learning rate value decreased, the number of opened stations decreased. Learning, which is an important part of real life, should be taken into account with the truncated position-based learning effect in solving DLB problems.

References

- Altekin, F. T. (2017). A comparison of piecewise linear programming formulations for stochastic disassembly line balancing. *International Journal of Production Research*, 55(24), 7412–7434. <https://doi.org/10.1080/00207543.2017.1351639>
- Bentaha, M. L., Battaïa, O., Dolgui, A., & Hu, S. J. (2015). Second order conic approximation for disassembly line design with joint probabilistic constraints. *European Journal of Operational Research*, 247(3), 957–967. <https://doi.org/10.1016/j.ejor.2015.06.019>
- Bentaha, M. L., Dolgui, A., Battaïa, O., Riggs, R. J., & Hu, J. (2018). Profit-oriented partial disassembly line design: dealing with hazardous parts and task processing times uncertainty. *International Journal of Production Research*, 56(24), 7220–7242. <https://doi.org/10.1080/00207543.2017.1418987>
- Biskup, D. (1999). Single-machine scheduling with learning considerations. *European Journal of Operational Research*, 115(1), 173–178. [https://doi.org/10.1016/S0377-2217\(98\)00246-X](https://doi.org/10.1016/S0377-2217(98)00246-X)
- Duta, L., Caciula, I., & Patic, P. C. (2016). Column generation approach for disassembly line balancing. *IFAC-PapersOnLine*, 49(12), 916–920. <https://doi.org/10.1016/j.ifacol.2016.07.892>
- Edis, E. B. (2021). Constraint programming approaches to disassembly line balancing problem with sequencing decisions. *Computers and Operations Research*, 126, 105111. <https://doi.org/10.1016/j.cor.2020.105111>
- Edis, E. B., Ilgin, M. A., & Edis, R. S. (2019). Disassembly line balancing with sequencing decisions: A mixed integer linear programming model and extensions. *Journal of Cleaner Production*, 238, 117826. <https://doi.org/10.1016/j.jclepro.2019.117826>
- Güngör, Askiner, & Gupta, S. M. (2001). A solution approach to the disassembly line balancing problem in the presence of task failures. *International Journal of Production Research*, 39(7), 1427–1467. <https://doi.org/10.1080/00207540110052157>
- Güngör, Aşkiner, & Gupta, S. (1999). *Disassembly Line Balancing*. <https://doi.org/10.1201/9781420018790.ch6>
- Güngör, Aşkiner, & Gupta, S. M. (2002). Disassembly line in product recovery. *International Journal of Production Research*, 40(11), 2569–2589. <https://doi.org/10.1080/00207540210135622>
- Guo, X., Wei, T., Wang, J., Liu, S., Qin, S., & Qi, L. (2022). Multiobjective U-Shaped Disassembly Line Balancing Problem Considering Human Fatigue Index and

- an Efficient Solution. *IEEE Transactions on Computational Social Systems*.
<https://doi.org/10.1109/TCSS.2022.3217101>
- Kalayci, C. B., Polat, O., & Gupta, S. M. (2016). A hybrid genetic algorithm for sequence-dependent disassembly line balancing problem. *Annals of Operations Research*, 242(2), 321–354. <https://doi.org/10.1007/s10479-014-1641-3>
- Kalaycilar, E. G., Azizoğlu, M., & Yeralan, S. (2016). A disassembly line balancing problem with fixed number of workstations. *European Journal of Operational Research*, 249(2), 592–604. <https://doi.org/10.1016/j.ejor.2015.09.004>
- Kucukkoc, I., Li, Z., & Li, Y. (2020). Type-E disassembly line balancing problem with multi-manned workstations. *Optimization and Engineering*, 21(2), 611–630. <https://doi.org/10.1007/s11081-019-09465-y>
- Li, Z., & Janardhanan, M. N. (2021). Modelling and solving profit-oriented U-shaped partial disassembly line balancing problem. *Expert Systems with Applications*, 183(October 2019), 115431. <https://doi.org/10.1016/j.eswa.2021.115431>
- Li, Z., Kucukkoc, I., Tang, Q., & Zhang, Z. (2023). Models and two-phase bee algorithms for multi-objective U-shaped disassembly line balancing problem. In *Optimization and Engineering* (Vol. 24). <https://doi.org/10.1007/s11081-021-09696-y>
- Liang, W., Zhang, Z., Yin, T., Zhang, Y., & Wu, T. (2023). Modelling and optimisation of energy consumption and profit-oriented multi-parallel partial disassembly line balancing problem. *International Journal of Production Economics*, 262(May), 108928. <https://doi.org/10.1016/j.ijpe.2023.108928>
- Liu, J., & Wang, S. (2017). Balancing disassembly line in product recovery to promote the coordinated development of economy and environment. *Sustainability (Switzerland)*, 9(2). <https://doi.org/10.3390/su9020309>
- McGovern, S. M., & Gupta, S. M. (2007). Combinatorial Optimization Analysis Of The Unary NP-Complete Disassembly Line Balancing Problem. *International Journal of Production Research*, 45(18–19), 4485–4511. <https://doi.org/10.1080/00207540701476281>
- McGovern, S. M., & Gupta, S. M. (2007). A balancing method and genetic algorithm for disassembly line balancing. *European Journal of Operational Research*, 179(3), 692–708. <https://doi.org/10.1016/j.ejor.2005.03.055>
- Mirjalili, S. (2015). Moth-flame optimization algorithm: A novel nature-inspired heuristic paradigm. *Knowledge-Based Systems*, 89, 228–249. <https://doi.org/10.1016/j.knsys.2015.07.006>
- Qin, S., Li, J., Wang, J., Guo, X., Liu, S., & Qi, L. (2023). A Salp Swarm Algorithm for

- Parallel Disassembly Line Balancing Considering Workers With Government Benefits. *IEEE Transactions on Computational Social Systems*, *PP*, 1–10. <https://doi.org/10.1109/TCSS.2023.3238965>
- Ren, Y., Meng, L., Zhang, C., Zhao, F., Saif, U., Huang, A., ... Sutherland, J. W. (2020). An Efficient Metaheuristics For A Sequence-Dependent Disassembly Planning. *Journal of Cleaner Production*, *245*, 118644. <https://doi.org/10.1016/j.jclepro.2019.118644>
- Ren, Y., Yu, D., Zhang, C., Tian, G., Meng, L., & Zhou, X. (2017). An improved gravitational search algorithm for profit-oriented partial disassembly line balancing problem. *International Journal of Production Research*, *55*(24), 7302–7316. <https://doi.org/10.1080/00207543.2017.1341066>
- Ren, Y., Zhang, C., Zhao, F., Tian, G., Lin, W., Meng, L., & Li, H. (2018). Disassembly line balancing problem using interdependent weights-based multi-criteria decision making and 2-Optimal algorithm. *Journal of Cleaner Production*, *174*, 1475–1486. <https://doi.org/10.1016/j.jclepro.2017.10.308>
- Saif, U., Guan, Z., Liu, W., Zhang, C., & Wang, B. (2014). Pareto based artificial bee colony algorithm for multi objective single model assembly line balancing with uncertain task times. *Computers and Industrial Engineering*, *76*(1), 1–15. <https://doi.org/10.1016/j.cie.2014.07.009>
- Scholl, A. (1995). Data of assembly line balancing problems. *Schriften Zur Quantitativen Betriebswirtschaftslehre*, Vol. 93, pp. 1–28.
- Wang, K., Gao, L., & Li, X. (2020). A multi-objective algorithm for U-shaped disassembly line balancing with partial destructive mode. *Neural Computing and Applications*, *32*(16), 12715–12736. <https://doi.org/10.1007/s00521-020-04721-0>
- Wang, K., Li, X., & Gao, L. (2019a). A Multi-Objective Discrete Flower Pollination Algorithm For Stochastic Two-Sided Partial Disassembly Line Balancing Problem. *Computers and Industrial Engineering*, *130*(March), 634–649. <https://doi.org/10.1016/j.cie.2019.03.017>
- Wang, K., Li, X., & Gao, L. (2019b). Modeling and optimization of multi-objective partial disassembly line balancing problem considering hazard and profit. *Journal of Cleaner Production*, *211*, 115–133. <https://doi.org/10.1016/j.jclepro.2018.11.114>
- Wang, K., Li, X., Gao, L., Li, P., & Sutherland, J. W. (2022). A Discrete Artificial Bee Colony Algorithm for Multiobjective Disassembly Line Balancing of End-of-Life Products. *IEEE Transactions on Cybernetics*, *52*(8), 7415–7426. <https://doi.org/10.1109/TCYB.2020.3042896>

- Wang, X. Y., Zhou, Z., Zhang, X., Ji, P., & Wang, J. B. (2013). Several flow shop scheduling problems with truncated position-based learning effect. *Computers and Operations Research*, 40(12), 2906–2929. <https://doi.org/10.1016/j.cor.2013.07.001>
- Wu, C. C., Yin, Y., & Cheng, S. R. (2013). Single-Machine And Two-Machine Flowshop Scheduling Problems With Truncated Position-Based Learning Functions. *Journal of the Operational Research Society*, 64(1), 147–156. <https://doi.org/10.1057/jors.2012.46>
- Xiao, S., Wang, Y., Yu, H., & Nie, S. (2017). An entropy-based adaptive hybrid particle swarm optimization for disassembly line balancing problems. *Entropy*, 19(11). <https://doi.org/10.3390/e19110596>
- Yin, T., Zhang, Z., & Jiang, J. (2021). A Pareto-discrete hummingbird algorithm for partial sequence-dependent disassembly line balancing problem considering tool requirements. *Journal of Manufacturing Systems*, 60(August 2020), 406–428. <https://doi.org/10.1016/j.jmsy.2021.07.005>
- Yin, T., Zhang, Z., Wu, T., Zeng, Y., Zhang, Y., & Liu, J. (2023). Multimanned partial disassembly line balancing optimization considering end-of-life states of products and skill differences of workers. *Journal of Manufacturing Systems*, 66(July 2022), 107–126. <https://doi.org/10.1016/j.jmsy.2022.12.002>
- Yin, T., Zhang, Z., Zhang, Y., Wu, T., & Liang, W. (2022a). Mixed-integer programming model and hybrid driving algorithm for multi-product partial disassembly line balancing problem with multi-robot workstations. *Robotics and Computer-Integrated Manufacturing*, 73(August 2021), 102251. <https://doi.org/10.1016/j.rcim.2021.102251>
- Yin, T., Zhang, Z., Zhang, Y., Wu, T., & Liang, W. (2022b). Mixed-integer programming model and hybrid driving algorithm for multi-product partial disassembly line balancing problem with multi-robot workstations. *Robotics and Computer-Integrated Manufacturing*, 73(April 2021), 102251. <https://doi.org/10.1016/j.rcim.2021.102251>
- Zhang, Y., Zhang, Z., Guan, C., & Xu, P. (2022). Improved whale optimisation algorithm for two-sided disassembly line balancing problems considering part characteristic indexes. *International Journal of Production Research*, 60(8), 2553–2571. <https://doi.org/10.1080/00207543.2021.1897178>
- Zhang, Z., Wang, K., Zhu, L., & Wang, Y. (2017). A Pareto improved artificial fish swarm algorithm for solving a multi-objective fuzzy disassembly line balancing problem. *Expert Systems with Applications*, 86, 1339–1351. <https://doi.org/10.1016/j.eswa.2017.05.053>

- Zhou, B., & Bian, J. (2022). Multi-mechanism-based modified bi-objective Harris Hawks optimization for sustainable robotic disassembly line balancing problems. *Engineering Applications of Artificial Intelligence*, 116(September), 105479. <https://doi.org/10.1016/j.engappai.2022.105479>
- Zhu, L., Zhang, Z., & Guan, C. (2020). Multi-objective partial parallel disassembly line balancing problem using hybrid group neighbourhood search algorithm. *Journal of Manufacturing Systems*, 56(May), 252–269. <https://doi.org/10.1016/j.jmsy.2020.06.013>
- Zhu, L., Zhang, Z., & Wang, Y. (2018). A Pareto firefly algorithm for multi-objective disassembly line balancing problems with hazard evaluation. *International Journal of Production Research*, 56(24), 7354–7374. <https://doi.org/10.1080/00207543.2018.1471238>



Chapter 17

INVESTIGATION OF CFD ANALYSIS OF RECTANGULAR SHAPE OF TALL BUILDINGS AT DIFFERENT ASPECT RATIOS FOR SAME CROSS-SECTIONAL AREA

Ahmet ŞUMNU¹

¹ Assist. Prof. Dr., Ahmet ŞUMNU, Iskenderun Technical University, Faculty of Aeronautics and Astronautics, Aerospace Engineering Department, ahmet.sumnu@iste.edu.tr, ORCID: 0000-0003-1514-6048.

INTRODUCTION

The tall buildings can be exposed to high wind loads that produced noise, vibration and structural stress on buildings. Therefore, the wind load analysis on buildings has been performed and its effects have been taken into account when designing the especially tall buildings. For this, the engineers and architects have been proposed different designs and solution to improve the aerodynamics of buildings and reduce negative effects. The various aerodynamic shape optimization methods can also applied to increase resistance of the structure of building against to wind and minimize the cost. Enhancing the effectiveness and obtaining reasonable results, it is important to perform aerodynamic and optimization solutions in early stage of design (Xie, 2014). The some studies related with aerodynamic analysis of tall buildings are mentioned in the followings.

The study of tall buildings of aerodynamics is performed for the development of different building form since the wind speed and loads increase as the building height (Paltun et al., 2015). The some techniques were proposed to reduce wind loads on buildings. One of them is aerodynamic mitigation techniques that are used to modify the aerodynamic shape of buildings. Another method is aerodynamic shape optimization that is performed to reduce aerodynamic loads, noise and vibration (Mooneghi and Kargarmoakhar, 2016). In order to decide aerodynamic load, both CFD and experimental methods are used and the results are visualized to examine flow physics on designed building. Gnatowska (2019) performed CFD analysis for finding pressure distributions on tall buildings and investigated the flow physics among two buildings at various angle of attacks. Toja-Silva et al. (2015) also proposed CFD study for tall buildings and investigated to find the turbulence model that gives reasonable result since the solutions may show differences according to selected turbulence model. For finding the accurate results especially at wake region that occurs behind the buildings, the stochastic and Monte Carlo technique was used to improve the CFD simulation since the used CFD tools doesn't efficient for Atmospheric boundary layer flow model (Shirzadi et al., 2017).

The aerodynamic analysis was presented to investigate building roof shape in terms of wind energy and optimization was applied to find optimal shape of building by Toja-Silva et al. (2016). The optimization study for the wind

energy was performed using CFD simulation. Energy generation from the wind by opening the hole on buildings was carried out and shape optimization was performed using its design parameters (Ruiz et al., 2021). The CFD solutions were presented for a building with and without balconies using different turbulence model and the results were compared with experimental data (Montazeri and Blocken, 2013). The turbulence model optimization was carried out for bluff body solution by Duarte et al. (2020). Aerodynamic modifications were performed to reduce wind effect load for different shape of buildings (Neethi and Joby, 2018). The another study related with multi-objective aerodynamic shape optimization for the three opening tall buildings was implemented to show effect of wind load using LES (Large Eddy Simulation) method by Elshaer et al. (2018). Daemei and Eghbali (2019) proposed study to reduce length of the wake region for tall buildings by modifying corner of different geometries that are square and triangular shapes. Bernardini et al. (2015) studied on aerodynamic shape optimization of tall buildings and bridges using kriging model and CFD method for determining aerodynamic parameters and enhancing performance. The optimization study was performed for rectangular shape building using CFD method by Paul and Dalui (2021). In this study, design parameters were selected limbs position and wind incidence angle. Optimization proses were done by selecting randomly design of parameters using Multi-Objective Genetic Algorithms.

Huang et al. (2007) presented to observe effect of wind load on tall buildings using CFD method. LES (Large Eddy Simulation) and RANS (Reynolds Averaged Navier-Stokes) models were used and compered each other. Iqbal and Chan (2016) investigated effect of wind incident angle and passage width for high-rise buildings at different wind direction using standard $k-\epsilon$ turbulence model. Zhang et al. (2017) investigate the effect of lift-up buildings at pedestrian level wind for five different aspect ratios. Ekman layer effect was investigated for high-rise buildings using CFD method by Feng et al. (2019). In this study, wind veering effect was observed and simulated with LES method. Fouad et al. (2018) investigated pressure distribution and drag coefficient for low rise buildings using CFD method. The CFD technique with international wind standards and code were applied and validated with wind tunnel test results. Lohade and Kulkarni (2016) performed CFD analysis to observe shape effect at same plan area for high rise buildings using ANSYS Fluent. Roy and Bairagi (2016) carried out analysis of stepped tall buildings

using CFD simulation with $k-\varepsilon$ turbulence method at various wind angles and different height of buildings to show flow field and pressure distribution for designing the building. Kumar et al. (2023) investigated wind effects numerically for irregular cross-section shape using ANSYS CFX. Bairagi and Dalui (2021) investigated stepped tall building for observation effect of wind load using CFD method at four different configurations that are scaled 1:300. The 'E' shaped tall building was analysed to show mean pressure coefficient using both experimentally (wind tunnel test) and numerically (CFD simulation) by Bhattacharyya and Dalui (2018). Revuz et al. (2012) presented CFD simulation using RNG $k-\varepsilon$ turbulence model to indicate proper size of computational domain and effect of changing domain size for tall building. You and Lee (2021) investigated pressure coefficient at various wind directions and it was concluded that maximum pressure that occurs in urban areas was larger than suburban areas.

As a result of review previous studies, it can be said that wind effect creates many problems in tall buildings such as statics of the building. In addition, it can be inferred that the height to width ratio or aspect ratio of building are directly affected from wind. Hence, the aim of the study is to observe aspect ratio and speed effects for tall buildings. In this study, the effects of wind loads for rectangular shape tall buildings are investigated in terms of aerodynamics using CFD (Computational Fluid Dynamics) method. For this, the CFD analyses are performed at same cross-sectional area and different aspect ratios of buildings. In addition, the solutions are performed at various velocity of air that are 10 m/s, 20 m/s and 30 m/s. The CFD solutions are carried out at different turbulence models, which are SST (Shear Stress Transport) $k-\omega$ and Standard $k-\varepsilon$, to show which models are convenient for this application. The results are presented visually and compared with each other. It was concluded that SST $k-\omega$ model show superior performance due to capture flow field at boundary layer. In addition, the building with higher aspect ratio was observed that low velocity contours occurred at rear region of building when compared with building that has lower aspect ratio.

SOLUTION SETUP

In this study, CFD method was used to solve flow field by means of software programming. The beginning of study, the scaled rectangular tall building geometry was drawn for three different aspect ratios. If the geometry is not

scaled, solution would be complicated and it requires excessive solution time and power. The processes to perform solution are presented in the following.

COMPUTATIONAL DOMAIN AND MESH GENERATION

Mesh generation around the geometries are critical process to observe flow field and perform aerodynamic analysis. Therefore, hybrid mesh structure that includes both structured (prismatic) and unstructured mesh was generated around the geometries. The prismatic mesh was generated around the building to capture flow field correctly. In order to observe external flow around the body, the computational domain was generated and its dimensions are enough that the free-stream velocity is not affected by geometry. The height of computational domain is 4 times of building height and its width is also 10 times of building height. The mesh generation around the geometry is presented in Figure 1 and computational domain is also shown in Figure 2.

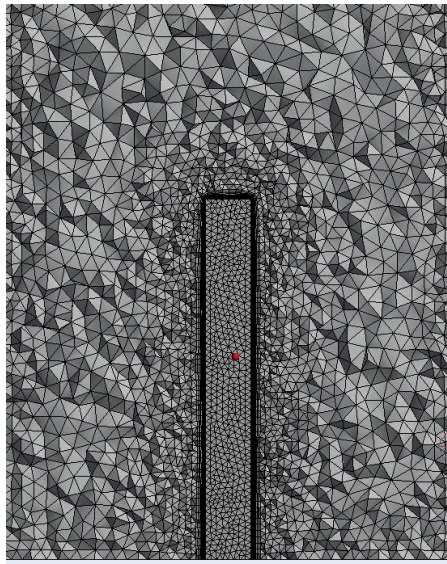


Figure 1. Mesh generation around the Geometry

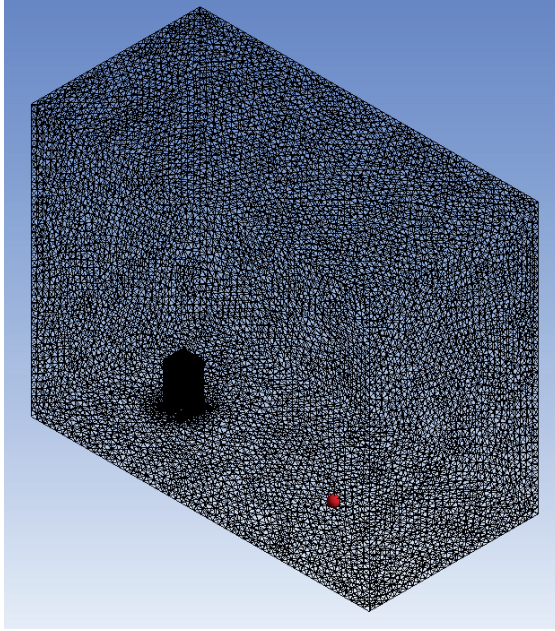


Figure 2. Computational Domain for Solution

The mesh sensitivity analysis was carried out to find sufficient number of mesh for correct solution. This process should be performed for different geometries to conduct CFD analysis correctly (Güzelbey et al. 2019). Mesh dependency process was carried out at 20 m/s for 4,5 aspect ratio. For this study, all of the models were prepared to have number of mesh elements higher than 1.7 Million to have accurate results independent from mesh. The Figure 3 shows the mesh numbers versus C_d values for CFD solutions.

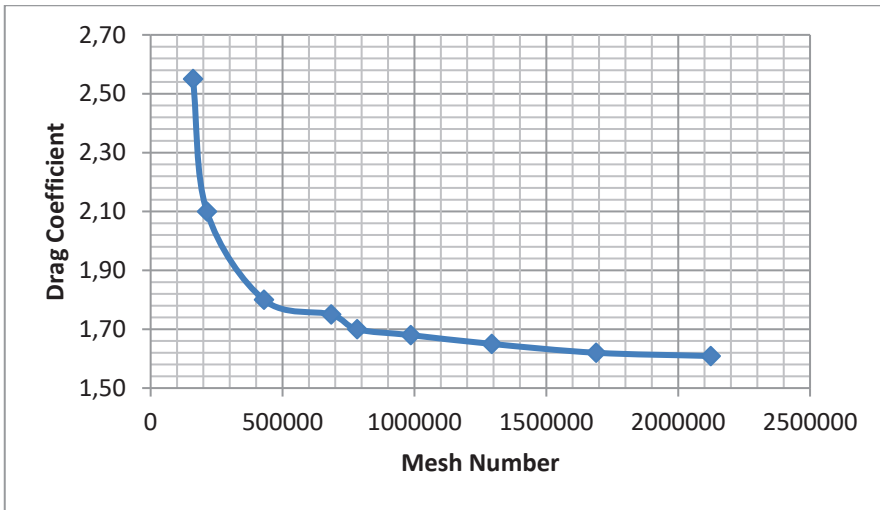


Figure 3. Mesh Sensitivity analysis for rectangular shape

CFD SOLUTION AND MATHEMATICAL MODELLING

CFD solution was performed using software programming. The solutions were 3-Dimensional, density based and steady for all cases. The Navier-Stokes equations were utilized for the solution. The governing equations of continuity, momentum and energy are given as conservation form following equations (1) to (6) (Anderson and Wendt, 1995).

$$\frac{\partial}{\partial t} \vec{U} + \frac{\partial}{\partial x} \vec{F} + \frac{\partial}{\partial y} \vec{G} + \frac{\partial}{\partial z} \vec{H} = 0 \quad (1)$$

$$\vec{U} = \begin{Bmatrix} \rho \\ \rho u \\ \rho v \\ \rho w \\ \rho E \end{Bmatrix} \quad (2)$$

$$\vec{F} = \begin{Bmatrix} \rho u \\ \rho u^2 + p - \tau_{xx} \\ \rho v u - \tau_{xy} \\ \rho w u - \tau_{xz} \\ \rho u E + p u - q_x - u \tau_{xx} - v \tau_{xy} - w \tau_{xz} \end{Bmatrix} \quad (3)$$

$$\vec{G} = \left\{ \begin{array}{c} \rho v \\ \rho uv - \tau_{yx} \\ \rho v^2 + p - \tau_{yy} \\ \rho wv - \tau_{yz} \\ \rho vE + pv - q_y - u\tau_{yx} - v\tau_{yy} - w\tau_{yz} \end{array} \right\} \quad (4)$$

$$\vec{H} = \left\{ \begin{array}{c} \rho w \\ \rho uw - \tau_{zx} \\ \rho vw - \tau_{zy} \\ \rho w^2 + p - \tau_{zz} \\ \rho wE + pw - q_z - u\tau_{zx} - v\tau_{zy} - w\tau_{zz} \end{array} \right\} \quad (5)$$

\vec{F} , \vec{G} and \vec{H} are the called the flux terms. The solution vector is called \vec{U} since the elements in $\vec{U}(\rho, \rho u, \rho v, \rho w, \rho E)$ are dependent variables that are acquired in steps of time. τ is the viscous stress tensor and ρ , E and p are the density, total energy and pressure, respectively. q is the heat flux vector.

The selection of turbulence model is important for simulation of flow field around the body. Therefore, two different turbulence models that are SST $k-\omega$ and Standard $k-\varepsilon$ models were used to simulate flow and the differences between them were observed visually. SST $k-\omega$ model can simulate the complex flow and gives accurate results in case of separation and circulation combining $k-\omega$ and standard $k-\varepsilon$ models (Menter, 1994). This turbulence model can capture unsteadiness and separation therefore, it suitable to simulate complex turbulent flow. However, it is difficult to converge so, finer mesh that generate near the wall of body requires and high solution power and computational time may be needed.

The Standard $k-\varepsilon$ turbulence model (k is kinetic energy and ε is turbulent dissipation) includes two transport equations. Diffusion of turbulent energy and convection can be evaluated. This model can be used to capture the flow under strong adverse pressure gradient, recirculation and separation. To minimize the unknowns terms and present the equations used for turbulent flow, the Standard $k-\varepsilon$ model is used since $k-\varepsilon$ turbulence contain some immeasurable and unknown terms (Launder and Sharma, 1974)(Launder and Spalding, 1983)(Ansys inc., 2009).

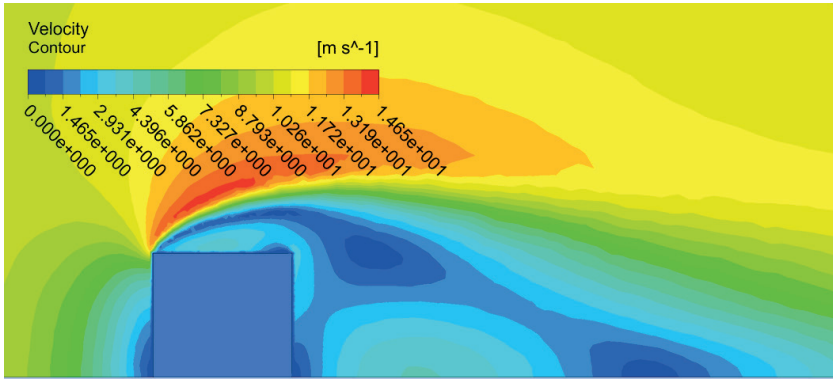
The CFD solution is performed by using Green-Gauss cell based that is discretization model and gives reasonable results for second order finite volume method. The convergence criteria are decided by investigating flow

residuals and aerodynamic coefficients. If the flow residuals reach the 10^{-5} and the change of aerodynamic coefficients value is negligible small during the last 100 iterations, the computation is finished. The results of CFD solution is given as visually for all cases in the following section.

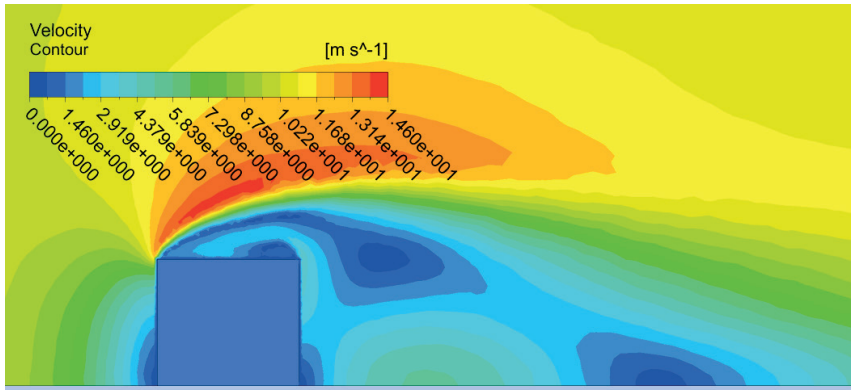
CFD RESULTS AND DISCUSSIONS

In this study, the effect of aspect ratio of tall buildings were investigated at various velocity of air using Standard $k-\epsilon$ and SST $k-\omega$ turbulence models by means of CFD simulation. Three different aspect ratios were determined as 0.89, 4.5, 8 at same cross-sectional area and three velocities of air were determined as 10 m/s, 20 m/s and 30 m/s. The velocity contours that occur around the tall buildings were presented for each case. Figures 4, 5 and 6 show velocity contours at 10 m/s, 20 m/s, 30 m/s velocities and 0.89 aspect ratio for both selected turbulence models, respectively. Figures 7, 8 and 9 show velocity contours at 10 m/s, 20 m/s, 30 m/s velocities and 4.5 aspect ratio for both selected turbulence models, respectively. Figures 10, 11 and 12 show velocity contours at 10 m/s, 20 m/s, 30 m/s velocities and 8 aspect ratio for both selected turbulence models, respectively.

It was concluded that SST $k-\omega$ show superior performance at boundary layer since it can capture flow more closely than standard $k-\epsilon$ model. This situation has been observed in almost all solutions. In addition, the top of end corner of building was observed that the size of vortices increases with increasing of air velocity. The velocity contours that occur back of building were observed that minimum pressure area increase with increasing of air velocity. When the comparison was made between aspect ratios, it was observed that the vortex sizes formed on top of buildings with higher aspect ratios were smaller at the same air speeds. Moreover, for high aspect ratio, high pressure occurred when compared with lower aspect ratio at the back surface of tall building due to low velocity region. It has been observed that high pressure areas in the rear areas of buildings with higher aspect ratios are greater than those of buildings with lower aspect ratios.

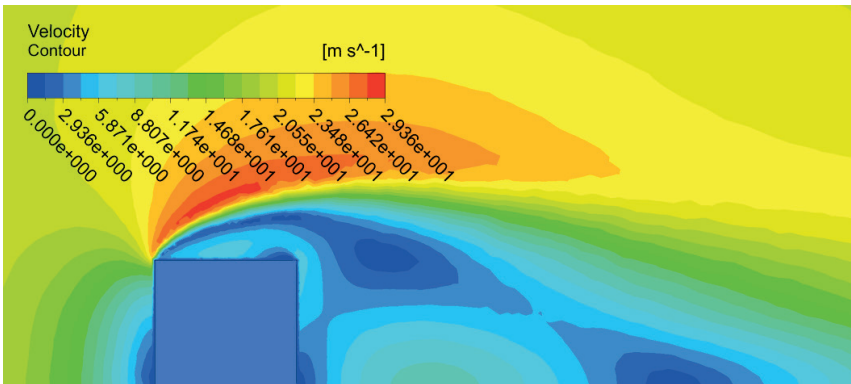


(a)

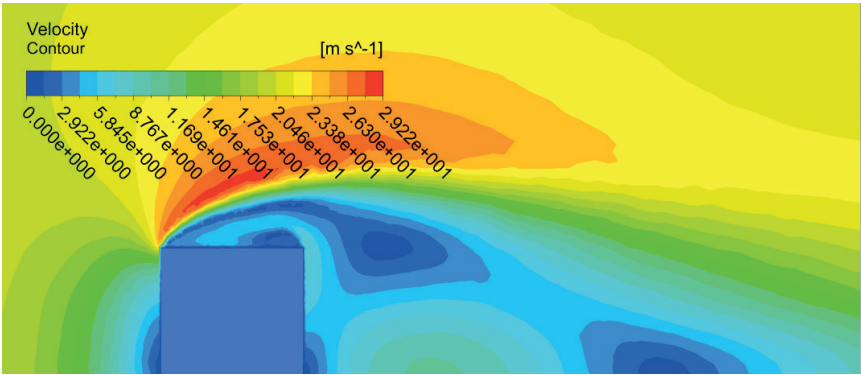


(b)

Figure 4. CFD solutions at 10 m/s air velocity and aspect ratio 0.89 (80H/90W) (a: standard k- ϵ , b: SST k- ω turbulence models)

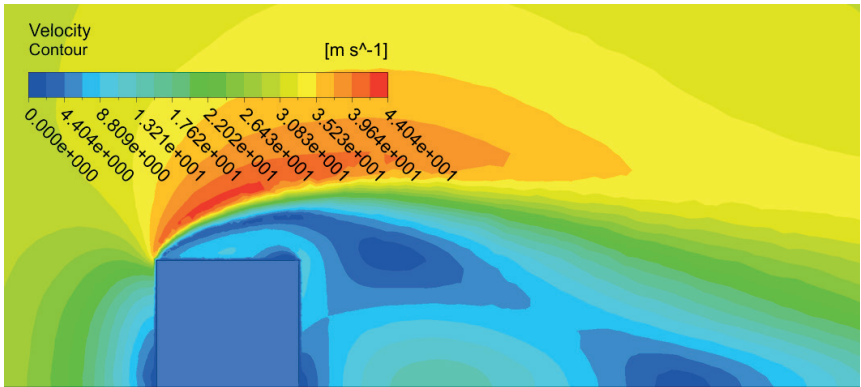


(a)

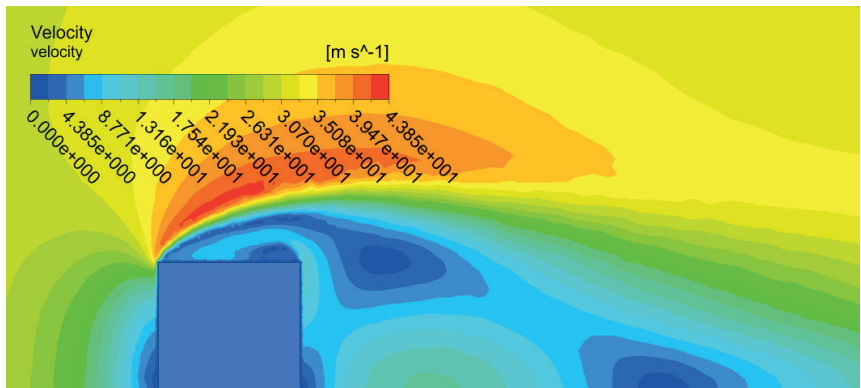


(b)

Figure 5. CFD solutions at 20 m/s air velocity and aspect ratio 0.89 (80H/90W) (a: standard k-ε b: SST k-ω turbulence models)

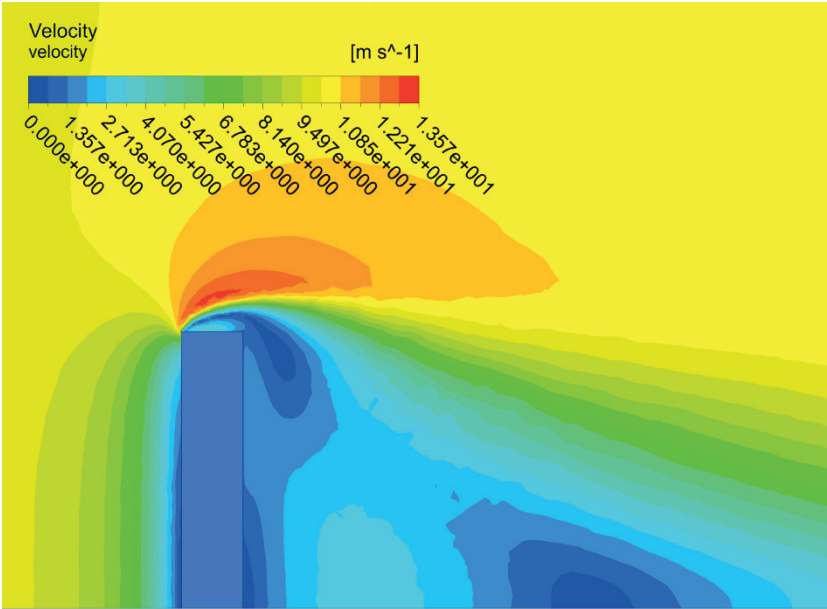


(a)

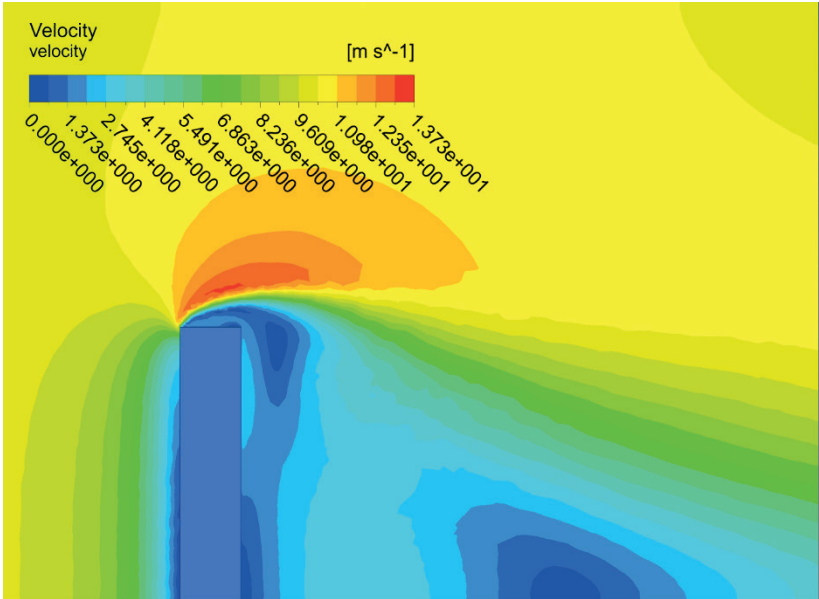


(b)

Figure 6. CFD solutions at 30 m/s air velocity and aspect ratio 0.89 (80H/90W) (a: standard k-ε b: SST k-ω turbulence models)

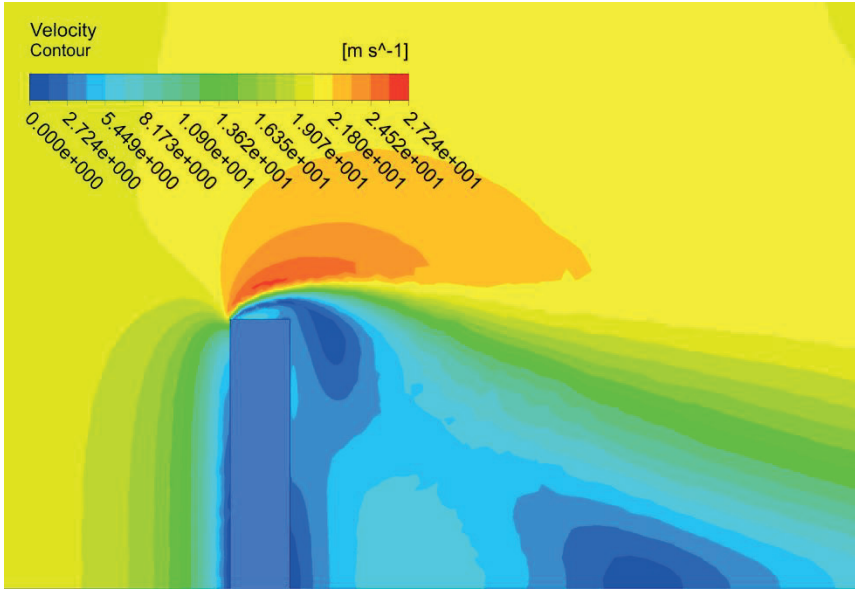


(a)

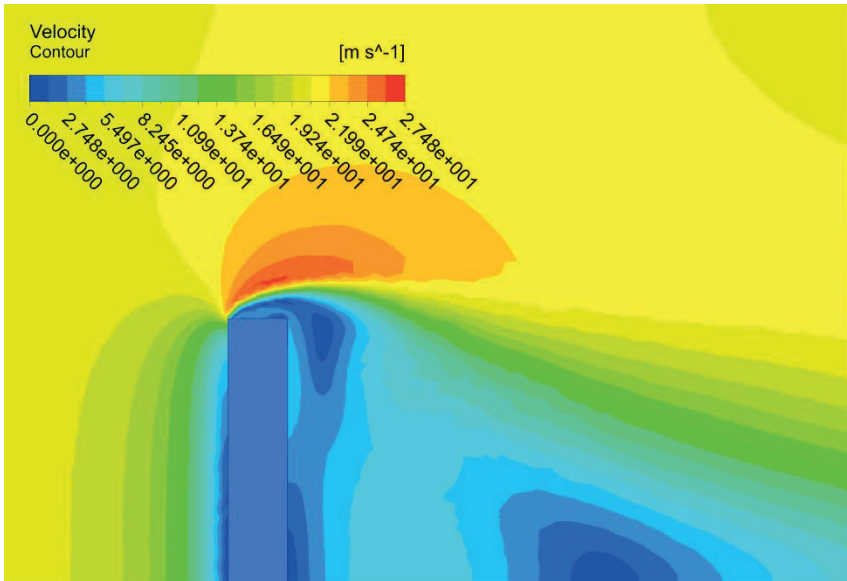


(b)

Figure 7. CFD solutions at 10 m/s air velocity and aspect ratio 4.5 (180H/40W)
 (a: standard k- ϵ b: SST k- ω turbulence models)

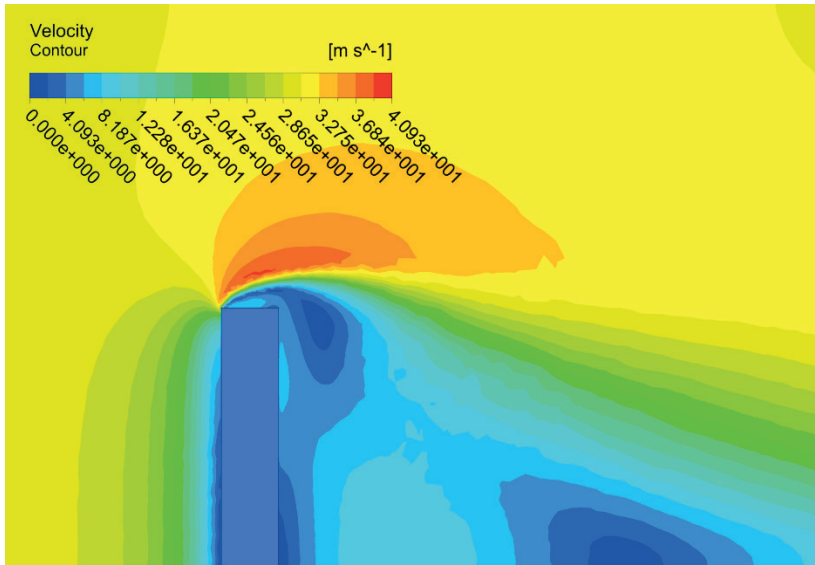


(a)

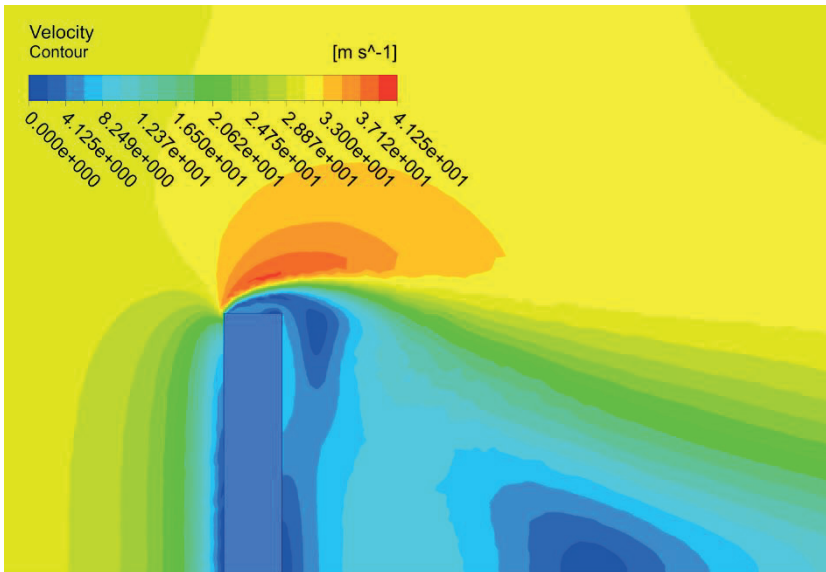


(b)

Figure 8. CFD solutions at 20 m/s air velocity and aspect ratio 4.5 (180H/40W)
(a: standard k- ϵ b: SST k- ω turbulence models)

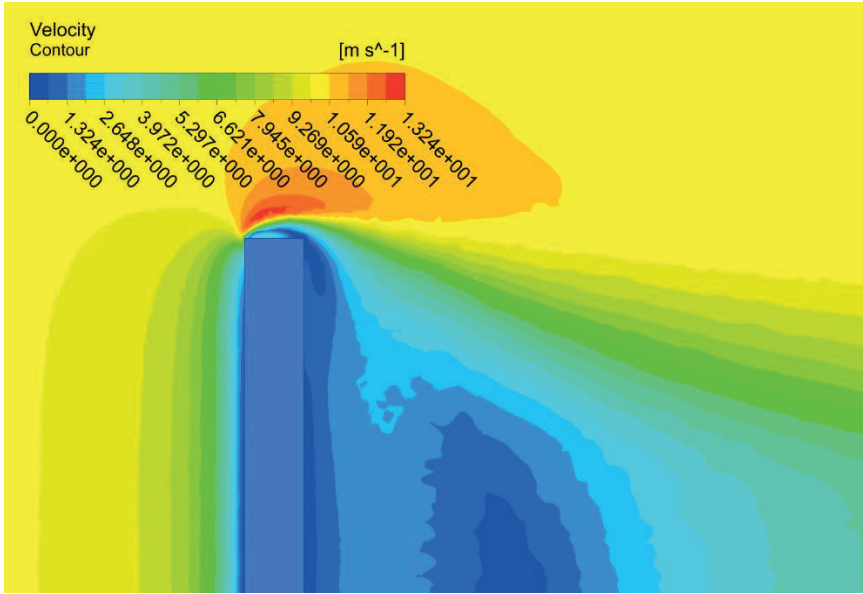


(a)

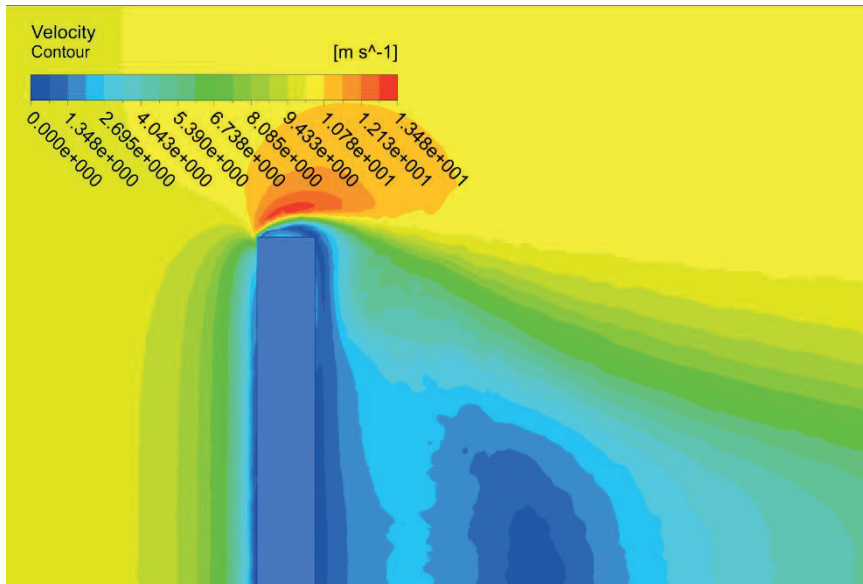


(b)

Figure 9. CFD solutions at 30 m/s air velocity and aspect ratio 4.5 (180H/40W)
 (a: standard k- ϵ b: SST k- ω turbulence models)

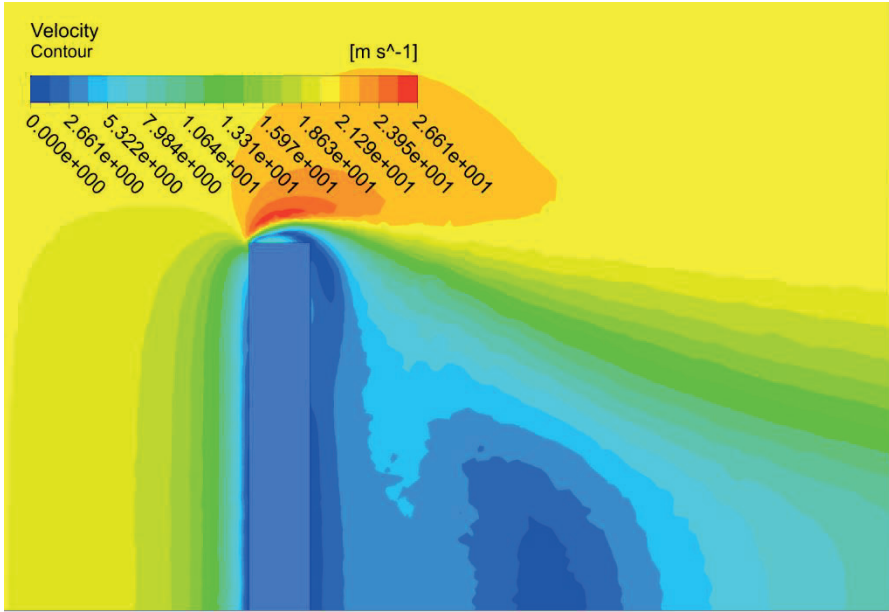


(a)

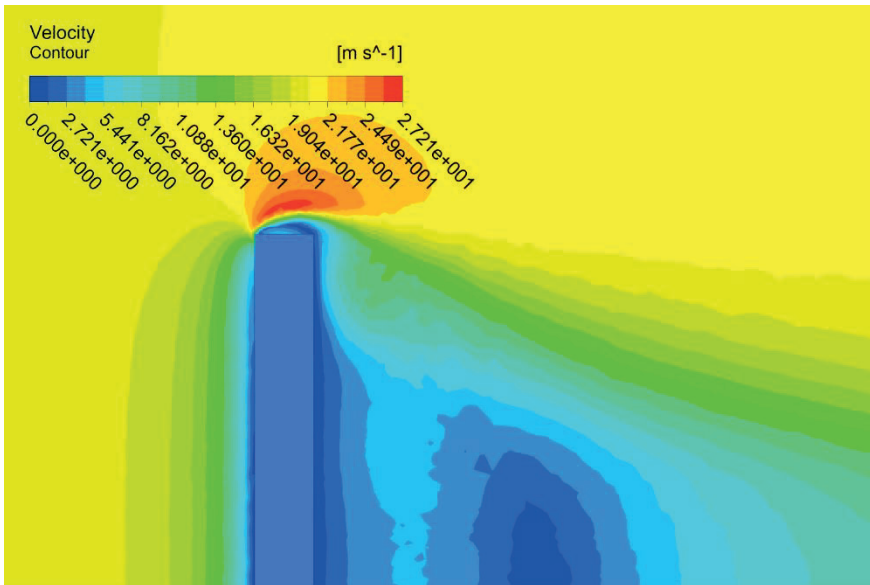


(b)

Figure 10. CFD solutions at 10 m/s air velocity and aspect ratio 8 (240H/30W)
(a: standard k- ϵ b: SST k- ω turbulence models)

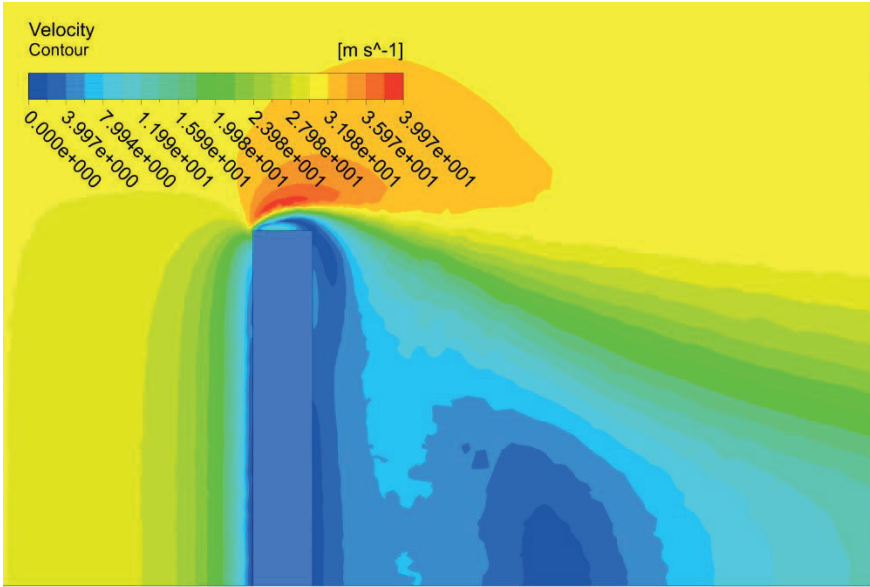


(a)

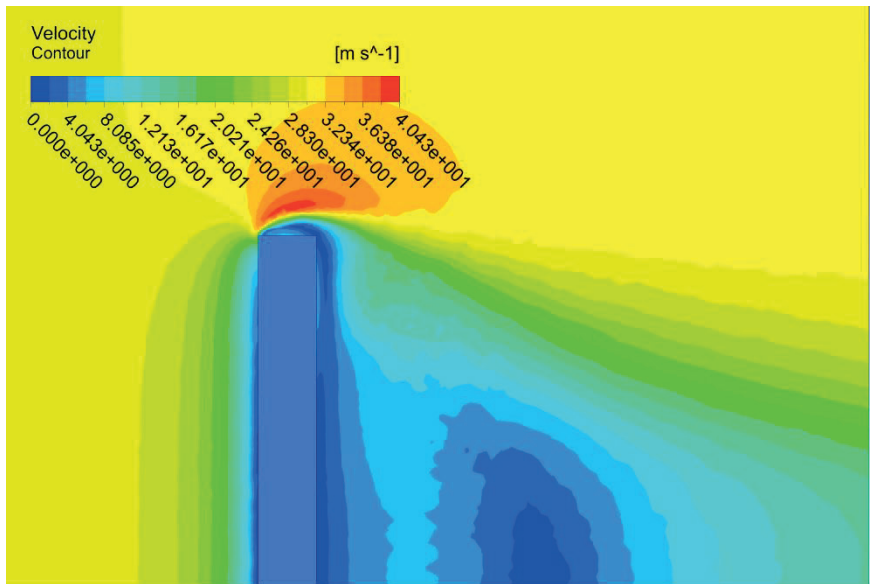


(b)

Figure 11. CFD solutions at 20 m/s air velocity and aspect ratio 8 (240H/30W)
 (a: standard k- ϵ b: SST k- ω turbulence models)



(a)



(b)

Figure 12. CFD solutions at 30 m/s air velocity and aspect ratio 8 (240H/30W) (a: standard k- ϵ b: SST k- ω turbulence models)

CONCLUSION

In this study, CFD simulation analysis was performed for scaled tall buildings at three different velocity of air (10 m/s, 20 m/s, 30 m/s) and three different aspect ratios (0.89, 4.5, 8) using SST k- ω and Standard k- ϵ turbulence models. Cross sectional area was same for all cases due to observe the effect of aspect ratio and velocity of air. The mesh dependency performed to find sufficient mesh number for obtained correct solution. In order to capture flow around the tall buildings, prismatic mesh structure was generated. The mesh number was decided as 1.7 Million since CFD solution results were negligible change for the higher mesh number. The Navier-Stokes equations were used to conduct CFD solution by means of software programming. The results were presented visually as velocity contours for all cases. It was concluded that SST k- ω turbulence model show superior performance especially at boundary layer in which near the wall when compared with Standard k- ϵ model. In addition, the size of vortex that occur the top of building is higher for the lower aspect ratio at same velocity when observed the results. It was also inferred from the presented figure, high pressure region was observed at rear region of building that has high aspect ratio since the minimum velocity contour was observed at that region. The analysis can be conducted using different shape of building and wind incidence angles as experimentally and numerically for future works.

REFERENCES

- Anderson JD, Wendt J. Computational Fluid Dynamics, McGraw-Hill, New York, USA; 1995.
- Bairagi, A. K., & Dalui, S. K. (2021). Estimation of wind load on stepped tall building using CFD simulation. *Iranian Journal of Science and Technology, Transactions of Civil Engineering*, 45(2), 707-727.
- Bernardini, E., Spence, S. M., Wei, D., & Kareem, A. (2015). Aerodynamic shape optimization of civil structures: A CFD-enabled Kriging-based approach. *Journal of Wind Engineering and Industrial Aerodynamics*, 144, 154-164.
- Bhattacharyya, B., & Dalui, S. K. (2018). Investigation of mean wind pressures on 'E'plan shaped tall building. *Wind and structures*, 26(2), 99-114.
- Daemei, A. B., & Eghbali, S. R. (2019). Study on aerodynamic shape optimization of tall buildings using architectural modifications in order to reduce wake region. *Wind and Structures*, 29(2), 139-147.
- Duarte, C. A. R., Duarte, L. E. R., de Lima, B. S., & de Souza, F. J. (2020). Performance of an optimized k- ϵ turbulence model for flows around bluff bodies. *Mechanics Research Communications*, 105, 103518.
- Elshaer, A., & Bitsuamlak, G. (2018). Multiobjective aerodynamic optimization of tall building openings for wind-induced load reduction. *Journal of Structural Engineering*, 144(10), 04018198.
- Feng, C., Gu, M., & Zheng, D. (2019). Numerical simulation of wind effects on super high-rise buildings considering wind veering with height based on CFD. *Journal of Fluids and Structures*, 91, 102715.
- Fluent, A.N.S.Y.S. ANSYS Fluent 12.0 Theory Guide. ANSYS Inc., Canonsburg, PA. 2009.
- Fouad, N. S., Mahmoud, G. H., & Nasr, N. E. (2018). Comparative study of international codes wind loads and CFD results for low rise buildings. *Alexandria engineering journal*, 57(4), 3623-3639.
- Gnatowska, R. (2019). Wind-induced pressure loads on buildings in tandem arrangement in urban environment. *Environmental Fluid Mechanics*, 19(3), 699-718.

Güzelbey, İ. H., Eraslan, Y., & Dođru, M. H. (2019). Effects of Taper Ratio on Aircraft Wing Aerodynamic Parameters: A Comparative Study. *European Mechanical Science*, 3(1), 18-23.

Huang, S., Li, Q. S., & Xu, S. (2007). Numerical evaluation of wind effects on a tall steel building by CFD. *Journal of constructional steel research*, 63(5), 612-627.

Iqbal, Q. M. Z., & Chan, A. L. S. (2016). Pedestrian level wind environment assessment around group of high-rise cross-shaped buildings: Effect of building shape, separation and orientation. *Building and environment*, 101, 45-63.

Kumar, A., Meena, R. K., Raj, R., Khan, M. I., & Khatib, J. M. (2023). CFD Study of Pressure Distribution on Recessed Faces of a Diamond C-Shaped Building. *Buildings*, 13(11), 2800.

Launder, B. E., & Sharma, B. I. (1974). Application of the energy-dissipation model of turbulence to the calculation of flow near a spinning disc. *Letters in heat and mass transfer*, 1(2), 131-137.

Launder, B. E., & Spalding, D. B. (1983). The numerical computation of turbulent flows. In *Numerical prediction of flow, heat transfer, turbulence and combustion* (pp. 96-116). Pergamon.

Lohade, S., & Kulkarni, S. (2016). Shape effects of wind induced response on tall buildings using CFD. *International Journal of Engineering and Applied Sciences*, 3(6), 257650.

Menter, F. R. (1994). Two-equation eddy-viscosity turbulence models for engineering applications. *AIAA journal*, 32(8), 1598-1605.

Montazeri, H., & Blocken, B. (2013). CFD simulation of wind-induced pressure coefficients on buildings with and without balconies: validation and sensitivity analysis. *Building and Environment*, 60, 137-149.

Moonoghi, M. A., & Kargarmoakhar, R. (2016). Aerodynamic mitigation and shape optimization of buildings. *Journal of building engineering*, 6, 225-235.

Neethi, B., & Joby, E. (2018). Aerodynamic Modifications against Wind Excitation on Tall Buildings-Shape Optimization. *International Journal of Engineering Research & Technology*, 7(5).

Paltun, S., Gültekin, A., & Çelebi, G. (May, 2015) Binaların Aerodinamik Biçimsel Yapısının İrdelenmesi Bina Formu Ve Rüzgar İlişkisi. 2nd International Sustainable Buildings Symposium, Ankara, Türkiye.

Paul, R., & Dalui, S. (2021). Shape optimization to reduce wind pressure on the surfaces of a rectangular building with horizontal limbs. *Periodica Polytechnica Civil Engineering*, 65(1), 134-149.

Revuz, J., Hargreaves, D. M., & Owen, J. S. (2012). On the domain size for the steady-state CFD modelling of a tall building. *Wind and structures*, 15(4), 313.

Roy, K., & Bairagi, A. K. (2016). Wind pressure and velocity around stepped unsymmetrical plan shape tall building using CFD simulation—A case study. *Asian Journal of Civil Engineering (BHRC)*, 17(8), 1055-1075.

Ruiz, C. A., Kalkman, I., & Blocken, B. (2021). Aerodynamic design optimization of ducted openings through high-rise buildings for wind energy harvesting. *Building and Environment*, 202, 108028.

Shirzadi, M., Mirzaei, P. A., & Naghashzadegan, M. (2017). Improvement of k-epsilon turbulence model for CFD simulation of atmospheric boundary layer around a high-rise building using stochastic optimization and Monte Carlo Sampling technique. *Journal of Wind Engineering and Industrial Aerodynamics*, 171, 366-379.

Toja-Silva, F., Lopez-Garcia, O., Peralta, C., Navarro, J., & Cruz, I. (2016). An empirical-heuristic optimization of the building-roof geometry for urban wind energy exploitation on high-rise buildings. *Applied energy*, 164, 769-794.

Toja-Silva, F., Peralta, C., Lopez-Garcia, O., Navarro, J., & Cruz, I. (2015). Roof region dependent wind potential assessment with different RANS turbulence models. *Journal of Wind Engineering and Industrial Aerodynamics*, 142, 258-271.

Xie, J. (2014). Aerodynamic optimization of super-tall buildings and its effectiveness assessment. *Journal of Wind Engineering and Industrial Aerodynamics*, 130, 88-98.

You, J., & Lee, C. (2021). Experimental Study on the Effects of Aspect Ratio on the Wind Pressure Coefficient of Piloti Buildings. *Sustainability*, 13(9), 5206.

Zhang, X., Tse, K. T., Weerasuriya, A. U., Li, S. W., Kwok, K. C., Mak, C. M., ... & Lin, Z. (2017). Evaluation of pedestrian wind comfort near 'lift-up' buildings with different aspect ratios and central core modifications. *Building and Environment*, 124, 245-257



Chapter 18

REVIEW OF BRAKING AND BATTERY SYSTEMS IN ELECTRIC VEHICLES

*Mehmet ŞEN¹
Muciz ÖZCAN²*

1 PhD(c) Necmettin Erbakan University, Faculty of Engineering,
Department of Electric Electronic Engineering,
Konya, Türkiye
E-mail: mehmet.sen@asbu.edu.tr
ORCID: 0000-0001-7609-2210

2 Professor, Dr.
Necmettin Erbakan University, Faculty of Engineering,
Department of Electric Electronic Engineering,
Konya, Türkiye
E-mail: mozcan@erbakan.edu.tr
ORCID: 0000-0001-5277-6650

INTRODUCTION

Electric vehicles (EVs) completed their journey from R&D centers to prototype workshops in the early 1990s. Ten years ago, mass production of EVs started (Chan, 2013). Today, hybrid electric vehicles (HEAs) and EVs constitute the majority of vehicle production. HEAs are preferred by users because of their innovative features and the equipment found in conventional vehicles. HEAs do not directly require stationary charging systems and have a similar or greater range than conventional vehicles. Battery studies are gaining momentum every day for EVs to have higher ranges (Cogen, 2010). EVs will have longer ranges than conventional vehicles in the coming years.

The production of EVs has a rapidly increased momentum. While the total number of EVs worldwide was less than 20,000 in 2010, it has increased 55 times in the last 10 years with the increase in mass production and reached 11 million (Demir et al., 2012). With the increase in the number of EVs on the roads, the automotive sector has undergone major changes. Increasing the growth rate of EVs is a necessity to achieve the net-zero emissions targeted by the 2015 Paris Climate Agreement and 2021 COP26 Conference, in which Turkey is a stakeholder (Demir, 2022). In order to achieve the net-zero emission target, all road transportation should be provided by electric vehicles until 2050. In order to achieve this transformation, rapid development in EV production must also be ensured in electricity distribution networks and charging stations.

The biggest challenge in the deployment of EVs lies in the development of low-cost and high-range battery systems. Because the production of low-cost batteries will enable us to see more EVs on the road, battery manufacturers are investing heavily in their facilities. Batteries used in EVs must have high power and energy densities. However, EVs have not yet reached the desired energy density. This situation brings along the necessity of using energy in the most efficient way in EVs. Studies have shown that useful braking can increase the range of EVs by 20%-30% (Jung et al., 2021). However, this situation has negative effects on the battery. In addition to increasing the range of batteries, preventing battery aging is important for ensuring economic and environmental sustainability.

1. BRAKING SYSTEMS USED IN ELECTRIC VEHICLES

There are three different methods for the electrical braking of electric vehicles. First, energy recovery braking, which is known as beneficial braking,

stores energy in the battery by braking to increase vehicle efficiency when the vehicle is above a certain speed. Another method is the dynamic braking system, which is used to stop at vehicle safely at low speeds. Because there is not enough current in the dynamic braking system, no recovery can be made (Demirci and Çelikoğlu, 2018). However, by upgrading this method, the required recovery can be achieved by reaching the desired current value at low speeds. The last method ensures that the vehicle stops as soon as possible by providing current flow in the opposite direction in cases where sudden braking is required (Cornic, 2010).

In order to study the braking characteristics of EVs, the energy flow from the electric machine to the battery must be known. In a rotary system, power is equal to the moment and angular velocity, expressed in Formula 1. When this power is reduced to the motor shaft, it is expressed as follows:

$$P_{tk}(t) = \omega_{tk}(t) \cdot r_{tk}(t) \quad (1)$$

$$P_{tk}(t) = \eta_{ak} \cdot P_{EM}(t) \quad (2)$$

In formulas,

- $P_{tk}(t)$; power at the vehicle wheels (*Watt*),
- $\omega_{tk}(t)$; wheel speed (*1/s*),
- $r_{tk}(t)$; wheel moment (*N.m*),
- η_{ak} ; efficiency in the transfer sections,
- $P_{EM}(t)$; power of the electric machine (*Watt*).

The current conditions for a brushless direct current (DC) motor in EVs when powered by a battery are given in Formula 3.

$$E_a - V_{bt} = I_{fr} \cdot (R_{bt} + R_{pp} + R_{sc}) \quad (3)$$

In formulas,

- E_a ; voltage induced during braking (*V*),
- V_{bt} ; end voltage of the battery at braking (*V*),
- I_{fr} ; brake current (*A*),
- R_{bt} ; internal resistance of the battery (*ohm*),
- R_{pp} ; resistance of the electric machine (*ohm*),
- R_{sc} ; resistance of semiconductor materials (*ohm*).

The driver connection diagram of the DA machine with the battery is shown in Fig.1.

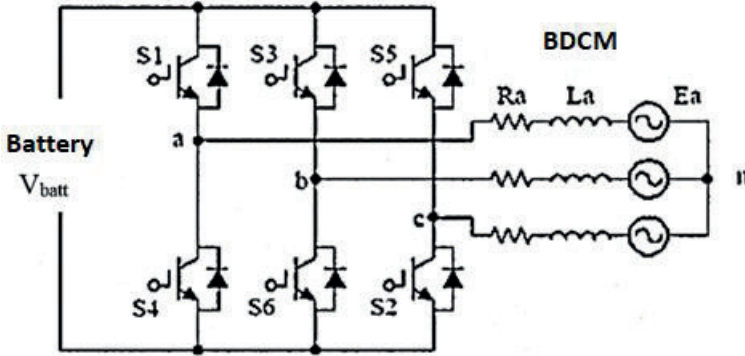


Figure 1. Connection diagram between the DA machine and the battery

1.1. Regenerative Braking

When the braking characteristics of EVs are analyzed, energy recovery from useful braking cannot be achieved below certain speeds. Useful braking occurs when the voltage higher than the battery voltage after all losses are subtracted (Lee and Chen, 2003). The voltage that must be induced is given in Formula 4, otherwise useful braking will not occur.

$$E_a > V_{bt} + (R_{bt} + R_{PP} + R_{SC}) \cdot I_{fr} \quad (4)$$

In EVs, energy storage is achieved by increasing the voltage obtained during braking. This can be achieved by controlling the current to maintain the braking torque. More important than useful braking in electric vehicles is battery safety. Another limiting factor for useful braking is the state of battery charge. Even if a speed level sufficient for useful braking is reached, the battery begins to act as a resistor when it is charged. This high internal resistance in the battery causes the battery to heat up and then burn or explode. The battery reacts in direct proportion to the current it draws (González-Gil et al., 2013). Useful braking is limited when the I_{fr} current given in Formula 4 exceeds the maximum current value that the battery will accept.

2.2. Dynamic Braking

In dynamic braking, unlike utility braking, the braking resistance takes the battery resistance (Xu and Zheng, 2016). The torque occurring during braking can be calculated from Formula 5 and the induced voltage can be calculated from Formula 6.

$$T = k_t \cdot I_{fr} = k_t \cdot \frac{E_a}{R_{fr} + R_{pp} + R_{SC}} \quad (5)$$

$$E_a = I_{fr} \cdot (R_{fr} + R_{PP} + R_{SC}) \quad (6)$$

Dynamic braking is also called electrical braking. The voltage value to be applied to the coil during dynamic braking depends on the speed of the vehicle. Sufficient current must be generated for the braking moment. In cases where the vehicle speed is low, a sufficient current value may not be reached, in which case an upgrade is made. High torque is needed in powerful motors and when the vehicle weight is high. The current passing through the windings during braking should not exceed the nominal current of the motor (Boerboom, 2012). Otherwise, the stator windings may burn, and vehicle safety may be jeopardized.

2.3. Reverse Current Braking

Reverse current braking can be applied to EVs where sudden braking is required. It is applied by abruptly changing the direction of the motor speed. Reverse current braking can be applied to machines with high inertia and requiring sudden stopping (Zhao et al., 2014). In this type of braking, current flows in the opposite direction by expending energy and braking occurs. In other words, the direction of current and voltage is from the battery to the machine. Braking characteristics are expressed in Formulas 7 and 8.

$$V_{rev} + E_a = I_{fr} \cdot (R_{PP} + R_{SC}) \quad (7)$$

$$T = k_t \cdot I_{fr} = k_t \cdot \frac{V_{rev} + E_a}{R_{pp} + R_{SC}} \quad (8)$$

There are issues to be considered in the design of machines to be braked with reverse current. When braking starts, a serious current will occur on the

system. In this case, it is important to choose the electronic devices correctly to prevent damage to the devices. This type of braking is not preferred for EVs, except for panic braking, as it reduces the range (Boerboom, 2012). In addition to electrical braking, mechanical braking is preferred as a complement.

2.4. Optimal and Safe Braking

To ensure safe braking, vehicle dynamics must first be examined. To move a vehicle safely, the wheels, which are the points of contact with the road, must always be attached to the road. Indeed, the "slip" that occurs at the base of the tire wheel moves and steers the vehicle. When the tire contacts the road under a positive moment, it compresses toward travel and the rear of the tire is stretched (Lee and Chen, 2003). Fig. 2 shows the effect of positive moment on the tire.

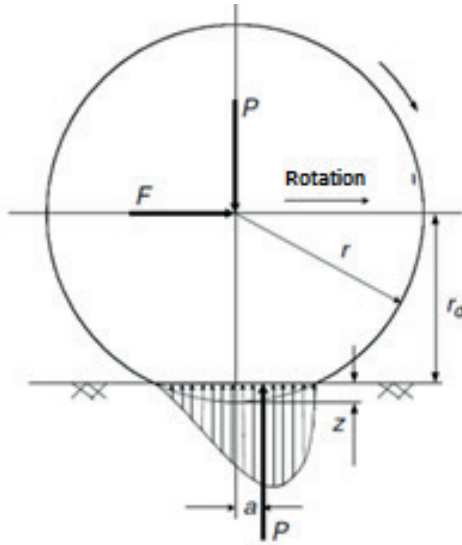


Figure 2. Pressure created in the tire by the positive moment

The positive and negative moments at the tire tread are expressed in Formulas 9 and 10, respectively.

$$s = \left(1 - \frac{v}{r-w}\right) \times 100\% \quad (9)$$

$$s = \left(1 - \frac{v}{r-w}\right) \times 100\% \quad (10)$$

In formulas,

s ; slip,

v ; vehicle speed,

r ; wheel radius,

w ; wheel rotation speed.

After a certain point, when a moment is applied to the wheel, this base reaction becomes large enough to break the bond between the wheel and the road. Apart from the drive and brake units, the ability of a vehicle's wheels to transmit the effects of these units to the road determines the traction or braking performance of the vehicle. This is possible as long as the wheel and road have a cohesive effect. In general, this effect limits overall vehicle performance. This effect is especially minimal on wet, muddy, or icy roads, where the vehicle's ability to move and stop is greatly reduced. The situation where the wheel contact with the road is maximized is expressed in Formula 11.

$$F_{maks} = P_n \cdot \mu \quad (11)$$

In formulas,

F_{maks} ; maximum force,

P_n ; wheel load,

μ ; road contact coefficient.

Fig.3 shows the plot of the relationship between the slip and contact coefficients in the vehicle.

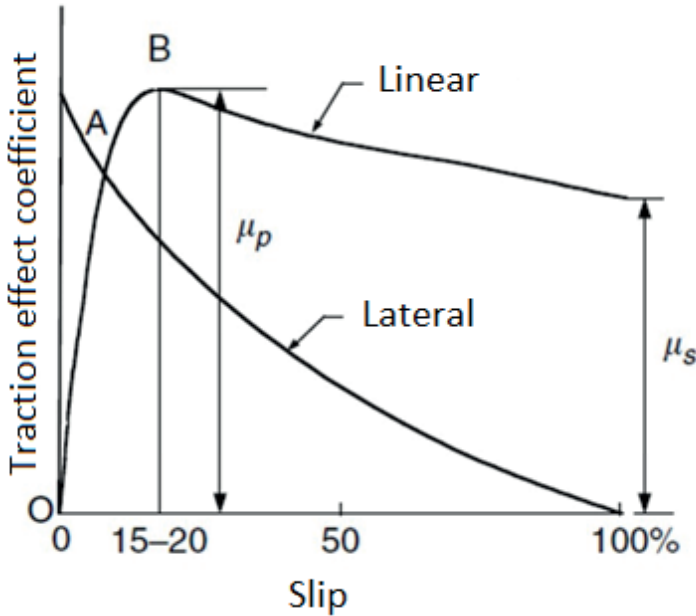


Figure 3. Relationship between vehicle slip and road contact

As shown in Fig. 3, after the maximum μ_p point, the wheel becomes unstable and the relationship between the skid and traction changes inversely. The skidding condition of the vehicles varies according to the road surface. Table 1 shows the grip and skid values for various road surfaces (Demirci and Çelikoğlu, 2018).

Table 1. Contact coefficients on various road surfaces

| Surface | Maximum value (μ_p) | Skid value (μ_s) |
|--------------------|---------------------------|------------------------|
| Asphalt dry ground | 0,8-0,9 | 0,75 |
| Asphalt wet ground | 0,5-0,7 | 0,45-0,6 |
| Gravel floor | 0,6 | 0,55 |
| Soil dry ground | 0,68 | 0,65 |
| Soil wet ground | 0,55 | 0,4-0,5 |
| Stuck snow ground | 0,2 | 0,15 |
| Ice floor | 0,1 | 0,07 |

The braking of the vehicle generates a braking force limited by the maximum contact (grip) value. Table 1 shows that the least braking will occur on an icy surface and the highest quality braking force will occur on a dry asphalt surface. In a vehicle without a sophisticated braking system, standard braking is performed according to the ratio between the front and rear wheels.

In terms of vehicle dynamics, locking the front brakes is safer than locking the rear wheels. When the rear brakes are locked, the understeer and yaw rate of the vehicle increase. In this case, locking the front wheels is preferred. In today's vehicles, advanced electronic systems provide safe braking by applying different brake forces to each wheel.

2.5. Comfortable Braking

In conventional vehicles, when the pilot brakes, he adapts to the braking force in a time inversely proportional to his driving experience. In this way, he/she easily predicts how hard he/she should apply the brakes and how long it will take to stop. Similarly, when the pilot takes his foot off the brake, he knows when the vehicle will slow down with the negative moment effect. This conventional situation should also be applied in EVs to provide a comfortable braking system. For comfortable braking, Figure 4 shows the braking acceleration for various situations (Cornic, 2010).

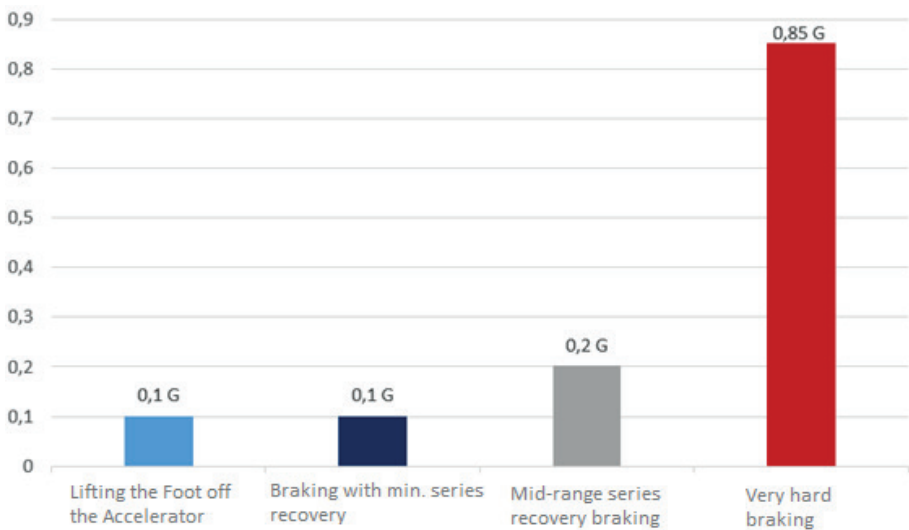


Figure 4. Braking acceleration for different cases ($G=10 \text{ m/s}^2$)

$$F_{brake} = (M \cdot j) - F_{load} \quad (12)$$

$$T_{brake} = r_{wheel} \cdot F_{brake} \quad (13)$$

In formulas,

F_{brake} ; braking force on vehicle wheels,

F_{load} ; vehicle load on the wheel,

T_{brake} ; braking moment on the vehicle,
 r_{wheel} ; vehicle wheel radius,
 M ; vehicle mass,
 j ; braking acceleration.

The loads acting on the vehicle and the braking moment play a role in the deceleration of the vehicle. The braking moment and vehicle speed are inversely proportional. In other words, in the total forces acting on the vehicle, there is a relationship between the vehicle speed and the load force proportional to the square of the speed.

2. BATTERY SYSTEMS USED IN ELECTRIC VEHICLES

There are three basic types of battery cells used in electric vehicles. These are,

- Cylindrical batteries,
- Prismatic batteries and
- Pouch batteries.

Lithium coin cells are also used for testing in research and development but have never been used in electric vehicles. The number of cells in EV varies greatly depending on the cell format. On average, EVs with cylindrical cells have 5,000 - 9,000 cells (Asghar et al., 2021). However, there are prismatic cells with only a few hundred cells.

Cylindrical cells are the cheapest format to manufacture because they are already enclosed in a protective sheath that offers good mechanical resistance. Cylindrical cells are not only cost-effective, but also highly protected and easy to manufacture. Cylindrical cells have limitations in terms of power because of their shape (Bentley and Heacock, 1996). Therefore, vehicles with smaller batteries, such as hybrid vehicles, use pouch or prismatic cells to provide more power during acceleration. Cylindrical batteries need to be manufactured in a smaller format than other battery types to ensure that they dissipate heat well and extend battery life. Therefore, the most common cylindrical cell formats are 18650 and 21700 (Burd et al., 2021).

Prismatic cells can be 20 to 100 times larger than cylindrical cells. They can typically deliver more power and store more energy for the same volume because less material is used in the enclosure. The shape and

thickness of the enclosure also allows for better heat management than cylindrical cells. Prismatic cells are popular among Chinese manufacturers because their preferred cell chemistry (lithium, iron, phosphate) is currently mostly available in prismatic format (Catenacci, 2013). Recently, prismatic cells have gained importance elsewhere in the world. While cylindrical cells used to be the most popular format, prismatic cells are expected to take a large share of the market in EVs in the coming years (Chu and Majumdar, 2012).

Pouch cells are designed to deliver more power than other types of cells. They are also very efficient in terms of space utilization. However, their soft plastic casing means that they have the lowest mechanical resistance of all cell types. Therefore, an additional structure must be added to protect the pouch cell from mechanical damage during pouch cell assembly. There are many types of batteries used in the industry, and they are classified according to the material used in their plates or electrolytes. The evolution of the main battery types used in EVs is shown in Fig. 5 (Budde et al., 2013).

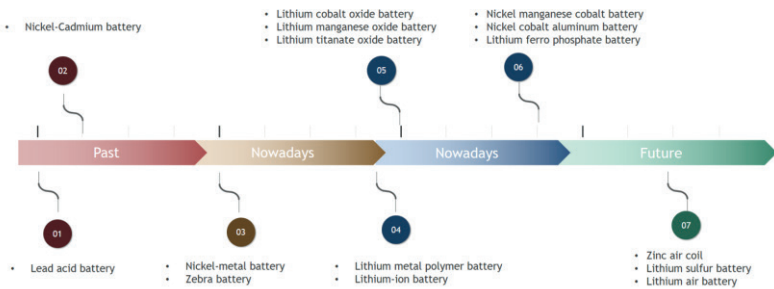


Figure 5. Temporal chart of battery development in electric vehicles

Today's EV batteries have a low energy density, which directly affects their range. However, EV battery technology has advanced significantly in recent years. Today, there are many battery technologies with different nominal voltages and energy densities. Fig. 6 shows a comparison of different battery types in terms of energy density (Chu and Majumdar, 2012).

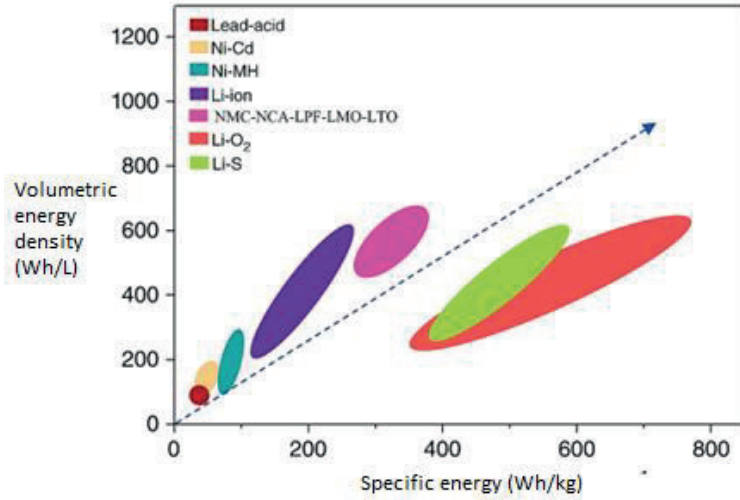


Figure 6. Comparison of battery types in terms of energy density

3.1. Lead Acid Batteries

Invented in 1859, the lead-acid battery is still used in many vehicles with both internal combustion and electric motors. In 1899, the EV "La Jamais Contente" with this technology was in fact the first car to exceed 100 km/h, long before internal combustion engine vehicles (Asghar et al., 2021). Today, lead-acid batteries are no longer used for traction control, but to power the electrical circuitry of accessories or components typical of internal combustion engines, such as starters. Despite its volume and weight, the lead-acid battery offers only a limited capacity, but it has the advantage of being both cheap and easy to produce and recycle. Used as the main energy storage mechanism for electric cars until the 1980s, it is rapidly being replaced by other more efficient technologies (Hu et al., 2019). Fig.7 shows a graph showing the battery health of a sulfur acid battery depending on the charge cycle.

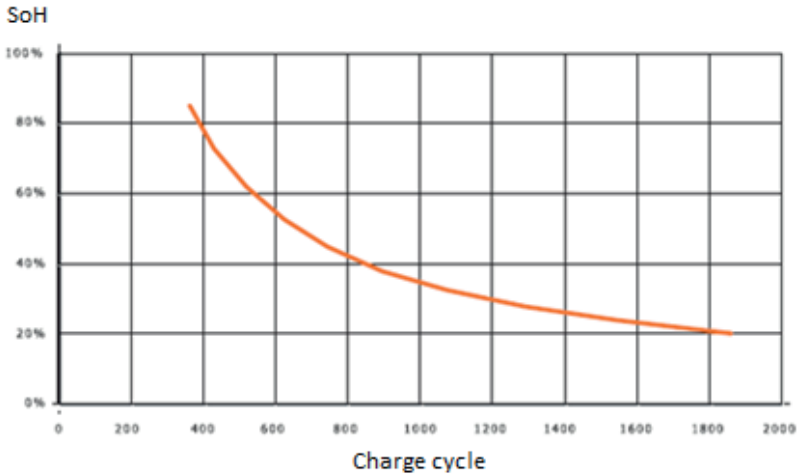


Figure 7. Battery health depending on the charge cycle of sulfur acid batteries

3.2. Alkaline Batteries

Alkaline batteries were invented in the early twentieth century. Inventor Lewis Urry created the Eveready alkaline battery in 1949. Although these batteries were not immediately accepted by consumers, they became successful a few years later. Thirty years after its invention, the company changed its name to Energizer (Enache et al., 2014).

An alkaline battery is a battery created by chemical reactions between zinc and manganese dioxide. Alkaline batteries have a higher energy concentration than other battery types. Therefore, they are more durable than other battery types. Initially, alkaline batteries were unpopular when they were invented in 1906. It took about fifty years for alkaline batteries to be used worldwide, and they were used as part of consumer products such as children's toys. Over time, they began to be used as consumer goods in their own right. Today, alkaline batteries are the most common type of batteries sold worldwide. Approximately four billion alkaline AA batteries are produced each year. To this number, millions of other alkaline batteries (C, AAA, D) can be added (Hawkins et al., 2012). AA batteries are the most common type of alkaline battery produced in the world and are generally used to power children's toys and in homes and workplaces to power lamps, battery-operated drills, flashlights, and many other portable electrical products.

The physical components of an alkaline battery are complex; however, the physical appearance of an alkaline battery is not very different from that of other types of batteries. The cathode is at one end of the battery and the anode at the other. The positive end of the alkaline batteries has a circular portion extending from the main battery body. The other end of the anode has a flat surface. Fig. 8 shows the general structure of an alkaline battery (Enache et al., 2014).

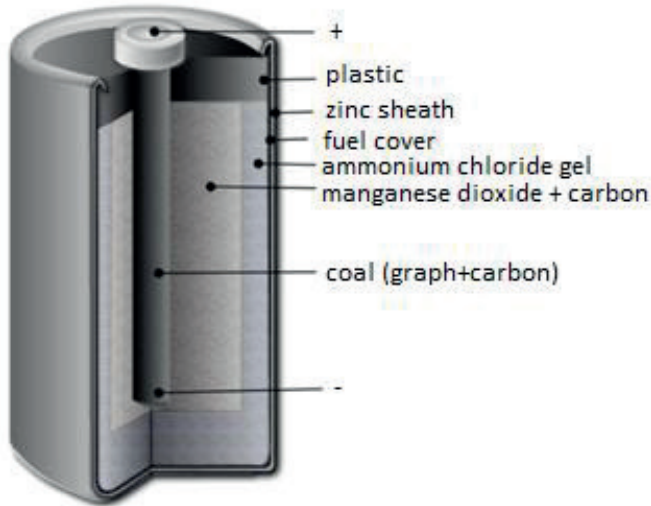


Figure 8. Internal structure of the alkaline battery

The basic operating principle of an alkaline battery is the conversion of chemical energy from the interactions between zinc and manganese oxide into electrical energy. Battery chemistry always involves two or more materials. The specific chemical reactions that occur in an alkaline battery occur between the materials in the battery.

First, electricity comes into contact with the zinc material of the battery anode. This causes ionic power to flow from the anode into the battery. Zinc combines with manganese dioxide and water to form zinc monoxide and manganese dioxide hydroxyl (Muratoğlu and Akkaya, 2015). Manganese dioxide, water, and electrons then interact to form hydroxide ions and more hydroxyls. Zinc and hydroxide then interact to form zinc oxide, water, and electrons. These interactions build up from each other and produce a flow of energy. The electrons formed as a result of these interactions transmit electrical energy.

3.3. Zebra Batteries

The zebra battery for EVs is a low-temperature variant of sodium sulfur (NaS) batteries and was developed as part of the "Zero Emission Batteries Research Project". Since the beginning, zebra batteries have been developed for EV applications. NaAlCl₄ is used as the battery component. Zebra batteries offer safe use in EVs because of their high-temperature operation. The long-life cycle, short-circuit tolerance and low-cost components have enabled zebra batteries to be used for EVs for more than a decade. Because the battery has very high discharge characteristics when not in use, it is mostly preferred in commercial vehicles with intensive use (Sun et al., 2020; Enache et al., 2014).

3.4. Lithium-Ion Batteries

A lithium ion (Li-ion) battery is an advanced battery technology that uses lithium ions as a key component of its electrochemistry. During a discharge cycle, lithium atoms at the anode are ionized and stripped of their electrons. The lithium ions move from the anode and pass through the electrolyte until they reach the cathode, where they recombine with their electrons and become electrically neutralized. Lithium ions are small enough to pass through a micro permeable separator between the anode and cathode. Partly because of the small size of lithium, Li-ion batteries have very high voltage and charge storage per unit mass and per unit volume (Lin et al. 2017).

Li-ion batteries can use some different materials as electrodes. The most common combination are lithium cobalt oxide (cathode) and graphite (anode), which are most commonly found in portable electronic devices such as mobile phones and laptops. Other cathode materials include lithium manganese oxide (used in hybrid electric and electric cars) and lithium iron phosphate. Fig. 9 schematically illustrates the charge-discharge process of Li-ion batteries (Matthews et al., 2017; Şen and Özcan, 2023).

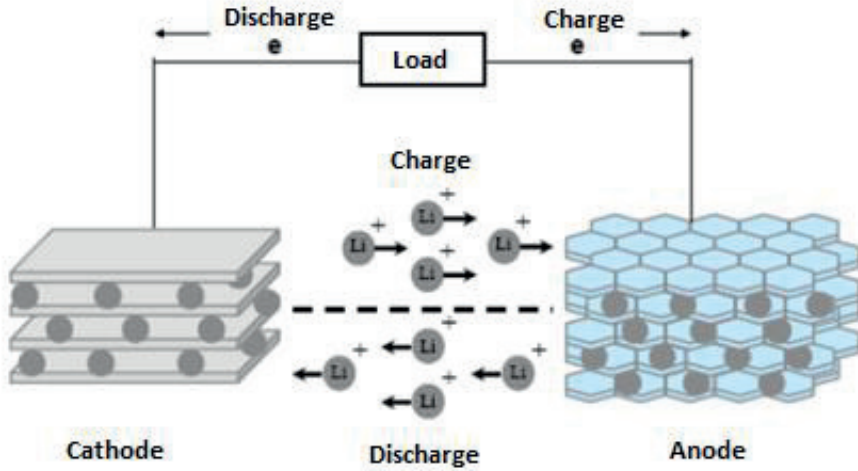


Figure 9. Charge-discharge processes of Li-ion batteries

Compared with other high-quality rechargeable battery technologies (nickel-cadmium or nickel-metal-hydride), Li-ion batteries have several advantages. They have one of the highest energy densities among today's battery technologies (100-265 Wh/kg or 250-670 Wh/L). In addition, Li-ion battery cells can charge-discharge 3 times more than battery technologies such as Ni-Cd or Ni-Mh (Miller, 2015). This means that Li-ion batteries can provide large amounts of current for high-power applications with relatively low maintenance compared with other batteries. Li-ion batteries also have a low self-discharge rate of approximately 1.5% - 2% per month.

Due to these advantages, Li-ion batteries have replaced Ni-Cd batteries as the market leader in portable electronic devices (such as smartphones and laptops). Li-ion batteries are also used to power electrical systems on the new and more environmentally friendly Boeing 787, where weight is a significant cost factor, and for some aerospace applications. From a clean energy perspective, much of the promise of Li-ion technology stems from its potential applications in EVs. The Nissan Leaf and Tesla Model S, currently the best-selling EVs, use Li-ion batteries as their primary fuel source (Stan et al., 2014; Matthews et al., 2017).

Despite these advantages, Li-ion batteries still have some disadvantages, especially in terms of safety. Li-ion batteries tend to

overheat and can be damaged at high voltages. In some cases, this can lead to thermal runaway and combustion. On a Boeing 787 passenger plane, thermal leakage in a li-on battery caused a fire.

Li-ion batteries are also subject to aging, which means that they can lose capacity and often fail after a few years. Another factor limiting their widespread use is their cost, which is about 40% higher than that of Ni-Cd. Addressing these issues is an important component of current research into technology. Finally, despite Li-ion's high energy density compared to other battery types, it has about a hundred times less energy density than gasoline (which contains 12,700 Wh/kg by mass or 8760 Wh/L by volume).

3.5. Lithium Air Batteries

Lithium-air batteries are a type of metal-air electrochemical cell or battery chemistry that generates electricity by oxidizing lithium at the anode and reducing oxygen at the cathode. They are not yet mass-produced but could one day become the ultimate rechargeable battery. Lightweight and high-capacity, they have a much higher potential energy density than conventional lithium-ion batteries. Because of these potential benefits, they will be used in the future in places such as electric vehicles and electricity storage systems. However, only a few lithium-air batteries have been successfully manufactured. This is partly because a significant proportion of lithium-air batteries by weight contain heavy inactive components that are not directly involved in battery processes (Lin et al. 2017).

3.6. Lithium Sulfur Batteries

Lithium sulfur (Li-S) can store much more energy than a similar battery using existing lithium ion (Li-ion) technology. This means that they can last significantly longer on a single charge. They can also be produced in the same factories where Li-ion batteries are produced, so it should be relatively easy to get them into production. Instead of using expensive cobalt, sulfur, a cheap raw material available as a by-product of the petroleum industry, is used (Hawkins et al., 2012). This can lead to significant savings in costs per unit of power.

However, existing Li-S batteries cannot be sufficiently charged before they become commercially viable. This is because charging a Li-S battery leads to the accumulation of chemical deposits that degrade the cell and shorten its lifetime. The deposits form on thin, tree-like structures called dendrites that emerge from the lithium anode, which is the negative

electrode inside the battery. The deposits thus disrupt the anode and the electrolyte, the medium through which the lithium ions travel back and forth. This reduces the power that the battery can provide and can short-circuit and cause a flammable electrolyte to ignite (Tredeau et al., 2009).

While Li-S cells can theoretically store up to five times the energies of Li-ion batteries in terms of mass, they also consume more volume. The fact that the life cycle of the batteries is half that of Li-ion batteries is another obstacle to their use in EVs for the time being.

3.7. Supercapacitor

A supercapacitor, also called an ultracapacitor, is used to store and discharge electricity similar to a battery. However, instead of storing energy in chemical form, supercapacitors are better at charging and discharging energy quickly by storing electricity in a static state. Therefore, supercapacitors have high power density but low energy density (Winter and Brodd, 2004).

In many ways, a supercapacitor is similar to a larger capacitor with larger electrode plates and less distance between them, allowing a larger charge to be stored in the form of electrical potential energy. A supercapacitor does not use a dielectric; instead, porous electrode plates are immersed in an electrolyte and separated by a very thin separator material. When a charge passes through the electrodes, the atoms in them polarize, giving the electrodes a positive or negative charge (Lin et al. 2017).

Supercapacitors are suitable for use in vehicles equipped with regenerative braking systems. This is due to their higher power density than batteries based on chemical reaction, which allows them to store and discharge electricity quickly, collecting the energy generated during braking and then quickly discharging it during acceleration (Hawkins et al., 2012). Full cell-based cars, such as the Toyota FCHV, also use supercapacitors to provide auxiliary power, which hydrogen fuel cells alone struggle to do. Li-ion batteries are still used as the primary power source (Enache et al., 2014). However, the number of electric and hybrid vehicles is increasing every day, so supercapacitors can play a bigger role in the next generation of electric cars.

4. CONCLUSION

The biggest challenge in the deployment of EVs lies in the development of low-cost and high-range battery systems. Because the production of low-cost batteries will enable us to see more EVs on the road, battery manufacturers are investing heavily in their facilities. Batteries used in EVs must have high power density and energy density. However, EVs have not yet reached the desired energy density. This situation brings along the necessity of using energy in the most efficient way in EVs. Studies have shown that useful braking can increase the range of EVs by 20% to 30% (Jung et al., 2021). However, this situation causes negative effects on the battery. In addition to increasing the range in batteries, preventing battery aging is important in terms of ensuring economic and environmental sustainability.

The general problem with today's EVs is their battery capacity and battery life. With the increase in the number of EVs in the coming years, the lack of charging stations and long charging times will provide users with an uncomfortable experience. In this context, energy recovery with beneficial braking will become more important in EVs in the future. Research and development of battery technologies that can offer a longer range without increasing the volume and mass of EVs continues. This chapter describes the braking and battery systems used in EVs.

REFERENCES

- Asghar, R., Rehman, F., Ullah, Z., Qamar, A., Ullah, K., Iqbal, K., Aman, A., and Nawaz, A. A. (2021). Electric vehicles and key adaptation challenges and prospects in Pakistan: A comprehensive review. *Journal of Cleaner Production*, 278,123375.
- Bentley, W. F., Heacock, D. K. (1996). Battery management considerations for multichemistry systems. *IEEE Aerospace and Electronic Systems Magazine*, 11(5), 23-26.
- Boerboom M. (2012). Electric Vehicle Blended Braking Maximizing Energy Recovery While Maintaining Vehicle Stability and Maneuverability, Master's Thesis in Chalmers Automotive Engineering and in European Master of Automotive Engineering, Göteborg, Sweden.
- Budde-Meiwes, H., Drillkens, J., Lunz, B., Muennix, J., Rothgang, S., Kowal, J., and Sauer, D. U. (2013). A review of current automotive battery technology and future prospects. *Proceedings of the Institution of Mechanical Engineers, Part D: Journal of Automobile Engineering*, 227(5), 761-776.
- Burd, J., Moore, E. A., Ezzat, H., Kirchain, R. and Roth, R. (2021). Improvements in electric vehicle battery technology influence vehicle lightweighting and material substitution decisions. *Applied Energy*, 283, 116269.
- Catenacci, M., Verdolini, E., Bosetti, V. and Fiorese, G. (2013). Going electric: Expert survey on the future of battery technologies for electric vehicles. *Energy Policy*, 61, 403-413.
- Chan, C.C., 2013. The rise & fall of electric vehicles in 1828–1930: lessons learned, *Proceedings of the IEEE*, 101(1):206 – 212.
- Chu, S., Majumdar, A. (2012). Opportunities and challenges for a sustainable energy future. *Nature*, 488(7411), 294-303.
- Cogen, J. (2010). Report of the alternative fuel vehicle infrastructure of working group, Oregon State Reports, USA.
- Cornic, D. (2010). October. Efficient recovery of braking energy through a reversible dc substation. In *Electrical systems for aircraft, railway and ship propulsion* (pp. 1-9). IEEE.
- Demir, A. (2022). Paris Anlaşması ve 26. Taraflar Konferansı (COP 26)'nda Türkiye Değerlendirmesi: Yükümlülükler ve Sorumluluklar . *Biyolojik Çeşitlilik ve Koruma* , 15 (2) , 162-170.
- Demir, A., Gümüş, M., Sayın, C., Boztoprak, Y., Yılmaz, M. (2012). Geçmişten günümüze otomobil teknolojileri, *Mimar ve Mühendis Dergisi*, 64: 60-63.
- Demirci, I. E., & Celikoglu, H. B. (2018). November. Timetable Optimization for Utilization of Regenerative Braking Energy: *A Single Line Case over Istanbul Metro Network*. In *2018 21st International Conference on Intelligent Transportation Systems (ITSC)* pp. 2309-2314. IEEE.
- Enache, B., Lefter, E., & Cepisca, C. (2014). Batteries for Electrical Vehicles: A Review. In: N. Bizon, L. Dascalescu, and N. M. Tabatabaei (Eds.), *Autonomous Vehicles* (pp. 409-429). *Intelligent Transport Systems and Smart Technologies*, Nova Science Publishers, New York.
- González-Gil, A., Palacin, R., & Batty, P. (2013). Sustainable urban rail systems: Strategies and technologies for optimal management of regenerative braking energy. *Energy conversion and management*, 75, 374-388.

- Hawkins, T., Singh, B., Bettez, G.M. & Stromman, A. H. (2012). Comparative Environmental Life Cycle Assessment of Conventional and Electric Vehicles. *Journal of Industrial Ecology*, 17(1), 53-64.
- Hu, H-Y., Xie, N., Wang, C., Wu, F., Pan, M., Li, H-F., Wu, P., Wang, X-D, Zeng, Z., Deng, S., Wu, M. H., Vinodgopal, K., & Dai, G-P. (2019). Enhancing the performance of motive power lead-acid batteries by high surface area carbon black additives. *Applied Sciences*, 9(1).
- Jung, H. Y., Kim, S. C., Shim, J. Y., Mandal, S., Thangarasu, S., & Thong, T. P. (2021). Positive electrode active material development opportunities through carbon addition in the lead-acid batteries: A recent progress. *Journal of Power Sources*, 485.
- Lee, C. K., Chen, C. H. (2003). Scheduling of train driver for Taiwan railway administration. *Journal of Eastern Asia Society of Transportation Studies*, 5, 292-306.
- Lin, D., Liu, Y. and Cui, Y. (2017). Reviving the lithium metal anode for high-energy batteries. *Nature Nanotechnology*, 12(3), 194-206.
- Matthews, L., Lynes, J., Riemer, M., Del Matto, T., & Cloet, N. (2017). Do we have a car for you? Encouraging the uptake of electric vehicles at point of sale. *Energy Policy*, 100, 79-88.
- Miller, P. (2015). Automotive lithium-ion batteries. *Johnson Matthey Technology Review*, 59(1), 4-13.
- Muratoğlu, Y., Akkaya, A. (2015). Elektrikli Araç Teknolojisi ve Pil Yönetim Sistemi-İnceleme. *Elektrik Mühendisliği Dergisi*, 458, 10-14.
- Stan, A. I., Swierczynski, M., Stroe, D. I., Teodorescu, R., and Andreassen, S. J. (2014). Lithium ion battery chemistries from renewable energy storage to automotive and back-up power applications - An overview. *2014 International Conference on Optimization of Electrical and Electronic Equipment, OPTIM 2014*, 713-720, 22- 24 May, Bran, Romania.
- Sun, X., Li, Z., Wang, X., & Li, C. (2020). Technology development of electric vehicles: A review. *Energies*, 13(1), 1-29.
- Şen, M., & Özcan, M. (2023). A novel method for SoC estimation of lithium-ion batteries based on Kalman filter in electric vehicle. *International Journal of Advanced Natural Sciences and Engineering Researches*, 7(5), 1-6.
- Tredeau, F. P., & Salameh, Z. M. (2009). Evaluation of lithium iron phosphate batteries for electric vehicles application. *5th IEEE Vehicle Power and Propulsion Conference, 1266-1270, 7-10 September, Dearborn, MI, USA*.
- Winter, M., & Brodd, R. J. (2004). What are batteries, fuel cells, and supercapacitors?. *Chemical Reviews*, 104(10), 4245-4270.
- Xu, G. & Zheng, C. (2016). Fully Electrified Regenerative Braking Control for Deep Energy Recovery and Maintaining Safety of Electric Vehicle. *IEEE Transactions on Vehicular Technology*, 65 (3), 1186-1198.
- Zhao, L., Li, K., & Su, S. (2014). A multi-objective timetable optimization model for subway systems. In *Proceedings of the 2013 International Conference on Electrical and Information Technologies for Rail Transportation (EITRT2013)*, 557-565. Springer, Berlin, Heidelberg.



Chapter 19

THE ART OF TIMELESS LEATHER: SUSTAINABILITY AND LIFE CYCLE ASSESSMENT OF THE LEATHER INDUSTRY

Fazlı AKYÜZ¹

Nuray Olcay IŞIK EMEKSİZ²

Khashim BEGALIEV³

1 Assist.Prof.Dr., Istanbul University – Cerrahpasa, Vocational School of Tehnical Sciences, Orcid ID: 0000-0001-5629-8764

2 Assoc.Prof.Dr., Tekirdag Namik Kemal University, Çorlu Vocational School, Orchid ID: 0000-0003-4749-336X

3 Assoc.Prof.Dr., Tashkent Institute of Textile and Light Industry, Orchid ID: 0009-0005-5907-9854

The Basics of Leather Processing

Leather is a timeless and versatile material that has been widely used for centuries due to its durability, luxurious appeal, and natural aesthetics. Also, the leather is an exceptional material that is well-suited to produce consumer goods, and efforts to enhance the longevity of items made from leather are critical for fostering sustainable practices and safeguarding the environment. By limiting waste volume, these initiatives promote eco-consciousness and extend the useful life of leather-based products. The leather industry employs extensive processing techniques to transform animal hides, which possess a fundamental histological structure comprised of collagen protein, into highly desirable and unique materials. These materials, characterized by their breathability, flexibility, durability, and distinctive surface and structural features, are versatile and resilient, making them suitable for use in various industries.

The primary objective of leather enterprises extends beyond the conversion of animal hides, derived as by-products from slaughterhouses, into economically viable and practical items while adhering to a sustainable production approach. Additionally, such endeavours aim to conduct operations with due sensitivity and in an environmentally responsible manner throughout the industrial process. (Krishnamoorthy, Sadulla, Sehgal, & Mandal, 2012) (Hassan, Harris, Busfield, & Bilotti, 2023). The refined products generated by this industry culminate at the end of a process that is enhanced by the expertise of art and craftsmanship, complemented by a wealth of scientific knowledge. These products are versatile and can be utilized in a broad range of final products, including footwear, apparel, automotive and furniture upholstery, accessories, and works of art.

This lengthy and labour-intensive process, which has been carried out for centuries, is capable of processing not only mammalian hides from animals such as cattle, sheep, goats, and pigs, which are commonly used in the meat and meat products industry, but also hides from various species and types of animals including fur animals, reptiles, fish, and birds.

The leather processing process begins with the initial stage of separating the animal's hide from its carcass after slaughter. When the raw animal hides cannot be processed immediately, they undergo protective treatments, known as conservation processes, to prevent the loss of quality until they reach tanneries where they will undergo tanning processes. These conservation processes include drying, salting, cooling, freezing, and pickling. Essentially, this process ensures that the raw hides can withstand microbial activity and storage conditions without deterioration or putrefaction.

The leather processing procedure involves subjecting raw animal hides to comprehensive chemical and mechanical treatments, not only to preserve

the leather from hot water, microbial influences, and chemical damages but also to meet the demands of fashion by rendering it aesthetically appealing, durable, and flexible (Inbasekar, Raghava Rao, & Fathima, 2021). The resultant finished leather, thus obtained, distinguishes itself as a natural material, drawing attention with its elegance and quality, which are a manifestation of the amalgamation of aesthetic and technical knowledge in every application.

Upon reaching a tannery, the primary processing steps applied to raw hides can be categorized into four main groups: i) pre-tanning, ii) tanning, iii) post-tanning, and iv) finishing processes (Buljan, Reich, & Ludvik, 1998), (European Commission, 2003).

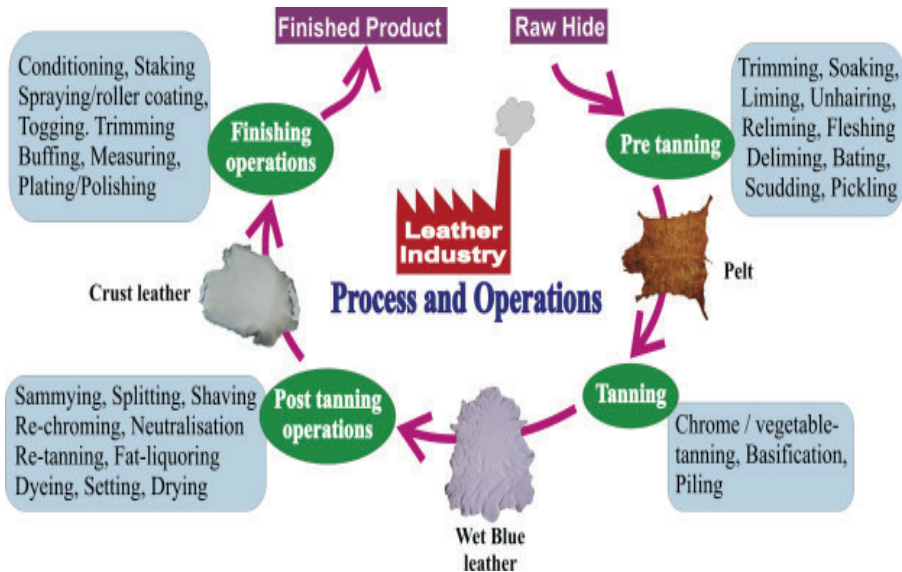


Figure 1. Leather manufacturing schema (Dixit, Yadav, Dwivedi, & Das, 2015)

The raw hides processed in tanneries undergo a series of operations known as 'pre-tanning processes' in preparation for the tanning phase. These operations include soaking, softening, fleshing, hair removal, liming, splitting, deliming, bating, and degreasing to remove interfibrillar substances along with hair, wool, grease, and impurities. These steps are undertaken with the aim of preparing the hides for the tanning process by eliminating unwanted materials and are essential for the effective execution of subsequent stages in leather production.

Through these processes, the aim is to clean and purify the collagen network, which has a fibrous structure due to the removal of some components inherent in the natural structure of rawhide. This involves loosening and isolating the collagen fibres by making certain changes to its structure. If these processes are not carried out properly, they can impede both the intended purposes of the treatments and access to the desired characteristics sought to

be imparted to the leather.

After the pre-tanning processes, the leather is subjected to the most crucial stage in the leather production process, known as the ‘tanning process’. (Ahmed & Maraz, 2021). Tanning is the process of transforming raw hides and skins obtained from different animals into a sustainable and manageable material known as finished leather. In this process, reactions are induced under suitable conditions between the fibrous collagen protein structure of the hides and specific agents with tanning effects, resulting in the formation of new chemical bonds. Consequently, the leather is strengthened, its hydrothermal resistance and resistance to degradation caused by microorganisms are enhanced, and the potential for deterioration over time is prevented. In other words, tanned leather, unlike raw hides, undergoes minimal dimensional changes when dried or immersed in water, possesses a higher shrinkage temperature, and exhibits increased resistance against microbial activity.

Traditionally, the tanning process involves the ionic compatibility of the tanning agent with the leather, the penetration of the tanning agent into the leather, its homogeneous distribution, and binding in the final stage. In the contemporary world, more than 85-90% of the leathers produced are tanned with trivalent basic chromium sulfate due to its effectiveness in producing high-quality leather (Ahmed & Maraz, 2021)(Ražić, ve diğerleri, 2022). Chromium tanning is followed by vegetable tanning, which involves the use of tannins obtained from high-tannin content plants and plant parts, representing one of the oldest tanning methods. In addition to these, synthetic tannins (syntans), aldehydes, oils, various polymers, and other mineral tanning agents are also employed.

Tanned hides undergo ‘post-tanning processes’ to impart and enhance properties suitable for the final application. Essentially, this stage, comprising neutralization, lubrication, dyeing, and fixation processes, aims to align the leather’s strength, feel, softness, waterproofing, color, and similar characteristics with fashion requirements. Starting from soaking, the processes leading up to this stage primarily involve chemical treatments conducted in aqueous environments. However, mechanical processes such as fleshing, splitting, and shaving are also employed to both remove undesirable portions of the leather and adjust its thickness according to the final product.

The final stage of leather processing is referred to as the ‘finishing’ stage, also known as ‘dry finishing processes.’ This stage is also described as the ‘make-up’ of the leather. The process involves initially drying the leather, mechanically preparing it into smooth layers, and subsequently applying coating processes that reflect the desired properties of the final product onto the leather surface. In this way, the finishing stage not only imparts a fashionable appearance to the leather but also addresses imperfections and

flaws on the leather surface, corrects deficiencies from aging processes, and adds a protective transparent coating to the leather against external factors.

Environmental Impacts of the Leather Industry

Leather is a renewable industrial product obtained as a by-product/waste after the slaughter of animals such as cattle, sheep, pigs, goats, etc., used in the meat and dairy industries. The leather industry functions within a circular economy framework by transforming raw hides into finished leather products (Dixit et al., 2015; Jaegler, 2016; Joseph & Nithya, 2009). Consequently, leather can be fundamentally recognized as a unique sustainable material.

For centuries, the leather industry has held an indispensable position among sectors due to its enduring charm, economic contribution, and versatile usability in producing a strong and valuable material. However, aspects of environmental pollution, such as solid and liquid waste as well as emissions of gases and odors, generated during the transformation of raw hide into leather, have become focal points highlighting the industry's environmental challenges (Durai & Rajasimman, 2011) (Haroun & Ahmed, 2023).

As mentioned in the introduction section, the key stages in leather processing include curing, soaking, liming, dehairing, detaining, deliming, bating, picking, degreasing, and tanning. Throughout these steps, various chemicals such as sodium sulphide, sodium bicarbonate, chromate, chloride, sodium sulphite, chromium sulphate, calcium salts, ammonium salts, acids, alkalis, fat, liquor, organic dyes, hydrogen peroxide, and formate are employed. The utilization of these chemicals releases potentially toxic substances such as organic chlorinated phenols (e.g., 3,5-dichlorophenol), inorganic pollutants like Cr(VI), and other hazardous compounds including sulphides, phenolic compounds, magnesium, sodium, potassium, azo-dyes, cadmium compounds, cobalt, copper, antimony, barium, lead, selenium, mercury, zinc, arsenic, PCB, nickel, formaldehyde resins, dyes, solvents, pesticide residues, and other mineral salts (Ros & Ganter, 1998), resulting in significant health risks and environmental challenges throughout all stages, thereby impacting entire ecosystems.

As a result of these, the leather industry faces pressure to optimize its processes and reduce environmental impacts in response to high demands for sustainability and ecological development. The transformation of raw hides into finished leather involves the use of various chemicals, including some considered hazardous such as chromium, which can lead to significant environmental effects. The leather industry contributes to serious environmental issues by generating substantial amounts of liquid and solid waste, posing a potential threat to biodiversity in receiving environments (Figure 2, 3 and 4).

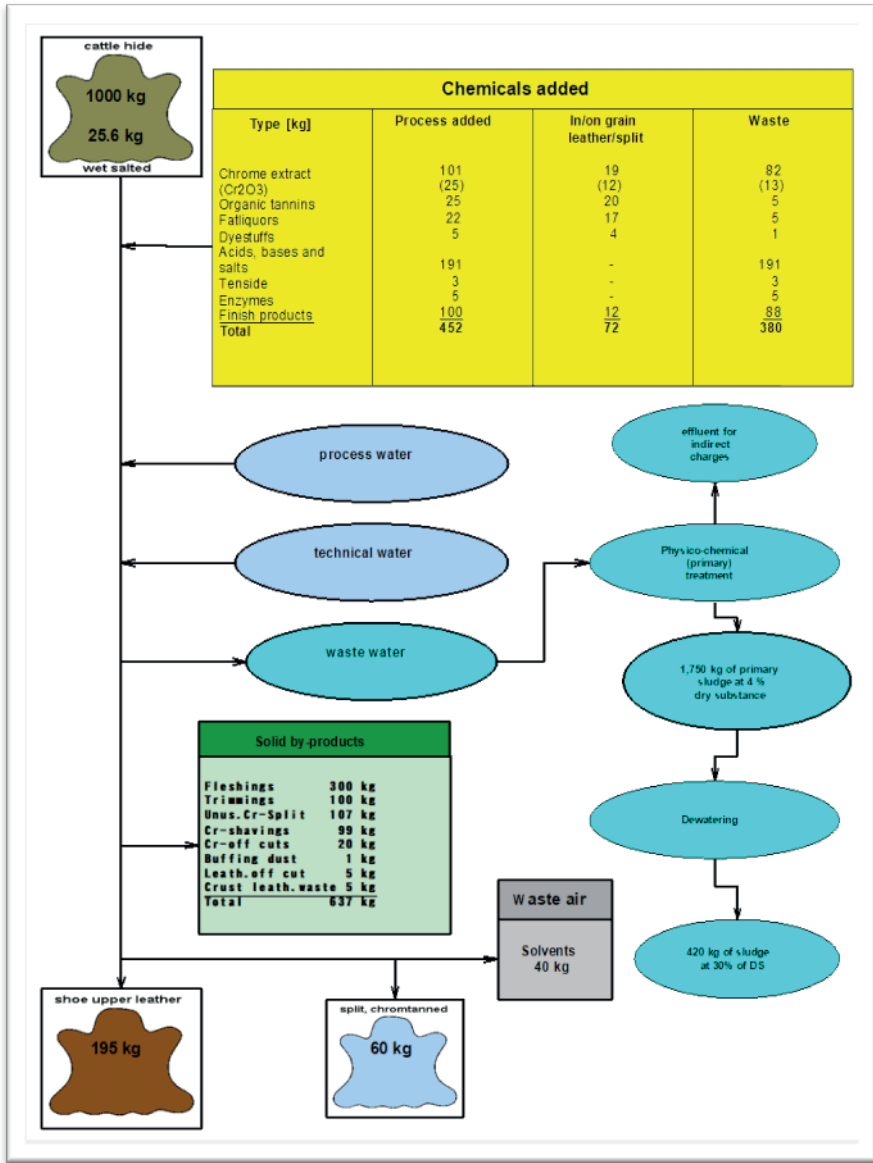


Figure 2. Mass balance in leather processing (Buljan et al.,1998)



Figure 3. Waste profile of the leather production

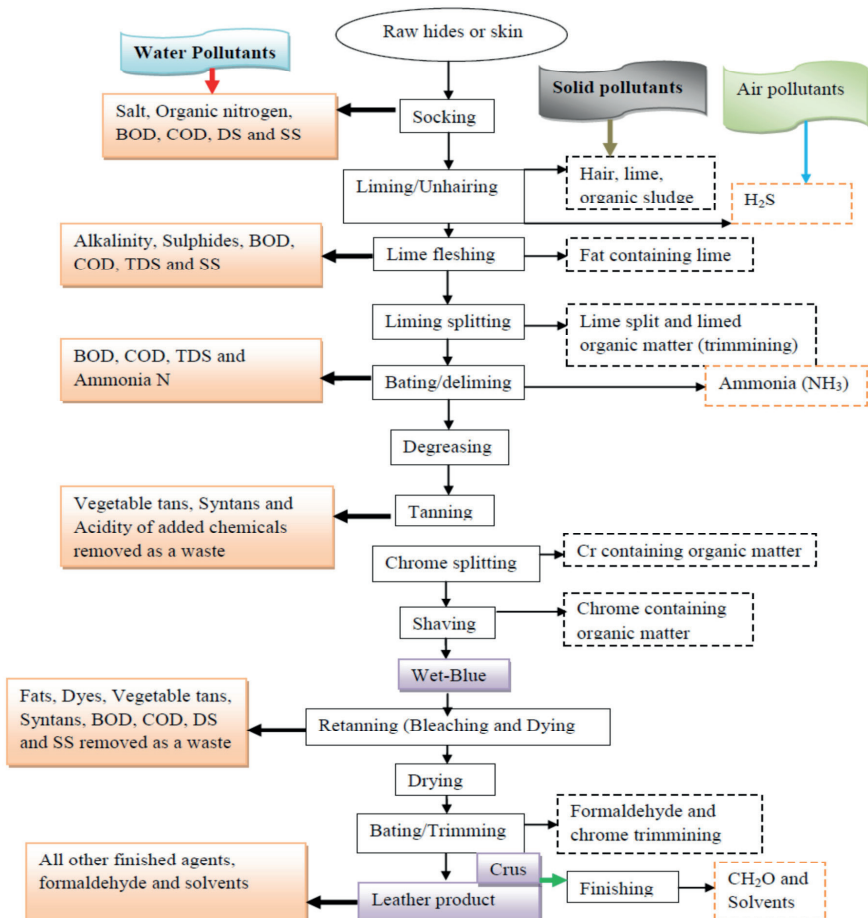


Figure 3. Type of pollutants during the tanning process (UNEP 1994)

In essence, the leather industry makes a significant contribution to the global economy, yet it is also associated with various environmental impacts. These impacts arise from the use of chemicals, water consumption, and waste generation during the leather tanning process. Studies have emphasized the environmental effects of the leather tanning industry, shedding light on challenges and the need for sustainable practices. Researches have focused on evaluating the conditions that govern chromium release during leather processing and highlighting potential environmental and health risks associated with chromium exposure (Hedberg et al., 2015). Efforts have been made to develop chrome-free tanning systems to address the environmental impact of chromium in leather tanning (Tang et al., 2015). Life cycle assessment studies have identified the tanning process as a primary contributor to environmental impact categories in leather production, emphasizing the need for cleaner production methods (Cui & Qiang, 2019). The current state of research on sustainability in the leather industry reveals a concentration of studies in developing countries, primarily focusing on economic and environmental sustainability issues. However, the area of social sustainability, as highlighted in the third pillar of sustainability, has received limited attention, with most research concentrated on health and occupational safety (Omoloso et al., 2021). In response to growing customer demand for sustainable products, increasingly stringent regulations, and heightened user awareness of the environmental impact of their purchases, the leather industry is now faced with the pressing need to adopt more sustainable practices in tanneries. For instance, the United Nations' 2030 Sustainable Development Goals, which aim to create an economically, socially, and environmentally sustainable system without compromising the needs of future generations, have not only embedded the concept of sustainability but also directed the leather industry to improve its environmental carbon footprint (United Nations, 2016).

In the leather industry, the term “carbon footprint” refers to determining the amount of carbon emissions generated during the production process and working towards their reduction (Nugraha, Suparno, & Indrasti, 2020). Conducting a Life Cycle Assessment of Leather and determining the amount of CO₂ emitted during leather processing enable more accurate and controlled analyses to achieve a more sustainable leather production.

the leather tanning industry is associated with various environmental impacts, including the release of toxic compounds, water pollution, and chemical usage. The environmental concerns have prompted extensive research into sustainable and eco-friendly tanning methods, waste management strategies, and the development of alternative tanning agents. Addressing the environmental impact of leather tanning is crucial for promoting sustainable practices and minimizing the industry's ecological footprint.

Environmental Consciousness: Sustainable Practices in the Leather Industry

The leather industry has historically been associated with significant environmental impacts, including the release of hazardous chemicals, water consumption, and waste generation. However, there is a growing awareness of the need for sustainable practices in leather production to minimize environmental harm and promote eco-friendly processes.

The environmental impact of the leather industry has been a subject of concern, particularly regarding the use of chromium in tanning processes. Chromium, particularly hexavalent chromium (Cr (VI)), is a toxic and carcinogenic compound, posing risks to both human health and the environment (Hansen et al., 2003). In response to these concerns, researchers have focused on developing chrome-free and chrome-less tanning systems to mitigate the environmental impact of chromium in leather tanning (Jiang et al., 2020). The development of eco-friendly chrome-free metal tanning agents has been identified as crucial for the sustainable development of the leather industry (Jiang et al., 2020).

Furthermore, Loffrano et al. (2008) have studied the characterization, fluxes, and toxicity of leather tanning bath chemicals to evaluate their environmental impact, emphasizing the need for optimal resource management within tanneries to achieve a sustainable industry for the future (Loffrano et al., 2008). Additionally, the reduction of water consumption in leather processing has been recognized as a critical aspect of sustainable leather production, with efforts to improve leather quality while minimizing water usage (Ferdous et al., 2023). The implementation of cleaner beam house processes and salt-free pickling and chrome-free tanning technologies has been explored as sustainable approaches for cleaner leather manufacturing, reflecting the industry's commitment to reducing environmental impact (Liu et al., 2010; Mala et al., 2020).

The development of chrome-free tanning agents using renewable materials, such as biomass-derived compounds, has gained attention as a sustainable approach to leather tanning. The utilization of biomass materials in the leather industry offers a fundamental step towards sustainable and environmentally friendly tanning agents (Shen et al., 2023). Additionally, the use of natural plants as sources of substances for cleaner leather tanning technologies has been explored, aiming to minimize or prevent pollution caused by hazardous chemicals (Nalyanya et al., 2021) (Pons, Rius, Vintró, & Gallart, 2022).

The environmental impact of leather tanning extends to the generation of tannery effluent, which can contribute to water pollution and health risks. Studies have highlighted the environmental hazards associated with the

uncontrolled release of chrome in tannery effluent, emphasizing the need for effective waste management and treatment strategies (Fernández-Rodríguez et al., 2022).

In addition to addressing the environmental impact of tanning processes, the leather industry has focused on developing sustainable and eco-friendly tanning agents. The utilization of natural organic pigments with excellent tanning capabilities has been explored as a novel strategy for sustainable leather manufacturing, reflecting the industry's commitment to eco-friendly practices (Ding et al., 2022). Furthermore, the development of a salt-free pickling and chrome-free tanning technology has been identified as a sustainable approach for cleaner leather manufacturing, aligning with the industry's shift towards environmental consciousness (Liu et al., 2022).

The shift towards sustainable practices in the leather industry is also evident in the development of cleaner production methods for the synthesis of bactericides used in leather making, reflecting the industry's commitment to minimizing environmental impact (Muthusubramanian & Mitra, 2006). Moreover, the reduction of chromium use in combined chromium-gambier tanning processes has been explored to minimize the environmental impact of chromium in leather production, highlighting the industry's efforts to adopt sustainable and eco-friendly practices (Kasim et al., 2014).

The leather industry is undergoing a transformation towards environmental consciousness and sustainable practices. The adoption of chrome-free tanning agents, cleaner production methods, and the utilization of renewable materials reflects the industry's commitment to minimizing environmental impact and promoting eco-friendly processes. The shift towards sustainable practices in the leather industry is essential for achieving a balance between economic viability and environmental responsibility.

Balancing Act: Sustainability and Lifecycle Assessment in Leather Tanning

The nexus between sustainability and life cycle assessment (LCA) is vital in the leather industry, particularly in leather tanning, where economic significance coexists with environmental challenges. To achieve sustainability and perform LCA in this sector is necessary to comprehend and tackle the environmental consequences of leather production.

In the leather tanning industry, sustainability entails adopting environmentally-friendly practices, efficient resource utilization, and minimal environmental harm. LCA, on the other hand, is a holistic approach for evaluating the environmental impacts of a product or process throughout its entire lifecycle, from raw material extraction to end-of-life disposal. Integrating sustainability and LCA in the leather tanning sector is crucial

for pinpointing areas of environmental concern, implementing sustainable solutions, and guiding decision-making and policy development.

Several studies have highlighted the importance of conducting life cycle assessments to evaluate the environmental impacts of leather production processes. For example, a study by Pradeep et al. (2021) emphasized the benefits of a melamine-based polymeric crosslinker for cleaner leather production, which resulted in a reduction in chromium input and total dissolved solids generation. This demonstrates how life cycle assessment serves as a tool for identifying opportunities to improve sustainability in the leather industry.

The development of cleaner production methods and eco-friendly tanning agents is another area where the relationship between sustainability and life cycle assessment is evident. For instance, Xiao et al. (2023) discussed sustainable metal-free leather manufacture via the synergistic effects of a triazine derivative and vegetable tannins, highlighting the potential for achieving a more ecological and sustainable leather industry through life cycle assessment. Additionally, the use of glucose to improve the environmental aspects of the chrome tanning process, as discussed by (Puccini & Castiello, 2014), demonstrates the integration of sustainability and life cycle assessment to achieve more environmentally sound tanning processes.

The relationship between sustainability and life cycle assessment in the leather tanning industry also extends to the development of catalysts and cleaner alternative products. Shen et al. (2023) discussed the one-step synthesis of starch-based composite chrome-free tanning agents via in situ catalysis using hydrotalcites, emphasizing the improved catalytic efficiency and the avoidance of pollution generation. Additionally, Cui & Qiang (2019) highlighted the pressure from importing countries to source finished leathers, prompting researchers to seek cleaner alternative products and relevant processing technologies, reflecting the industry's commitment to sustainability guided by life cycle assessment.

Life cycle assessment also plays a crucial role in identifying areas of environmental concern and guiding policy formulation in the leather tanning industry. For example, Yang et al. (2021) conducted a life cycle assessment of processing for chrome-tanned cowhide upper leather, demonstrating the sensitivity of inventory data and the environmental impact of different tanning processes.

The interconnection between sustainability and life cycle assessment (LCA) within the leather tanning industry plays a pivotal role in comprehending and mitigating the environmental implications associated with leather production. Life cycle assessment emerges as a valuable instrument, facilitating the scrutiny of the environmental dynamics inherent in the processes of leather production. This approach aids in pinpointing areas necessitating enhancement, thus

steering the formulation of sustainable practices and policies. The integration of life cycle assessment into sustainability frameworks empowers the leather industry to actively pursue the diminution of its environmental impact, fostering the adoption of ecologically sound and sustainable methodologies.

Result

The leather industry is a significant contributor to the global economy, but it also presents environmental challenges. To address these challenges, sustainability and life cycle assessment (LCA) are crucial in the leather industry. Sustainability involves adopting practices that minimize environmental harm, promote eco-friendly processes, and ensure efficient resource use. LCA is a comprehensive method for evaluating the environmental impacts of a product or process throughout its entire life cycle. The integration of sustainability and LCA in the leather industry is essential for identifying areas of environmental concern, implementing sustainable solutions, and guiding decision-making and policy formulation.

Several studies have emphasized the importance of conducting life cycle assessments to evaluate the environmental impacts of leather production processes. For example, LCA studies have been used to identify opportunities to improve sustainability in the leather industry, such as the development of cleaner production methods and eco-friendly tanning agents. Additionally, LCA plays a crucial role in identifying areas of environmental concern and guiding policy formulation in the leather tanning industry.

The relationship between sustainability and LCA in the leather industry also extends to the utilization of natural resources and bio-based materials, as well as the development of catalysts and cleaner alternative products. Furthermore, the integration of sustainability and LCA in the leather industry is essential for guiding decision-making and policy formulation, as well as for identifying areas of environmental concern and implementing sustainable solutions.

In conclusion, the relationship between sustainability and life cycle assessment in the leather industry is crucial for understanding and addressing the environmental impact of leather production. By integrating life cycle assessment into sustainability initiatives, the leather industry can work towards reducing its environmental footprint and promoting eco-friendly and sustainable practices.

Literature

- Buljan, J., Reich, G., & Ludvik, J. (1998). Mass balance in leather processing. *Leder und Haute Markt*, 24(4), 30-27.
- Cui, L. and Qiang, X. (2019). Clean production for chrome free leather by using a novel triazine compound. *Journal of Renewable Materials*, 7(1), 57-71. <https://doi.org/10.32604/jrm.2019.00118>
- Ding, W., Liu, H., Li, S., Remón, J., Pang, X., & Ding, Z. (2022). Providing natural organic pigments with excellent tanning capabilities: a novel “one-pot” tanning–dyeing integration strategy for sustainable leather manufacturing. *ACS Sustainable Chemistry & Engineering*, 10(51), 17346-17354. <https://doi.org/10.1021/acssuschemeng.2c06144>
- Dixit, S., Yadav, A., Dwivedi, P.D., Das, M. (2015). Toxic hazards of leather industry and technologies to combat threat: a review. *J. Clean. Prod.* 87, 39–49. <https://doi.org/10.1016/J.JCLEPRO.2014.10.017>
- Durai, G. and Rajasimman M., (2011). Biological treatment of tannery waste water, a Review. *Journal of Environmental Science and Technology*, 4 (1): 1-17.
- European Commission. (2003). Integrated Pollution Prevention and Control (IPPC), Reference Document on Best Available Techniques for the Tanning of Hides and Skins.
- Ferdous, S., Mottalib, M. A., Goni, M. A., Abdulla-Al-Mamun, M., & Sheikh, M. A. A. (2023). Reduction of water consumption in leather processing and an investigation of the leather quality. *Textile & Leather Review*, 6, 132-150. <https://doi.org/10.31881/tlr.2023.001>
- Fernández-Rodríguez, J., Lorea, B., & González-Gaitano, G. (2022). Biological solubilisation of leather industry waste in anaerobic conditions: effect of chromium (iii) presence, pre-treatments and temperature strategies. *International Journal of Molecular Sciences*, 23(21), 13647. <https://doi.org/10.3390/ijms232113647>
- Hansen, M. B., Johansen, J. D., & Menné, T. (2003). Chromium allergy: significance of both cr(iii) and cr(vi). *Contact Dermatitis*, 49(4), 206-212. <https://doi.org/10.1111/j.0105-1873.2003.0230.x>
- Haroun, M., & Ahmed, M. M. (2023). Reducing chromium discharge in tanning: The salt-free chrome tanning process. *GSC Advanced Research and Reviews*, 15(01), 015–020.
- Hassan, M. M., Harris, J., Busfield, J. J., & Bilotti, E. (2023). A review of the green chemistry approaches to leather tanning in imparting sustainable leather manufacturing. *Green Chemistry*, 25, 7441-7469.
- Hedberg, Y., Lidén, C., & Wallinder, I. O. (2015). Chromium released from leather – i: exposure conditions that govern the release of chromium(iii) and chromium(-vi). *Contact Dermatitis*, 72(4), 206-215. <https://doi.org/10.1111/cod.12329>

- Inbasekar, C., Raghava Rao, J., & Fathima, N. N. (2021). Strategizing the development of a metal- and formaldehyde-free tanning process using (3,5-dimethyl-1h,3h,5h-oxazol[3,4-c]oxazol-7a(7h)-yl) methanol heterocyclic derivative oxazolidine and polyallylamine. *ACS Sustainable Chemistry & Engineering*, 9(44), 15053-15062.
- Jiang, Z., Ding, W., Xu, S., Remón, J., Shi, B., Hu, C., & Clark, J. H. (2020). A 'trojan horse strategy' for the development of a renewable leather tanning agent produced via an alcl₃-catalyzed cellulose depolymerization. *Green Chemistry*, 22(2), 316-321. <https://doi.org/10.1039/c9gc03538a>
- Kasim, A., Novia, D., Mutiar, S., & Efendi, A. (2014). Diminishing chromium use on combined chromium-gambier tanning process upon the characteristics of tanned leather. *Media Peternakan*, 37(1), 24-29. <https://doi.org/10.5398/medpet.2014.37.1.24>
- Muthusubramanian, L. and Mitra, R. B. (2006). A cleaner production method for the synthesis of bronopol – a bactericide that is useful in leather making. *Journal of Cleaner Production*, 14(5), 536-538. <https://doi.org/10.1016/j.jclepro.2005.03.020>
- Nugraha, A., Suparno, O., & Indrasti, N. (2020). Analisis Potensi Jejak Karbon Limbah Cair dan Listrik Pada Proses Penyamakan Kulit., 30, 256-264. <https://doi.org/10.24961/J.TEK.IND.PERT.2020.30.3.256>
- Itanola, M., & Saka, N. (2019). Life Cycle Costing and Assessment of Building Slab Materials. *Journal of Sustainable Construction Materials and Technologies*, 4(2), 332-343.
- Jaegler, A. (2016). A sustainable supply chain in the leather sector: dilemmas, challenges and learnings. *Supply Chain Forum An Int. J.* 17, 136-142. <https://doi.org/10.1080/16258312.2016.1211833>
- Joseph, K., Nithya, N. (2009). Material flows in the life cycle of leather. *J. Clean. Prod.* 17, 676-682. <https://doi.org/10.1016/j.jclepro.2008.11.018>
- Krishnamoorthy, G., Sadulla, S., Sehgal, P. K., & Mandal, A. B. (2012, 15 5). Green chemistry approaches to leather tanning process for making chrome-free leather by unnatural amino acids. *Journal of Hazardous Materials*, 215-216, 173-182.
- Liu, S., Li, J., Yi, J., & Zhi-hua, S. (2010). Cleaner beam house processes trial on cattle sofa leather. *Journal of Cleaner Production*, 18(5), 471-477. <https://doi.org/10.1016/j.jclepro.2009.11.010>
- Liu, X., Wang, Y., Wang, X., Han, T., Wang, W., & Jiang, H. (2022). A salt-free pickling and chrome-free tanning technology: a sustainable approach for cleaner leather manufacturing. *Green Chemistry*, 24(5), 2179-2192. <https://doi.org/10.1039/d1gc04105c>
- Lofrano, G., Aydın, E., Russo, F., Guida, M., Belgiorno, V., & Meriç, S. (2008). Characterization, fluxes and toxicity of leather tanning bath chemicals in a large tan-

- ning district area (it). *Water, Air, & Soil Pollution: Focus*, 8(5-6), 529-542. <https://doi.org/10.1007/s11267-008-9177-7>
- Mala, J. G. S., Takeuchi, S., & Mani, U. (2020). Microbial chromate reductases: novel and potent mediators in chromium bioremediation-a review. *Applied Microbiology: Theory Technology*, 32-44. <https://doi.org/10.37256/amtt.112020222>
- Nalyanya, K. M., Rop, R. K., Onyuka, A., & Birech, Z. (2021). A review of natural plants as sources of substances for cleaner leather tanning technologies. *Textile & Leather Review*, 4(3), 137-148. <https://doi.org/10.31881/tlr.2021.03>
- Navarro, D., Wu, J., Lin, W., Fullana-i-Palmer, P., & Puig, R. (2020). Life cycle assessment and leather production. *Journal of Leather Science and Engineering*, 2, 1-13. <https://doi.org/10.1186/s42825-020-00035-y>.
- Pons, A., Rius, J., Vintró, C., & Gallart, A. (2022). Analysis of Twitter posts for evaluation of Corporate Social Responsibility in the leather industry. *Journal of Engineered Fibers and Fabrics*, 17(155892502211318).
- Pradeep, S., Sathish, M., Sreeram, K. J., & Rao, J. R. (2021). Melamine-based polymeric crosslinker for cleaner leather production. *ACS Omega*, 6(20), 12965-12976. <https://doi.org/10.1021/acsomega.0c05668>
- Ros M, Ganter A., (1998). Possibilities of reduction of recipient loading of tannery waste Slovenia. *Water Science Technology*. 37.
- Omoloso, O., Mortimer, K., Wise, W.R. & Jraisat, L (2021). Sustainability research in the leather industry: A critical review of progress and oppurtunities for future research. *Journal of Cleaner Production.*, 285, DOI: <https://doi.org/10.1016/j.jclepro.2020.125441>
- Puccini, M. and Castiello, D. (2014). Use of glucose to improve the environmental aspects of chrome tanning process. *Advanced Materials Research*, 933, 144-150. <https://doi.org/10.4028/www.scientific.net/amr.933.144>
- Ražić, S. E., Kopjar, N., Kašuba, V., Skenderi, Z., Akalović, J., & Hrenović, J. (2022). Evaluation of DNA-Damaging Effects Induced by Different Tanning Agents Used in the Processing of Natural Leather—Pilot Study on HepG2 Cell Line. *Molecules*, 27(20), 7030.
- Rao, J. R., Thanikaivelan, P., Sreeram, K. J., & Nair, B. U. (2002). Green Route for the Utilization of Chrome Shavings (Chromium-Containing Solid Waste) in Tanning Industry. *Environ. Sci. Technol.*, 36(6), 1372 - 1376.
- Shen, Y., Ma, J., Fan, Q., Han, Y., Zhang, J. H., Zhang, W., ... & Yan, H. (2023). One-step synthesis of starch-based composite chrome-free tanning agents via in situ catalysis using hydrotalcites. *ACS Sustainable Chemistry & Engineering*, 11(30), 11342-11352. <https://doi.org/10.1021/acssuschemeng.3c03526>
- Tang, Q., Gao, X., Ren, J., Chen, X., & Wang, X. (2015). A chrome-free and chrome-less tanning system based on the hyperbranched polymer. *ACS Sustainable Chemistry & Engineering*, 4(3), 701-707. <https://doi.org/10.1021/acssuschemeng.5b00917>

UNEP IE/PAC, (1994). *Tanneries and Environment - A Technical Guide*, Technical Report (2nd Print) Series, No:4, ISBN 92 807 12764

United Nations. 2016. *Transforming our world: The 2030 agenda for sustainable development*. <https://sdgs.un.org/2030agenda>.

Yang, H., An, D., Gaidău, C., Zhang, J., & Jin, Z. (2021). Life cycle assessment of processing for chrome tanned cowhide upper leather. *Leather and Footwear Journal*, 21(2), 75-86. <https://doi.org/10.24264/lfj.21.2.1>

Xiao, Y., Zhou, J., Wang, C., Zhang, J., Radnaeva, V., & Lin, W. (2023). Sustainable metal-free leather manufacture via synergistic effects of triazine derivative and vegetable tannins. *Collagen and Leather*, 5(1). <https://doi.org/10.1186/s42825-022-00108-0>